

Fe-Mg AND Ni PARTITIONING BETWEEN  
OLIVINE AND SILICATE MELT

Thesis by

Andrew Keith Matzen

In Partial Fulfillment of the Requirements for the  
degree of

Doctorate of Philosophy

CALIFORNIA INSTITUTE OF TECHNOLOGY

Pasadena, California

2012

(Defended January 20<sup>th</sup>, 2012)

© 2012

Andrew Keith Matzen

All Rights Reserved

## ACKNOWLEDGEMENTS

First, I would like to thank my thesis advisor, Edward Stolper, for bringing me to Caltech in the summer of 2004 to work in his laboratory. While here, I was able to work with Mike Baker and John Beckett on the “small” project that would eventually turn into Chapter II of this thesis. The exceptionally positive experience I had is what, ultimately, led me to pursue my PhD at Caltech. I am very grateful for Ed’s excitement about new experiments, his demands for excellent scientific writing, and his understanding when things just didn’t work. I am also indebted to Mike and John for teaching me how to be a careful experimentalist and analyst, in addition to their friendship. I would also like to acknowledge the other members of my thesis committee: Paul Asimow for his long sessions working on thermodynamics, and his commitment to teaching new and engaging classes; George Rossman for his willingness to let me destroy beautiful mineral samples, and his open door; and John Eiler, for his patience with me as young graduate student and his commitment to PRG.

I would also like to thank my fellow graduate students, especially Alan Chapman, Steve Kidder, and Steve Chemtob, for their amazing vocal abilities; Willy Amidon for mountain bike rides in the San Gabes; and June Wicks for being a fantastic office mate. My time in the L.A. area has also been made wonderful by the many friends I have made along the way, Tim, Lisa, Cam, Tom, and the entire 860 entourage. I am extremely grateful of your friendship. Lastly, I would like to thank my family, Keith, Terri, and (especially) Kelly: I wouldn’t have been able to do this without your support and love.

## ABSTRACT

The mineral olivine is abundant in a wide range of mafic igneous rocks from around the solar system. The fractionation, or accumulation, of olivine often exerts a major control on the observed variations in magma and whole-rock compositions. We performed experiments on a synthetic Hawaiian picrite and examined the olivine (ol)-liquid (liq) partitioning of Mg and  $\text{Fe}^{2+}$ . These experiments show that the exchange coefficient,  $K_{D, \text{Fe}^{2+}\text{-Mg}} = (\text{FeO}/\text{MgO})^{\text{ol}} / (\text{FeO}/\text{MgO})^{\text{liq}}$ , by weight, is  $0.345 \pm 0.009$  ( $1\sigma$ ) and is independent of temperature and liquid composition. Using this result, we estimate that parental liquids for tholeiites from Kilauea, Mauna Loa, and Mauna Kea have approximately 19-21 wt. % MgO. Published experiments on model Martian compositions suggest that for the Fe-enriched and Al-depleted Martian basalts a slightly higher  $K_{D, \text{Fe}^{2+}\text{-Mg}}$  of 0.36 is more appropriate. Using this value we conclude that the olivine-phyric shergottites Y 980459, NWA 5789, 2990, and EETA 79001 are possible liquid compositions (others are not); if the canonical  $K_{D, \text{Fe}^{2+}\text{-Mg}}$  of 0.30 were used, we would have concluded that none of the bulk meteorites represent liquids.

The behavior of Ni is nearly unique among most other major and trace elements: it is compatible in olivine. This compatibility is useful in constraining the evolution of lavas, as their Ni contents will be very sensitive to the fractionation or accumulation of olivine. We performed experiments investigating the partitioning of Ni between a liquid and olivine of approximately constant composition over a range of temperatures and pressures. These experiments successfully separate the effects of composition from those of temperature and pressure, showing that, for our liquid with ~ 18 wt. % MgO, the ol-liq Ni partition

coefficient (by wt.) decreases from 5.0 to 3.8 as the temperature and pressure increase from 1400 to 1550°C and 1-atm to 3.0 GPa, respectively. We show that this temperature and pressure effect may contribute to the generation of high-NiO olivines observed in Hawaiian and other ocean-island basalts.

## TABLE OF CONTENTS

|   |       |
|---|-------|
| Acknowledgements .....  | iii   |
| Abstract .....  | iv    |
| Table of Contents .....   | vi    |
| List of Tables and Figures .....  | ix    |
| <b>Chapter I</b>  |       |
| Introduction.....   | I-1   |
| References.....   | I-6   |
| <b>Chapter II</b>   |       |
| Fe-Mg Partitioning Between Olivine and High-Magnesian Melts<br>and the Nature of Hawaiian Parental Liquids .....      | II-1  |
| Abstract.....   | II-2  |
| Introduction.....   | II-3  |
| Experimental and Analytical Techniques .....  | II-6  |
| <i>Starting Composition</i> .....   | II-6  |
| <i>Experimental Techniques</i> .....  | II-8  |
| <i>Analytical Techniques</i> .....  | II-10 |
| Experimental Results.....   | II-12 |
| <i>Phase Compositions</i> .....   | II-12 |
| <i>Phase Proportions</i> .....  | II-16 |
| <i>Olivine-Liquid Fe<sup>2+</sup>-Mg Exchange Coefficients</i> .....  | II-19 |
| Discussion.....   | II-21 |
| <i>Comparison of Our Data with Exchange Coefficients from<br/>        Literature-Based Olivine-Liquid Pairs</i> ..... | II-22 |
| <i>Hawaiian Parental Liquids</i> .....  | II-31 |
| Conclusions.....  | II-36 |
| Acknowledgements .....  | II-38 |
| References.....   | II-38 |
| Supplementary Material .....  | II-66 |
| 1. An Assessment of the Experimental Data of Roeder and<br>Emslie (1970).....   | II-66 |
| 1.1 <i>Introduction</i> .....   | II-66 |
| 1.2 <i>K<sub>D,Fe<sup>2+</sup>-Mg</sub></i> as Determined by Roeder and Emslie (1970).....                            | II-68 |
| 1.3 <i>Some Basic Acceptance Criteria for Roeder and Emslie's<br/>            Experiments</i> .....                   | II-71 |
| 1.4 <i>Mass Balance Calculations on Roeder and Emslie's<br/>            (1970) Data</i> .....                         | II-72 |
| 1.5 <i>Discussion</i> .....   | II-83 |
| 1.6 <i>Concluding Thoughts</i> .....  | II-85 |
| 2. Projection of Olivine-Liquid Exchange Coefficients .....   | II-86 |

|   |        |
|---|--------|
| 3. Comparison of Our Data with Predictions of the Models of Ford et al. (1983) and Toplis (2005) .....  | II-89  |
| 4. References for Sections 1-3 .....  | II-92  |
| 5. Experimental Database References .....   | II-98  |
| <b>Chapter III</b>  |        |
| Fe-Mg Partitioning Between Olivine and Basaltic Martian Melts .....   | III-1  |
| Abstract .....  | III-2  |
| Introduction.....   | III-3  |
| Experiments on Martian Compositions .....   | III-4  |
| <i>One-Atmosphere Martian Experiments</i> .....   | III-4  |
| <i>High-Pressure Martian Experiments</i> .....  | III-5  |
| <i>Compositional Dependence of <math>K_{D, Fe^{2+}-Mg}</math></i> .....   | III-8  |
| Comparison with Other One-Atmosphere Experiments .....  | III-9  |
| Olivine-Phyric Shergottites .....   | III-10 |
| Using $K_{D, Fe^{2+}-Mg}$ to Estimate Oxygen Fugacity .....   | III-11 |
| Conclusions.....  | III-12 |
| References.....   | III-14 |
| <b>Chapter IV</b>   |        |
| The Temperature and Pressure Dependence of Nickel Partitioning between Olivine and Silicate Melt .....  | IV-1   |
| Abstract .....  | IV-2   |
| Introduction.....   | IV-2   |
| Experimental Methods .....  | IV-6   |
| Experimental Results.....   | IV-10  |
| <i>Phase Compositions</i> .....   | IV-10  |
| <i>Mass Balance</i> .....   | IV-13  |
| <i>Attainment of Equilibrium</i> .....  | IV-15  |
| Discussion.....   | IV-17  |
| <i>Possible Contributions of Melt Compositional Variations in our Experiments to the Observed Temperature and Pressure Dependence of <math>D_{Ni}^{ol/liq}</math></i> ..... | IV-17  |
| <i>Fitting <math>D_{Ni}^{ol/liq}</math> : Previous Partitioning Expressions</i> .....   | IV-19  |
| <i>Fitting <math>D_{Ni}^{ol/liq}</math> : Ideal Exchange Reaction</i> .....   | IV-20  |
| <i>Fitting <math>D_{Ni}^{ol/liq}</math> : Ideal Formation Reaction</i> .....  | IV-27  |
| <i>Fitting <math>D_{Ni}^{ol/liq}</math> : Regular Solution Model</i> .....  | IV-29  |
| <i>Comparison of Ni with Other Divalent Cations</i> .....   | IV-34  |
| Modeling High NiO Olivines.....   | IV-35  |
| <i>Ocean Island Magmas</i> .....  | IV-35  |
| <i>Komatiites</i> .....   | IV-39  |
| Conclusions.....  | IV-42  |
| Acknowledgements .....  | IV-43  |
| References.....   | IV-43  |

|   |       |
|---|-------|
| Supplementary Material .....  | IV-71 |
| 1. Example Calculation Using our Preferred Partitioning<br>Expression (Equation 5) from the Main Text ..... | IV-71 |
| 1.1 <i>Initial Information</i> .....  | IV-71 |
| 1.2 <i>Transforming to Molar Components</i> .....   | IV-72 |
| 1.3 <i>Predicting a Partition Coefficient</i> .....   | IV-75 |
| 1.4 <i>Converting <math>D_{Ni}^{molar}</math> to <math>D_{Ni}^{ol/liq}</math></i> .....                     | IV-76 |
| 2. Comparing Fitted and Tabulated Standard-State Enthalpies<br>and Entropies.....                           | IV-77 |
| 3. Mass-Balance Calculations.....   | IV-78 |
| 4. Constructing the Filter-B Dataset.....   | IV-82 |
| References for Sections 1-4 .....   | IV-85 |
| 5. Experimental Database References .....   | IV-87 |

## LIST OF TABLES AND FIGURES

| <b>Chapter II</b>  | <i>Page</i> |
|--|-------------|
| Table 1: Starting Composition .....  | II-50       |
| Table 2: Run Conditions and Experimental Results .....   | II-51       |
| Table 3: Phase Compositions .....  | II-53       |
| Figure Captions.....   | II-55       |
| Figure 1: Concentrations of Oxides in Experimental Glasses .....   | II-59       |
| Figure 2: Mass Balance Results .....   | II-60       |
| Figure 3: $K_{D,Fe^{+2}-Mg}$ vs. MgO Content of the Liquid and<br>Temperature .....                                | II-61       |
| Figure 4: Histograms of Projected $K_{D,Fe^{+2}-Mg}$ S .....   | II-62       |
| Figure 5: Median and Projected $K_{D,Fe^{+2}-Mg}$ S .....  | II-63       |
| Figure 6: $K_{D,Fe^{+2}-Mg}$ vs. $Na_2O+K_2O$ .....  | II-64       |
| Figure 7: Parental Liquids .....   | II-65       |
| Supplementary Material .....   | II-106      |
| Table A1: Results of the Mass Balance Calculations Using the<br>Experimental Data of Roeder and Emslie (1970)..... | II-106      |
| Table A2: Compositions Used for Olivine-Addition Calculations.....   | II-110      |
| Table A3: Compositions of Calculated Parental Hawaiian Magmas ..   | II-111      |
| Supplementary Material Figure Captions .....   | II-113      |
| Figure A1: Reproducing the Roeder and Emslie $K_{D,Fe^{2+}-Mg}$ .....  | II-122      |
| Figure A2: Histogram of Roeder and Emslie $K_{D,Fe^{2+}-Mg}$ .....   | II-123      |
| Figure A3: $SiO_2$ and MgO of Roeder and Emslie's Liquids.....   | II-124      |
| Figure A4: CaO and MgO of Roeder and Emslie's Liquids.....   | II-125      |
| Figure A5: Roeder and Emslie Mass Balance .....  | II-126      |
| Figure A6: $K_{D,Fe^{2+}-Mg}$ as a Function of Mass Balance and Iron<br>Loss .....                                 | II-127      |
| Figure A7: $K_{D,Fe^{2+}-Mg}$ as a Function of Iron Loss .....   | II-128      |
| Figure A8: Ferric-Ferrous Ratios at Constant Temperature .....   | II-129      |
| Figure A9: Roeder and Emslie's Ferric-Ferrous Ratios at Constant<br>Temperature.....                               | II-130      |
| Figure A10: Ferric-Ferrous Ratios for Composition 654.....   | II-131      |
| Figure A11: Sensitivity of Ferric-Ferrous Ratio to Temperature .....   | II-132      |

|   |             |
|---|-------------|
| Figure A12: Roeder and Emslie Ferric-Ferrous Ratio vs. Temperature.....           | II-133      |
| Figure A13: $K_{D, Fe^{2+}-Mg}$ as a Function of Iron Loss.....                   | II-134      |
| Figure A14: The Sensitivity of $K_{D, Fe^{2+}-Mg}$ .....                          | II-135      |
| Figure A15: Projecting $K_{D, Fe^{2+}-Mg}$ .....                                  | II-136      |
| Figure A16: Histograms of Projected and Unprojected $K_{D, Fe^{2+}-Mg}$ .....     | II-137      |
| Figure A17: Comparing the Predicted and measured $K_{D, Fe^{2+}-Mg}$ S.....       | II-138      |
| Figure A18: Predicted Ferric-Ferrous Ratios.....                                  | II-139      |
| Figure A19: Temperature Distribution of High-Pressure and 1-atm Experiments.....  | II-140      |
| <b>Chapter III</b>  | <i>Page</i> |
| Figure Captions.....  | III-23      |
| Figure 1: $D_{Fe^{2+}}$ vs. $D_{Mg}$ : One-Atm Experiments.....                   | III-26      |
| Figure 2: $D_{Fe^{2+}}$ vs. $D_{Mg}$ : One-Atm and High-P Experiments.....        | III-27      |
| Figure 3: Compositional Dependence of $K_{D, Fe^{2+}-Mg}$ .....                   | III-28      |
| Figure 4: Comparison with Other One-Atm Experiments.....                          | III-29      |
| Figure 5: Olivine-Phyric Shergottites.....  | III-30      |
| Figure 6: Estimating $fO_2$ .....   | III-31      |
| <b>Chapter IV</b>   | <i>Page</i> |
| Table 1: Starting Composition.....  | IV-55       |
| Table 2: Run Conditions and Phase Information.....                                | IV-56       |
| Table 3: Phase Compositions.....  | IV-57       |
| Table 4: Fit Parameters.....  | IV-59       |
| Figure Captions.....  | IV-60       |
| Figure 1: $D_{Ni}^{ol/liq}$ for This Study and Predicting $D_{Ni}^{ol/liq}$ ..... | IV-64       |
| Figure 2: Fitting Equation (5).....   | IV-65       |
| Figure 3: Fitting Equation (9).....   | IV-66       |
| Figure 4: $D_{Ni}^{ol/liq}$ for a Constant Composition.....                       | IV-67       |
| Figure 5: Comparison with Other Divalent Cations.....                             | IV-68       |
| Figure 6a: Generating High-NiO Olivines: Mauna Kea.....                           | IV-69       |
| Figure 6b: Generating High-NiO Olivines: Komatiites.....                          | IV-70       |
| Supplementary Material.....   | IV-71       |
| Supplementary Material Figure Caption.....  | IV-91       |
| Figure S1: Fitting Fractional Errors.....   | IV-92       |

I-1  
*Chapter 1*

INTRODUCTION

Andrew K. Matzen

The Hawaiian-Emperor seamount chain is a striking feature on the surface of the Earth: the islands record more than 60 million years of volcanic activity (e.g., Garcia et al., 1987) and contain the Earth's largest volcano. As a result, the Hawaiian Islands have been at the center of many geochemical and geophysical inquiries aimed at gaining insights into the mantle source, or sources, of such abundant volcanism (e.g., Dapeng, 2001; Ji et al., 1998; Putirka et al., 2007; Sobolev et al., 2005; Weis et al., 2011). Inferring the composition of the deep mantle sources by examining the eruptive products is not a simple task: like many mafic lavas from around the solar system, olivine is often the primary crystalline phase of Hawaiian liquids and the chemical composition of lavas that are erupted on the surface are often influenced by the removal of olivine as they cool in shallow level magma chambers (e.g., Clague et al., 1991; Macdonald et al., 1964; Powers, 1955; Roedder, 1983). We can reverse this low-pressure olivine removal by numerically adding olivine back to the erupted liquid composition that we measure at the surface, but the accuracy of such a calculation depends critically on our knowledge of the solid-liquid partition coefficients. We performed experiments examining the partitioning of  $\text{Fe}^{2+}$  and Mg between olivine and a synthetic Hawaiian picrite. By focusing on  $\text{Fe}^{2+}$  and Mg, the dominant exchangeable cations in olivine, we should be able to better reconstruct the major element compositions of the unfractionated—or, more commonly, parental—liquids. Armed with a better understanding of parental liquids, we may then be able to place tighter constraints on the composition of the mantle source(s) beneath Hawaii. Although  $\text{Fe}^{2+}$  and Mg partition coefficients (i.e.,  $D_{\text{Mg}} = \text{MgO}^{\text{olivine}}/\text{MgO}^{\text{liquid}}$ , by wt.) are functions of temperature (and liquid composition) individually, Roeder and Emslie (1970) were the first

to show that a ratio of partition coefficients (or exchange coefficient,  $K_{D, Fe^{2+}-Mg} = (FeO/MgO)^{olivine}/(FeO/MgO)^{liquid}$ ) is constant, independent of temperature and/or liquid composition. Our experiments, along with additional data from the literature, show that a  $K_{D, Fe^{2+}-Mg}$  of approximately 0.34 is appropriate for Hawaiian lavas, and although this value is significantly higher than the value of 0.30 first proposed by Roeder and Emslie (1970) [see the Chapter II Supplement for a discussion of the Roeder and Emslie (1970) data], it is also independent of temperature and liquid composition. When we use the results of our study to numerically add olivine back to erupted glass compositions, we come to the conclusion that the parental liquids were highly magnesian, having approximately 19-21 wt. % MgO.

Olivine is present in a broad range of mafic and ultramafic magmas throughout the solar system (BVSP, 1981). Roeder and Emslie (1970) showed that  $K_{D, Fe^{2+}-Mg}$  was independent of liquid composition, however later work (e.g., Sack et al., 1987) has shown that liquid composition does, in fact, play a significant role. Given the well-known fact that Martian basalts tend to have higher FeO and lower  $Al_2O_3$  than most terrestrial basalts, what is the appropriate  $K_{D, Fe^{2+}-Mg}$  (s) to use when studying Martian volcanics? Using data from the literature, we found that a  $K_{D, Fe^{2+}-Mg}$  of  $\sim 0.36$  is more appropriate for Martian basalts than the canonical value of 0.30. We can then use this value to test if any of the olivine-bearing meteorite compositions represent liquids. We conclude that, based on olivine-liquid equilibria, Yamato 980459, Northwest Africa 5789, 2990, and Elephant Moraine A79001 are possible liquid compositions, similar to the recent results of Filiberto et al. (2011).

Another way we can investigate the mantle beneath Hawaii is by examining the partitioning of Ni between olivine and melt. The behavior of Ni is nearly unique among minor and trace elements in that it is compatible in olivine (i.e.,  $D_{\text{Ni}} = \text{NiO}^{\text{olivine}}/\text{NiO}^{\text{liquid}}$ , by wt., is greater than one). Additionally, the NiO contents of olivine phenocrysts from Hawaii are high when compared to other ocean-island basalts, and to olivines from peridotites. This observation led Sobolev et al. (2005) to develop the hypothesis that the mantle source beneath Hawaii is, at least partially, olivine-free. To quantitatively test this hypothesis we need to know how the olivine-liquid partition coefficient varies as a function of temperature, pressure, and composition. Due to the long-recognized importance of Ni partitioning (e.g., Hart et al., 1978), there are many experiments, spanning a large pressure, temperature, and compositional range to help us test the hypotheses introduced above. In the current experimental database, however, temperature and liquid composition are correlated, making it difficult to separate out the compositional and temperature dependencies of the Ni partition coefficient. We performed a series of experiments examining the partitioning between an olivine and liquid of constant composition while simultaneously changing the temperature and pressure, effectively separating the effects of composition from that of temperature and pressure. Our experiments show that temperature and pressure have a significant effect: the partition coefficient decreases from ~ 5.0 to 3.8 as temperature and pressure increase from 1400 to 1550°C and 1-atm to 3.0 GPa, respectively. We then used a simple thermodynamic treatment to fit our data, in conjunction with data from the literature. Our predictive equation shows that partial melting of an olivine-bearing source at elevated pressure and temperature in the mantle

followed by melt segregation, transport to the Earth's surface and crystallization of olivine at lower temperature will generate phenocrysts with higher NiO contents than those of the olivines in the mantle source of the magmas. This suggests that the high-NiO olivines seen in Hawaii are not necessarily indicative of a distinctive mineralogy of the mantle source.

In the above example we highlighted the fact that the temperature difference between the partial melting and subsequent crystallization (i.e.,  $\Delta T = T_{\text{melting}} - T_{\text{crystallization}}$ ) was the driving force behind the generation of high-NiO olivines. However, the absolute temperature also plays an important role. We show that as the absolute temperature increases, for the same temperature difference, the NiO contents of the low-temperature olivine phenocrysts will decrease. This is an important observation that may help explain why olivines from komattites (which are generally thought to be rapidly erupting, high-temperature liquids) tend to show only moderate Ni enrichment when compared to those of Hawaii.

## REFERENCES

- BVSP 1981. *Basaltic Volcanism on the Terrestrial Planets* New York: Pergamon Press. 1286 p.
- Clague D. A., Weber W. S., and Dixon J. E. 1991. Picritic Glasses from Hawaii. *Nature* 353(6344):553-556.
- Dapeng Z. 2001. Seismic structure and origin of hotspots and mantle plumes. *Earth and Planetary Science Letters* 192(3):251-265.
- Filiberto J. and Dasgupta R. 2011. Fe<sup>2+</sup>-Mg partitioning between olivine and basaltic melts: Applications to genesis of olivine-phyric shergottites and conditions of melting in the Martian interior. *Earth and Planetary Science Letters* 304(3-4):527-537.
- Garcia M. O., Grooms D. G., and Naughton J. J. 1987. Petrology and geochronology of volcanic rocks from seamounts along and near the Hawaiian Ridge: Implications for propagation rate of the ridge. *Lithos* 20(4):323-336.
- Hart S. R. and Davis K. E. 1978. Nickel Partitioning between Olivine and Silicate Melt. *Earth and Planetary Science Letters* 40(2):203-219.
- Ji Y. and Nataf H.-C. 1998. Detection of mantle plumes in the lower mantle by diffraction tomography: Hawaii. *Earth and Planetary Science Letters* 159(3-4):99-115.
- Macdonald G. A. and Katsura T. 1964. Chemical composition of Hawaiian lavas. *Journal of Petrology* 5(1):82-133.
- Powers H. A. 1955. Composition and origin of basaltic magma of the Hawaiian Islands. *Geochimica et Cosmochimica Acta* 7(1-2):77-107.
- Putirka K. D., Perfit M., Ryerson F. J., and Jackson M. G. 2007. Ambient and excess mantle temperatures, olivine thermometry, and active vs. passive upwelling. *Chemical Geology* 241(3-4):177-206.
- Roedder E. 1983. Geobarometry of ultramafic xenoliths from Loihi Seamount, Hawaii, on the basis of CO<sub>2</sub> inclusions in olivine. *Earth and Planetary Science Letters* 66(1-3):369-379.
- Roeder P. L. and Emslie R. F. 1970. Olivine-liquid equilibrium. *Contributions to Mineralogy and Petrology* 29(4):275-289.
- Sobolev A. V., Hofmann A. W., Sobolev S. V., and Nikogosian I. K. 2005. An olivine-free mantle source of Hawaiian shield basalts. *Nature* 434:590-597.
- Weis D., Garcia M. O., Rhodes J. M., Jellinek M., and Scoates J. S. 2011. Role of the deep mantle in generating the compositional asymmetry of the Hawaiian mantle plume. *Nature Geosci* 4(12):831-838.

II-1

*Chapter 2*

Fe-Mg PARTITIONING BETWEEN OLIVINE AND HIGH-MAGNESIAN MELTS  
AND THE NATURE OF HAWAIIAN PARENTAL LIQUIDS

Andrew K. Matzen

Michael B. Baker

John R. Beckett

Edward M. Stolper

Accepted to

*Journal of Petrology*

November 30, 2010

**ABSTRACT**

We conducted 1-atm experiments on a synthetic Hawaiian picrite at  $fO_2$ s ranging from the quartz-fayalite-magnetite (QFM) buffer to air and temperatures ranging from 1302–1600°C. Along the QFM buffer, olivine is the liquidus phase at ~1540°C and small amounts of spinel (< 0.2 wt %) are present in experiments conducted at and below 1350°C. The olivine becomes progressively more ferrous with decreasing temperature (Fo<sub>92.3</sub> to Fo<sub>87.3</sub>, where Fo = 100×Mg/[Mg + Fe], atomic); compositions of coexisting liquids reflect the mode and composition of the olivine with concentrations of SiO<sub>2</sub>, TiO<sub>2</sub>, Al<sub>2</sub>O<sub>3</sub>, and CaO increasing monotonically with decreasing temperature, those of NiO and MgO decreasing, and FeO\* (all Fe as FeO) remaining roughly constant. An empirical relationship based on our data,  $T(^{\circ}\text{C}) = 19.2 \times (\text{MgO in liquid, wt \%}) + 1048$ , provides a semi-quantitative geothermometer applicable to a range of Hawaiian magma compositions.

The olivine-liquid exchange coefficient,  $K_{\text{D,Fe}^{+2}\text{-Mg}} = (\text{FeO/MgO})^{\text{ol}}/(\text{FeO/MgO})^{\text{liq}}$ , is  $0.345 \pm 0.009$  (1 $\sigma$ ) for our 11 experiments. A literature database of 446 1-atm experiments conducted within 0.25 *log* units of the QFM buffer (QFM $\pm$ 0.25) yields a median  $K_{\text{D,Fe}^{+2}\text{-Mg}}$  of 0.34;  $K_{\text{D,Fe}^{+2}\text{-Mg}}$ s from individual experiments range from 0.41 to 0.13 and are correlated with SiO<sub>2</sub> and alkalis in the liquid as well as the forsterite (Fo) content of the olivine. For 78 experiments with broadly tholeiitic liquid compositions (46–52 wt % SiO<sub>2</sub>,  $\leq 3$  wt % Na<sub>2</sub>O + K<sub>2</sub>O) coexisting with Fo<sub>92–80</sub> olivines, and run near QFM (QFM $\pm$ 0.25),  $K_{\text{D,Fe}^{+2}\text{-Mg}}$  is approximately independent of composition with a median value of  $0.340 \pm 0.012$  (error is the mean absolute deviation of the 78 olivine-glass pairs from the

database that meet these compositional criteria), a value close to the mean value of  $0.343 \pm 0.008$  from our QFM experiments. Thus, over the composition range encompassed by Hawaiian tholeiitic lavas and their parental melts,  $K_{D,Fe^{+2}-Mg} \sim 0.34$  and, given the redox conditions and a Fo content for the most magnesian olivine phenocrysts, a parental melt composition can be reconstructed. The calculated compositions of the parental melts are sensitive to these input parameters, decreasing by  $\sim 1$  wt % MgO for every *log* unit increase in the selected  $fO_2$ , every 0.5 decrease in the Fo# of the target olivine, and every 0.015 decrease in  $K_{D,Fe^{+2}-Mg}$ . For plausible ranges in redox conditions and Fo# of the most MgO-rich olivine phenocrysts, the parental liquids for Hawaiian tholeiites are highly magnesian, in the range of 19–21 wt % MgO for Kilauea, Mauna Loa and Mauna Kea.

## INTRODUCTION

Knowledge of the partitioning of elements between coexisting solid and liquid phases is critical for deciphering and modeling igneous processes. Hardly a paper is written on igneous petrogenesis today without referring to solid-liquid partition coefficients: Examples include the modeling of evolving liquid compositions generated during partial melting and the liquid lines of descent of cooling magmas (e.g., Grove *et al.*, 1992; Nielsen & DeLong, 1992; Herzberg & O'Hara, 2002), reconstruction of the compositions of parental or primary liquids from the compositions of fractionated magmas (e.g., Baker *et al.*, 1996; Putirka *et al.*, 2007), and modeling the evolution of liquid compositions on the basis of cumulus phases (e.g., Longhi, 1982; Bédard, 1994; Thy *et al.*, 2006). The partitioning of major and minor elements between olivine and liquid is of particular

importance because olivine is a ubiquitous phase in a broad range of mafic and ultramafic igneous rocks in the upper mantle, and the fractionation or accumulation of this phase exerts a major control on observed variations in magma composition (e.g., for Hawaii: Powers, 1955; Macdonald & Katsura, 1964; Clague *et al.*, 1991). It is therefore not surprising that there has been considerable experimental work over several decades aimed at quantifying the partitioning of major and minor elements between olivine and liquid in relevant igneous systems (e.g., Roeder & Emslie, 1970; Hart & Davis, 1978; Beattie *et al.*, 1991; Mallmann & O'Neill, 2009) and complementary development of empirical and thermodynamic models of the experimental data (e.g., Longhi *et al.*, 1978; Ford *et al.*, 1983; Hirschmann & Ghiorso, 1994; Toplis, 2005). Partitioning of Fe<sup>+2</sup> and Mg between olivine and liquid is a natural starting point for such studies given that these are the dominant exchangeable cations in olivine from the earth and other planets. Roeder & Emslie (1970) were the first to pair these elements in an exchange reaction between olivine and melt for use in correlating data in both experimental and natural systems. Based on 1-atm experiments on three Hawaiian basalts, they showed that the olivine (ol)-liquid (liq) exchange coefficient,  $K_{D,Fe^{+2}-Mg} = (FeO/MgO)^{ol}/(FeO/MgO)^{liq}$ , where FeO and MgO refer to concentrations (by weight), is  $0.30 \pm 0.03$  and, within the resolution of their data, is independent of temperature and liquid composition. Later work considerably expanded the range of pressure, temperature, and liquid composition and showed that liquid composition does in fact exert a significant effect on  $K_{D,Fe^{+2}-Mg}$  (e.g., Sack *et al.*, 1987; Gee & Sack, 1988). There have been numerous attempts to formulate expressions for  $K_{D,Fe^{+2}-Mg}$  as a function of these variables (e.g., Longhi *et al.*, 1978; Ford *et al.*, 1983; Gee & Sack, 1988;

Snyder & Carmichael, 1992; Sobolev & Nikogosian, 1994; Herzberg & O'Hara, 2002; Toplis, 2005) and various constant values of  $K_{D,Fe^{+2}-Mg}$  have been proposed for specific applications (e.g., Nisbet *et al.*, 1987; Putirka *et al.*, 2007). Nevertheless, the Roeder and Emslie value of 0.30 is still a convenient reference point commonly used in petrologic modeling (e.g., Garcia, 1996; Rhodes & Vollinger, 2004).

The paucity of experiments on high-magnesian liquids with compositions similar to naturally occurring magmas is problematic because estimates of parental/primary liquid compositions for Hawaii and other localities (e.g., Gorgona komatiites and picrites from Baffin Island, western Greenland, and Ontong Java Plateau: Clague *et al.*, 1991; Baker *et al.*, 1996; Herzberg & O'Hara, 2002; Stolper *et al.*, 2004; Herzberg *et al.*, 2007) and liquids produced in high-pressure melting experiments on ultramafic compositions (e.g., Kushiro & Walter, 1998; Walter, 1998) often have more than 16 wt % MgO. Although a large number of olivine-liquid pairs are available in the literature (we have a compilation containing 1179 pairs), we are aware of only 24 with glass compositions similar to naturally occurring liquids (nonzero concentrations of TiO<sub>2</sub>, Al<sub>2</sub>O<sub>3</sub>, FeO, MgO, CaO, and Na<sub>2</sub>O) with  $\geq 16$  wt % MgO and for none of these high MgO liquids was Fe<sup>+3</sup>/Fe<sup>+2</sup> actually measured. Thus, the effects of high MgO and the Fe<sup>+3</sup>/Fe<sup>+2</sup> ratio on Fe-Mg partitioning between olivine and liquid are poorly known, yet they are important for petrologic modeling. A major motivation for the study reported here is to extend the data set on  $K_{D,Fe^{+2}-Mg}$  to include experiments on magmatic liquids with high MgO conducted under well characterized and controlled redox conditions.

In this study, we present the results of 1-atm experiments on a synthetic analog to a Hawaiian picrite (25.7 wt % MgO, 45.7 wt % SiO<sub>2</sub>). Most of the experiments were done near the quartz-fayalite-magnetite buffer (QFM), but two experiments were conducted under more oxidizing conditions (nickel-nickel oxide buffer (NNO) and air) to explore the effect of varying Fe<sup>+3</sup>/Fe<sup>+2</sup> in the liquid on  $K_{D,Fe^{+2}-Mg}$ . Glasses from two of the experiments (air and QFM) were also analyzed for FeO by wet chemistry, thereby allowing the determination of  $K_{D,Fe^{+2}-Mg}$  independent of any Fe<sup>+3</sup>/Fe<sup>+2</sup> algorithm. In addition, we compiled a set of 1-atm olivine-liquid pairs from the literature encompassing  $fO_2$ s ranging from slightly below the iron-wüstite (IW) buffer to air and MgO concentrations in the liquid from 1.3 to 28.6 wt %. Finally, we used this database together with the results of our experiments to constrain  $K_{D,Fe^{+2}-Mg}$  for highly magnesian liquids and to reconstruct parental Hawaiian magma compositions.

## EXPERIMENTAL AND ANALYTICAL TECHNIQUES

### Starting composition

The starting composition for this study, Syn-HP1 (Table 1), is based on whole-rock analyses of “low-SiO<sub>2</sub>” Mauna Kea basalts from the Hawaii Scientific Drilling Project (HSDP) (Rhodes & Vollinger, 2004). We chose the “low-SiO<sub>2</sub>” array (Stolper *et al.*, 2004) because these rocks lie on an olivine control line along which liquids of roughly constant composition (with ~6–7 wt % MgO) are variably affected by olivine accumulation (Rhodes & Vollinger, 2004) and because they are compositionally distinct from higher SiO<sub>2</sub> bulk compositions used in previous experiments on Hawaiian lavas (e.g., Eggins, 1992; Wagner

& Grove, 1998). We selected 25 wt % MgO for the bulk composition to ensure a large olivine primary phase volume with magnesian liquids and then computed corresponding values for eleven additional major and minor oxides from linear least-squares fits of oxide-MgO variations along the array of “low-SiO<sub>2</sub>” basalts. The resulting target composition, HP-25, is listed in Table 1. Numerous 1-atm experimental studies have shown that Na<sub>2</sub>O, K<sub>2</sub>O, and P<sub>2</sub>O<sub>5</sub> display varying degrees of volatility at high temperatures (Corrigan & Gibb, 1979; Tsuchiyama *et al.*, 1981; Kilinc *et al.*, 1983; Yu *et al.*, 2003), so we left these three oxides out of the Syn-HP1 composition. In addition, we increased the NiO content in the synthetic composition relative to the HP-25 target composition by a small amount to facilitate measurement of NiO in the experimental glasses. Note that all experiments reported in this paper were done on the alkali- and P-free syn-HP1 composition (in the Discussion section, we address the issue of applying our results to alkali-bearing tholeiitic magmas). The MgO content on the array of “low SiO<sub>2</sub>” Mauna Kea basalts chosen for this study was a compromise between the desire for an MgO-rich starting composition with a broad range of olivine stability and the more practical goal of keeping the liquidus within the normal operational limits of our gas-mixing furnaces. Based on MELTS (Ghiorso & Sack, 1995) calculations, the selected alkali- and phosphorus-free nominal composition Syn-HP1 (Table 1) has a 1-atm liquidus at QFM of 1535°C.

A starting mix was prepared from high-purity oxides and carbonates ground for ~5 h under ethanol in an automated alumina mortar. After decarbonation, splits of the resulting powder were reduced for ~1 h at ~900°C at QFM using flowing H<sub>2</sub>-CO<sub>2</sub> gas mixtures and a Pt catalyst to facilitate equilibrium within the gas (Beckett & Mendybaev, 1997). The reduced powder, as well as an unreduced split, were pressed into ~0.4 cm thick, 1.27 cm

diameter pellets using ethanol as a binder. Chips weighing 60–100 mg were broken from these pellets and used in the experiments. Analyses of glass from a superliquidus experiment (run 43 in Table 3; see Table 2 for run conditions) show that the oxide mix gained ~0.7 wt % alumina through the grinding process. Minor Na<sub>2</sub>O (0.05 wt %) was also present in this glass and low levels of Na<sub>2</sub>O were detected in nearly all our experimental glasses. The presence and amounts of Na in the glasses observed in this nominally Na-free bulk composition are discussed below. Weight percents of the other oxides overlap those of the target composition at the 1 $\sigma$  level.

### **Experimental techniques**

One-atmosphere experiments were conducted in a vertical Deltech furnace at roughly 50°C intervals between 1300 and 1600°C using H<sub>2</sub>-CO<sub>2</sub> gas mixtures to control  $f_{\text{O}_2}$ .

Temperature was monitored using a type-S thermocouple placed in the hot-spot of the furnace and calibrated at the boiling point of water and the melting point of gold referenced to ITS<sub>90</sub> (Goldberg & Weir, 1992). Most of the experiments were conducted at QFM since  $f_{\text{O}_2}$  estimates for Hawaiian magmas generally lie at or somewhat more reducing than this buffer (e.g., Rhodes & Vollinger, 2005). However, experiments were also run at the nickel-nickel oxide (NNO) buffer and under a continuous flow of air to examine the effect of  $f_{\text{O}_2}$  on the olivine-liquid Fe<sup>+2</sup>-Mg exchange coefficient. For the purpose of guiding our choice of particular experimental  $f_{\text{O}_2}$ s, we used expressions for the QFM and NNO buffers from the compilation of Huebner (1971). Except for the superliquidus runs, the  $f_{\text{O}_2}$  was monitored using a yttria-stabilized zirconia oxygen sensor (SIRO2; Ceramic Oxide Fabricators, Eaglehawk, Australia) calibrated at the IW buffer (Huebner, 1971). For the

two superliquidus runs, the gas mixture was adjusted with the aid of an oxygen sensor to yield the appropriate  $fO_2$  at each run temperature, but the oxygen sensor was not present in the furnace during the run. Samples were suspended on 0.2 mm diameter FePt alloy loops using polyvinyl alcohol as a binding agent. Experiments were initiated by introducing the sample into the hot spot of the furnace at  $\sim 1100^\circ\text{C}$  under a mixture of  $\text{H}_2\text{-CO}_2$  set to provide the  $fO_2$  of interest at the final run temperature. The furnace was then ramped to the desired temperature at  $400\text{--}500^\circ\text{C/hr}$  (this initial ramp up is not included in the reported run-times). Experiments were terminated by drop quenching the wire loop and attached sample into de-ionized water. Although no quench crystals were observed in our experimental glasses, thin ( $< 1\ \mu\text{m}$ ) overgrowths were present on the olivines.

Even under the relatively oxidizing conditions of QFM, considerable Fe and Ni can be lost from a sample to a Pt loop (e.g., Hart & Davis, 1978; Grove, 1981). We therefore pre-conditioned loops by first conducting three to four 24 h doping runs using syn-HP1 at the same temperature and  $fO_2$  as desired for the first experiment that the loop was to be used for. At the end of each pre- saturation run, the sample was dissolved off of the loop using an  $\sim 1:1$  mixture (by volume) of HF and  $\text{HNO}_3$ . Once preconditioned, a loop was then used for one or more experiments conducted at the same conditions, except for loop 8, which was used at both  $1551$  and  $1600^\circ\text{C}$ . Table 2 lists the loop used for each experiment and the combined number of doping runs and experiments that had previously been run on it. Run times for experiments at a given temperature and  $fO_2$  ranged from 72 h at  $1300^\circ\text{C}$  to 0.5 h at  $1600^\circ\text{C}$ . Chips from each experiment were broken off the loop, mounted in epoxy, and polished for electron microprobe analysis. Temperatures,  $fO_2$ s, run times,

observed phases, and their proportions calculated by mass balance (see below and footnote to Table 2) are also reported in Table 2.

### **Analytical techniques**

Glass and crystalline phases produced in the experiments were analyzed with a five-spectrometer JEOL JXA-8200 electron microprobe at Caltech and all data were reduced using a modified ZAF procedure (CITZAF; Armstrong, 1988).

Quenched glasses were analyzed using a 15 keV accelerating voltage, 10 nA beam current, 10  $\mu\text{m}$  spot, and glass, mineral, and oxide standards. Approximately ten glass analyses were collected for each experiment. Counting times typically ranged from 20–40 s on peak and half that at high and low backgrounds. On-peak counting times on glasses from runs 43 and 46 were slightly longer for most elements and 100 s for Ni. Secondary glass standards (BHVO-2g, BIR-1g, and BCR-2g) were all analyzed during three separate periods during each microprobe session for a total of 9–12 points each. The mean BHVO-2g composition from each session coupled with the accepted composition of BHVO-2; ([http://minerals.cr.usgs.gov/geo\\_chem\\_stand/](http://minerals.cr.usgs.gov/geo_chem_stand/)) was used to reprocess the k-ratios for all glass analyses from a session; post-correction compositions of BIR-1g and BCR-2g overlap their accepted bulk rock compositions ([http://minerals.cr.usgs.gov/geo\\_chem\\_stand/](http://minerals.cr.usgs.gov/geo_chem_stand/)). Glass analyses reported in Table 3 were accepted if their post correction totals were between 98.5 and 101.5 wt %.

Experimentally produced olivines were analyzed using a 15 keV accelerating voltage, 40 nA beam current, 1  $\mu\text{m}$  diameter spot size, and mineral and oxide standards.

Counting times were 20–60 s on peak, and 10–30 s each on high and low backgrounds. In general, ten olivine grains were analyzed from each charge. Most olivines have cross-sections of 25–100  $\mu\text{m}$  in longest dimension and, for these, a single analysis was generally taken from the central portion of the grain. Run 39 produced large ( $\sim 250 \mu\text{m}$ ) olivines, and for this experiment both core and rim analyses were collected; these indicate that the olivine grains in this run product are homogeneous at the  $2\sigma$  level. To help remove inter-session variability, olivine analyses from a given probe session were referenced to the mean of the multiple (7–28) analyses of San Carlos olivine obtained during the session. The occasional olivine analysis showing obvious signs of contamination (e.g.,  $\text{Al}_2\text{O}_3 > 1 \text{ wt } \%$ ) was rejected. The remaining olivine analyses were accepted if they had (1) an oxide total of  $100 \pm 1.5 \text{ wt } \%$  and (2) a cation sum (on a four oxygen basis) of  $3.000 \pm 0.015$ . The analyses reported in Table 3 are averages of all olivine analyses from a given experiment that passed through this filter.

Spinel were analyzed using a 15 keV accelerating voltage, 25 nA beam current, a focused beam (nominal spot size of  $\sim 0.2 \mu\text{m}$ ), and mineral and synthetic oxide standards. Peak counting times were 30 s with 15 s on high and low backgrounds. We analyzed seven to 12 spinels in each run product containing this phase; most of these analyses were contaminated by adjacent phases due to their small sizes (e.g.,  $\sim 3 \mu\text{m}$  in diameter at  $1300^\circ\text{C}$  and  $\sim 9 \mu\text{m}$  at  $1350^\circ\text{C}$ ). We used  $\text{SiO}_2$  contents, which show a rough negative correlation with apparent grain size as a measure of “contamination”. After calculating  $\text{Fe}^{+2}$  and  $\text{Fe}^{+3}$  assuming ideal  $\text{R}_3\text{O}_4$  stoichiometry, we accepted spinel analyses from runs 28 and 46 with  $\leq 0.5 \text{ wt } \%$   $\text{SiO}_2$  and  $2.000 \pm 0.015$  cations in the octahedral site. In runs 6, 8, and 15, few spinel analyses contained  $\leq 0.5 \text{ wt } \%$   $\text{SiO}_2$  so for these we corrected the spinel analyses for

contamination from the coexisting glass and/or olivine (details are given in the notes to Table 3).

## **EXPERIMENTAL RESULTS**

The temperature, run duration,  $f_{O_2}$ , and phase assemblage of each experiment are reported in Table 2. Also listed are phase proportions and estimated changes in bulk Na and Fe (discussed below). Phase compositions are reported in Table 3.

### **Phase compositions**

#### *Olivine*

Olivine is observed in all subliquidus experiments. For experiments conducted along the QFM buffer, the Fo content of olivine ( $100 \times \text{Mg}/[\text{Mg} + \text{Fe}]$ , atomic) increases monotonically with increasing temperature from 87.3 at  $\sim 1300^\circ\text{C}$  to 92.3 at  $1500^\circ\text{C}$ .

Olivine from the air-equilibrated experiment, performed at  $1396^\circ\text{C}$ , is much more magnesian than comparable QFM experiments (Fo<sub>97.0</sub> vs. Fo<sub>90.0</sub>), whereas olivine from the NNO experiment, done at  $1350^\circ\text{C}$ , has a nearly identical Fo content to the comparable QFM experiment (Fo<sub>88.8</sub>). In the experiments conducted at QFM, concentrations of MnO (0.10–0.15 wt %) and CaO (0.21–0.28 wt %) in olivine decrease slightly with increasing temperature; concentrations of Al<sub>2</sub>O<sub>3</sub> and Cr<sub>2</sub>O<sub>3</sub> are constant within error (0.07–0.11 and 0.09–0.12 wt %); and NiO contents (0.53–0.65 wt %) increase with temperature. The Cr, Mn, and Al olivine-liquid partition coefficients obtained in our experiments agree well with other experimental studies (e.g., Mäkipää, 1980; Murck & Campbell, 1986; Agee & Walker, 1990; Parman *et al.*, 1997; Hanson & Jones, 1998; Bédard, 2005), and the Ca

olivine-liquid partition coefficients are similar to the results of previous studies and the predictions of Libourel (1999), keeping in mind that no effort was made in this study to correct olivine analyses for the fluorescence of Ca from adjacent glass.

### *Spinel*

The experiments at 1300–1350°C contain small amounts of Al-rich chromite (< 0.2 wt %; Table 2) in addition to glass and olivine. Despite their low abundance, the spinels account for as much as 36% of the Cr budget in these experiments ( $\text{Cr\#} = \text{Cr}/[\text{Cr} + \text{Al}]$ , atomic, ranges from 0.59–0.64 in the spinels).  $\text{Fe}^{+3}/\text{Fe}^*$  ( $\text{Fe}^*$  is all Fe as  $\text{Fe}^{+2}$ ) ratios calculated assuming an  $\text{R}_3\text{O}_4$  stoichiometry are between 0.24–0.26 for the QFM experiments, but they are distinctly higher, 0.37, in the NNO run (28).  $\text{TiO}_2$  contents (1.1–1.2 wt %), Cr#s, and Mg#s (0.65–0.68) of the experimental spinels are comparable to those observed in spinels from Hawaiian lavas (e.g., Clague *et al.*, 1995; Baker *et al.*, 1996; Kamenetsky *et al.*, 2001; Roeder *et al.*, 2003).

### *Glass*

Figure 1 shows concentrations of selected oxides from the experimental glasses as a function of temperature. Taking the QFM and NNO data together, concentrations of  $\text{SiO}_2$ ,  $\text{TiO}_2$ , and  $\text{MgO}$  in the glass are monotonic functions of temperature (as are concentrations of  $\text{Al}_2\text{O}_3$  and  $\text{CaO}$ , which are not shown), reflecting the absence of major crystalline phases other than olivine.  $\text{FeO}^*$  contents of the QFM glasses are essentially independent of temperature, reflecting the similar  $\text{FeO}^*$  contents of olivine and glass in these experiments (Fig. 1d; note the  $\text{FeO}^*$  plot is noisier than for other oxides, due to the minor Fe loss or

gain in these experiments). The glass from the air experiment (39) plots off the trends for all oxides shown in Fig. 1 due to the high  $\text{Fe}^{+3}/\text{Fe}^{+2}$  in the glass (e.g., Kilinc *et al.*, 1983) and the correspondingly  $\text{Fe}^{+2}$ -poor coexisting olivine.

Figure 1c shows that MgO contents of the olivine-bearing experimental glasses at QFM and NNO are approximately linear as a function of temperature; an unweighted least-squares fit to our QFM data yields:  $T(^{\circ}\text{C}) = 19.2 \times (\text{MgO, wt \%}) + 1048$ . The slope ( $\sim 19$ ) is similar to values (16–23) calculated using 1-atm experiments on Hawaiian basaltic compositions (Helz & Thornber, 1987; Montierth *et al.*, 1995) and komatiitic compositions (Thy, 1995; Parman *et al.*, 1997) (see Fig. 1c). Transforming the  $T(\text{K})$  vs. mole % MgO global fit of olivine-saturated 1-atm experiments given by Sugawara (2000) into  $T(^{\circ}\text{C})$  vs. wt % MgO space yields a slope of  $\sim 17.8$  (for liquids with  $\sim 2$  to 26 wt % MgO). Note that liquids from the highest temperature experiments for the Hawaiian studies,  $1261^{\circ}\text{C}$ , (Helz & Thornber, 1987);  $1310^{\circ}\text{C}$ , (Montierth *et al.*, 1995) contained 1.7–2 wt %  $\text{Na}_2\text{O}$ . The fact that our glasses with much lower alkali contents yield a trend line with a similar slope to the more Na + K-rich Hawaiian data suggests that sodium values between  $\sim 0.1$  and  $\sim 2$  wt % have little effect on these trends and that the expression derived from our data is applicable to a broad range of liquid compositions. In a recent study, Putirka (2008b) obtained a higher slope (26) for the Mg-in-glass thermometer than reported by other workers. This reflects Putirka's (2008b) use of both high- and low-pressure data from the LEPR database (Hirschmann *et al.*, 2008) without including a pressure term in the equation. Considering only the 1-atm experiments in the LEPR database yields a slope of 18.1, consistent with values obtained by previous workers.

Two elements, Na and Cr, were affected by volatility during our experiments. Although no sodium was added to our starting mix and care was taken to avoid inadvertent sodium addition during its preparation, all but one of our glasses contain Na concentrations above background, with abundances of 0.05–0.6 wt % (Table 3). We believe these relatively small amounts of Na were acquired through re-volatilization, either deposited by previous Na-bearing experiments or as a contaminant on new furnace tubes. The concentration of Na<sub>2</sub>O in our experimental glasses declined with each successive experiment unless temperature was increased, thereby accessing Na further from the hot spot. This suggests a gradual depletion of Na from the inner wall of the Al<sub>2</sub>O<sub>3</sub> furnace tube as the reservoir of Na on the inner tube surface was depleted. We analyzed glasses for K<sub>2</sub>O and P<sub>2</sub>O<sub>5</sub> but concentrations of these oxides were negligible; see notes for Table 3. Generally, Cr was conserved during experiments but the 1400°C run in air lost nearly all of its Cr due to volatility under oxidizing conditions (Hanson & Jones, 1998).

Experiments run under the same conditions but for different times provide information on the approach to equilibrium in the experiments. For example, we conducted two QFM experiments each at ~ 1400°C and ~1450°C (25 and 48 hr), and three at ~1300°C (22, 48, and 72 hr). Although there are differences in the concentrations of Na<sub>2</sub>O in glasses run at similar conditions but for different durations (reflecting, as discussed above, re-mobilization of previously deposited/condensed Na on the alumina furnace tubes), for the most part all other oxide concentrations in the glasses overlap at the 2σ level in each time series. Exceptions (in the 1300°C experiments) largely reflect variable amounts of Fe loss/gain, but even in these cases we infer that exchange equilibrium

between olivine and liquid was closely approached given that values of  $K_{D,Fe^{+2}-Mg}$  within each time series, including the one at 1300°C, overlap at the  $1\sigma$  level.

### **Phase proportions**

The proportions of phases in subliquidus experiments were determined by mass balance using the non-linear approach of Albarède & Provost (1977), which incorporates uncertainties on the bulk and phase compositions. The analyzed glass from superliquidus run 43 (1600°C) was taken as representative of the bulk composition (except for the air experiment, where the bulk  $Cr_2O_3$  was set equal to zero; using run 34 (1551°C) for these calculations yields virtually identical results). We included  $FeO^*$ ,  $Na_2O$ , and  $NiO$  as variables in the bulk composition because these components may have varied and, according to our calculations, did vary from experiment to experiment. The oxide sum of the bulk composition was held constant, and any changes in the bulk concentrations of  $FeO^*$ ,  $Na_2O$ , or  $NiO$  required to minimize  $\chi^2$  were compensated by corresponding proportional changes to concentrations of all the remaining oxides (with 10 equations and either five or six—if spinel is present—unknowns, our mass balance problems are still over-determined). All experiments yielded mass balance solutions acceptable at the 95% confidence level (i.e., goodness of fit values,  $Q \geq 0.05$ ; see Press *et al.*, 1992). Our mass balance calculations suggest that loop preconditioning was successful in limiting iron loss to the Pt wire; bulk  $FeO$  changed by  $-6.4\%$  (loss) to  $+1.5\%$  (gain) with most in the range  $-2.2$  to  $+1.5\%$  (relative).

The proportions of liquid and olivine in our experiments are plotted in Fig. 2a as functions of temperature for the ~QFM data with quadratic fits for each phase. The wt % of liquid steadily increases and that of olivine decreases with increasing temperature until, at 1538°C according to the 2<sup>nd</sup> order polynomial fit of the olivine mode, the bulk composition is at the liquidus. This predicted liquidus temperature is consistent with our experimental constraint that the bulk composition is above the liquidus at 1551°C and below it at 1500°C and with the prediction of 1531°C for the “as analyzed” bulk composition (run 43; Table 3) obtained from MELTS (which is also similar to the 1535°C value cited above for the nominal alkali-free version of this bulk composition, Table 1). Although the olivine content was fit to a quadratic, the slope of the olivine vs. temperature curve in Fig. 2a is relatively constant at ~0.14 wt %/°C over the range of our experiments. Fits to modes in the olivine-primary phase field from the 1-atm experiments of Thy (1995) and Parman *et al.* (1997) on komatiitic compositions (16 and 23 wt % MgO), yield similar slopes of ~0.15 and ~0.14 wt %/°C. Although not shown in Fig. 2a, modes from the MELTS calculations (Ghiorso & Sack, 1995; Smith & Asimow, 2005) are almost indistinguishable from the quadratic fits in Fig. 2a.

Increasing oxygen fugacity at constant temperature suppresses olivine crystallization in syn-HP1; for example, there is 1.5 wt % less olivine at NNO and 1350°C than there is at QFM and 6.4 wt % less olivine at 1396°C in air than there is at QFM at 1400°C. Although the best-fit olivine proportions in the NNO and QFM experiments at ~1350°C overlap at 2 $\sigma$  (see Table 2), the difference in the modes is in the same direction as that seen in the air and QFM experiments at ~1400°C. This effect can also be seen in simple systems such as MgO-FeO-SiO<sub>2</sub>-O<sub>2</sub> (e.g., Muan and Osborn, 1956) in which

olivine-liquid tie lines for a given temperature must rotate and extend towards more magnesian olivine compositions with increasing  $fO_2$ . Since the position of the liquidus isotherm is a relatively weak function of  $fO_2$ , the lever principle dictates that the olivine/liquid ratio for a given bulk composition decreases with increasing  $fO_2$ . This destabilization of olivine with increasing  $fO_2$  is the flip side of the well-known stabilization of spinel in basaltic melts with increasing  $fO_2$  (e.g., Hill & Roeder, 1974): Both phases respond to increases in  $Fe^{+3}/Fe^{+2}$  in the melt as  $fO_2$  is increased. For spinel, stabilization of magnetite and magnesioferrite components in the spinel due to increased activities of these components in the melt offsets any destabilization of  $Fe^{+2}$ -bearing components. Olivine, in contrast, has a negligible solubility for  $Fe^{+3}$  and, since  $K_{D,Fe^{+2}-Mg}$  in air and QFM are nearly identical for syn-HP1 (Fig. 3 and discussion below), higher  $Fe^{+3}/Fe^{+2}$  in the melt translates into lower activities of the fayalite component in the melt and, therefore, higher  $Mg/Fe^{+2}$  in the coexisting olivine and this requires a decrease in the modal abundance of olivine. Figure 2b shows wt % liquid by mass balance for the ~1350 and ~1400°C experiments (Table 2) and spinel-suppressed MELTS calculations using the glass composition from run 43 (Table 3) at these two temperatures as a function of  $\log fO_2$  relative to the QFM buffer. Both MELTS curves show an increase in liquid fraction with increasing  $fO_2$  and, in particular, the 1350°C MELTS curve overlaps the liquid modes of our 1350°C QFM and NNO experiments (noting that typical  $1\sigma$  errors from the mass balance for the liquid fraction are 0.3–0.4 wt%). At higher  $fO_2$ s, the MELTS curves are qualitatively consistent with our data. The Fo content of olivine predicted by MELTS is, however, higher at 1396°C and air than is observed in our experiment (98.4 vs. 97.0), and the predicted

MELTS  $K_{D,Fe^{+2}-Mg}$  is much lower (0.130 vs. 0.353). We suspect that these differences are, in part, related to the  $Fe^{+3}/Fe^{+2}$  equation of Kress & Carmichael (1991), which is used in MELTS.

### **Olivine-liquid $Fe^{+2}$ -Mg exchange coefficients**

Knowledge of the  $Fe^{+2}$  (or equivalently the FeO) content of an olivine-saturated liquid is a prerequisite for calculating  $K_{D,Fe^{+2}-Mg}$ . FeO contents of glasses can be measured by wet chemistry (e.g., Yokoyama & Nakamura, 2002), Mössbauer spectroscopy (e.g., Partzsch *et al.*, 2004), and/or XANES spectroscopy (e.g., Cottrell *et al.*, 2009); more often, however, parameterizations based on such measurements are used to calculate  $Fe^{+3}/Fe^{+2}$  as a function of temperature,  $fO_2$ , and liquid composition (e.g., Sack *et al.*, 1980; Kilinc *et al.*, 1983; Kress & Carmichael, 1991). In Fig. 3, we show calculated  $K_{D,Fe^{+2}-Mg}$  values from our experiments as a function of liquid MgO content (Fig. 3a) and temperature (Fig. 3b): For the data points shown in black, we used the algorithm of Jayasuriya *et al.* (2004, eqn 12) to calculate  $Fe^{+3}/Fe^{+2}$  in the liquid; we justify the choice of this parameterization in the discussion below. For the two experiments shown in gray (runs at 1500°C and QFM and 1396°C in air), we have wet chemical determinations of the abundance of FeO in the glasses provided by R.A. Lange (see notes to Table 3), which lead to  $K_{D,Fe^{+2}-Mg}$  values of  $0.338 \pm 0.006$  and  $0.353 \pm 0.013$ , respectively. The  $1\sigma$  error bars in Fig. 3 are based on Monte Carlo propagation of uncertainties on (1) the concentrations of FeO and MgO in the olivines as measured by electron microprobe (Table 3); (2) the concentrations of FeO\* and MgO in the glasses as measured by electron microprobe (Table 3); and (3) the

concentrations of FeO in the glasses as measured by R.A. Lange (see Table 3). For those experiments where we calculated FeO in the glasses using eqn 12 of Jayasuriya *et al.* (2004), the Monte Carlo calculations assumed flat distributions of  $\pm 3^\circ\text{C}$  and  $\pm 0.05 \log$  units for  $f\text{O}_2$ , but we ignored the errors associated with the equation's fit parameters.

The data in Fig. 3 show that all of the  $K_{\text{D,Fe}^{+2}\text{-Mg}}$  values, except for the air experiment calculated via Jayasuriya *et al.* (2004), are in the narrow range of 0.33 to 0.36 (the unweighted average for all 11 experiments is  $0.345 \pm 0.009$ ,  $1\sigma$ ; for runs 26 and 39,  $K_{\text{D,Fe}^{+2}\text{-Mg}}$  values used to calculate this average were based on the FeO concentration in the glass as measured by wet chemistry). This mean  $K_{\text{D,Fe}^{+2}\text{-Mg}}$  is substantially higher than the canonical value of 0.30 of Roeder and Emslie (1970). There is no statistically significant correlation (at the 95% confidence level) with either temperature (over a  $200^\circ\text{C}$  range,  $1300\text{--}1500^\circ\text{C}$ ), consistent with Roeder and Emslie's observation at  $1152\text{--}1266^\circ\text{C}$  or MgO (over the interval of  $\sim 13$  to 24 wt %; unless otherwise stated, statistical tests for correlation are based on the non-parametric Spearman rank-order correlation coefficient,  $r_s$ ; Press *et al.*, 1992). Thus, for this MgO-rich bulk composition, over the range of conditions we have studied,  $K_{\text{D,Fe}^{+2}\text{-Mg}}$  appears to be independent of temperature, melt composition, and  $f\text{O}_2$ .

The only significant discrepancy shown in Fig. 3 is between the two  $K_{\text{D,Fe}^{+2}\text{-Mg}}$  values in air, one based on a wet chemical measurement of  $\text{Fe}^{+2}$  and the other based on a calculation of  $\text{Fe}^{+3}/\text{Fe}^{+2}$  ratio using the algorithm of Jayasuriya *et al.* (2004). Although we do not know the source of the discrepancy, it is unlikely to be olivine contamination of the glass separate analyzed by wet chemistry since the measured FeO contents of the glass and olivine in the

air experiment are nearly identical (3.08 and 3.05 wt %, respectively; Table 3), and thus any addition of olivine to the glass separate would have almost no effect on the wet chemical FeO measurement. We note that most of the other  $\text{Fe}^{+3}/\text{Fe}^{+2}$  models tested also predict a low  $K_{\text{D,Fe}^{+2}\text{-Mg}}$  for our experiment in air—a discrepancy that is puzzling since all of the models published after Sack *et al.* (1980) include the air experiments of Kilinc *et al.* (1983), and the available air experiments cover a region of composition space (other than  $\text{Fe}^{+3}/\text{Fe}^{+2}$ ) comparable to coverage for the more reducing experiments.

## DISCUSSION

In their landmark study, Roeder & Emslie (1970) found for a range of basaltic bulk compositions that the logarithm of the partition coefficients for MgO and FeO between olivine and silicate melt are each a linear function of inverse temperature of roughly equal slope. Thus, when a ratio of the two partition coefficients is taken to form an exchange coefficient,  $K_{\text{D,Fe}^{+2}\text{-Mg}}$ , the temperature dependences of the partition coefficients essentially cancel, leaving  $K_{\text{D,Fe}^{+2}\text{-Mg}} = 0.30 \pm 0.03$  ( $1\sigma$ ), independent of both temperature and liquid composition. Subsequent experimental work (e.g., Sack *et al.*, 1987; Gee & Sack, 1988) demonstrated that  $K_{\text{D,Fe}^{+2}\text{-Mg}}$  decreases with increasing alkali content in the melt, reaching values as low as 0.18 for highly nepheline- and/or leucite-normative bulk compositions. Moreover, Kushiro & Walter (1998) and Kushiro & Mysen (2002) found  $K_{\text{D,Fe}^{+2}\text{-Mg}}$  values ranging from 0.25–0.35 (without correcting for the presence of  $\text{Fe}^{+3}$ ), and noted that  $K_{\text{D,Fe}^{+2}\text{-Mg}}$  correlates with the degree of polymerization of the melt as measured by NBO/T.

In contrast, Toplis (2005) attributed most of the variation in  $K_{D,Fe^{+2}-Mg}$  to variations in silica and alkali contents of the coexisting liquids rather than to NBO/T. The essential point, however, is that  $K_{D,Fe^{+2}-Mg}$  is a function of melt composition if a sufficiently large range is considered. In light of substantial variations in  $K_{D,Fe^{+2}-Mg}$  apparent in the literature data and the discrepancy between  $K_{D,Fe^{+2}-Mg}$  obtained through wet chemistry and the algorithm of Jayasuriya *et al.* (2004) for our air experiment, several questions arise in the context of our experiments: (1) Are our data for MgO-rich liquids consistent with previous 1-atm experiments from the literature? (2) How much does the choice of  $Fe^{+3}/Fe^{+2}$  algorithm affect the calculated  $K_{D,Fe^{+2}-Mg}$  values from experiments conducted under  $fO_2$ s most relevant for terrestrial basalts (i.e., ~QFM; Carmichael, 1991)? And (3) are there compositional ranges for basaltic melts (e.g., Hawaiian tholeiites or mid-ocean ridge basalts) over which  $K_{D,Fe^{+2}-Mg}$  can be safely approximated to be constant?

### **Comparison of our data with exchange coefficients from literature-based olivine-liquid pairs**

We assembled a comprehensive database of 1-atm experiments with coexisting olivine and glass analyses from the literature for comparison with our data. We chose not to consider high-pressure experiments in graphite capsules because, although these experiments are reducing (Médard *et al.*, 2008), the  $fO_2$ s are not so low that  $Fe^{+3}$  can be ignored in calculating  $K_{D,Fe^{+2}-Mg}$ . Moreover, given the lack of oxygen buffers or independent measures of  $fO_2$  in most of these experiments and the paucity of data on pressure

corrections to  $\text{Fe}^{+3}/\text{Fe}^{+2}$  in the melt (O'Neill *et al.*, 2006),  $K_{\text{D,Fe}^{+2}\text{-Mg}}$  is inherently less well constrained in graphite capsule experiments conducted at high-pressures than it is in 1-atm experiments. All selected bulk compositions contain at least the elements Si, Al, Fe, Mg, and Ca and a majority resemble natural basalts. In an effort to remove low-quality analyses from the data set, we applied the following compositional filters: oxide totals for glass of  $100.0 \pm 1.5$  and olivine tetrahedral and total cation sums per four oxygens of  $1.000 \pm 0.015$  and  $3.00 \pm 0.015$ , respectively. We also applied the following three compositional filters: olivine NiO and CoO contents  $< 6$  wt %, a conservative upper limit for Henry's law behavior (e.g., Mäkipää, 1980; Drake & Holloway, 1981) and  $\text{TiO}_2$  contents of glass  $< 6$  wt %, as higher  $\text{TiO}_2$  contents are known to affect  $K_{\text{D,Fe}^{+2}\text{-Mg}}$  (Longhi *et al.*, 1978; see Xirouchakis *et al.*, 2001 for a discussion of the effect of increasing  $\text{TiO}_2$  on olivine-liquid  $K_{\text{D,Fe}^{+2}\text{-Mg}}$  at constant silica activity). The glass oxide sum constraint was applied to highly reduced experiments ( $f\text{O}_2 \leq \text{IW}+0.5$ ; IW buffer calculated using the equation in Huebner, 1971) based on the assumption that all Fe is present as FeO (i.e.,  $\text{FeO}^*$ ); for more oxidized runs, this constraint was applied after first calculating FeO and  $\text{Fe}_2\text{O}_3$  abundances using eqn 12 of Jayasuriya *et al.* (2004). The 964 experiments (from our database of 1179 olivine-liquid pairs from the literature) that passed these filtering constraints span temperatures from 1009 to 1600°C and  $f\text{O}_2$ s from  $\sim\text{IW}-3$  to air (data references are given in the on-line Supplementary Material available at <http://www.petrology.oxfordjournals.org/>). The Fo contents of the olivines in this data set range from 28 to 99, and MgO contents in the glasses range from 1.3 to 28 wt %.

Olivine-liquid pairs in our literature data set can be divided into three categories: (1)  $\text{Fe}^{+3}/\text{Fe}^{+2}$  in the liquid is known by direct measurement of the quenched glass; (2)  $\text{Fe}^{+3}/\text{Fe}^{+2}$  was not measured but run conditions were sufficiently reducing so that  $\text{Fe}^{+3}$  can be neglected (e.g., at  $f\text{O}_2\text{s} \leq \text{IW}+0.5$  and 1-atm according to the model of Jayasuriya *et al.* (2004), molar  $\text{Fe}^{+3}/(\text{Fe}^*)$  is less than 0.035); (3)  $\text{Fe}^{+3}/\text{Fe}^{+2}$  was not measured but can be calculated using one of the algorithms developed for this purpose (e.g., Sack *et al.*, 1980; Kilinc *et al.*, 1983; Kress & Carmichael, 1991). Experiments in category 1 are ideally suited to answering the questions posed above since calculated  $K_{\text{D,Fe}^{+2}\text{-Mg}}$  values from these experiments are independent of any  $\text{Fe}^{+3}/\text{Fe}^{+2}$  algorithm. We are, however, aware of only 33 olivine-bearing experiments in the literature with reported  $\text{Fe}^{+3}/\text{Fe}^{+2}$  ratios (Mysen & Dubinsky, 2004; Partzsch *et al.*, 2004; Mysen & Shang, 2005; Mysen, 2006, 2007), 24 of which were done in air, and of the nine remaining, only six were run at  $f\text{O}_2\text{s} \leq \text{QFM}$ . The 172 experiments in category 2 are dominated by Fe-rich bulk compositions with low total alkalis (range in olivine Fo# is 33–96 with a median and mean absolute deviation of  $72 \pm 11$ ; from this point on we refer to the mean absolute deviation as “MAD”). We also constructed a data set from category 3 experiments run within 0.25 *log* units of the QFM buffer, as defined by O'Neill (1987); the median Fo content of olivine in these 446 experiments is  $79 \pm 7$  (MAD), with a range of 45–95. Since most of our experiments were done at QFM, this is a convenient data set for comparing literature data with our experimental results. Because of the small number of category 1 experiments and their bias towards highly oxidizing conditions, we emphasize category 2–3 experiments in the following discussion.

To test the viability of treating all Fe as Fe<sup>+2</sup> in the reduced experiments, we first computed Fe<sup>+3</sup>/Fe<sup>+2</sup> ratios in the melt by applying Jayasuriya *et al.* (2004) eqn 12 to experiments in the  $\leq$  IW+0.5 data set. For Fe-capsule experiments, the required  $f_{O_2}$ s were calculated based on expressions from Righter *et al.* (1997) and Snyder & Carmichael (1992) and data from Robie *et al.* (1978) (using the iron activity model of Roeder (1974) instead of Snyder & Carmichael's has a negligible effect on the calculated  $f_{O_2}$ s). These computations lead to a median  $K_{D,Fe^{+2}-Mg}$  value of  $0.34\pm 0.02$  (MAD; the range in  $K_{D,Fe^{+2}-Mg}$ s is 0.24–0.41). Assuming all Fe in the melt to be ferrous yields a median  $K_{D,Fe^{+2}-Mg}$  of  $0.33\pm 0.02$  (MAD; range is 0.23–0.40) for the same experiments. Thus, the influence of Fe<sup>+3</sup> in the melt on calculated  $K_{D,Fe^{+2}-Mg}$  is small for these reduced experiments. To test the consistency of the  $\leq$  IW+0.5 data set with the QFM $\pm$ 0.25 data set, for which Fe<sup>+3</sup>/Fe<sup>+2</sup> cannot be ignored, we calculated Fe<sup>+3</sup>/Fe<sup>+2</sup> for the QFM $\pm$ 0.25 literature glasses using eqn 12 of Jayasuriya *et al.* (2004), and then computed values of  $K_{D,Fe^{+2}-Mg}$ . The range of  $K_{D,Fe^{+2}-Mg}$  values for the QFM $\pm$ 0.25 experiments is 0.13–0.41, with a median of  $0.34\pm 0.03$ ; again, the uncertainty given here is the mean absolute deviation. The median  $K_{D,Fe^{+2}-Mg}$  values for both  $\leq$  IW+0.5 ( $0.34\pm 0.02$ ) and QFM $\pm$ 0.25 ( $0.34\pm 0.03$ ; median and MAD, respectively) data sets overlap the mean  $K_{D,Fe^{+2}-Mg}$  value calculated from our experiments ( $0.345\pm 0.009$ ; mean and  $1\sigma$ , all 11 experiments); indeed, they are essentially identical. The agreement is also good if we consider only the 78 glasses from the literature at QFM $\pm$ 0.25 with 46–52 wt % SiO<sub>2</sub>,  $\leq$  3 wt % Na<sub>2</sub>O + K<sub>2</sub>O and Fo<sub>92</sub> to Fo<sub>80</sub> olivines, bounds that overlap with our olivine-saturated experiments and incorporate most tholeiitic

magmas (Le Maitre, 1976; Rhodes & Vollinger, 2004; Stolper *et al.*, 2004)—the median  $K_{D,Fe^{+2}-Mg}$  for these 78 olivine-liquid pairs is  $0.340\pm 0.012$  (MAD), a value essentially identical to the mean value of  $0.343\pm 0.008$  from our QFM experiments and to the median from the full QFM $\pm 0.25$  literature data set ( $0.34\pm 0.03$ ). The agreement between our data and those in the literature that require no correction for the amount of  $Fe^{+3}$  in the melt and those that do require a correction is important in that it demonstrates a consistency between  $K_{D,Fe^{+2}-Mg}$  values measured in the experiments presented here and a large number of 1-atm experiments from the literature. Moreover, this consistency in  $K_{D,Fe^{+2}-Mg}$  spans a wide range of mafic to ultramafic liquid compositions and is significantly higher than the canonical value of 0.30. In the on-line Supplementary Material, we explore possible reasons for the discrepancy between the canonical  $K_{D,Fe^{+2}-Mg}$  value of 0.30 obtained by Roeder and Emslie (1970) and the higher values for our data and most of those in the literature. We also discuss predictions of the Ford *et al.* (1983) and Toplis (2005) models for  $K_{D,Fe^{+2}-Mg}$ .

Calculating  $Fe^{+3}/Fe^{+2}$  for a given liquid is a crucial step in obtaining an accurate  $K_{D,Fe^{+2}-Mg}$ . To assess how the different expressions for calculating  $Fe^{+3}/Fe^{+2}$  that are available in the literature affect calculated  $K_{D,Fe^{+2}-Mg}$  values at terrestrially relevant  $fO_{2S}$ , we calculated  $K_{D,Fe^{+2}-MgS}$  for glasses from the QFM $\pm 0.25$  data set after first calculating FeO contents using each of the following eight parameterizations: Sack *et al.* (1980), Kilinc *et al.* (1983), Kress & Carmichael (1988), Borisov & Shapkin (1989), Kress & Carmichael (1991), Jayasuriya *et al.* (2004) eqn 12 and 14, and Ghiorso & Kress (2004).

However, comparing how these different parameterizations affect  $K_{D,Fe^{+2}-Mg}$  is difficult because not only are the calculated  $Fe^{+3}/Fe^{+2}$  values functions of liquid composition but because the resulting  $K_{D,Fe^{+2}-Mg}$ s are also correlated with both liquid and olivine composition. In an effort to minimize the compositional effects on  $K_{D,Fe^{+2}-Mg}$  so that we could consider as large a body of olivine-liquid pairs as possible, we parameterized each data set as a function of “S”, a component in the CMAS projection scheme (“S” =  $S/(C + M + A + S)$ ); BVSP 1981, chapter 3.3; Gee & Sack, 1988; see also the on-line Supplementary Material), which we calculated on a molar basis. We used the expression  $K_{D,Fe^{+2}-Mg} = a + b \times \exp(c \times “S”)$  for this purpose, where a, b, and c are least-squares fit parameters. Correlation coefficients for the fits range from 0.72–0.84, although most lie between 0.82 and 0.84. Gee & Sack (1988) showed that  $K_{D,Fe^{+2}-Mg}$  is strongly correlated with “S”, which incorporates terms for  $Na_2O$  and  $K_2O$  in addition to  $SiO_2$ , and Toplis (2005) showed that  $K_{D,Fe^{+2}-Mg}$  is strongly correlated with silica content of the glass (after correcting for the effects of alkalis) and olivine Fo content. We therefore projected each  $K_{D,Fe^{+2}-Mg}$  value calculated using one of the  $Fe^{+3}/Fe^{+2}$  algorithms to “S” = 0.5, an arbitrary value close to the median “S” = 0.48 for all of the glass compositions. Each set of projected  $K_{D,Fe^{+2}-Mg}$  values was then fit to a linear function in Fo content and projected to an olivine composition of  $Fo_{88}$  (the on-line Supplementary Material provides a detailed description of the projection scheme). We emphasize that our goal is not to provide a formal parameterization of  $K_{D,Fe^{+2}-Mg}$ , but to minimize the compositional effects on  $K_{D,Fe^{+2}-Mg}$  so

as to compare the effect of different  $\text{Fe}^{+3}/\text{Fe}^{+2}$  calculation schemes using as large a population of olivine-liquid pairs as possible.

The projection procedure described above and in the on-line Supplementary Material removes the effect of olivine composition on  $K_{\text{D,Fe}^{+2}\text{-Mg}}$  and substantially reduces the effects of silica and total alkalis. Two of the projected data sets, those calculated using Borisov & Shapkin (1989) and Jayasuriya *et al.* (2004) eqn 14, show a weak but statistically significant correlation with wt %  $\text{SiO}_2$  ( $r_s$  is equal to  $-0.12$  and  $-0.13$ , respectively) and all of the projected data sets are weakly correlated with wt %  $\text{Na}_2\text{O} + \text{K}_2\text{O}$  ( $r_s$  lies between  $-0.30$  and  $-0.18$ ). Linear fits of the projected  $K_{\text{D,Fe}^{+2}\text{-Mg}}$ s as a function of wt %  $\text{Na}_2\text{O} + \text{K}_2\text{O}$  yield, however, slopes that are  $\leq 0.0014$  ( $\leq 0.0008$  for five of the seven sets), an order of magnitude lower than for the unprojected  $K_{\text{D,Fe}^{+2}\text{-Mg}}$ s. Figure 4 shows histograms of the projected  $K_{\text{D,Fe}^{+2}\text{-Mg}}$  values based on five of the eight  $\text{Fe}^{+3}/\text{Fe}^{+2}$  calculation schemes. Mean absolute deviations, which we use as an indication of the width of a distribution, are all in the range of 0.014 to 0.015, and, with the exception of  $K_{\text{D,Fe}^{+2}\text{-Mg}}$ s calculated using Borisov & Shapkin (1989), the median values all overlap at 1 MAD; the algorithms of Jayasuriya *et al.* (2004) yield the highest median  $K_{\text{D,Fe}^{+2}\text{-Mg}}$  values (0.336, eqn 12, Fig. 4d and 0.330, eqn 14, not shown) and those of Borisov & Shapkin (1989) yield the lowest (0.304). We applied the same projection procedure to the  $\leq \text{IW}+0.5$  data set as we did for  $\text{QFM}\pm 0.25$ . All median projected  $K_{\text{D,Fe}^{+2}\text{-Mg}}$  values lie between 0.332 and 0.337 and, with the exception of Borisov & Shapkin (1989), all of them overlap at 1 MAD. We selected eqn 12 of Jayasuriya *et al.* (2004) for calculating  $\text{Fe}^{+3}/\text{Fe}^{+2}$  in

Hawaiian parental liquids because it has the smallest difference between median projected  $K_{D,Fe^{+2}-Mg}$ s for the  $\leq IW+0.5$  and  $QFM\pm 0.25$  data sets. It is, however, important to stress that we lack sufficient data to determine which  $Fe^{+3}/Fe^{+2}$  model is the most accurate (many more  $Fe^{+3}/Fe^{+2}$  measurements are needed, especially under conditions more oxidizing than QFM). That said, self-consistency across ranges of redox conditions is important in any model and this leads us to favor eqn 12 of Jayasuriya *et al.* (2004).

We noted above (e.g., Fig. 3) that, under highly oxidizing conditions, there is a discrepancy between  $K_{D,Fe^{+2}-Mg}$  values for run 39 in which  $Fe^{+3}/Fe^{+2}$  was measured and for which  $Fe^{+3}/Fe^{+2}$  was calculated. Figure 5 shows projected  $K_{D,Fe^{+2}-Mg}$  values (thus removing most of the liquid and olivine compositional dependencies on  $K_{D,Fe^{+2}-Mg}$ ) as a function of the deviation in  $\log fO_2$  from QFM. Median projected  $K_{D,Fe^{+2}-Mg}$  values calculated using Jayasuriya *et al.* (2004; black symbols) and those for which  $Fe^{+3}/Fe^{+2}$  was measured, either by Mössbauer (open circles) or wet chemistry (gray circles), overlap for  $fO_2s \leq \sim QFM$  and are essentially constant. The Mössbauer and wet chemistry determinations are important because they are independent of  $Fe^{+3}/Fe^{+2}$  calculation schemes and they suggest that, for the redox conditions most relevant to terrestrial and planetary basalts,  $Fe^{+3}$  in the liquid does not significantly affect the solution properties of MgO and FeO in the melt and, therefore, the value of  $K_{D,Fe^{+2}-Mg}$ . As the  $fO_2$  is increased above these low levels, however, median projected  $K_{D,Fe^{+2}-Mg}$  values increasingly diverge from the  $\sim 0.34$  characteristic of more reducing conditions. This may reflect the influence of  $Fe^{+3}$  on the thermodynamic

properties of basaltic liquid and definitely implies that the application of constant  $K_{D,Fe^{+2}-Mg}$  values to highly oxidizing systems should be approached with caution.

Projected  $K_{D,Fe^{+2}-Mg}$  values can be used to compare  $Fe^{+3}/Fe^{+2}$  algorithms and the possible influence of  $Fe^{+3}$  on  $K_{D,Fe^{+2}-Mg}$ , as discussed above. It is, however, also important to establish the temperature- $fO_2$  and compositional bounds over which a single *unprojected* value of  $K_{D,Fe^{+2}-Mg}$  can be assumed as this greatly simplifies modeling olivine fractionation in natural systems. A variety of constant  $K_{D,Fe^{+2}-Mg}$  values have been offered, sometimes tailored to specific magmatic systems (e.g., Roeder & Emslie, 1970; Nisbet *et al.*, 1987; Putirka *et al.*, 2007), but none of these are applicable to all liquid and olivine compositions. Consider, for example, the variation of  $K_{D,Fe^{+2}-Mg}$  with alkalis in the liquid (Fig. 6). For low  $Na_2O + K_2O$  (e.g., < 3 wt %),  $K_{D,Fe^{+2}-Mg}$  can be regarded as independent of alkali content but, as  $Na_2O + K_2O$  is increased above a few wt %,  $K_{D,Fe^{+2}-Mg}$  decreases markedly. Thus, modeling of olivine fractionation for magmas ranging from alkali-poor to alkali-rich would need to account for variations in  $K_{D,Fe^{+2}-Mg}$  with changing alkali concentrations in the melt but the effect of alkalis on  $K_{D,Fe^{+2}-Mg}$  can be ignored for relatively low-alkali liquids. Similar arguments hold for silica. Low-silica melts yield low values of  $K_{D,Fe^{+2}-Mg}$ , although some of this may be an alkali effect (many silica-poor melts are also alkali-rich). Restricting melt compositions to 46–52 wt %  $SiO_2$  and  $\leq 3$  wt %  $Na_2O + K_2O$  avoids  $K_{D,Fe^{+2}-Mg}$ s that vary strongly with liquid composition but still includes a range of natural

basaltic to picritic liquids. The median  $K_{D,Fe^{+2}-Mg}$  (unprojected) for 337 experimental glasses equilibrated at  $fO_2 \leq QFM+0.25$  with 46–52 wt %  $SiO_2$  and  $\leq 3$  wt %  $Na_2O + K_2O$ , including those of the present study, is  $0.343 \pm 0.017$  (MAD); the range in temperature and Fo content for these experiments is 1009–1571°C and 36–95, respectively.  $K_{D,Fe^{+2}-Mg}$  is weakly correlated with temperature ( $r_s = -0.12$ ) and the  $SiO_2$  content of the glass ( $r_s = 0.12$ ), but for silica contents and temperatures for olivine crystallization from basaltic to picritic melts (46–52 wt %  $SiO_2$ ; 1150–1500°C), these dependences have little effect ( $< 0.013$ ).  $K_{D,Fe^{+2}-Mg}$  is negatively correlated with Fo content of the olivine but for experiments with  $Fo_{80}$ – $Fo_{92}$  olivines, a range encompassing ~96% of over 17,000 olivine phenocryst analyses from the global data set of Sobolev *et al.* (2007), the median  $K_{D,Fe^{+2}-Mg}$  only decreases from  $0.343 \pm 0.017$  to  $0.337 \pm 0.014$  (144 experiments). We conclude that for relatively low-alkali terrestrial basalts, a constant  $K_{D,Fe^{+2}-Mg}$  of 0.34 is adequate for simple petrologic modeling and we use this value below in constructing estimates of Hawaiian parental magmas.

### **Hawaiian parental liquids**

The compositions and characteristics of mantle sources and of liquids in shallow pre-eruptive magma chambers are critical to understanding the nature and origin of Hawaiian lavas (e.g., Maaløe, 1979; Wright, 1984; Herzberg & O'Hara, 2002). Trace element and isotopic data have been used to address these issues (e.g., Hofmann & Jochum, 1996; Blichert-Toft *et al.*, 2003), as has the major element chemistry (e.g., Stolper *et al.*, 2004;

Herzberg, 2006). For the major elements, different reconstruction approaches and model constraints have led to a range of inferred MgO contents in the parental/primary magmas (13–22 wt %; Wright, 1984; Clague *et al.*, 1991; Garcia *et al.*, 1995; Baker *et al.*, 1996; Rhodes, 1996; Norman & Garcia, 1999; Green *et al.*, 2001; Herzberg & O'Hara, 2002; Rhodes & Vollinger, 2004; Stolper *et al.*, 2004; Herzberg, 2006; Herzberg *et al.*, 2007; Putirka, 2008a). This range of estimates of the MgO contents of Hawaiian parental/primary magmas has not attracted much attention (after all, they are all high in MgO relative to commonly erupted magmas), but it actually has considerable petrogenetic significance (e.g., in the depth of separation of liquids from peridotitic residual sources and in estimates of mantle potential temperatures; e.g., Herzberg & O'Hara, 2002; Falloon *et al.*, 2007; Putirka *et al.*, 2007).

The usual approach to these types of parental liquid calculations (but see Norman & Garcia, 1999 for an alternative) is to posit the composition of a target olivine, define  $\text{Fe}^{+3}/\text{Fe}^{+2}$  in liquid either by specifying  $\text{Fe}^{+3}/\text{Fe}^{+2}$  or choosing the redox conditions and an algorithm to compute  $\text{Fe}^{+3}/\text{Fe}^{+2}$ , choose a single (unprojected) value of  $K_{\text{D,Fe}^{+2}\text{-Mg}}$  to connect liquid and olivine compositions, and select a glass or aphyric lava whose composition is thought to be related through olivine fractionation to the parental melt. The fractionation process is then reversed numerically by dissolving small increments of equilibrium olivine back into the selected glass/aphyric lava until the resulting liquid is in equilibrium with the assumed composition of the target olivine. In this section, we first consider input parameters for parental melt calculations applicable to Mauna Loa, Mauna Kea, and Kilauea and then evaluate parental magmas for these three Hawaiian volcanoes

using our constraints on  $K_{D,Fe^{+2}-Mg}$ .

Plausible target olivines for reversed fractionation calculations are usually either mantle phases postulated to be in equilibrium with the primary melt or the most Mg-rich olivine phenocryst found in lavas from the volcano in question (for a parental liquid). We chose the latter approach and have ignored the possible effects of pressure on  $Fe^{+3}/Fe^{+2}$  in the liquid and on  $K_{D,Fe^{+2}-Mg}$ ; the assumption that olivine fractionation occurs primarily at low pressures is justified by fluid inclusions in olivine phenocrysts from Hawaiian lavas that suggest low formation pressures in the 2–5 kbar range (Roedder, 1983) and gravity anomalies associated with the summits and rift zones of all of the volcanoes on the Big Island (Kauahikaua *et al.*, 2000) that suggest substantial olivine fractionation occurs at relatively low pressures (~2 kbar). Under these conditions, the effect of pressure on  $Fe^{+3}/Fe^{+2}$  and  $K_{D,Fe^{+2}-Mg}$  is believed to be modest (Toplis, 2005; O'Neill *et al.*, 2006).

Based on a large sample of olivine phenocryst compositions (Baker *et al.*, 1996; Clague *et al.*, 1995, Clague, unpublished data; Garcia *et al.*, 1995; Garcia, 1996; Sobolev *et al.*, 2007), the most magnesian olivines are Fo<sub>90.8</sub> for Kilauea, Fo<sub>91.0</sub> for Mauna Kea and Fo<sub>91.7</sub> for Mauna Loa.

Recent estimates of redox conditions for Hawaiian magmas based on  $Fe_2O_3/FeO$  determinations of glasses and aphyric lavas are generally in the vicinity of QFM–1 (see Rhodes & Vollinger, 2005, and references therein). Bulk  $Fe_2O_3/FeO$  measured on near-vent aphyric Mauna Loa lavas yield  $fO_2$ s of ~QFM–2 (Rhodes and Vollinger, 2005); Cr-in-glass and  $FeO/Fe_2O_3$  wet chemical measurements on near-vent, rapidly quenched Kilauea Pu'u 'O'o lavas yield values that range from ~QFM–0.4 to QFM–1.7 (Roeder *et al.*, 2003).

Pousovetov & Roeder (2001) studied the partitioning of Cr between melt and spinel in a Kilauea basalt and obtained  $\sim$ QFM-0.5. Similar measurements are not available for Mauna Kea, so we accepted the range of estimates for Mauna Loa and Kilauea, QFM-0.5 to QFM-2, as bounding the redox conditions during low-pressure fractionation of olivine in the shield-building tholeiitic phases of this volcano.

Below  $\sim$ 7 wt % MgO, Hawaiian tholeiitic liquids become saturated with plagioclase and/or augite (Montierth *et al.*, 1995; Thornber *et al.*, 2003; Seaman *et al.*, 2004), so we restricted consideration to glasses with  $\geq$  7 wt % MgO; Table A2 lists average glass compositions for Mauna Kea, Mauna Loa, and Kilauea volcanoes (given in the on-line Supplementary Material). All three of these compositions and their calculated parental liquids, as described below, are within the compositional bounds over which  $K_{D,Fe^{+2}-Mg}$  can assumed to be constant based on our analysis given above. We compare reconstructed parental magma compositions for two constant values of  $K_{D,Fe^{+2}-Mg}$ : 0.34, the value most consistent with both our experimental data and the literature data (46–52 wt % SiO<sub>2</sub>,  $\leq$  3 wt % Na<sub>2</sub>O + K<sub>2</sub>O) under relevant redox conditions (i.e.,  $\leq$  QFM+0.25); and 0.30, the canonical value of Roeder & Emslie (1970).

Results of the parental melt calculations are shown in Fig. 7. Figure 7a shows the results of olivine addition calculations (given in Table A3 in the on-line Supplementary Material) to the “low-SiO<sub>2</sub>” glass composition of Mauna Kea (Table A2). Here, we explore the effects of varying the  $fO_2$  (QFM-0.5 to QFM-2), the target olivine composition (Fo<sub>90</sub> to Fo<sub>91</sub>), and  $K_{D,Fe^{+2}-Mg}$  (0.30–0.34) on the resulting parental liquid composition. The MgO contents of the calculated parental liquids vary from 15.5 (QFM-0.5, Fo<sub>90</sub>,  $K_{D,Fe^{+2}-Mg} =$

0.30) to 21.4 wt % (QFM–2, Fo<sub>91</sub>,  $K_{D,Fe^{+2}-Mg} = 0.34$ ), nearly spanning the range of estimated parental/primary Hawaiian magmas from the literature (see Fig. 7b; filled gray circles). Over these ranges in composition and  $fO_2$ , the calculated parental liquid compositions decrease by ~1 wt % MgO for every *log* unit increase in the selected  $fO_2$  (from QFM–2 to QFM–0.5), for every 0.5 decrease in the forsterite content of the residual olivine (from Fo<sub>91</sub> to Fo<sub>90</sub>), and every 0.015 decrease in  $K_{D,Fe^{+2}-Mg}$  (0.34–0.30). An important conclusion from these calculations is that, while holding  $fO_2$  and the forsterite content of residual olivine constant, a change in  $K_{D,Fe^{+2}-Mg}$  from 0.30–0.34 leads to an ~2.6 wt % increase in the MgO content of the reconstructed parental liquid.

The results of olivine-addition calculations with Mauna Loa and Kilauea glasses and Mauna Kea low- and high-SiO<sub>2</sub> glass compositions (Table A3) are shown in Fig. 7b. Here we used  $K_{D,Fe^{+2}-Mg}$  of 0.34 and  $fO_2$ s calculated from measured Fe<sub>2</sub>O<sub>3</sub>/FeO ratios in Mauna Loa and Kilauea lavas (and in the case of Kilauea, the Cr contents of these near-vent glasses); for Mauna Kea we assumed an  $fO_2$  of QFM–1, a conservative value consistent with estimates on Mauna Loa and Kilauea lavas (see Rhodes and Vollinger, 2005). Target olivine compositions, i.e., the endpoint of each olivine-addition calculation, were Fo<sub>90.8</sub> (Kilauea), Fo<sub>91.7</sub> (Mauna Loa), and Fo<sub>91.0</sub> (Mauna Kea). Calculated MgO contents for the parental Kilauea composition range from 19.0 to 19.7 depending on whether the  $fO_2$  is assumed to be QFM–0.7 (from Cr measurements of Roeder *et al.* 2003) or QFM–1.4 (based on Fe<sub>2</sub>O<sub>3</sub>/FeO measurements; Roeder *et al.*, 2003). The calculated MgO content of the Mauna Loa parental composition is 21.2 wt %. For the low- and high-SiO<sub>2</sub> Mauna Kea glasses, calculated MgO contents are 20.5 and 19.0 wt %, respectively.

For comparison, the filled gray circles in Fig. 7b show estimated MgO contents of parental/primary Hawaiian magmas from the literature (Wright, 1984; Clague *et al.*, 1991; Garcia *et al.*, 1995; Baker *et al.*, 1996; Rhodes, 1996; Green *et al.*, 2001; Herzberg & O'Hara, 2002; Rhodes & Vollinger, 2004; Stolper *et al.*, 2004; Herzberg, 2006; Herzberg *et al.*, 2007; Putirka, 2008a). For a given target olivine composition, relatively low MgO values generally reflect the use of a  $K_{D,Fe^{+2}-Mg}$  of 0.30 and/or an  $fO_2$  of ~QFM (or a fixed FeO/FeO\* ratio of 0.9), whereas high MgO estimates reflect the use of a  $K_{D,Fe^{+2}-Mg}$  of ~0.34 (e.g., Herzberg & O'Hara, 2002) or conditions more reducing than QFM (note that the initial FeO\* content of the starting composition also influences the final MgO value). If Hawaiian tholeiitic magmas undergoing shallow-level fractionation are as reducing as the near-vent glass FeO contents seem to suggest and if the rare  $> Fo_{90}$  olivines represent the earliest fractionation products of these magma, then it seems hard to avoid parental magma estimates with at least 18–19 wt % MgO. Such MgO-rich magmas have obvious implications for melting temperatures within the Hawaiian plume—a topic that is beyond the scope of this work—but one that has been addressed in a number of recent papers (e.g., Falloon *et al.*, 2007; Herzberg *et al.*, 2007; Putirka *et al.*, 2007).

## CONCLUSIONS

Our 1-atm experiments on a synthetic Hawaiian picrite composition (25.7 wt % MgO) yielded olivine-liquid pairs over a temperature range of ~1300 to 1500°C. For experiments conducted along the QFM buffer, olivine becomes progressively less forsteritic with decreasing temperature, i.e.,  $Fo_{92.3}$  to  $Fo_{87.3}$ . With increasing  $fO_2$  at constant temperature,

the modal abundance of olivine in our experiments decreases and the olivine becomes more forsteritic (e.g., at 1400°C, olivines are Fo<sub>90</sub> at QFM and Fo<sub>97</sub> in air), observations qualitatively consistent with MELTS calculations on the same bulk composition. MgO contents of the olivine-bearing glasses at QFM and NNO are approximately linear functions of temperature; an unweighted least-squares fit to our QFM data yields  $T(^{\circ}\text{C}) = 19.2 \times (\text{wt \% MgO in liquid}) + 1048$ , which can be used as a semi-quantitative geothermometer for Hawaiian glass or whole rock compositions with  $> \sim 7$  wt % MgO.

The olivine-liquid Fe<sup>+2</sup>-Mg exchange coefficient for our 11 experiments is  $0.345 \pm 0.009$  (mean and  $1\sigma$ , respectively), and is independent of temperature and liquid composition. The mean value from our QFM experiments,  $0.343 \pm 0.008$ , agrees well with the median value of  $0.340 \pm 0.012$  (MAD) from 78 olivine-glass pairs from the literature with broadly tholeiitic compositions (46–52 wt % SiO<sub>2</sub>,  $\leq 3$  wt % Na<sub>2</sub>O + K<sub>2</sub>O, and Fo<sub>80</sub>–Fo<sub>92</sub>) and run under similar  $f\text{O}_2$ s (QFM $\pm 0.25$ ). Within these bounds, olivine-liquid  $K_{\text{D,Fe}^{+2}\text{-Mg}}$ s calculated using FeO contents in the liquid based on eqn 12 of Jayasuriya *et al.* (2004) are approximately independent of composition and temperature.

Over the compositional range encompassed by Hawaiian tholeiitic lavas and their parental melts,  $K_{\text{D,Fe}^{+2}\text{-Mg}}$  is  $\sim 0.34$  and, given the redox conditions and a Fo content for the most magnesian olivine phenocrysts, a parental melt composition can be predicted. The calculated compositions of the parental melts are sensitive to input parameters, decreasing by  $\sim 1$  wt % MgO for every  $\log$  unit increase in the selected  $f\text{O}_2$ , every 0.5 decrease in the Fo content of the target olivine, and every 0.015 decrease in  $K_{\text{D,Fe}^{+2}\text{-Mg}}$ . For plausible ranges of redox conditions and Fo contents of the most MgO-rich olivine phenocrysts, the

parental liquids for Hawaiian tholeiites were highly magnesian, in the range of 19–21 wt % MgO for Kilauea, Mauna Loa, and Mauna Kea.

## ACKNOWLEDGEMENTS

We thank Ma Chi for assistance with the analytical work on the electron microprobe and are especially appreciative of Rebecca Lange for providing FeO wet chemical measurements. The comments of S. Parman, K. Putirka, and M. Toplis led to significant improvements in the text and a more careful look at the seminal work of Roeder and Emslie. Finally, we would very much like to acknowledge Peter Roeder for the truly amazing feat of locating an unpublished data table four decades after it was produced and his willingness to share it. This work was supported by NSF grant EAR-9528594, NASA grant NNX09AG40G, and an NSF GRF (AKM).

## REFERENCES

- Agee, C. B. & Walker, D. (1990). Aluminum partitioning between olivine and ultrabasic silicate liquid to 6 GPa. *Contributions to Mineralogy and Petrology* **105**, 243–254.
- Albarède, F. & Provost, A. (1977). Petrological and geochemical mass-balance equations: an algorithm for least-square fitting and general error analysis. *Computers and Geosciences* **3**, 309–326.
- Armstrong, J. T. (1988). Quantitative analysis of silicate and oxide materials: comparison of Monte Carlo, ZAF and  $\phi(\rho z)$  procedures. In: Newbury, D. E. (ed.) *Microbeam Analysis*. San Francisco: San Francisco Press, pp. 239–246.

- Baker, M. B., Alves, S. & Stolper, E. M. (1996). Petrography and petrology of the Hawaii Scientific Drilling Project lavas: Inferences from olivine phenocryst abundances and compositions. *Journal of Geophysical Research* **101**, 11715–11727.
- Beattie, P. Ford, C. & Russell, D. (1991). Partition coefficients for olivine-melt and orthopyroxene-melt systems. *Contributions to Mineralogy and Petrology* **109**, 212–224.
- Beckett, J. R. & Mendybaev, R. A. (1997). The measurement of oxygen fugacities in flowing gas mixtures at temperatures below 1200°C. *Geochimica et Cosmochimica Acta* **61**, 4331–4336.
- Bédard, J. H. (1994). A procedure for calculating the equilibrium distribution of trace elements among the minerals of cumulate rocks, and the concentration of trace elements in the coexisting liquids. *Chemical Geology* **118**, 143–153.
- Bédard, J. H. (2005). Partitioning coefficients between olivine and silicate melts. *Lithos* **83**, 394–419.
- Blichert-Toft, J., Weis, D., Maerschalk, C., Agranier, A. & Albarède, F. (2003). Hawaiian hot spot dynamics as inferred from the Hf and Pb isotope evolution of Mauna Kea volcano. *Geochemistry Geophysics Geosystems* **4**, 8704, doi: 10/1029/2002GC000340.
- Borisov, A. A. & Shapkin, A. I. (1989). New empirical equation of dependence of  $\text{Fe}^{3+}/\text{Fe}^{2+}$  ratio in natural melts on their composition, oxygen fugacity and temperature. *Geokhimiya* **1989**, (6), 892–897 [*Geochemistry International* (1989) **27** (1), 111–116].
- BVSP (1981). *Basaltic Volcanism on the Terrestrial Planets*. New York: Pergamon Press.
- Carmichael, I. S. E. (1991). The redox states of basic and silicic magmas: a reflection of their source regions? *Contributions to Mineralogy and Petrology* **106**, 129–141.
- Clague, D. A., Moore, J. G., Dixon, J. E. & Friesen, W. B. (1995). Petrology of submarine lavas from Kilauea's Puna Ridge, Hawaii. *Journal of Petrology* **36**, 299–349.
- Clague, D. A., Weber, W. S. & Dixon, J. E. (1991). Picritic glasses from Hawaii. *Nature* **353**, 553–556.

- Corrigan, G. & Gibb, F. G. F. (1979). The loss of Fe and Na from a basaltic melt during experiments using the wire-loop method. *Mineralogical Magazine* **43**, 121–126.
- Cottrell, E., Kelley, K. A., Lanzirotti, A. & Fischer, R. A. (2009). High-precision determination of iron oxidation state in silicate glasses using XANES. *Chemical Geology* **268**, 167–179.
- Drake, M. J. & Holloway, J. R. (1981). Partitioning of Ni between olivine and silicate melt: the 'Henry's Law problem' reexamined. *Geochimica et Cosmochimica Acta* **45**, 431–437.
- Eggins, S. M. (1992). Petrogenesis of Hawaiian tholeiites: 1, phase equilibria constraints. *Contributions to Mineralogy and Petrology* **110**, 387–397.
- Eugster, H. P. & Wones, D. R. (1962). Stability relations of the ferruginous biotite, annite. *Journal of Petrology* **3**, 82–125.
- Falloon, T. J., Danyushevsky, L. V., Ariskin, A., Green, D. H. & Ford, C. E. (2007). The application of olivine geothermometry to infer crystallization temperatures of parental liquids: Implications for the temperature of MORB magmas. *Chemical Geology* **241**, 207–233.
- Ford, C. E., Russell, D. G., Craven, J. A. & Fisk, M. R. (1983). Olivine-liquid equilibria: Temperature, pressure and composition dependence of the crystal/liquid cation partition coefficients for Mg, Fe<sup>2+</sup>, Ca and Mn. *Journal of Petrology* **24**, 256–265.
- Garcia, M. O. (1996). Petrography and olivine and glass chemistry of lavas from the Hawaii Scientific Drilling Project. *Journal of Geophysical Research* **101**, 11701–11713.
- Garcia, M. O., Hulsebosch, T. P. & Rhodes, J. M. (1995). Olivine-rich submarine basalts from the southwest rift zone of Mauna Loa Volcano: implications for magmatic processes and geochemical evolution. In: Rhodes, J. M. & Lockwood, J. P. (eds.) *Mauna Loa Revealed: Structure, Composition, History, and Hazards, Geophysical Monograph 92*. Washington, DC: American Geophysical Union, pp. 219–239.
- Gee, L. L. & Sack, R. O. (1988). Experimental petrology of melilite nephelinites. *Journal of Petrology* **29**, 1233–1255.

- Ghiorso, M. S. & Kress, V. C. (2004). An equation of state for silicate melts. II. Calibration of volumetric properties at  $10^5$  Pa. *American Journal of Science* **304**, 679–751.
- Ghiorso, M. S. & Sack, R. O. (1995). Chemical mass transfer in magmatic processes IV. A revised and internally consistent thermodynamic model for the interpolation and extrapolation of liquid-solid equilibria in magmatic systems at elevated temperatures and pressures. *Contributions to Mineralogy and Petrology* **119**, 197–212.
- Goldberg, R. N. & Weir, R. D. (1992). Conversion of temperatures and thermodynamic properties to the basis of the international temperature scale of 1990. *Pure and Applied Chemistry* **64**, 1545–1562.
- Green, D. H., Falloon, T. J., Eggins, S. M. & Yaxley, G. M. (2001). Primary magmas and mantle temperatures. *European Journal of Mineralogy* **13**, 437–451.
- Grove, T. L. (1981). Use of FePt alloys to eliminate the iron loss problem in 1 atmosphere gas mixing experiments: Theoretical and practical considerations. *Contributions to Mineralogy and Petrology* **78**, 298–304.
- Grove, T. L., Kinzler, R. J. & Bryan, W. B. (1992). Fractionation of mid-ocean ridge basalt (MORB). In: Morgan, J. P., Blackman, D. K. & Sinton, J. M. (eds.) *Mantle Flow and Melt Generation at Mid-Ocean Ridges, Geophysical Monograph 71*. Washington, DC: American Geophysical Union, pp. 281–310.
- Hanson, B. & Jones, J. H. (1998). The systematics of  $\text{Cr}^{+3}$  and  $\text{Cr}^{+2}$  partitioning between olivine and liquid in the presence of spinel. *American Mineralogist* **83**, 669–684.
- Hart, S. R. & Davis, K. E. (1978). Nickel partitioning between olivine and silicate melt. *Earth and Planetary Science Letters* **40**, 203–219.
- Helz, R. T. & Thornber, C. R. (1987). Geothermometry of Kilauea Iki lava lake, Hawaii. *Bulletin of Volcanology* **49**, 651–668.
- Herzberg, C. (2006). Petrology and thermal structure of the Hawaiian plume from Mauna Kea volcano. *Nature* **444**, 605–609.
- Herzberg, C. & O'Hara, M. J. (2002). Plume-associated ultramafic magmas of Phanerozoic age. *Journal of Petrology* **43**, 1857–1883.

- Herzberg, C., Asimow, P. D., Arndt, N., Niu, Y., Leshner, C. M., Fitton, J. G., Cheadle, M. J. & Saunders, A. D. (2007). Temperatures in ambient mantle and plumes: Constraints from basalts, picrites, and komatiites. *Geochemistry Geophysics Geosystems* **8**, Q02006, doi:10.1029/2006GC001390.
- Hill, R. & Roeder, P. (1974). The crystallization of spinel from basaltic liquid as a function of oxygen fugacity. *Journal of Geology* **82**, 709–729.
- Hirschmann, M. & Ghiorso, M. S. (1994). Activities of nickel, cobalt, and manganese silicates in magmatic liquids and applications to olivine/liquid and to silicate/metal partitioning. *Geochimica et Cosmochimica Acta* **58**, 4109–4126.
- Hirschmann, M. M., Ghiorso, M. S., Davis, F. A., Gordon, S. M., Mukherjee, S., Grove, T. L., Krawczynski, M., Medard, E. & Till, C. B. (2008). Library of experimental phase relations (LEPR): a database and web portal for experimental magmatic phase equilibria data. *Geochemistry Geophysics Geosystems* **9**, Q03011, doi: 10/1029/2007GC001894.
- Hofmann, A. W. & Jochum, K. P. (1996). Source characteristics derived from very incompatible trace elements in Mauna Loa and Mauna Kea basalts, Hawaii Scientific Drilling Project. *Journal of Geophysical Research* **101**, 11831–11839.
- Huebner, J. S. (1971). Buffering techniques for hydrostatic systems at elevated pressures. In: Ulmer, G. C. (ed.) *Research Techniques for High Pressure and High Temperature*. New York: Springer-Verlag, pp. 123–177.
- Jayasuriya, K. D., O'Neill, H. St. C., Berry, A. J. & Campbell, S. J. (2004). A Mössbauer study of the oxidation state of Fe in silicate melts. *American Mineralogist* **89**, 1597–1609.
- Kamenetsky, V. S., Crawford, A. J. & Meffre, S. (2001). Factors controlling chemistry of magmatic spinel: an empirical study of associated olivine, Cr-spinel and melt inclusions from primitive rocks. *Journal of Petrology* **42**, 655–671.
- Kauahikaua, J., Hildenbrand, T. & Webring, M. (2000). Deep magmatic structures of Hawaiian volcanoes, imaged by three-dimensional gravity models. *Geology* **28**, 883–886.

- Kilinc, A., Carmichael, I. S. E., Rivers, M. L. & Sack, R. O. (1983). The ferric-ferrous ratio of natural silicate liquids equilibrated in air. *Contributions to Mineralogy and Petrology* **83**, 136–140.
- Kress, V. C. & Carmichael, I. S. E. (1988). Stoichiometry of the iron oxidation reaction in silicate melts. *American Mineralogist* **73**, 1267–1274.
- Kress, V. C. & Carmichael, I. S. E. (1991). The compressibility of silicate liquids containing Fe<sub>2</sub>O<sub>3</sub> and the effect of composition, temperature, oxygen fugacity and pressure on their redox states. *Contributions to Mineralogy and Petrology* **108**, 82–92.
- Kushiro, I. & Mysen, B. O. (2002). A possible effect of melt structure on the Mg-Fe<sup>2+</sup> partitioning between olivine and melt. *Geochimica et Cosmochimica Acta* **66**, 2267–2272.
- Kushiro, I. & Walter, M. J. (1998). Mg-Fe partitioning between olivine and mafic-ultramafic melts. *Geophysical Research Letters* **25**, 2337–2340.
- Le Maitre, R. W. (1976). The chemical variability of some common igneous rocks. *Journal of Petrology* **17**, 589–637.
- Libourel, G. (1999). Systematics of calcium partitioning between olivine and silicate melt: implications for melt structure and calcium content of magmatic olivines. *Contributions to Mineralogy and Petrology* **136**, 63–80.
- Longhi, J. (1982). Effects of fractional crystallization and cumulus processes on mineral composition trends of some lunar and terrestrial rock series. *Proceedings of the Thirteenth Lunar and Planetary Science Conference, Part 1, Journal of Geophysical Research* **87**, Supplement, A54–A64.
- Longhi, J., Walker, D. & Hays, J. F. (1978). The distribution of Fe and Mg between olivine and lunar basaltic liquids. *Geochimica et Cosmochimica Acta* **42**, 1545–1558.
- Maaløe, S. (1979). Compositional range of primary tholeiitic magmas evaluated from major-element trends. *Lithos* **12**, 59–72.
- Macdonald, G. A. & Katsura, T. (1964). Chemical composition of Hawaiian lavas. *Journal of Petrology* **5**, 82–133.

- Mäkipää, H. T. (1980). Partitioning of chromium, manganese, cobalt and nickel between olivine and basaltic liquid; an experimental study. *Bulletin of the Geological Society of Finland* **52**, 175–191.
- Mallmann, G. & O'Neill, H. St. C. (2009). The crystal/melt partitioning of V during mantle melting as a function of oxygen fugacity compared with some other elements (Al, P, Ca, Sc, Ti, Cr, Fe, Ga, Y, Zr and Nb). *Journal of Petrology* **50**, 1765–1794.
- Médard, E., McCammon, C. A., Barr, J. A. & Grove, T. L. (2008). Oxygen fugacity, temperature reproducibility, and H<sub>2</sub>O contents of nominally anhydrous piston-cylinder experiments using graphite capsules. *American Mineralogist* **93**, 1838–1844.
- Montierth, C., Johnston, A. D. & Cashman, K. V. (1995). An empirical glass-composition-based geothermometer for Mauna Loa lavas. In: Rhodes, J. M. & Lockwood, J. P. (eds.) *Mauna Loa Revealed: Structure, Composition, History, and Hazards, Geophysical Monograph 92*. Washington, DC: American Geophysical Union, pp. 207–217.
- Muan, A. & Osborn, E. F. (1956). Phase equilibria at liquidus temperatures in the system MgO-FeO-Fe<sub>2</sub>O<sub>3</sub>-SiO<sub>2</sub>. *Journal of the American Ceramic Society* **39**, 121–140.
- Murck, B. W. & Campbell, I. H. (1986). The effects of temperature, oxygen fugacity and melt composition on the behaviour of chromium in basic and ultrabasic melts. *Geochimica et Cosmochimica Acta* **50**, 1871–1887.
- Mysen, B. O. (2006). Redox equilibria of iron and silicate melt structure: Implications for olivine/melt element partitioning. *Geochimica et Cosmochimica Acta* **70**, 3121–3138.
- Mysen, B. (2007). Partitioning of calcium, magnesium, and transition metals between olivine and melt governed by the structure of the silicate melt at ambient pressure. *American Mineralogist* **92**, 844–862.
- Mysen, B. O. & Dubinsky, E. V. (2004). Melt structural control on olivine/melt element partitioning of Ca and Mn. *Geochimica et Cosmochimica Acta* **68**, 1617–1633.

- Mysen, B. O. & Shang, J. (2005). Evidence from olivine/melt element partitioning that nonbridging oxygen in silicate melts are not equivalent. *Geochimica et Cosmochimica Acta* **69**, 2861–2875.
- Nielsen, R. L. & DeLong, S. E. (1992). A numerical approach to boundary layer fractionation: application to differentiation in natural magma systems. *Contributions to Mineralogy and Petrology* **110**, 355–369.
- Nisbet, E. G., Arndt, N. T., Bickle, M.J., Cameron, W. E., Chauvel, C., Cheadle, M., Hegner, E., Kyser, T. K., Martin, A., Renner, R., & Roedder, E. (1987) Uniquely fresh 2.7 Ga komatiites from the Belingwe greenstone belt, Zimbabwe. *Geology* **15**, 1147–1150.
- Norman, M. D. & Garcia, M. O. (1999). Primitive magmas and source characteristics of the Hawaiian plume: petrology and geochemistry of shield picrites. *Earth and Planetary Science Letters* **168**, 27–34.
- O'Neill, H. St. C. (1987). Quartz-fayalite-iron and quartz-fayalite-magnetite equilibria and the free energy of formation of fayalite ( $\text{Fe}_2\text{SiO}_4$ ) and magnetite ( $\text{Fe}_3\text{O}_4$ ). *American Mineralogist* **72**, 67–75.
- O'Neill, H. St.C., Berry, A. J., McCammon, C. C., Jayasuriya, K. D., Campbell, S. J., & Foran, G. (2006). An experimental determination of the effect of pressure on the  $\text{Fe}^{3+}/\Sigma\text{Fe}$  ratio of an anhydrous silicate melt to 3.0 GPa. *American Mineralogist* **91**, 404–412.
- Parman, S. W., Dann, J. C., Grove, T. L., & deWit, M. J. (1997). Emplacement conditions of komatiite magmas from the 3.49 Ga Komati Formation, Barberton Greenstone Belt, South Africa. *Earth and Planetary Science Letters* **150**, 303–323.
- Partzsch, G. M., Lattard, D. & McCammon, C. (2004). Mössbauer spectroscopic determination of  $\text{Fe}^{3+}/\text{Fe}^{2+}$  in synthetic basaltic glass: a test of empirical  $f\text{O}_2$  equations under superliquidus and subliquidus conditions. *Contributions to Mineralogy and Petrology* **147**, 565–580.
- Poustovetov, A. A. & Roeder, P. L. (2001). The distribution of Cr between basaltic melt and chromian spinel as an oxygen geobarometer. *The Canadian Mineralogist* **39**, 309–317.

- Powers, H. A. (1955). Composition and origin of basaltic magma of the Hawaiian Islands. *Geochimica et Cosmochimica Acta* **7**, 77–107.
- Press, W. H., Teukolsky, S. A., Vetterling, W. T. & Flannery, B. P. (1992). *Numerical Recipes, 2<sup>nd</sup> ed.* Cambridge: Cambridge University Press.
- Putirka, K. (2008a). Excess temperatures at ocean islands: Implications for mantle layering and convection. *Geology* **36**, 283–286.
- Putirka K. (2008b) Thermometers and barometers for volcanic systems. *Reviews in Mineralogy & Geochemistry* **69**, 61–120.
- Putirka, K. D., Perfit, M., Ryerson, F. J. & Jackson, M. G. (2007). Ambient and excess mantle temperatures, olivine thermometry, and active vs. passive upwelling. *Chemical Geology* **241**, 177–206.
- Rhodes, J. M. (1996). Geochemical stratigraphy of lava flows sampled by the Hawaii Scientific Drilling Project. *Journal of Geophysical Research* **101**, 11729–11746.
- Rhodes, J. M. & Vollinger, M. J. (2004). Composition of basaltic lavas sampled by phase-2 of the Hawaii Scientific Drilling Project: Geochemical stratigraphy and magma types. *Geochemistry Geophysics Geosystems* **5**, Q03G13, doi:10.1029/2002GC000434.
- Rhodes, J. M. & Vollinger, M. J. (2005). Ferric/ferrous ratios in 1984 Mauna Loa lavas: a contribution to understanding the oxidation state of Hawaiian magmas. *Contributions to Mineralogy and Petrology* **149**, 666–674.
- Righter, K., Drake, M. J. & Yaxley, G. (1997). Prediction of siderophile element metal-silicate partition coefficients to 20 GPa and 2800°C: the effects of pressure, temperature, oxygen fugacity, and silicate and metallic melt compositions. *Physics of the Earth and Planetary Interiors* **100**, 115–134.
- Robie, R. A., Hemingway, B. S. & Fisher, J. R. (1978). Thermodynamic properties of minerals and related substances at 298.15 K and 1 bar ( $10^5$  Pascals) pressure and at higher temperatures. *Geological Survey Bulletin* **1452**.
- Roedder, E. (1983). Geobarometry of ultramafic xenoliths from Loihi Seamount, Hawaii, on the basis of CO<sub>2</sub> inclusions in olivine. *Earth and Planetary Science Letters* **66**, 369–379.

- Roeder, P. L. (1974). Activity of iron and olivine solubility in basaltic liquids. *Earth and Planetary Science Letters* **23**, 397–410.
- Roeder, P. L. & Emslie, R. F. (1970). Olivine-liquid equilibrium. *Contributions to Mineralogy and Petrology* **29**, 275–289.
- Roeder, P. L., Thornber, C., Poustovetov, A. & Grant, A. (2003). Morphology and composition of spinel in Pu'u 'O'o lava (1996–1998), Kilauea volcano, Hawaii. *Journal of Volcanology and Geothermal Research* **123**, 245–265.
- Sack, R. O. Carmichael, I. S. E., Rivers, M. & Ghiorso, M. S. (1980). Ferric-ferrous equilibria in natural silicate liquids at 1bar. *Contributions to Mineralogy and Petrology* **75**, 369–376.
- Sack, R. O., Walker, D., & Carmichael, I. S. E. (1987). Experimental petrology of alkalic lavas: constraints on cotectics of multiple saturation in natural basic liquids. *Contributions to Mineralogy and Petrology* **96**, 1–23.
- Seaman, C., Sherman, S. B., Garcia, M. O., Baker, M. B., Balta, B. & Stolper, E. (2004). Volatiles in glasses from the HSDP2 drill core. *Geochemistry, Geophysics, Geosystems* **5**, Q09G16, doi:10.1029/2003GC000596.
- Smith, P. M. & Asimow, P. D. (2005). Adibat\_1ph: A new public front-end to the MELTS, pMELTS, and pHMELTS models. *Geochemistry, Geophysics, Geosystems* **6**, Q02004, doi:10.1029/2004GC000816.
- Snyder, D. A. & Carmichael, I. S. E. (1992). Olivine-liquid equilibria and the chemical activities of FeO, NiO, Fe<sub>2</sub>O<sub>3</sub>, and MgO in natural basic melts. *Geochimica et Cosmochimica Acta* **56**, 303–318.
- Sobolev, A. V. & Nikogosian, I. K. (1994). Petrology of long-lived mantle plume magmatism: Hawaii, Pacific, and Reunion Island, Indian Ocean. *Petrology* **2**, 111–144.
- Sobolev, A. V., Hofmann, A. W., Kuzmin, D. V., Yaxley, G. M., Arndt, N. T., Chung, S-L., Danyushevsky, L. V., Elliott, T., Frey, F. A., Garcia, M. O., Gurenko, A. A., Kamenetsky, V. S., Kerr, A. C., Krivolustskaya, N. A., Matvienkov, V. V., Nikogosian, I. K., Rocholl, A., Sigurdsson, I. A., Sushchevskaya, N. M., & Teklay,

- M. .(2007). The amount of recycled crust in sources of mantle-derived melts. *Science* **316**, 412–417.
- Stolper, E., Sherman, S., Garcia, M., Baker, M. & Seaman, C. (2004). Glass in the submarine section of the HSDP2 drill core, Hilo, Hawaii. *Geochemistry, Geophysics, Geosystems* **5**, Q07G15, doi:10.1029/2003GC000553.
- Sugawara, T. (2000). Empirical relationships between temperature, pressure, and MgO content in olivine and pyroxene saturated liquid. *Journal of Geophysical Research* **105**, 8457–8472.
- Thornber, C. R., Heliker, C., Sherrod, D. R., Kauahikaua, J. P., Miklus, A., Okubo, P. G., Trusdell, F. A., Budahn, J. R., Ridley, W. I., & Meeker, G. P., (2003). Kilauea East Rift Zone magmatism: an episode 54 perspective. *Journal of Petrology* **44**, 1525–1559.
- Thy, P. (1995). Low-pressure experimental constraints on the evolution of komatiites. *Journal of Petrology* **36**, 1529–1548.
- Thy, P., Leshner, C. E., Nielsen, T. F. D. & Brooks, C. K. (2006). Experimental constraints on the Skaergaard liquid line of descent. *Lithos* **92**, 154–180.
- Toplis, M. J. (2005). The thermodynamics of iron and magnesium partitioning between olivine and liquid: criteria for assessing and predicting equilibrium in natural and experimental systems. *Contributions to Mineralogy and Petrology* **149**, 22–39.
- Tsuchiyama, A., Nagahara, H. & Kushiro, I. (1981). Volatilization of sodium from silicate melt spheres and its application to the formation of chondrules. *Geochimica et Cosmochimica Acta* **45**, 1357–1367.
- Wagner, T. P. & Grove, T. L. (1998). Melt/harzburgite reaction in the petrogenesis of tholeiitic magma from Kilauea volcano, Hawaii. *Contributions to Mineralogy and Petrology* **131**, 1–12.
- Walter, M. J. (1998). Melting of garnet peridotite and the origin of komatiite and depleted lithosphere. *Journal of Petrology* **39**, 29–60.
- Wilson, A. D. (1960). The micro determination of ferrous iron in silicate-minerals by a volumetric and a colorimetric method. *Analyst* **85**, 823–827.

- Wright, T. L. (1984). Origin of Hawaiian tholeiite: a metasomatic model. *Journal of Geophysical Research* **89**, 3233–3252.
- Xirouchakis, D., Hirschmann, M. M. & Simpson, J. A. (2001). The effect of titanium on the silica content and on mineral-liquid partitioning of mantle-equilibrated melts. *Geochimica et Cosmochimica Acta* **65**, 2201-2217.
- Yokoyama, T. & Nakamura, E. (2002). Precise determination of ferrous iron in silicate rocks. *Geochimica et Cosmochimica Acta* **66**, 1085–1093.
- Yu, Y., Hewins, R. H., Alexander, C. M. O'D. & Wang, J. (2003). Experimental study of evaporation and isotopic mass fractionation of potassium in silicate melts. *Geochimica et Cosmochimica Acta* **67**, 773–786.

**TABLES**

Table 1. Starting composition

|                      | SiO <sub>2</sub> | TiO <sub>2</sub> | Al <sub>2</sub> O <sub>3</sub> | Cr <sub>2</sub> O <sub>3</sub> | FeO*  | MnO   | MgO   | CaO  | Na <sub>2</sub> O | K <sub>2</sub> O | P <sub>2</sub> O <sub>5</sub> | NiO   |
|----------------------|------------------|------------------|--------------------------------|--------------------------------|-------|-------|-------|------|-------------------|------------------|-------------------------------|-------|
| HP-25 <sup>a</sup>   | 45.15            | 1.40             | 7.51                           | 0.217                          | 11.97 | 0.179 | 25.34 | 6.68 | 1.18              | 0.075            | 0.133                         | 0.155 |
| Syn-HP1 <sup>b</sup> | 45.72            | 1.42             | 7.61                           | 0.219                          | 12.12 | 0.182 | 25.67 | 6.77 | 0                 | 0                | 0                             | 0.292 |

<sup>a</sup> Mauna Kea picrite composition calculated from unweighted linear regression equations for bulk rock major- and minor-oxides versus MgO and an MgO value of 25; bulk rock data from Rhodes and Vollinger (2004). The reported composition is normalized to 100 wt % with all Fe as FeO (FeO\*), which leads to MgO slightly greater than 25.

<sup>b</sup> Syn-HP1 represents the HP-25 composition after increasing the NiO by 0.133 (the wt % of P<sub>2</sub>O<sub>5</sub> in HP-25) and then renormalizing the composition on an Na<sub>2</sub>O-, K<sub>2</sub>O-, and P<sub>2</sub>O<sub>5</sub>-free basis.

Table 2. Run conditions and experimental results

| Run# | Temp<br>(°C) | Time<br>(hrs) | logfO <sub>2</sub> | Loop #<br>& usage <sup>b</sup> | ΔFeO*<br>% <sup>c</sup> | ΔNa <sub>2</sub> O<br>wt % <sup>d</sup> | Phases<br>products <sup>e</sup> | Phase proportions <sup>f</sup> |
|------|--------------|---------------|--------------------|--------------------------------|-------------------------|---|---------------------------------|--------------------------------|
| 43   | 1600         | 0.5           | -4.7 <sup>a</sup>  | 8/6                            | -                       | 0.05                                    | gl                              | 100                            |
| 34   | 1551         | 5.0           | -5.1 <sup>a</sup>  | 8/5                            | -                       | bdl                                     | gl                              | 100                            |
| 26   | 1500         | 12.4          | -5.51              | 6/3                            | 0.8                     | 0.22                                    | gl, oliv                        | 93.3(5), 6.8(6)                |
| 24   | 1451         | 24.9          | -5.93              | 5/4                            | -2.2                    | 0.22                                    | gl, oliv                        | 83.6(4), 16.4(6)               |
| 21   | 1452         | 48.2          | -5.92              | 5/3                            | -5.2                    | 0.25                                    | gl, oliv                        | 83.5(4), 16.5(6)               |
| 17   | 1401         | 48.2          | -6.38              | 4/3                            | -2.6                    | 0.39                                    | gl, oliv                        | 76.3(4), 23.7(5)               |
| 27   | 1398         | 24.9          | -6.39              | 4/4                            | -3.3                    | 0.05                                    | gl, oliv                        | 77.1(4), 22.9(6)               |
| 39   | 1396         | 50.1          | -0.68              | 7/3                            | 0.3                     | 0.34                                    | gl, oliv                        | 83.1(4), 16.9(6)               |
| 28   | 1350         | 48.5          | -5.99              | 2/4                            | 0.3                     | 0.04                                    | gl, oliv, sp                    | 70.7(3), 29.2(5), 0.10(3)      |
| 15   | 1349         | 66.7          | -6.87              | 2/3                            | -2.2                    | 0.41                                    | gl, oliv, sp                    | 69.2(3), 30.7(5), 0.10(3)      |
| 6    | 1302         | 22.3          | -7.36              | 1/4                            | -6.4                    | 0.22                                    | gl, oliv, sp                    | 63.4(3), 36.4(5), 0.16(2)      |
| 46   | 1300         | 48.1          | -7.41              | 1/9                            | 0.5                     | 0.05                                    | gl, oliv, sp                    | 64.0(3), 35.8(4), 0.13(2)      |
| 8    | 1302         | 72.0          | -7.36              | 1/5                            | -0.4                    | 0.30                                    | gl, oliv, sp                    | 63.3(3), 36.6(5), 0.15(3)      |

Note: All runs except numbers 28 and 39 were conducted at ~QFM. The oxygen fugacity of run 28 was

held at ~NNO, while run 39 was equilibrated in air.

- <sup>a</sup> Oxygen fugacity was not measured during the superliquidus runs to prevent sensor degradation at these high temperatures. The gas mixture was set, at a lower T, to a value that would yield the desired  $f_{O_2}$  at the actual run temperature.
- <sup>b</sup> First number is the loop designation number; second value is the number of experiments that had been run with the loop prior to the present experiment.
- <sup>c</sup> Relative change (in percent) of FeO\* in the bulk composition based on mass balance; negative sign denotes a decrease in FeO\*.
- <sup>d</sup> Calculated addition of Na<sub>2</sub>O (in wt %) to the bulk composition based on the sodium content of the glass and mass balance. Na<sub>2</sub>O in run 34 was below the detection limit (bdl).
- <sup>e</sup> Abbreviations: gl=glass (quenched liquid), ol=olivine, sp=spinel.
- <sup>f</sup> Phase proportions (in wt %) in all subliquidus experiments are given in the same order as listed in the phase products column. Numbers in parenthesis are uncertainties in terms of the least units cited, e.g., 0.10(3) corresponds to  $0.10 \pm 0.03$ , where 0.03 is one standard deviation. Uncertainties were estimated using the method of Albarède & Provost (1977) after the sodium and iron gain/loss was calculated for each experiment.

Table 3. Phase compositions

| Run | Ph | SiO <sub>2</sub> | TiO <sub>2</sub> | Al <sub>2</sub> O <sub>3</sub> | Cr <sub>2</sub> O <sub>3</sub> | FeO*      | MnO     | MgO       | CaO      | NiO     | Na <sub>2</sub> O | Sum    |
|-----|----|------------------|------------------|--------------------------------|--------------------------------|-----------|---------|-----------|----------|---------|-------------------|--------|
| 43  | gl | 46.19(23)        | 1.38(2)          | 8.32(7)                        | 0.20(2)                        | 11.95(14) | 0.16(3) | 25.59(14) | 6.79(2)  | 0.22(1) | 0.05(1)           | 100.87 |
| 34  | gl | 45.87(22)        | 1.42(2)          | 8.35(9)                        | 0.21(2)                        | 11.65(19) | 0.15(3) | 25.89(10) | 6.83(3)  | 0.17(3) | bdl               | 100.59 |
| 26  | gl | 46.33(20)        | 1.49(3)          | 8.80(7)                        | 0.19(2)                        | 12.31(23) | 0.17(3) | 23.90(14) | 7.36(5)  | 0.18(5) | 0.09(4)           | 100.85 |
| 26  | ol | 41.30(14)        | 0.01(1)          | 0.09(2)                        | 0.09(1)                        | 7.52(8)   | 0.10(1) | 50.53(16) | 0.21(1)  | 0.65(1) | –                 | 100.51 |
| 24  | gl | 47.35(31)        | 1.64(2)          | 9.92(8)                        | 0.21(1)                        | 12.31(20) | 0.17(2) | 20.76(9)  | 8.13(7)  | 0.14(2) | 0.16(3)           | 100.81 |
| 24  | ol | 41.28(14)        | 0.01(1)          | 0.10(1)                        | 0.11(1)                        | 8.64(7)   | 0.10(1) | 49.93(19) | 0.23(1)  | 0.61(2) | –                 | 101.02 |
| 21  | gl | 47.10(25)        | 1.67(4)          | 9.96(9)                        | 0.19(1)                        | 11.8(2)   | 0.16(3) | 21.04(14) | 8.18(4)  | 0.15(4) | 0.29(4)           | 100.57 |
| 21  | ol | 41.00(12)        | 0.01(1)          | 0.10(2)                        | 0.10(1)                        | 8.39(7)   | 0.11(1) | 49.94(13) | 0.22(1)  | 0.58(1) | –                 | 100.45 |
| 17  | gl | 48.06(26)        | 1.81(4)          | 10.78(9)                       | 0.21(1)                        | 12.35(20) | 0.18(4) | 18.11(8)  | 8.86(5)  | 0.11(2) | 0.51(3)           | 101.01 |
| 17  | ol | 40.94(15)        | 0.02(1)          | 0.10(2)                        | 0.12(1)                        | 9.62(8)   | 0.12(1) | 49.12(10) | 0.25(1)  | 0.59(2) | –                 | 100.89 |
| 27  | gl | 47.87(28)        | 1.80(3)          | 10.64(6)                       | 0.23(2)                        | 12.01(26) | 0.16(3) | 18.41(20) | 8.81(4)  | 0.13(3) | 0.08(2)           | 100.17 |
| 27  | ol | 40.76(14)        | 0.02(1)          | 0.09(1)                        | 0.12(1)                        | 9.74(8)   | 0.12(1) | 48.49(24) | 0.23(1)  | 0.65(2) | –                 | 100.20 |
| 39  | gl | 46.71(23)        | 1.67(4)          | 9.86(10)                       | bdl                            | 13.80(16) | 0.17(3) | 19.51(16) | 8.15(5)  | 0.15(3) | 0.40(4)           | 100.45 |
| 39  | ol | 42.22(10)        | 0.01(1)          | 0.11(1)                        | bdl                            | 3.05(4)   | 0.10(1) | 54.68(13) | 0.16(1)  | 0.91(3) | –                 | 101.24 |
| 28  | gl | 48.40(27)        | 1.95(5)          | 11.47(7)                       | 0.18(2)                        | 12.45(23) | 0.17(3) | 15.95(13) | 9.63(4)  | 0.11(4) | 0.05(3)           | 100.36 |
| 28  | ol | 40.48(9)         | 0.02(1)          | 0.15(11)                       | 0.11(1)                        | 10.73(11) | 0.13(1) | 47.70(23) | 0.26(3)  | 0.80(1) | –                 | 100.39 |
| 28  | sp | 0.14(3)          | 1.07(2)          | 17.39(22)                      | 45.43(67)                      | 19.70(12) | 0.20(4) | 14.80(14) | –        | 0.51(2) | –                 | 99.24  |
| 15  | gl | 48.78(18)        | 1.97(3)          | 11.89(8)                       | 0.19(2)                        | 12.23(24) | 0.16(3) | 15.40(12) | 9.73(6)  | 0.09(3) | 0.60(4)           | 101.07 |
| 15  | ol | 40.82(12)        | 0.01(1)          | 0.09(1)                        | 0.12(1)                        | 10.87(8)  | 0.14(1) | 48.27(12) | 0.25(1)  | 0.60(2) | –                 | 101.17 |
| 15  | sp | 0.0              | 1.12(5)          | 18.7(4)                        | 47.3(1.0)                      | 17.45(14) | 0.22(3) | 14.4(9)   | –        | 0.34(3) | –                 | 99.23  |
| 6   | gl | 49.84(14)        | 2.18(4)          | 13.15(10)                      | 0.15(1)                        | 10.86(16) | 0.16(3) | 13.20(12) | 10.58(7) | 0.09(3) | 0.35(3)           | 100.56 |
| 6   | ol | 40.33(19)        | 0.03(1)          | 0.09(1)                        | 0.11(1)                        | 11.51(13) | 0.15(1) | 47.38(20) | 0.27(1)  | 0.53(2) | –                 | 100.38 |
| 6   | sp | 0.0              | 1.20(5)          | 20.7(1.4)                      | 44.8(1.7)                      | 17.54(16) | 0.21(2) | 14.74(49) | –        | 0.31(2) | –                 | 98.86  |
| 8   | gl | 49.18(28)        | 2.21(3)          | 12.74(13)                      | 0.16(2)                        | 11.65(16) | 0.16(2) | 13.37(10) | 10.69(7) | 0.08(4) | 0.48(5)           | 100.74 |
| 8   | ol | 40.26(15)        | 0.03(1)          | 0.08(2)                        | 0.10(1)                        | 12.17(11) | 0.15(1) | 46.87(12) | 0.27(1)  | 0.55(2) | –                 | 100.47 |
| 8   | sp | 0.0              | 1.23(1)          | 19.7(6)                        | 45.0(4)                        | 18.48(10) | 0.22(2) | 14.43(34) | –        | 0.33(3) | –                 | 99.18  |
| 46  | gl | 49.18(17)        | 2.16(2)          | 12.80(9)                       | 0.16(2)                        | 11.99(7)  | 0.17(2) | 14.01(11) | 10.51(3) | 0.07(1) | 0.07(1)           | 101.13 |
| 46  | ol | 40.69(29)        | 0.03(1)          | 0.07(3)                        | 0.12(1)                        | 12.03(5)  | 0.14(1) | 46.9(3)   | 0.26(2)  | 0.55(2) | –                 | 100.83 |
| 46  | sp | 0.08(15)         | 1.22(3)          | 21.0(6)                        | 43.71(3)                       | 17.69(11) | 0.22(2) | 15.1(4)   | –        | 0.31(3) | –                 | 99.33  |

Note: All compositions listed in wt %. Abbreviations: gl = glass; ol = olivine; sp = spinel. Numbers in parenthesis are analytical uncertainties in terms of the least units cited, e.g., 46.19(23) corresponds to  $46.19 \pm 0.23$  where 0.23 is one standard sample deviation; when the error is  $\geq 1.0$ , we include the decimal point. FeO\* = all Fe as FeO. Dashed line indicates that the element was not analyzed, bdl = below detection limit. K<sub>2</sub>O in the glass was measured but below detection limits for all but one of our experiments. Run 21 had  $0.03 \pm 0.02$  wt % K<sub>2</sub>O. Spinel compositions in runs 15, 6, and 8 were corrected for fluorescence and beam overlap onto adjacent glass and/or olivine (spinel in these three runs are  $< 5 \mu\text{m}$  in diameter). The silica content of the spinel was used as a proxy for the extent of glass and/or olivine “contamination”. The average compositions of olivine and glass (in wt %) were subtracted from each spinel analysis so as to minimize the sum of  $(\text{SiO}_2^{\text{sp}})^2 + (2-B)^2 + (1-A)^2 + (100-\Sigma)^2$ , where A and B are the sum of the cations in the A and B sites of an AB<sub>2</sub>O<sub>4</sub> spinel, respectively, and  $\Sigma$  is the oxide wt % sum of the spinel analysis (including calculated Fe<sub>2</sub>O<sub>3</sub>). Thus, the silica content of average spinel in these three runs is zero. In each of these runs, the average corrected spinel composition overlaps with the small number of low-silica spinel analyses ( $< 0.5$  wt % SiO<sub>2</sub>) suggesting that our correction procedure does not introduce a compositional bias. Glass FeO contents, measured by wet chemistry (Wilson, 1960), in runs 26 and 39 are 10.51(10) and 3.08(10) wt % respectively. The  $1\sigma$  uncertainty in parenthesis is based on replicate analyses of secondary standards.

**FIGURE CAPTIONS**

**Fig. 1.** Concentrations of oxides (wt %) in the experimental glasses as a function of run temperature (°C). Symbol indicates the oxygen fugacity: circles = QFM, diamond = NNO, triangle = air; open circles for the 1550 and 1600°C data indicate superliquidus experiments. Error bars represent one standard deviation and, where not visible, are smaller than the size of the symbols. (a) SiO<sub>2</sub>. (b) TiO<sub>2</sub>. (c) MgO. Lines are for MgO-T(°C) regressions from this study, for Kilauea (Kil) and Mauna Loa (ML) basalts by Helz & Thornber (1987) and Montierth *et al.* (1995), and for Barberton (BK) and Ontario (OK) komatiites by Thy (1995) and Parman *et al.* (1997). (d) FeO\*, all Fe as FeO.

**Fig. 2.** (a) Weight percent of liquid (closed symbols) and olivine (open symbols) determined by mass balance (Table 2) for ~QFM experiments. Solid black curves are polynomial fits: liquid (wt %) =  $243.1 - 0.3847(T) + 1.896 \times 10^{-4}(T)^2$ ; olivine (wt %) =  $-150.4 + 0.394(T) - 1.925 \times 10^{-4}(T)^2$ , where T is the temperature in °C. Proportions of liquid and olivine as calculated by MELTS at QFM (with spinel suppressed; i.e., not allowed to crystallized) are not shown as they are virtually identical to our polynomial fits. (b) Weight percent liquid versus the deviation in  $\log f_{O_2}$  from QFM (O'Neill, 1987) at the same temperature. Shape of the symbol indicates the oxygen fugacity of the experiment. The very slight offset of our QFM experiments from zero reflects differences between the QFM expression of Eugster & Wones (1962), which was quoted in Huebner (1971) and used to set the experimental conditions, and that of O'Neill (1987). MELTS calculations on our analyzed bulk composition (run 43, Table 3) at 1350 and 1400°C as a function of  $f_{O_2}$  are

shown by solid gray curves. Spinel was suppressed in the MELTS calculations because the program predicts substantially higher spinel modes (2–3 wt % in air at 1400°C) than are observed in our experiments (0.1–0.2 wt %).

**Fig. 3.** Olivine-liquid  $K_{D,Fe^{+2}-Mg}$  versus (a) MgO contents of the liquid and (b) temperature (°C). In both panels, symbol shape denotes the  $fO_2$  of the experiment (see also the caption to Fig. 1) and black symbols indicate that  $Fe^{+2}$  in the liquid was calculated using eqn 12 of Jayasuriya *et al.* (2004). Gray symbols represent experiments where the FeO content of the quenched liquid was measured by wet chemistry (see Table 2).

**Fig. 4.** Histograms of projected olivine-liquid  $K_{D,Fe^{+2}-Mg}$  values for QFM $\pm$ 0.25 experiments from the literature (see on-line Supplementary Material at <http://www.petrology.oxfordjournals.org/> for references) based on quenched liquid FeO contents calculated using  $Fe^{+3}/Fe^{+2}$  algorithms of: (a) Kilinc *et al.* (1983), (b) Kress & Carmichael (1991), (c) Borisov & Shapkin (1989), (d) eqn 12 of Jayasuriya *et al.* (2004), and (e) Ghiorso & Kress (2004). Median values and mean absolute deviations (based on the median value) are given for each panel. The projection scheme, which removes much (but not all) of the effects of liquid and olivine composition on  $K_{D,Fe^{+2}-Mg}$ , is described in the text and in more detail in the on-line Supplemental Material.

**Fig. 5.** Median and individual projected  $K_{D,Fe^{+2}-Mg}$  values as a function of the deviation in  $\log fO_2$  from QFM (O'Neill, 1987); projection methods are described in the text and in

more detail in the on-line Supplementary Material. Filled black circles are median values for literature data based on eqn 12 of Jayasuriya *et al.* (2004); data were binned in groups with  $\log fO_2$  in the range of  $\leq IW+0.5$ ,  $QFM\pm 0.25$ ,  $QFM+1.5\pm 0.5$ ,  $QFM+4.5\pm 0.5$ , and air. Open circles are from literature experiments with measured FeO contents; filled gray circles are the QFM and air experiments from this study (Table 2). Numbers adjacent to symbols are the number of experiments represented by the point; if  $> 1$ , then the plotted values are medians, the y-axis error bars represent mean absolute deviations, and the x-axis error bars are 1 standard deviation with respect to  $\Delta QFM$ , the deviation in  $\log fO_2$  from the QFM buffer at the same temperature. For the three open circles that represent a single  $K_{D,Fe^{+2}-Mg}$  value (Mysen 2006, and the two filled-gray circles (this study), the y-axis errors represent uncertainties on the  $K_{D,Fe^{+2}-Mg}$  obtained from propagating the  $1\sigma$  uncertainties associated with the FeO and MgO contents of the quenched melts and olivines. The unusually large error bars associated with the three open circles reflect the uncertainties associated with the MgO and FeO contents of the olivines in the experiments of Mysen (2006). References for the other literature data are given in the on-line Supplementary Material.

**Fig. 6.**  $K_{D,Fe^{+2}-Mg}$  vs. function of  $Na_2O + K_2O$  (wt %) for  $QFM\pm 0.25$  data from this study (filled black circles) and literature data (filled gray circles) based on eqn. 12 of Jayasuriya *et al.* (2004). References for the literature data are given in the on-line Supplementary Material.

**Fig. 7.** (a) Ol-liq  $K_{D,Fe^{+2}-Mg}$  and the MgO content (in wt %) of calculated parental magmas produced by near-fractional olivine addition to the mean composition of the undegassed “low-SiO<sub>2</sub>” glasses (Table A2; see the on-line Supplementary Material) from the Mauna Kea portion of the HSDP2 core (Stolper *et al.*, 2004). The near-fractional olivine-addition calculation is described in the notes to Table A3 (see the on-line Supplementary Material); the  $fO_2$  (relative to QFM; O’Neill, 1987) and the endpoint olivine composition is given for each pair of calculations (closed circles for  $K_{D,Fe^{+2}-Mg} = 0.30$ ; open circles for  $K_{D,Fe^{+2}-Mg} = 0.34$ ). Calculated compositions are reported in Table A3. (b) Estimated parental MgO contents for Mauna Loa, Kilauea, and Mauna Kea volcanoes (this study) as a function of target olivine  $100 \times Mg/(Mg + Fe)$ , atomic. Starting compositions are given in Table A2; calculated liquids are reported in Table A3. All calculations were carried out using  $K_{D,Fe^{+2}-Mg} = 0.34$  and various  $\log fO_2$  values relative to QFM (O’Neill, 1987), which are given next to symbol in the panel. Values of  $-1.8$  (Mauna Loa) and  $-1.4$  (Kilauea) represent median  $\Delta QFM$  values based on  $Fe^{+3}/Fe^{+2}$  measurements of Rhodes & Vollinger (2005) and Roeder *et al.* (2003), respectively. The value of  $-0.7$  for one of the Kilauea points is the median  $\Delta QFM$  based on glass Cr contents (Roeder *et al.*, 2003) and the algorithm of Poustovetov and Roeder (2001). For the two Mauna Kea (MK) calculations,  $\Delta QFM$  was assumed to be  $-1$ . The small filled gray circles are estimates of parental or primary Hawaiian magma compositions from Wright (1984), Clague *et al.* (1991), Garcia (1995), Baker *et al.* (1996), Rhodes (1996), Green *et al.* (2001), Herzberg and O’Hara (2002), Rhodes & Vollinger (2004), Stolper *et al.* (2004), Herzberg (2006), Herzberg *et al.* (2007), and Putirka (2008a).

## FIGURES

Fig. 1.

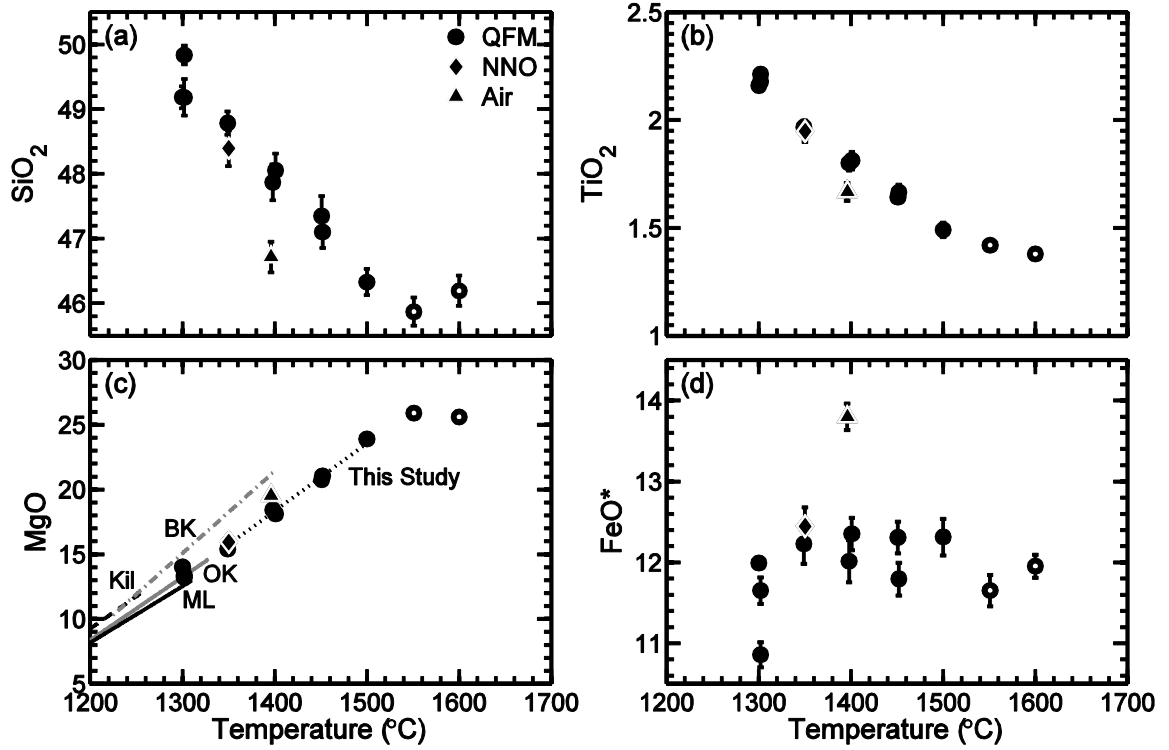


Fig. 2.

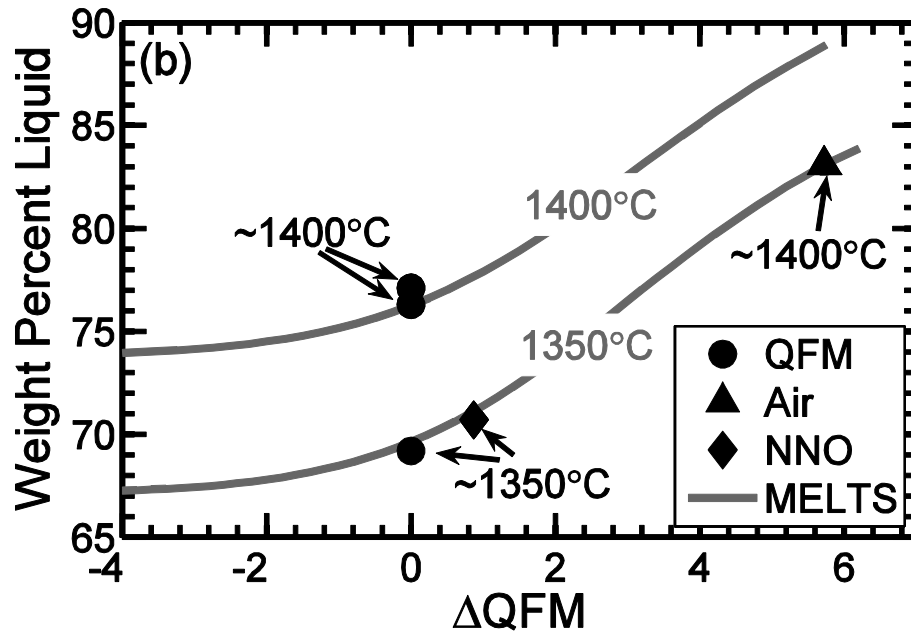
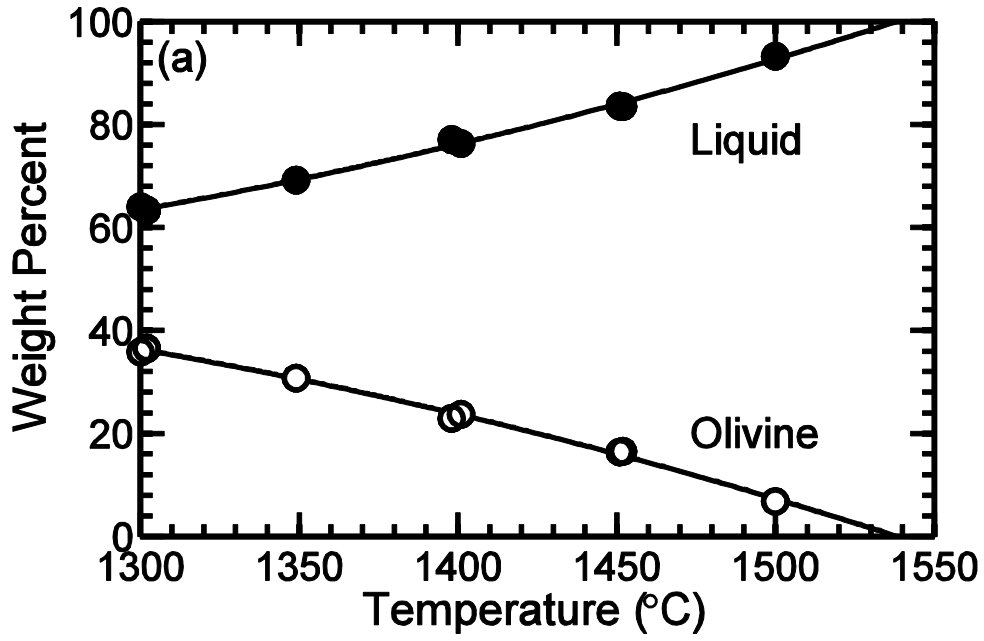


Fig. 3.

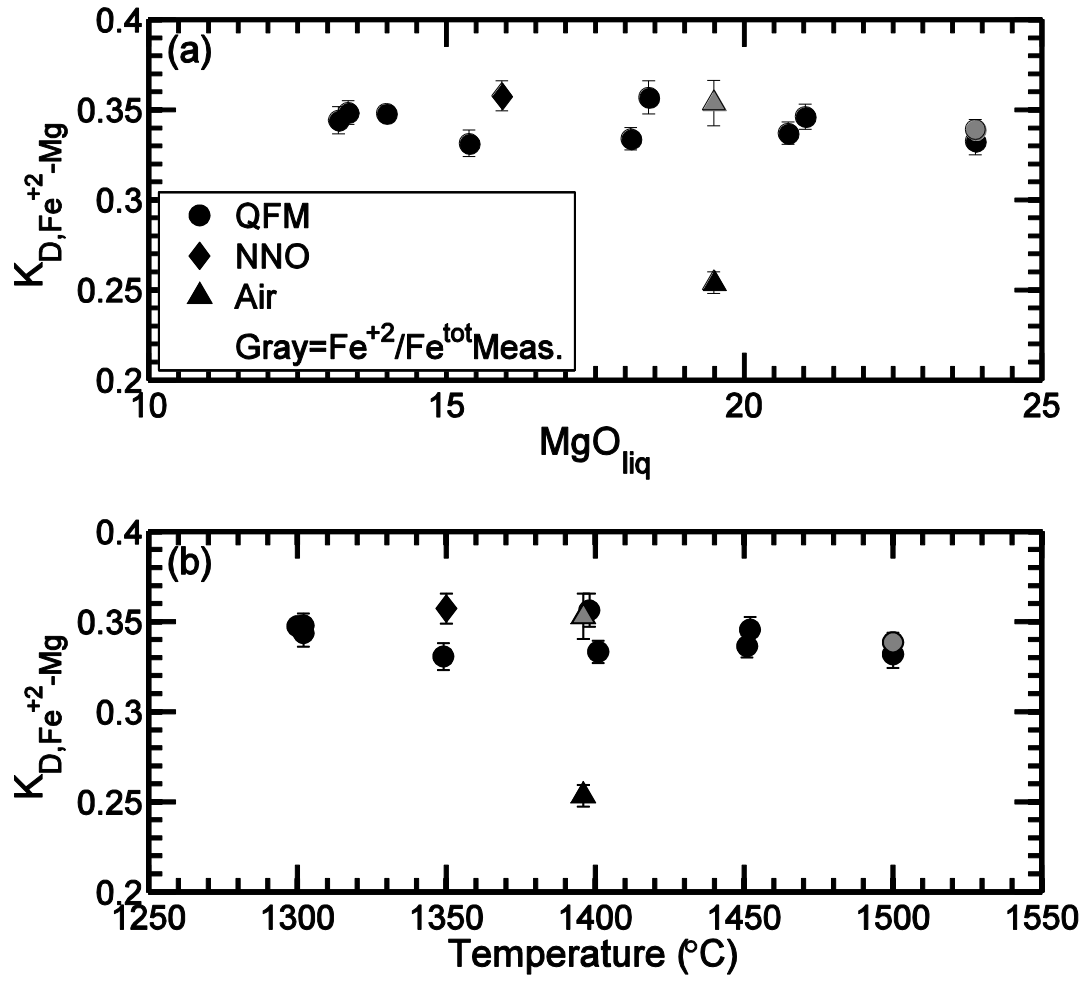


Fig. 4.

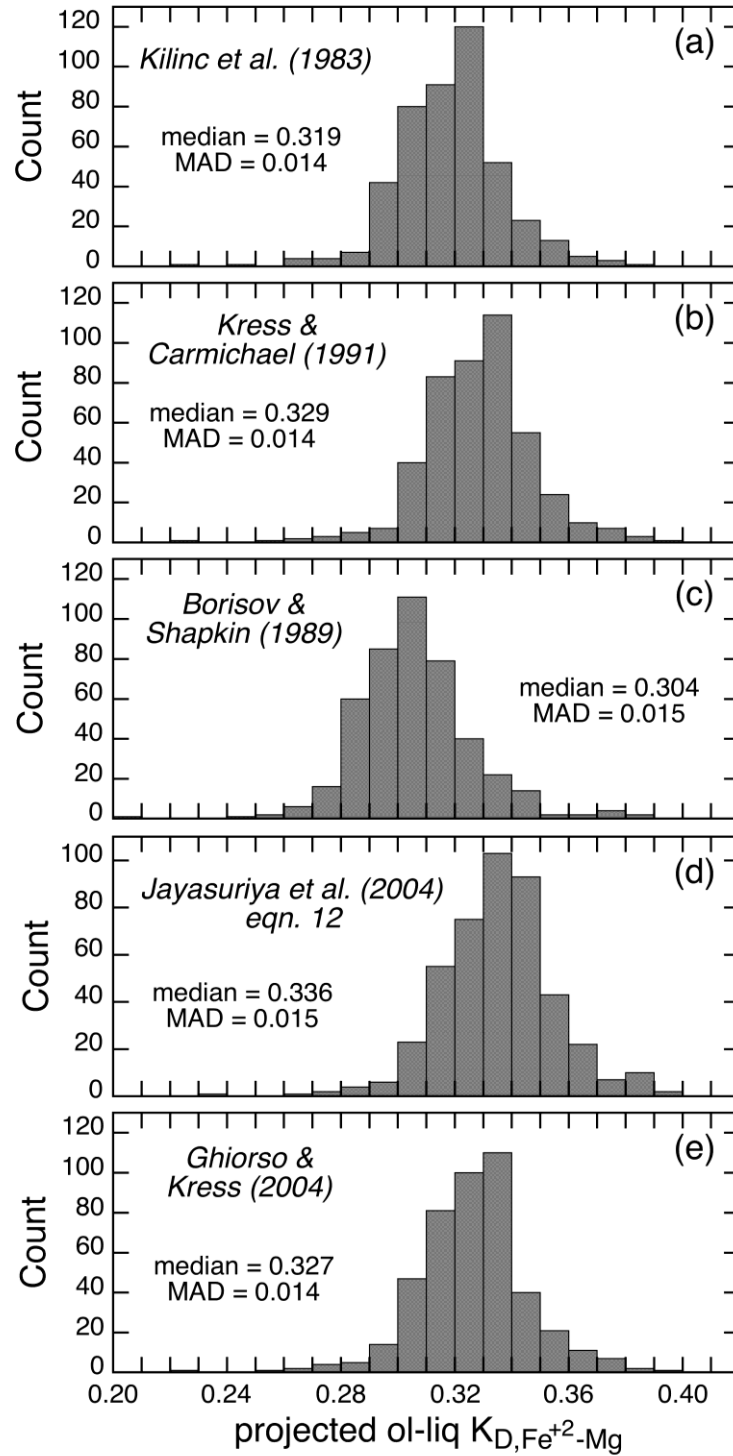


Fig. 5.

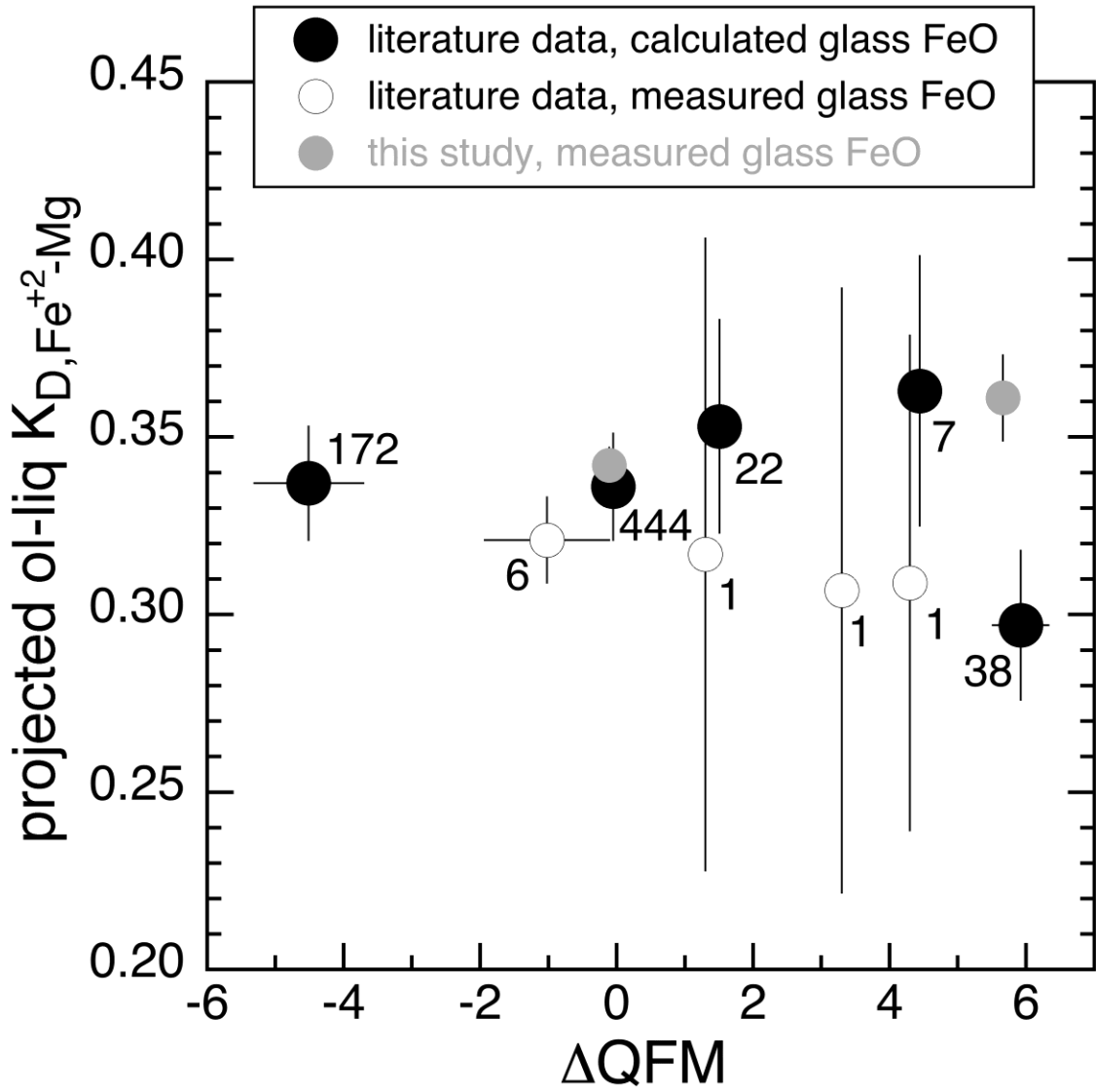


Fig. 6.

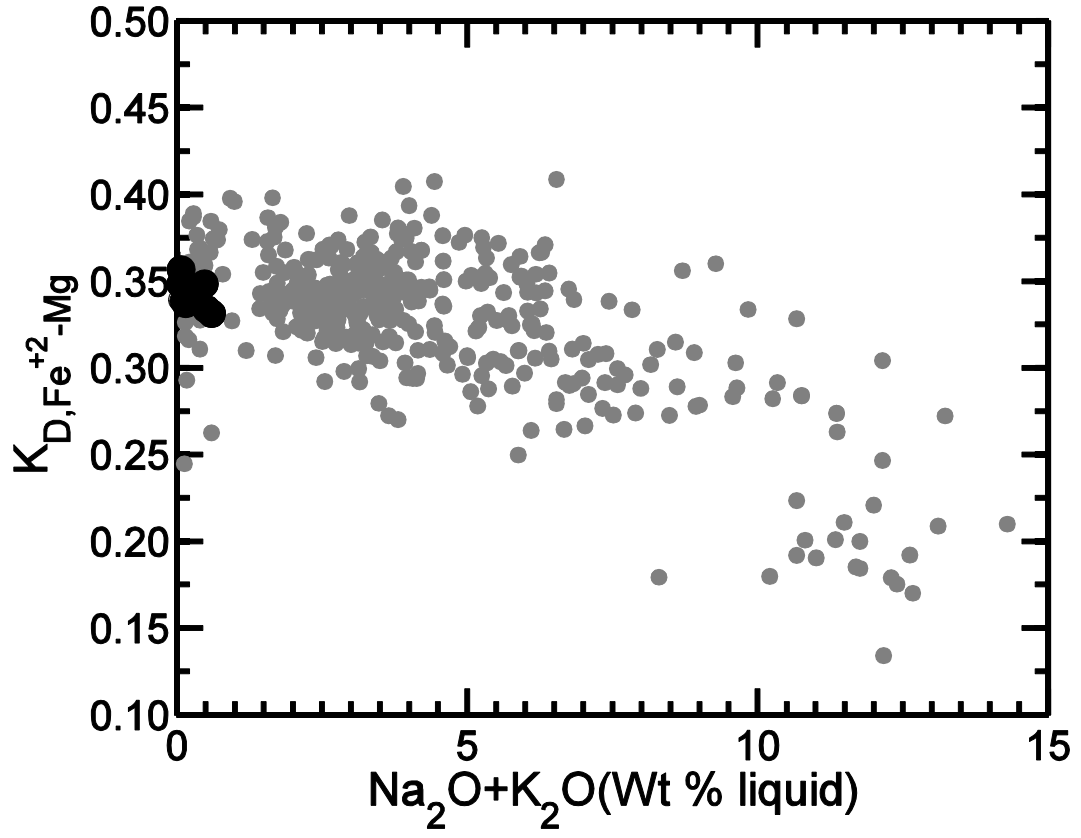
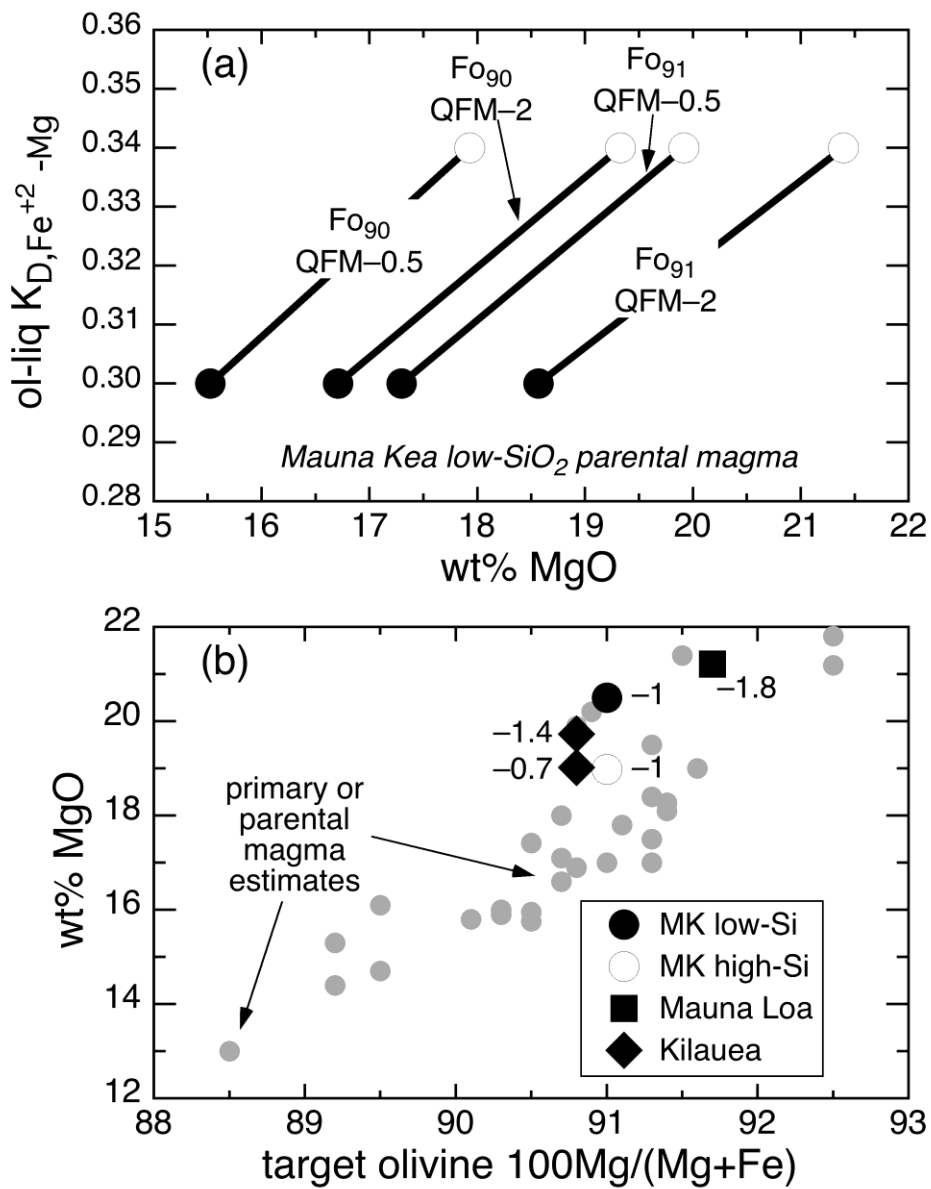


Fig. 7.



## SUPPLEMENTARY MATERIAL

In this supplement, we provide four sections intended to amplify and/or expand on specific topics raised in the main text. The first section is an assessment of the data underlying Roeder and Emslie (1970) as given in an unpublished table made available by the senior author. We assess general quality and consider possible sources for the discrepancy in  $K_{D,Fe^{+2}-Mg}$  values between the canonical 0.30 obtained by Roeder and Emslie (1970) and the ~0.34 preferred in this study. Section 2 provides a detailed description of the projection technique used in the main text to reduce compositional dependences of  $K_{D,Fe^{+2}-Mg}$  on melt and olivine composition for literature data. In Section 3, we evaluate the sources of discrepancies between predictions of the Ford *et al.* (1983) and Toplis (2005) models for  $K_{D,Fe^{+2}-Mg}$  and our experimental data. Finally, Section 4 is a listing of all of the references for data incorporated into our database of olivine-liquid pairs from the literature.

### **1. An Assessment of the Experimental Data of Roeder and Emslie (1970)**

#### ***1.1. Introduction***

Roeder and Emslie (1970) is an enormously influential paper, marking one of the great advances in igneous petrology. By experimentally determining the partitioning of magnesium and iron between olivine and liquid and using an exchange equilibrium involving the two cations, Mg and  $Fe^{+2}$ , they showed that the temperature and composition dependences of single-element partitioning between phases largely canceled. Thus, given

nothing but the composition of an olivine, it became possible to directly calculate the  $\text{Mg}/\text{Fe}^{+2}$  ratio of the coexisting liquid. By focusing on olivine, Roeder and Emslie (1970) established that even the most common, compositionally simple minerals had a lot to say about their environment of formation.

Although the work of Roeder and Emslie (1970) has provided an intellectual motivation for hundreds of subsequent papers, the vast majority of the experimental data remained unpublished and has, to our knowledge, never been compared quantitatively with later work. At the time the paper was published, the editorial policies at Contributions to Mineralogy and Petrology were not conducive to printing large data tables and electronic supplements did not exist. Moreover, all of the data used in Roeder and Emslie (1970) were made freely available by the senior author upon request and, indeed, we obtained a copy of the data table (hereafter referred to as REUPDT), nearly forty years after publication.

Our in-depth examination of the data of Roeder and Emslie (1970) was motivated by two of our reviewers who asked us to reconcile the discrepancy between our data and those in the recent literature suggesting that  $K_{\text{D,Fe}^{+2}\text{-Mg}}$  for Hawaiian basaltic liquids is  $\sim 0.34$  with the canonical value of 0.30 obtained by Roeder and Emslie (1970).  $K_{\text{D,Fe}^{+2}\text{-Mg}} = 0.30$  is still commonly used for generic petrologic calculations and a 0.04 difference in the selected  $K_{\text{D,Fe}^{+2}\text{-Mg}}$  can have a large effect on the results, so it is important to see if the source of this discrepancy can be inferred. Moreover, because Roeder and Emslie measured FeO and  $\text{Fe}_2\text{O}_3$  by wet chemistry (albeit on their bulk experimental charges), this discrepancy does not simply reflect a difference in  $\text{Fe}^{+3}/\text{Fe}^{+2}$  algorithm. In section 1.2, we

begin our analysis of Roeder and Emslie (1970) by reproducing their calculations. These results establish a quantitative basis for determining the effect of different approaches to analyzing the data on  $K_{D,Fe^{+2}-Mg}$ . We also confirm that a facial interpretation of their data using the procedures outlined in Roeder and Emslie (1970) does in fact lead to  $K_{D,Fe^{+2}-Mg} \sim 0.30$ . In sections 1.3 through 1.5, we apply our mass balance approach and other tools to evaluate the REUPDT data and discuss the implications of our results for the canonical value of  $K_{D,Fe^{+2}-Mg}$  and the connectivity between results of our study and those of Roeder and Emslie (1970).

### ***1.2. $K_{D,Fe^{+2}-Mg}$ as determined by Roeder and Emslie (1970)***

As a first step towards analyzing the data of Roeder and Emslie (1970), we sought to reproduce their calculation of  $K_{D,Fe^{+2}-Mg}$  as summarized in their Fig. 4. This computation requires four pieces of information, the concentrations of MgO and FeO in the olivine and the concentrations of MgO and FeO in liquid. Roeder and Emslie (1970) used electron microprobe analyses for both oxides in olivine (only forsterite and fayalite contents are given in REUPDT but these are readily converted to oxides). For the liquid, Roeder and Emslie (1970) determined MgO and FeO\* (i.e., total Fe as FeO) from electron microprobe analyses of the glass but there are no direct analyses of FeO and, although wet chemical measurements were made of FeO (and Fe<sub>2</sub>O<sub>3</sub>), these were done on bulk splits, not on glass separates. Thus, prior to calculating a value for  $K_{D,Fe^{+2}-Mg}$ , FeO for the whole sample had to be disaggregated into FeO residing in olivine and FeO in the liquid. Roeder and Emslie (1970) approached this problem through mass balance using MgO in olivine

and glass, assuming that only these two phases contributed to bulk MgO. From the relative weights of the two phases, they then partitioned the known bulk FeO between liquid and olivine, also assumed to be present only in these two phases, and computed  $K_{D,Fe^{+2}-Mg}$ . Roeder and Emslie (1970) used the results of 27 experiments for this purpose (22 on a Kilauea olivine basalt, sample 654; three on a Hualalai ankaramite, sample C71; and two on a Hualalai alkali olivine basalt, sample C218). Results for olivine-liquid experiments conducted in air are also given in REUPDT but  $K_{D,Fe^{+2}-Mg}$  for these experiments were ignored due to the extreme sensitivity of calculated values on phase composition.

Figure A1 shows the results of our MgO-based olivine and liquid mass balance calculations to produce, in combination with electron microprobe data, the molar FeO/MgO ratios in the experimental olivines and glasses. We use the same symbol set as Roeder and Emslie (1970) and a comparison of Fig. A1 with their Fig. 4 shows very good agreement in the distribution of points. The very subtle differences between the two figures likely reflect round-off errors and the different modes of plot generation. Our unweighted least-squares fit through the origin yields a slope (equal to  $K_{D,Fe^{+2}-Mg}$ ) of  $0.305 \pm 0.005$ , in complete agreement with the value of 0.30 reported by Roeder and Emslie (1970). Considering the 27 individual  $K_{D,Fe^{+2}-Mg}$  values, the overall range is from 0.26 to 0.36, almost all of which (0.27–0.36) is encompassed by the 22 olivine basalt experiments (composition 654). The mean and standard deviation for the entire data set is  $0.31 \pm 0.03$  (the median value is also 0.31).

The individual  $K_{D,Fe^{+2}-Mg}$  values based on MgO mass balance are not simply a random distribution of values with a large standard deviation as there is structure in the

data associated with bulk composition, phase assemblage, and container material. In Fig. A2a,  $K_{D,Fe^{+2}-Mg}$  is plotted in the form of a histogram and disaggregated according to the bulk composition. Experiments on the alkali olivine basalt (C218) and ankaramite bulk compositions (C71) generally yield  $K_{D,Fe^{+2}-Mg}$  values at the lower end of the distribution, except that  $K_{D,Fe^{+2}-Mg}$  for 7-2-C71 is among the highest of the study. Similarly,  $K_{D,Fe^{+2}-Mg}$  values for olivine  $\pm$  trace spinel experiments are skewed to high values relative to the mean of all of the data (means of 0.33 vs. 0.30). We can't appeal to fractionation to dramatically alter liquid compositions from one experiment to the next because the calculated melt fractions are all greater than 0.87. Moreover, the bulk compositions are all similar, the range in  $SiO_2$  and  $Na_2O+K_2O$  values being 47.9–49.4 and 2.6–3.3 wt % when each bulk composition is normalized to 100 wt %. Given the relatively small differences in glass compositions among the Roeder and Emslie (1970) experiments and literature data for basaltic melts, the large spread in  $K_{D,Fe^{+2}-Mg}$  from 0.26–0.36 is surprising.

An additional type of systematic behavior can be seen when the  $K_{D,Fe^{+2}-Mg}$  values are parsed by the experimental container material. For the most reducing conditions, Roeder and Emslie (1970) generally used alumina crucibles with the other experiments being conducted in either  $Ag_{55}Pd_{45}$  or  $Ag_{60}Pd_{40}$  alloy capsules. Figure A2b shows a histogram of  $K_{D,Fe^{+2}-Mg}$  separated according to container material.  $K_{D,Fe^{+2}-Mg}$  values obtained from the alumina crucible experiments form a coherent group ranging from 0.327–0.344 ( $0.337 \pm 0.008$ , mean and  $1\sigma$ ), whereas the Ag-Pd capsule runs display far greater variations (0.260–0.362;  $0.303 \pm 0.026$ ) that are not correlated with temperature or redox conditions. We conclude that we can reproduce Roeder and Emslie's (1970)

calculations as they described them, but that the large scatter in the data, particularly among the Ag-Pd experiments, gives cause for concern. In the following two sections, we provide an independent critical assessment of the internal consistency of their data.

### ***1.3. Some basic acceptance criteria for Roeder and Emslie's experiments***

Before discussing the results of our mass balance calculations, we present some basic acceptance criteria as an initial quality check for the 27 experiments used by Roeder and Emslie (1970) to define  $K_{D,Fe^{+2}-Mg}$ . REUPDT gives full probe analyses of glass, excluding  $Cr_2O_3$ , but provides only wt % fayalite and forsterite for the olivine (2 digits), so that some of the usual tests of data quality for a crystalline phase, such as oxide totals or stoichiometry constraints, can't be used directly. We can, however, take advantage of the low concentrations of elements other than Mg, Fe, and Si in olivine from basalts (e.g., Simkin and Smith, 1970; Sobolev *et al.*, 2007, and data therein). We accepted sums for olivine analyses between 97-103 but rejected run 8-2-C218 (wt % forsterite plus fayalite = 95) as requiring an implausible minor element contribution to bring the sum up to at least 97%. This run is excluded from any further consideration. Liquid compositions in terms of oxides also provide constraints on acceptable data. Oxide totals for probe analyses in REUPDT used to compute  $K_{D,Fe^{+2}-Mg}$  range from 98.0 to 100.8 (computed with all Fe as FeO) and we accepted this range as being viable. The concentration of  $SiO_2$  in glass from 7-8-654 is, however, anomalously high relative to other glass compositions from runs on the 654 bulk composition (Fig. A3) and we therefore rejected this experiment. A second

experiment, 7-5-654, also has unusually high SiO<sub>2</sub> relative to other experiments whose glass compositions are shown in Fig. A3 but we retain it for the time being.

The REUPDT notes that two experiments, 7-1-654 and 9-1-654, contain clinopyroxene but there are no accompanying analyses. Clinopyroxene crystallization in basaltic magmas is often associated with major shifts in melt composition (e.g., Seaman *et al.*, 2004) and we would be forced to reject these experiments if significant amounts of clinopyroxene were present because we would be unable to perform an accurate mass balance calculation. We therefore conducted a simple check for the onset of clinopyroxene crystallization by plotting CaO concentrations in the melt as a function of MgO, a variable sensitive to olivine fractionation (Fig. A4). Note that the open symbols (clinopyroxene present) in Fig. A4 are indistinguishable from values expected from a simple linear extension of the line calculated for the clinopyroxene-absent experiments. Had significant crystallization of clinopyroxene occurred, the open symbols would have plotted well below the line. We conclude that clinopyroxene crystallization can be neglected for these two experiments and have, therefore, included them in our subsequent analysis.

#### ***1.4. Mass balance calculations on Roeder and Emslie's (1970) data***

Roeder and Emslie (1970) used MgO to mass balance olivine and glass so that they could determine  $K_{D,Fe^{+2}-Mg}$ . The major advantage to this approach is that it is not computationally intensive, an important consideration in the 1960s. However, using only MgO also carries a major penalty because it neglects constraints on mass balance available through other elements. In this section, we consider the results of all phase (excluding

clinopyroxene)-all oxide mass balance calculations as applied to REUPDT. We excluded two of Roeder and Emslie's 27 diagnostic experiments for reasons described above and performed mass balance calculations on the remaining 25, using the phase assemblage and compositions for each experiment as reported in REUPDT. As with our experiments, the mass balance calculations are based on a non-linear system of equations presented by Albarède and Provost (1977), which incorporates uncertainties on the bulk and phase compositions. Since most of Roeder and Emslie's experiments contained phases that weren't analyzed and some of the uncertainties are not given, we describe in the notes to Table A3 how we estimated required data not explicitly reported by Roeder and Emslie. For those experiments containing clinopyroxene, we assumed that the modal abundance was very small and could be neglected.

Modes,  $\chi^2$  values, sum of squared residuals, FeO and Fe<sub>2</sub>O<sub>3</sub> in the melt, and  $K_{D,Fe^{+2}-Mg}$  obtained from the full mass balance calculations for Roeder and Emslie's experiments are given in Table A3. Twenty-four of the 25 mass balance calculations yield  $\chi^2$  values between 0.2 and 8.4. All of these mass balance solutions are acceptable at the 95% confidence interval, i.e., the calculated  $Q$  value for the degrees of freedom associated with each mass balance calculation was  $\geq 0.05$ , a consequence of the relatively large errors cited by Roeder and Emslie (1970). The  $\chi^2$  value for the mass balance fit of run 10-1-654 is, however, 29.6, yielding a  $Q$  of 0.00005 and we therefore rejected it from further consideration.

Calculated liquid abundances in the 24 provisionally accepted experiments range from 81.5 to 98.4 wt % with most or all of the balance being olivine. One experiment, 7-5-

654, has anomalously low olivine (Fig. A5a) and high spinel (Fig. A5b) in the calculated mode relative to expectations based on the other 7-X-654 experiments (those conducted on the 654 bulk composition with  $\log fO_2 \sim -7$  and at variable temperatures). It also has high  $SiO_2$  relative to other 654 experiments (Fig. A3) and the second highest discrepancy we observed between  $FeO^*$  of the bulk composition as measured by electron microprobe of the completely fused starting material and  $FeO^*$  for the bulk run product obtained by wet chemistry (Table A3). It seems likely that a significant problem exists with this experiment and we therefore rejected it. Of the 27 experiments used by Roeder and Emslie (1970) to evaluate  $K_{D,Fe^{+2}-Mg}$ , we have thus far rejected four (8-2-C218 for low olivine sum, 7-8-654 for anomalously high  $SiO_2$  in the glass, 7-5-654 for an inconsistent calculated mode, and 10-1-654 because of a poor fit in the mass balance calculation). For accepted experiments, the calculated olivine mode (Table A3) is between 1.4 and 12.2 wt %; when present, the spinel mode lies between 0.2 and 0.8 wt % and plagioclase abundances are  $< 6$  wt %. As noted above, the clinopyroxene mode is assumed to be zero, even when present according to REUPDT.

In Fig. A6a, we compare calculated  $K_{D,Fe^{+2}-Mg}$  values from our complete mass balance fits to those based solely on MgO, as used by Roeder and Emslie (1970). For individual experiments,  $K_{D,Fe^{+2}-Mg}$  for the two calculation schemes differ by as much as 0.04 and MgO-based  $K_{D,Fe^{+2}-Mg} > 0.32$  all convert to lower values in the full oxide mass balance calculations (but note that others are increased). Differences in  $K_{D,Fe^{+2}-Mg}$  that are apparent in Fig. A6a are mostly a consequence of our using  $FeO^*$  in the liquid as a mass balance constraint. For most experiments, the ratio of calculated  $K_{D,Fe^{+2}-Mg}$  values is a

linear function of  $\Delta\text{FeO}^*$  (liq), which we define as the percentage difference between ( $\text{FeO} + 0.89981 \times \text{Fe}_2\text{O}_3$ ) in the liquid determined by mass balance and  $\text{FeO}^*$  for the glass obtained using the electron microprobe (Fig. A6b; note that the liquid  $\text{FeO}$  and  $\text{Fe}_2\text{O}_3$  contents determined by mass balance largely reflect the olivine  $\text{FeO}$  value and the wet chemistry bulk  $\text{FeO}$  and  $\text{Fe}_2\text{O}_3$  values). In general,  $\Delta\text{FeO}^*$  (liq)  $> 0$  leads to higher  $K_{\text{D,Fe}^{+2}\text{-Mg}}$  values than expected from MgO-based mass balance and  $\Delta\text{FeO}^*$  (liq)  $< 0$  leads to lower values. Overall, the all oxide-all phase mass balance yields a smaller standard deviation suggesting that some of the scatter in Roeder and Emslie's (1970) data is an artifact of their mass balance technique. The averages are nevertheless similar ( $0.312 \pm 0.027$  for MgO-based mass balance versus  $0.305 \pm 0.020$ ) and systematic behaviors noted above in discussing Fig. A2 remain intact or are strengthened. For example, experiments conducted in  $\text{Al}_2\text{O}_3$  crucibles yield a fairly tight cluster of  $K_{\text{D,Fe}^{+2}\text{-Mg}}$  values ( $0.321 \pm 0.007$ ) at the higher end of the distribution of all  $K_{\text{D,Fe}^{+2}\text{-Mg}}$ s whereas the Ag-Pd results are more scattered and generally lower ( $0.301 \pm 0.020$ ). Similarly, data for the C71 and C218 bulk compositions are mostly at the low end of calculated  $K_{\text{D,Fe}^{+2}\text{-Mg}}$  values. Note that  $K_{\text{D,Fe}^{+2}\text{-Mg}}$  for 7-2-C71, which is at the high end of  $K_{\text{D,Fe}^{+2}\text{-Mg}}$  values when using MgO-based mass balance (0.343) becomes 0.301 and, mostly as a consequence of this, the average of the four C71 plus C218 experiments for an all-oxide all-phase mass balance calculation is lower, 0.28 instead of 0.30.

Figure A7 shows olivine-liquid  $K_{\text{D,Fe}^{+2}\text{-Mg}}$  values calculated using all oxides and reported phases in REUPDT as a function of bulk  $\Delta\text{FeO}^*$ . There is no correlation between bulk  $\Delta\text{FeO}^*$  and  $K_{\text{D,Fe}^{+2}\text{-Mg}}$  but we can distinguish three clusters of data, seven Ag-Pd

experiments with bulk  $\Delta\text{FeO}^* < -3$ , two of which have bulk  $\Delta\text{FeO}^* < -5$ , a central region of five  $\text{Al}_2\text{O}_3$  and eight Ag-Pd experiments with  $-3 < \text{bulk } \Delta\text{FeO}^* < +3$ , and four Ag-Pd experiments with bulk  $\Delta\text{FeO}^* > +3$ , three of which are  $> +5$ . Splits analyzed by wet chemistry are both Fe-enriched and Fe-depleted relative to the true bulk composition, consistent with wet chemistry splits being both crystal-enriched and crystal-depleted relative to the bulk composition. Variable amounts of Ag-Pd contamination in the analyzed splits may also play a role. We show below that there are questions concerning the quality of most of the data with very high or very low bulk  $\Delta\text{FeO}^*$  in Fig. A7.

The primary purpose of the mass balance calculations is to determine the FeO content of the melt so that  $K_{\text{D,Fe}^{+2}\text{-Mg}}$  can be computed but it can also find use in testing for internal consistency. In the remainder of this section, we focus on the mass-balance generated  $\text{Fe}^{+3}/\text{Fe}^{+2}$  of the experimental glasses, because this allows us to more easily consider Roeder and Emslie's (1970) data in light of a large body of work on  $\text{Fe}^{+3}/\text{Fe}^{+2}$  values in melts as a function of temperature and  $f\text{O}_2$ .

For equilibrium between ferric and ferrous iron in a melt, the free energy of reaction for  $\text{FeO} + 0.25 \text{O}_2 = \text{FeO}_{3/2}$  can be expressed in the form

$$\ln\left(\frac{X_{\text{FeO}_{3/2}}}{X_{\text{FeO}}}\right) = \frac{1}{4} \ln f_{\text{O}_2} + \left[ \frac{-G^\circ}{RT} - \ln\left(\frac{\gamma_{\text{FeO}_{3/2}}}{\gamma_{\text{FeO}}}\right) \right]$$

where  $G^\circ$ , which is a function of temperature but not composition, is the standard state free energy of reaction and  $X_i$  and  $\gamma_i$  are the mole fraction and activity coefficient of  $i$ . If

the last term on the right is independent of oxygen fugacity, then a plot of  $\ln(X_{\text{FeO}_{3/2}}/X_{\text{FeO}})$  at constant temperature against  $\ln f\text{O}_2$  will yield a slope of 0.25. In practice,  $\gamma_{\text{FeO}_{3/2}}/\gamma_{\text{FeO}}$  is generally a function of composition and, therefore of  $f\text{O}_2$ , and thus the slope deviates from the ideal value of 0.25. Figure A8a shows an example for a basaltic liquid at 1200°C taken from data of Hill and Roeder (1974). An unweighted regression yields a slope of 0.20 and this is typical of results for basaltic liquids reported in the literature, which yield slopes of 0.19 to 0.23 (Fudali, 1965; Shibata, 1967; Hill and Roeder, 1974; Kress and Carmichael, 1988). Note that the slope in Fig. A8a is well defined and that all of the points are within  $\sim 2\sigma$  of the line. Note also that experiments in different container materials (alumina, Ag-Pd, and Pt) are all consistent with each other. We show below that consistency among the results of experiments produced in different container materials is an important issue for the data of Roeder and Emslie.

Figure A8b is a histogram compiling slopes for plots of  $\ln f\text{O}_2$  versus  $\ln(X_{\text{FeO}_{3/2}}/X_{\text{FeO}})$  from literature experimental data and models for calculating  $\text{Fe}^{3+}/\text{Fe}^{2+}$  (see caption to Fig. A8 for references). We restrict attention to melts for which the experimental range in  $\ln f\text{O}_2$  exceeded 4.6 (i.e., 2 log units) because the scatter in best-fit slopes rose sharply when smaller ranges were considered. For simple systems, slopes ranged between 0.13 and 0.37 and for magmatic liquids, it was 0.19–0.23. We take the observed range for magmatic liquids, 0.19–0.23, to contain the expected value for Roeder and Emslie's liquids; values outside this range are problematic and any slope outside the range 0.13–0.37 can certainly be regarded as indicating a very serious problem. We use these criteria below to analyze the REUPDT for self-consistency.

Although run temperatures for the 23 provisionally accepted experiments in REUPDT range from 1152–1256, most of the data can be clustered into one of four groups, ~1153°C, ~1180°C, ~1200°C, and ~1225°C. There are four experiments conducted at higher temperatures (>1235°C), but the  $fO_2$ s are virtually identical, so we can't conduct an isothermal slope test for them. Figure A9 is a set of approximately isothermal plots of  $\ln fO_2$  versus  $\ln(Fe^{+3}/Fe^{+2})$  in order of ascending temperature. Figure A9a shows runs conducted in the vicinity of 1153°C. These are all experiments conducted in Ag-Pd capsules on bulk composition 654. An unweighted regression through the three points yields a slope of 0.32, which is well outside the expected range for a basaltic liquid (0.19–0.23). It is not possible to construct a line with a viable slope using any pair of experiments involving the most ferric glass (7-1-654); the other two experiments, 8-1-654 and 9-1-654, do form a line with a viable slope (0.20), although the range in  $\ln fO_2$  is small (2.2  $\ln$  units). We conclude that 7-1-654 was compromised although the precise nature of the problem(s) is unclear. We tentatively accept 8-1-654 and 9-1-654. Fig. A9b shows a somewhat different case. Here, three Ag-Pd experiments generate a slope of 0.23, within the expected range, albeit via a very small range in  $\ln fO_2$  (2.5  $\ln$  units). The calculated slope for all four data points, one an  $Al_2O_3$  experiment and three conducted in Ag-Pd capsules, is, however,  $0.176 < 0.19$ , suggesting that either the  $Al_2O_3$  datum is in error or that the alumina and Ag-Pd experiments are inconsistent with each other (e.g., if both sets are correct, then the  $Al_2O_3$  and Ag-Pd data are on different lines). Since we can't distinguish between these possibilities based solely on this plot, we accept all of the data in Fig. A9b for the purposes of this test. Figure A9c shows a clearer inconsistency between the alumina and Ag-Pd experiments. The three  $Al_2O_3$  experiments yield a slope of 0.19, within the expected range

and, therefore, acceptable. A very different result is obtained for the five Ag-Pd experiments. Here the slope is 0.41, an implausibly high value. Deleting 6-1-654, the most ferric point, which is anomalous in Fig. A6b, does not lead to a viable line for the remaining Ag-Pd data (slope of 0.247). It is possible to draw a line sub parallel to the alumina data that goes through these lower four Ag-Pd data but this would imply that the alumina and Ag-Pd liquids have significantly different bulk compositions and that alumina addition to melts in the alumina experiments was very important in determining the  $\text{Fe}^{+3}/\text{Fe}^{+2}$  ratio (i.e., the bulk compositions are sufficiently different so that the data lie on different lines). This appears unlikely because the amount of alumina contamination in the alumina crucible experiments varies from experiment to experiment and yet all three points are consistent with the same line. Moreover,  $\text{Fe}^{+3}/\text{Fe}^{+2}$  models in the literature (e.g., Jayasuriya *et al.*, 2004) show that Al is a modest driver of this ratio and we would therefore not expect the alumina and Ag-Pd experiments to produce significantly different lines. In addition, Hill and Roeder's (1974) data shown in Fig. A8a, which reflects experiments conducted in both alumina and Ag-Pd containers, are consistent with being on the same line. We conclude that some, if not all, of the  $\sim 1200^\circ\text{C}$  Ag-Pd experiments reported in REUPDT are in error and, since we can't distinguish reliably which, if any, might be valid, we reject all of them. For data obtained in the vicinity of  $1225^\circ\text{C}$  (Fig. A9d), the slope of 0.27 for the Ag-Pd data is higher than expectations for a basaltic melt (0.19–0.23) but, given the small range in  $\ln f\text{O}_2$  (2.3 *ln* units), we didn't enforce the slope consistency criterion for them. The alumina crucible experiment and the Ag-Pd data are consistent with a line whose slope is 0.18 (i.e.,  $< 0.19$ ). A higher slope could be obtained if the least ferric of the Ag-Pd experiments (7-6-654) were to be deleted or shifted in  $\ln f\text{O}_2$  but this would

again be an arbitrary exercise and therefore, in the absence of additional data, we simply accepted all of the ~1225°C data. We conclude, based on Fig. A9, that the Al<sub>2</sub>O<sub>3</sub> data can't be simultaneously consistent with all of the Ag-Pd data and that, even if one ignores the Al<sub>2</sub>O<sub>3</sub> data, many of the Ag-Pd data are demonstrably inconsistent with expectations based on literature determinations of Fe<sup>+3</sup>/Fe<sup>+2</sup> at constant temperature. Where there is sufficient range in *ln*fO<sub>2</sub> to confidently determine the slope for Ag-Pd runs in an isothermal *ln*fO<sub>2</sub> vs. *ln*(Fe<sup>+3</sup>/Fe<sup>+2</sup>) plot (Figs. A9a and A9c), the data fail the slope test. Overall, we accepted twelve Ag-Pd experiments in the aftermath of the isothermal *ln*fO<sub>2</sub> vs. *ln*(Fe<sup>+3</sup>/Fe<sup>+2</sup>) slope test (two runs in Fig. A9a, three runs each shown in Figs. A9b and A9d and untested runs 7-2-C71 (1237°C), 7-10-654 (1238°C), 7-11-654 (1251°C) and 7-4-C71 (1266°C)) but it is important to note that this collection largely reflects insufficient data to apply the slope test for a given temperature and not a successful passage through it.

Figure A10, shows data for three ~1200°C alumina crucible experiments from REUPDT (Fig. 9c) together with the result for an additional basalt experiment, also run in an alumina crucible, reported by Hill and Roeder (1974). The slope based on all four experiments is 0.22, which is within the expected range. This result suggests that the alumina data of Roeder and Emslie (1970) are consistent with the alumina data of Hill and Roeder (1974). Since the alumina, Ag-Pd and Pt experiments of Hill and Roeder (1974) also yield a consistent Fe<sup>+3</sup>/Fe<sup>+2</sup> (Fig. A8a), this implies that the alumina crucible experiments of Roeder and Emslie (1970) are also consistent with the Ag-Pd experiments of Hill and Roeder (1974) and, therefore, the inconsistency of Roeder and Emslie's alumina and Ag-Pd data is not inherent to their use of these different container materials.

Our analysis through Fig. A9 was restricted to nearly isothermal sets of data but it is also possible to construct a test based on the temperature dependence of  $\text{Fe}^{+3}/\text{Fe}^{+2}$ . A wide variety of studies have demonstrated that  $\ln(\text{Fe}^{3+}/\text{Fe}^{2+})$  in an otherwise constant composition liquid is a linear function of inverse temperature but we are aware of only one determination for a magmatic liquid, a basalt studied by Kennedy (1948). Figure A11 is a histogram of the temperature dependence for Kennedy's basalt, a variety of simple systems, and models for magmatic liquids (see caption to Fig. A11 for references). Coefficients of  $10^4/T(\text{K})$  range from 0.7 to 2.5 but the range 0.7–1.4 captures Kennedy's basalt (1.04), all of the models for magmatic liquids (0.85–1.27), and all but three of the simple system determinations. We take the range of 0.7–1.4 as including the coefficient of  $10^4/T(\text{K})$  for all plausible basaltic liquids including those studied by Roeder and Emslie (1970).

A temperature dependence test can provide a constraint independent of the isothermal slope test because it can be used to test data from temperatures for which data are too sparse or too close in  $\ln f\text{O}_2$  to allow a testable isothermal slope to be determined. To correct  $\text{Fe}^{+3}/\text{Fe}^{+2}$  to some reference temperature  $T_{\text{ref}}(\text{K})$ , we use the equation  $\ln(\text{Fe}^{+3}/\text{Fe}^{+2})$  at  $T_{\text{ref}} = \ln(\text{Fe}^{+3}/\text{Fe}^{+2})$  at  $T_{\text{exp}} + C \times (10^4) \times (1/T_{\text{ref}} - 1/T_{\text{exp}})$ , where  $T_{\text{exp}}$  refers to the run temperature and  $C$  is an empirical constant whose value is in the range 0.7–1.4 for Roeder and Emslie's liquids. The temperature test is essentially a special form of the isothermal slope test and it will be most sensitive when the difference between the experimental and reference temperature is maximized.

We selected a reference temperature of 1155°C for our variable temperature test because the highest temperature experiments were not tested using the isothermal slope test and because ~1155°C is the lowest temperature for which we conducted an isothermal test.

In Fig. A12, we adjusted the  $\text{Fe}^{+3}/\text{Fe}^{+2}$  of the five alumina and twelve Ag-Pd experiments that provisionally passed all of the previously described tests to a reference temperature of  $1155^\circ\text{C}$ . Each point was weighted by the inverse of its variance in  $\ln(\text{Fe}^{+3}/\text{Fe}^{+2})$  and the value of  $C$ , the coefficient of  $10^4/T(\text{K})$  was allowed to float within the range 0.7–1.4 so that squared deviations of all points from the best-fit line were minimized. The resulting value of  $C$  is 0.94 and this is consistent to first order with the value of 1.04 obtained by Kennedy (1948) for a basalt. The temperature corrections are relatively small,  $<0.36 \ln$  units but noticeable, especially for the highest temperature data. If the data are all consistent with each other, we expect them to lie along a single line with a slope within the range 0.19–0.23 and since the best-fit line has a slope of 0.186, we regard this as a plausible result. Only two points (6-2-654 and, especially, 7-4-C71) lie much more than  $2\sigma$  off the line and are, therefore, potential candidates for rejection and only one of these (7-4-C71) is outside the 95% confidence interval for placement of the line. However, we tentatively accept both.

As a final test, we again consider  $K_{\text{D,Fe}^{+2}\text{-Mg}}$  as a function of bulk  $\Delta\text{FeO}^*$  (last shown in Fig. A7), but now plot only the data that passed all of our previous tests (Fig. A13). Upon comparing Figs. A7 and A13, it is immediately apparent that the Ag-Pd experiments at bulk  $\Delta\text{FeO}^* > +3$  observed in Fig. A7 have disappeared, except for 7-1-C218 (bulk  $\Delta\text{FeO}^* = +6.7$ ), and that, although there are still several experiments with bulk  $\Delta\text{FeO}^* < -3$ , only one of these, 7-4-C71 (bulk  $\Delta\text{FeO}^* = -8.5$ ), is below  $-5$ . We note that 7-4-C71 is also anomalous in Fig. A12. Given the natural gaps between the central cluster at  $-5 < \text{bulk } \Delta\text{FeO}^* < +3$  and the two anomalous points and the fact that all of the other

data with similarly large deviations in bulk  $\Delta\text{FeO}^*$  from zero can be shown to be compromised, we reject both 7-4-C71 and 7-1-C218.

### ***1.5. Discussion***

Overall, 15 of 27 experiments used by Roeder and Emslie (1970) pass all of our quality filters giving us an accepted collection of experiments to interrogate for  $K_{\text{D,Fe}^{+2}\text{-Mg}}$  values and, finally, to address the issue of what Roeder and Emslie's data imply for  $K_{\text{D,Fe}^{+2}\text{-Mg}}$ . For the alumina crucible experiments, we obtain  $K_{\text{D,Fe}^{+2}\text{-Mg}}$  of  $0.321\pm 0.007$ . For accepted Ag-Pd experiments, we find  $K_{\text{D,Fe}^{+2}\text{-Mg}}$  of  $0.306\pm 0.011$  and, for the entire data set, we obtain  $K_{\text{D,Fe}^{+2}\text{-Mg}}$  of  $0.311\pm 0.012$ . Note that our analysis of Roeder and Emslie's data has reduced the scatter for the entire data set relative to that of the original ( $K_{\text{D,Fe}^{+2}\text{-Mg}} = 0.312\pm 0.027$ ) but the means are virtually identical. It is also noteworthy that, although our inferred means for Roeder and Emslie's data are low relative to the  $0.345\pm 0.009$  we obtained for our data and the  $0.340\pm 0.012$  for literature data on broadly tholeiitic compositions, all of these estimates overlap at  $2\sigma$ .

At first glance, it would seem that we have expended considerable effort to end up in essentially the same place as Roeder and Emslie (1970). The canonical value for  $K_{\text{D,Fe}^{+2}\text{-Mg}}$  is 0.30 (cf. Fig. A1) and the average for their individual experiments is 0.31. Our average for all accepted experiments from REUPDT is 0.31 (0.32 if the alumina experiments are preferred), which is lower than the  $\sim 0.34$  we obtained and we are, therefore, left with a gap of 0.02–0.03 in  $K_{\text{D,Fe}^{+2}\text{-Mg}}$ . In Fig. A14, we show a sensitivity diagram for a typical run with 8.2 wt % FeO in the melt and  $K_{\text{D,Fe}^{+2}\text{-Mg}} = 0.30$ . The wet

chemical determination of FeO in a bulk run product can significantly affect  $K_{D,Fe^{+2}-Mg}$  and if a FeO determination was 10% high, this could explain a  $K_{D,Fe^{+2}-Mg}$  difference of 0.03. However, bulk  $\Delta FeO^*$  deviations of accepted data (-5 to +3 %; Fig. A13) limit possible systematic errors in bulk FeO such that this source is unlikely to shift  $K_{D,Fe^{+2}-Mg}$  by no more than a few hundredths. Systematic microprobe errors can also significantly affect  $K_{D,Fe^{+2}-Mg}$ , and it is important to remember that a microprobe in the late 60s was a very different instrument than we have today. A clear indication of this can be seen in the fact that Roeder and Emslie used working curves to obtain quantitative compositional information and it is possible that this led to systematic errors. If, for example, their fayalite numbers were low relative to forsterite by just 1 on average, their inferred  $K_{D,Fe^{+2}-Mg}$  would be low by  $\sim 0.02$  (Fig. A14); we note that the olivine totals (Fa + Fo) in REUPDT are generally low. Similarly, if MgO concentrations in the liquid from REUPDT are low by  $2\sigma$ , this would shift  $K_{D,Fe^{+2}-Mg}$  up by  $\sim 0.03$ . Roeder and Emslie (1970) note that their errors are probably overstated, so that the nominal  $2\sigma$  MgO effect shown in Fig. A14 may well refer to more than  $2\sigma$ , but the point remains that systematic errors in glass composition can account for substantial differences in  $K_{D,Fe^{+2}-Mg}$ .

Finally, it is worth considering what the average  $K_{D,Fe^{+2}-Mg}$  value would be using the individual MgO-based  $K_{D,Fe^{+2}-Mg}$ s and our collection of “accepted” experiments, i.e., what might Roeder and Emslie have reported as the average olivine-liquid  $K_{D,Fe^{+2}-Mg}$  given this set of experiments. The average  $K_{D,Fe^{+2}-Mg}$  value (both alumina and Ag-Pd experiments) using MgO-based mass balance calculations on olivine and liquid would have been  $0.315 \pm 0.021$ , higher than the canonical 0.30 and within error of the 0.34 we inferred

in this work. As was the case with the full data set, the alumina experiments yield  $K_{D,Fe^{+2}-Mg}$ s that define a tight cluster (mean =  $0.336 \pm 0.008$ ,  $1\sigma$ ), whereas the remaining Ag-Pd experiments vary from a high of 0.34 to a low of 0.28, with a mean of  $0.305 \pm 0.017$  (virtually identical to the canonical value). Note that accepting the alumina data yields an average olivine-liquid  $K_{D,Fe^{+2}-Mg}$  that is essentially identical to the one obtained in our work.

### ***1.6. Concluding thoughts***

Finally, it is important to put our analysis of Roeder and Emslie's data in its proper place. The essence of Roeder and Emslie (1970) is not to be found in any specific value of  $K_{D,Fe^{+2}-Mg}$ . Nor is it in the efficacy of any particular experiment or collection of experiments. It is in the realization that an experimental study of crystal-liquid partitioning in a complex system can yield quantitative insights into the origin and evolution of natural magmatic liquids. It is in the realization that modern analytical techniques are tools that can provide great insight into igneous processes, especially if supported quantitatively through experimentation. It is in the motivation provided to many hundreds of later researchers, some of whom took the basic concepts of Roeder and Emslie and transformed them into new but related ways of looking at geological problems. These are the true legacies of Roeder and Emslie and there is nothing here that can or should affect them.

## 2. Projection of Olivine-Liquid Exchange Coefficients

In this section, we expand on the brief summary given in the main text of the projection scheme we used to reduce the dependence of olivine-liquid  $K_{D,Fe^{+2}-Mg}$  on the phase compositions.

We begin by computing molar CMAS components of the liquid as defined by the projection scheme used in BVSP (1981, chapter 3.3):

$$C = (\text{CaO} - \text{P}_2\text{O}_5/3 + \text{K}_2\text{O} + \text{Na}_2\text{O}) \quad (\text{A1a})$$

$$M = (\text{MgO} + \text{FeO} + \text{MnO}) \quad (\text{A1b})$$

$$A = (\text{Al}_2\text{O}_3 + \text{Cr}_2\text{O}_3 + \text{Fe}_2\text{O}_3 + \text{Na}_2\text{O}) \quad (\text{A1c})$$

$$S = \text{SiO}_2 - 2 \times \text{Na}_2\text{O} - 4 \times \text{K}_2\text{O}, \quad (\text{A1d})$$

where the oxides are on a molar basis (e.g., mole % or mole fractions). The value of “S” as used here and in the main article is then defined as

$$\text{“S”} = S / (C + M + A + S). \quad (\text{A1e})$$

Figure A15a shows values of  $K_{D,Fe^{+2}-Mg}$  vs. “S” for our nine QFM experiments (Table 3) and a collection of 446 experimentally determined olivine-liquid pairs obtained at  $\text{QFM} \pm 0.25$  taken from the literature (see section 4 for references to the data used). Values

of FeO/Fe<sub>2</sub>O<sub>3</sub> in the liquids for this figure were calculated using eqn 12 of Jarasuriya *et al.* (2004), one of the several available Fe<sup>2+</sup>/Fe<sup>3+</sup> algorithms discussed in the main text. The solid black curve is an unweighted least-squares fit to the equation:

$$K_{D,Fe^{+2}-Mg} = a + b \times \exp(c \times "S"), \quad (A2)$$

for all of the data, where a (0.4523), b (-0.5372), and c (-3.2001) are the least-squares fit parameters. To obtain the projection of an experimentally determined value of  $K_{D,Fe^{+2}-Mg}$  to a value of "S" = 0.5, we project along a curve parallel to the global fit, i.e.,

$$[K_{D,Fe^{+2}-Mg}]_{0.5} = K_{D,Fe^{+2}-Mg} - [a + b \times \exp(c \times "S")] + [a + b \times \exp(c \times 0.5)] \quad (A3)$$

where "S" in the equation above is the value of "S" associated with the particular  $K_{D,Fe^{+2}-Mg}$  value being projected. Two sample projection paths are shown schematically as red curves in Fig. A15a for experimentally determined points with "S" = 0.3994 (i.e., experimental "S" < 0.5) and the other with an experimental "S" = 0.5508 (i.e., experimental "S" > 0.5; both points are plotted as larger open circles).

The purpose of this initial projection (eqns A1–A3; Fig. A15a) is to remove first order effects of the liquid composition on  $K_{D,Fe^{+2}-Mg}$ . These projected data points are, however, correlated with the experimentally determined Fo contents of the olivine as shown in Fig. A15b. This suggests a dependence of  $K_{D,Fe^{+2}-Mg}$  on the olivine composition, a point discussed by Toplis (2005) and Tuff and O'Neill (2010), and thus we can use the

olivine composition to construct a second projection. We begin by defining a global unweighted linear least-squares fit to our QFM±0.25 database (black line in Fig. A15b):

$$[K_{D,Fe^{+2}-Mg}]_{0.5} = d + e \times [Mg/(Mg+Fe)]^{ol} \quad (A4)$$

where  $d$  (0.4045) and  $e$  (0.07799) are least-squares fit parameters. Individual data points are then projected to  $Fo_{88}$ :

$$[K_{D,Fe^{+2}-Mg}]_{0.5,88} = [K_{D,Fe^{+2}-Mg}]_{0.5} - \{d + e \times [Mg/(Mg+Fe)]^{ol}\} + \{d + e \times [0.88]^{ol}\} \quad (A5)$$

This is shown schematically in Fig. A15b for two points shown as larger open blue circles (the same two points that are plotted as larger open black circles in panel a). Red lines extend from these two points parallel to the global fit to the open gray circles at an olivine  $Mg/(Mg+Fe)$  value of 0.88. Projecting the solid blue circles parallel to the least-squares line. These doubly projected points appear in histogram form in Fig. 4 of the main article. Figure A16 compares unprojected  $K_{D,Fe^{+2}-Mg}$  values from the QFM±0.25 data set to the doubly-projected  $K_{D,Fe^{+2}-Mg}$ s. Although the mean values of the two data sets are very similar, projecting the  $K_{D,Fe^{+2}-Mg}$ s to “S” = 0.5 and  $Fo_{88}$  has decreased the standard deviation by a factor of two and removed essentially all of the skewness apparent in the distribution in Fig. A16a. In our view this makes it much easier to visually compare histograms of  $K_{D,Fe^{+2}-Mg}$ s that have been calculated using different  $Fe^{+3}/Fe^{+2}$  algorithms.

### 3. Comparisons of Our Data with predictions of the Models of Ford *et al.* (1983) and Toplis (2005)

Ford *et al.* (1983) and Toplis (2005) parameterized Fe<sup>+2</sup>-Mg partitioning between olivine and melt based on large numbers of 1-atm and high-pressure experiments. Both parameterizations have been used in olivine-addition calculations where the goal is to estimate the compositions of parental mantle melts (e.g., Herzberg *et al.*, 2007; Putirka *et al.*, 2007) but both models predict substantially lower  $K_{D,Fe^{+2}-Mg}$  values than we obtain for our QFM and NNO experiments and of the QFM±0.25 data set from the literature if Jayasuriya *et al.* (2004) equation 12 is used to compute Fe<sup>+3</sup>/Fe<sup>+2</sup> in the melt. In this section, we examine the causes of differences between predictions of the Ford *et al.* and Toplis models and observed and calculated results for our experiments and those from the literature.

Both the Ford *et al.* (1983) and Toplis (2005) models depend critically on the Fe<sup>+3</sup>/Fe<sup>+2</sup> algorithm used to calculate FeO in the liquid as this is required to calculate  $K_{D,Fe^{+2}-Mg}$ . Consider first Ford *et al.* (1983), who used the equation presented by Sack *et al.* (1980).  $K_{D,Fe^{+2}-Mg}$  values calculated using Sack *et al.* (1980) to obtain Fe<sup>+3</sup>/Fe<sup>+2</sup> in the liquid for the QFM±0.25 data set are 0.014±0.008 lower than they are if eqn 12 of Jayasuriya *et al.* (2004) is used with differences ranging between -0.014 (i.e., using Sack *et al.* yields a higher  $K_{D,Fe^{+2}-Mg}$ ) and +0.041. Thus, the Ford *et al.* expression will on average predict  $K_{D,Fe^{+2}-Mg}$ s for liquids at  $fO_2$ s near QFM that are ~0.014 lower than those preferred here due solely to the different choice of Fe<sup>+3</sup>/Fe<sup>+2</sup> algorithm. However, we obtain a larger

difference if we apply either the Sack *et al.* (1980)  $\text{Fe}^{+3}/\text{Fe}^{+2}$  algorithm or the  $K_{\text{D,Fe}^{+2}\text{-Mg}}$  expression of Ford *et al.* (1983) to our QFM experiments. If we calculate  $K_{\text{D,Fe}^{+2}\text{-Mg}}$  using the  $\text{Fe}^{+3}/\text{Fe}^{+2}$  expression of Sack *et al.* (1980), we obtain  $0.320\pm 0.009$ . The model of Ford *et al.* (1983) gives  $0.318\pm 0.009$ . These calculations are in good agreement with each other but are 0.023 and 0.025 lower (not  $\sim 0.014$ ) than the mean  $K_{\text{D,Fe}^{+2}\text{-Mg}}$  calculated for the same runs ( $0.343\pm 0.008$ ) using the wet chemistry FeO value for run # 26 and eqn 12 of Jayasuriya *et al.* (2004) for the remaining experiments. For run # 26 (1500°C, QFM), the deviation is even larger. A  $K_{\text{D,Fe}^{+2}\text{-Mg}}$  value of  $0.338\pm 0.005$  is observed experimentally for our run #26 (QFM, 1500°C) and, since  $\text{Fe}^{+3}/\text{Fe}^{+2}$  was determined through wet chemistry, it is independent of  $\text{Fe}^{+3}/\text{Fe}^{+2}$  algorithm. This  $K_{\text{D,Fe}^{+2}\text{-Mg}}$  value is 0.034 higher than the 0.304 predicted by the Ford *et al.* model, well outside the  $0.014\pm 0.008$  expected based on the literature QFM $\pm 0.25$  data set. The discrepancies we have just described with respect to model predictions for our data are closely tied to the temperature dependence of Ford *et al.*'s (1983) model as the deviations generally increase with increasing temperature (Fig. A17). This effect appears to be driven primarily by the temperature dependence of  $\text{Fe}^{+3}/\text{Fe}^{+2}$  as calculated by Sack *et al.* (1980) relative to that calculated by Jayasuriya *et al.* (2004), as shown in Fig. A18. This different temperature dependence is propagated through the Ford *et al.* (1983) model, which uses Sack *et al.* (1980), to yield low  $K_{\text{D,Fe}^{+2}\text{-Mg}}$  values at high temperatures (or high MgO contents) and suggests that the Ford *et al.* (1983)  $K_{\text{D,Fe}^{+2}\text{-Mg}}$  model is inaccurate for the highly magnesian liquids relevant to parental melts.

We can perform a similar analysis using the Toplis (2005) model to calculate  $K_{D,Fe^{+2}-Mg}$ . Toplis (2005) incorporates the  $Fe^{+3}/Fe^{+2}$  expression of Kilinc *et al.* (1983) into his model with an additional term for  $P_2O_5$  taken from Toplis *et al.* (1994). For the QFM $\pm$ 0.25 data set from the literature, the Kilinc *et al.* (1983) model yields  $K_{D,Fe^{+2}-Mg}$  values that are  $0.015\pm 0.007$  lower than those generated using Jayasuriya *et al.* (2004). This is similar to our observations described above for the Sack *et al.* (1980)  $Fe^{+3}/Fe^{+2}$  model. The mean  $K_{D,Fe^{+2}-Mg}$  value for our QFM data calculated using the model of Toplis (2005) is  $0.313\pm 0.009$ , 0.030 lower than our mean  $K_{D,Fe^{+2}-Mg}$  value of  $0.343\pm 0.008$  (i.e., this is twice the deviation expected based solely on the different calculation schemes for  $Fe^{+3}/Fe^{+2}$ ). In contrast to the Sack *et al.* (1980) model described above, there is no substantive and systematic temperature difference in the Kilinc *et al.* (1983) model for  $Fe^{+3}/Fe^{+2}$  relative to Jayasuriya *et al.* (2004) and yet there is a clear temperature dependence implicit in Fig. A17 for  $K_{D,Fe^{+2}-Mg}$  values calculated using the Toplis (2005) model. A possible source for the unexpectedly large deviations and temperature dependence is the use of high-pressure olivine-liquid data in parameterizing equations for  $K_{D,Fe^{+2}-Mg}$ . Such data extends to significantly higher temperatures than the 1-atm data set (Fig. A19) so that values for temperature and pressure coefficients are likely to be dominated by these data and, since pressure and temperature are correlated for these experiments, the coefficients are also likely to be correlated. Also, since the high pressure data used by Toplis (2005) include experiments run in Re (probably quite oxidizing), graphite (oxidizing enough to require a correction for the presence of  $Fe^{+3}$ ) and iron

(probably reducing enough not to require a correction for  $\text{Fe}^{+3}$ ), there are likely to be trade-offs among the coefficients of temperature, pressure, and chemical terms to compensate for variable  $\text{Fe}^{+3}/\text{Fe}^{+2}$  ratios that are not taken into account. Refitting the model of Toplis (2005) to establish the influences of specific data on the coefficients is beyond the scope of this study but, as noted in the main text, neglecting  $\text{Fe}^{+3}$  in the melt for high pressure graphite experiments leads to low estimates of  $K_{\text{D,Fe}^{+2}\text{-Mg}}$ , which would be consistent with the Toplis (2005) model underestimating  $K_{\text{D,Fe}^{+2}\text{-Mg}}$  values for our experiments (Fig. A17) and, by extension,  $K_{\text{D,Fe}^{+2}\text{-Mg}}$  values for high-temperature, magnesian parental melts.

### References for Sections 1 - 3:

- Albarède, F. & Provost, A. (1977). Petrological and geochemical mass-balance equations: an algorithm for least-square fitting and general error analysis. *Computers and Geosciences* **3**, 309–326.
- Ariskin, A. A. & Barmina, G. S. (1999). An empirical model for the calculation of spinel-melt equilibria in mafic igneous systems at atmospheric pressure: 2. Fe-Ti oxides. *Contributions to Mineralogy and Petrology* **134**, 251–263.
- Beattie, P. (1993). Olivine-melt and orthopyroxene-melt equilibria. *Contributions to Mineralogy and Petrology* **115**, 103–111.
- Beattie, P., Ford, C. & Russell, D. (1991). Partition coefficients for olivine-melt and orthopyroxene-melt systems. *Contributions to Mineralogy and Petrology* **109**, 212–224.
- Borisov, A. A. & Shapkin, A. I. (1989). New empirical equation of dependence of  $\text{Fe}^{3+}/\text{Fe}^{2+}$  ratio in natural melts on their composition, oxygen fugacity and temperature. *Geokhimiya* **1989**, (6), 892–897 [*Geochemistry International* (1989) **27** (1), 111–116].

- Bowker, J. C., Lupis, C. H. P. & Flinns, P. A. (1981). Structural studies of slags by Mössbauer spectroscopy. *Canadian Metallurgical Quarterly* **20**, 69–78.
- BVSP (1981) *Basaltic Volcanism on the Terrestrial Planets*. New York: Pergamon Press.
- Dingwell, D. B. & Virgo, D. (1987). The effect of oxidation state on the viscosity of melts in the system  $\text{Na}_2\text{O}-\text{FeO}-\text{Fe}_2\text{O}_3-\text{SiO}_2$ . *Geochimica et Cosmochimica Acta* **51**, 195–205.
- Ford, C. E., Russell, D. G., Craven, J. A. & Fisk, M. R. (1983). Olivine-liquid equilibria: Temperature, pressure and composition dependence of the crystal/liquid cation partition coefficients for Mg,  $\text{Fe}^{2+}$ , Ca and Mn. *Journal of Petrology* **24**, 256–265.
- Fudali, R. F. (1965). Oxygen fugacities of basaltic and andesitic magmas. *Geochimica et Cosmochimica Acta* **29**, 1063–1075.
- Ghiorso, M. S. & Kress, V. C. (2004). An equation of state for silicate melts. II. Calibration of volumetric properties at  $10^5$  Pa. *American Journal of Science* **304**, 679–751.
- Herzberg, C., Asimow, P. D., Arndt, N., Niu, Y., Leshner, C. M., Fitton, J. G., Chedle, M. J. & Saunders, A. D. (2007). Temperatures in ambient mantle and plumes: Constraints from basalts, picrites, and komatiites. *Geochemistry Geophysics Geosystems* **8**, Q02006, doi:10.1029/2006GC001390.
- Hill, R. & Roeder, P. (1974). The crystallization of spinel from basaltic liquid as a function of oxygen fugacity. *Journal of Geology* **82**, 709–729.
- Iwase, M., Okumura, T., Kawamura, K., Miyamoto, Y. & Oh-uchi, H. (1998). Oxidation-reduction equilibrium of  $\text{Fe}^{3+}/\text{Fe}^{2+}$  in a candidate glass for immobilisation of high level nuclear waste. *Glass Technology* **39**, 142–146.
- Jayasuriya, K. D., O'Neill, H. St. C., Berry, A. J. & Campbell, S. J. (2004). A Mössbauer study of the oxidation state of Fe in silicate melts. *American Mineralogist* **89**, 1597–609.
- Johnston, W. D. (1964). Oxidation-reduction equilibria in iron-containing glass. *Journal of the American Ceramic Society* **47**, 198–201.
- Kennedy, G. C. (1948). Equilibrium between volatiles and iron oxides in igneous rocks. *American Journal of Science* **246**, 529–549.

- Kilinc, A., Carmichael, I. S. E., Rivers, M. L. & Sack, R. O. (1983). The ferric-ferrous ratio of natural silicate liquids equilibrated in air. *Contributions to Mineralogy and Petrology* **83**, 136–140.
- Kress, V. C. & Carmichael, I. S. E. (1988). Stoichiometry of the iron oxidation reaction in silicate melts. *American Mineralogist* **73**, 1267–1274.
- Kress, V. C. & Carmichael, I. S. E. (1989). The lime-iron-silicate melt system: Redox and volume systematics. *Geochimica et Cosmochimica Acta* **53**, 2883–2892.
- Kress, V. C. & Carmichael, I. S. E. (1991). The compressibility of silicate liquids containing Fe<sub>2</sub>O<sub>3</sub> and the effect of composition, temperature, oxygen fugacity and pressure on their redox states. *Contributions to Mineralogy and Petrology* **108**, 82–92.
- Lange, R. A. & Carmichael, I. S. E. (1989). Ferric-ferrous equilibria in Na<sub>2</sub>O-FeO-Fe<sub>2</sub>O<sub>3</sub>-SiO<sub>2</sub> melts: Effects of analytical techniques on derived partial molar volumes. *Geochimica et Cosmochimica Acta* **53**, 2195–2204.
- Larson, H. & Chipman, J. (1953). Oxygen activity in iron oxide slags. *Transactions of the American Institute of Mining and Metallurgical Engineers* **197**, 1089–1096.
- Libourel, G. (1999). Systematics of calcium partitioning between olivine and silicate melt: implications for melt structure and calcium content of magmatic olivines. *Contributions to Mineralogy and Petrology* **136**, 63–80.
- Mysen, B. O. & Virgo, D. (1983). Redox equilibria, structure, and melt properties in the system Na<sub>2</sub>O-Al<sub>2</sub>O<sub>3</sub>-SiO<sub>2</sub>-Fe-O. *Carnegie Institution of Washington Yearbook* **82**, 313–317.
- Mysen, B. O., Virgo, D., & Seifert, F. A. (1984). Redox equilibria of iron in alkaline earth silicate melts: relationships between melt structure, oxygen fugacity, temperature and properties of iron-bearing silicate liquids. *American Mineralogist* **69**, 834–847.
- Mysen, B. O., Virgo, D., Neumann, E. G. & Seifert, F. A. (1985a). Redox equilibria and the structural states of ferric and ferrous iron in melts in the system CaO-MgO-Al<sub>2</sub>O<sub>3</sub>-SiO<sub>2</sub>-Fe-O: relationships between redox equilibria, melt structure and liquidus phase equilibria. *American Mineralogist* **70**, 317–331.

- Mysen, B. O., Virgo, D., Scarfe, C. M. & Cronin, D. J. (1985b). Viscosity and structure of iron- and aluminum-bearing calcium silicate melts at 1 atm. *American Mineralogist* **70**, 487–498.
- Nikolaev, G. S., Borisov, A. A. & Ariskin, A. A. (1996). Calculation of ferric-ferrous ratio in magmatic melts: Testing and additional calibration of empirical equations for various magmatic series. *Geokhimiya* **1996**, (8), 713–722 [*Geochemistry International* (1996) **34** (8), 641–649].
- Ohashi, S., Kashimura, N., Uchida, Y., McLean, A. & Iwase, N. (2000). Oxidation-reduction equilibria of ferrous/ferric ions in oxide melts. *Steel Research* **71**, 375–380.
- O'Horo, M. P. & Levy, R. A. (1978). Effect of melt atmosphere on the magnetic properties of a  $[(\text{SiO}_2)_{45}(\text{CaO})_{55}]_{65}[\text{Fe}_2\text{O}_3]_{35}$  glass. *Journal of Applied Physics* **49**, 1635–1637.
- O'Neill, H. St. C. (1987). Quartz-fayalite-iron and quartz-fayalite-magnetite equilibria and the free energy of formation of fayalite ( $\text{Fe}_2\text{SiO}_4$ ) and magnetite ( $\text{Fe}_3\text{O}_4$ ). *American Mineralogist* **72**, 67–75.
- Poustovetov, A. A. & Roeder, P. L. (2001). Numerical modeling of major element distribution between chromian spinel and basaltic melt, with application to chromian spinel in MORBs. *Contributions to Mineralogy and Petrology* **142**, 58–71.
- Putirka, K. (2005). Igneous thermometers and barometers based on plagioclase plus liquid equilibria: Tests of some existing models and new calibrations. *American Mineralogist* **90**, 336–346.
- Putirka, K. D., Perfit, M., Ryerson, F. J. & Jackson, M. G. (2007). Ambient and excess mantle temperatures, olivine thermometry, and active vs. passive upwelling. *Chemical Geology* **241**, 177–206.
- Rhodes, J. M. (1996). Geochemical stratigraphy of lava flows sampled by the Hawaii Scientific Drilling Project. *Journal of Geophysical Research* **101**, 11729–11746.
- Rhodes, J. M. & Vollinger, M. J. (2004). Composition of basaltic lavas sampled by phase-2 of the Hawaii Scientific Drilling Project: Geochemical stratigraphy and magma

- types. *Geochemistry, Geophysics, Geosystems* **5**, Q07G13, doi:10.1029/2002GC000434.
- Roeder, P. L. & Emslie, R. F. (1970). Olivine-liquid equilibrium. *Contributions to Mineralogy and Petrology* **29**, 275–289.
- Sack, R. O., Carmichael, I. S. E., Rivers, M. & Ghiorso, M.S. (1980). Ferric-ferrous equilibria in natural silicate liquids at 1bar. *Contributions to Mineralogy and Petrology* **75**, 369–376.
- Schreiber, H. D., Lauer, H. V. & Thanyasiri, T. (1980). The redox state of cerium in basaltic magmas: an experimental study of iron-cerium interactions in silicate melts. *Geochimica et Cosmochimica Acta* **44**, 1599–1612.
- Schreiber, H. D., Kozak, S. J., Merkel, R.C., Balazs, G.B. & Jones, P.W. (1986). Redox equilibria and kinetics of iron in a borosilicate glass-forming melt. *Journal of Non-Crystalline Solids* **84**, 186–195.
- Seaman, C., Sherman, S. B., Garcia, M.O., Baker, M.B., Balta, B. & Stolper, E. (2004). Volatiles in glasses from the HSDP2 drill core. *Geochemistry Geophysics Geosystems* **5**, Q09G16, doi:10.1029/2003GC000596, 42 pp.
- Shibata, K. (1967). The oxygen pressure of the magma from Mihara volcano, O-sima, Japan. *Bulletin of the Chemical Society of Japan* **40**, 830–834.
- Simkin, T. & Smith, J. V. (1970). Minor-element distribution in olivine. *Journal of Geology* **78**, 304–325.
- Sobolev, A. V., Hofmann, A. W., *et al.* (2007). The amount of recycled crust in sources of mantle-derived melts. *Science* **316**, 412–417.
- Stolper, E., Sherman, S., Garcia, M., Baker, M. & Seaman, C. (2004). Glass in the submarine section of the HSDP2 drill core, Hilo, Hawaii. *Geochemistry, Geophysics, Geosystems* **5**, Q07G15, doi:10.1029/2003GC000553.
- Timucin, M. & Morris, A. E. (1970). Phase equilibria and thermodynamic studies in the system CaO-FeO-Fe<sub>2</sub>O<sub>3</sub>-SiO<sub>2</sub>. *Metallurgical Transactions* **1**, 3193–3201.
- Toplis, M. J. (2005). The thermodynamics of iron and magnesium partitioning between olivine and liquid: criteria for assessing and predicting equilibrium in natural and experimental systems. *Contributions to Mineralogy and Petrology* **149**, 22–39.

- Toplis, M. J., Dingwell, D. B. & Libourel, G. (1994). The effect of phosphorus on the iron redox ratio, viscosity, and density of an evolved ferro-basalt. *Contributions to Mineralogy and Petrology* **117**, 293–304.
- Tsuchiyama, A., Nagahara, H. & Kushiro, I. (1981). Volatilization of sodium from silicate melt spheres and its application to the formation of chondrules. *Geochimica et Cosmochimica Acta* **45**, 1357–1367.
- Tuff, J. & O'Neill, H. St. C. (2010). The effect of sulfur on the partitioning of Ni and other first-row transition elements between olivine and silicate melt. *Geochimica et Cosmochimica Acta* **74**, 6180–6205.
- Virgo, D., Mysen, B. O. & Danckwerth, P. (1983). The coordination of Fe<sup>3+</sup> in oxidized vs. reduced sodium aluminosilicate glasses: <sup>57</sup>Fe Mössbauer study. *Carnegie Institution of Washington Yearbook* **82**, 309–313.

#### 4. Experimental Database References

In addition to data from this work, we drew from the following literature sources for olivine-liquid pairs. Criteria for data selection are discussed in the main text.

- Agee, C. B. & Walker, D. (1990). Aluminum partitioning between olivine and ultrabasic silicate liquid to 6 GPa. *Contributions to Mineralogy and Petrology* **105**, 243–254.
- Akella, J., Williams, R. J. & Mullins, O. (1976). Solubility of Cr, Ti, and Al in co-existing olivine, spinel, and liquid at 1 atm. *Proceedings of the Seventh Lunar Science Conference*, 1179–1194.
- Auwers, J. V. & Longhi, J. (1994). Experimental study of the jotunite (hypersthene monzodiorite): constraints on the parent magma composition and crystallization conditions (P,T,  $fO_2$ ) of the Bjerkreim-Sokndal layered intrusion (Norway). *Contributions to Mineralogy and Petrology* **118**, 60–78.
- Baker, M. B., Grove, T. L. & Price, R. (1994). Primitive basalts and andesites from the Mt. Shasta region, N. California: products of varying melt fraction and water content. *Contributions to Mineralogy and Petrology* **118**, 111–129.
- Bartels, K. S. & Furman, T. (2002). Effect of sonic and ultrasonic frequencies on the crystallization of basalt. *American Mineralogist* **87**, 217–226.
- Bartels, K. S. & Grove, T. L. (1991). High-pressure experiments on magnesian eucrite compositions: Constraints on magmatic processes in the eucrite parent body. *Proceedings of the Lunar and Planetary Science Conference* **21**, 351–365.
- Bartels, K. S., Kinzler, R. J. & Grove, T. L. (1991). High pressure phase relations of primitive high-alumina basalts from Medicine Lake volcano, northern California. *Contributions to Mineralogy and Petrology* **108**, 253–270.
- Bickle, M. J. (1978). Melting experiments on peridotitic komatiites. In: W. S. MacKenzie (ed.) *Progress in experimental petrology; fourth progress report of research supported by N.E.R.C., 1975–1978*. pp. 187–195. Natural Environment Research Council: London, United Kingdom.

- Brophy, J. G. (1995). 1-atm melting study of a Leg 142 basalt: implications for fractionation processes beneath the East Pacific Rise at 9°30'N. *Proceedings of the Ocean Drilling Program, Scientific Results* **142**, 41–49.
- Delano, J. W. (1977). Experimental melting relations of 63545, 76015, and 76055. *Proceedings of the Eighth Lunar Science Conference*, 2097–2123.
- Delano, J. W. (1980). Chemistry and liquidus phase relations of Apollo 15 red glass: Implications for the deep lunar interior. *Proceedings of the Eleventh Lunar and Planetary Science Conference*, 251–288.
- Donaldson, C. H., Usselman, T. M., Williams, R. J. & Lofgren, G. E. (1975). Experimental modeling of the cooling history of Apollo 12 olivine basalts. *Proceedings of the Sixth Lunar Science Conference*, 843–869.
- Draper, D. S. & Johnston, A. D. (1992). Anhydrous PT phase relations of an Aleutian high-MgO basalt: an investigation of the role of olivine-liquid reaction in the generation of arc high-alumina basalts. *Contributions to Mineralogy and Petrology* **112**, 501–519.
- Dunn, T. & Sen, C. (1994). Mineral/matrix partition coefficients for orthopyroxene, plagioclase, and olivine in basaltic to andesitic systems: A combined analytical and experimental study. *Geochimica et Cosmochimica Acta* **58**, 717–733.
- Dunn, T. & Stringer, P. (1990). Petrology and petrogenesis of the Ministers Island dike, southwest New Brunswick, Canada. *Contributions to Mineralogy and Petrology* **105**, 55–65.
- Ehlers, K., Grove, T. L., Sisson, T. W., Recca, S. I. & Zervas, D. A. (1992). The effect of oxygen fugacity on the partitioning of nickel and cobalt between olivine, silicate melt, and metal. *Geochimica et Cosmochimica Acta* **56**, 3733–3743.
- Gaetani, G. A., Grove, T. L. & Bryan, W. B. (1994). Experimental phase relations of basaltic andesites from hole 839B under hydrous and anhydrous conditions. *Proceedings of the Ocean Drilling Program, Scientific Results* **135**, 557–563.
- Gee, L. L. & Sack, R. O. (1988). Experimental petrology of melilite nephelinites. *Journal of Petrology* **29**, 1233–1255.

- Grove, T. L. (1981). Use of FePt alloys to eliminate the iron loss problem in 1-atmosphere gas mixing experiments: Theoretical and practical considerations. *Contributions to Mineralogy and Petrology* **78**, 298–304.
- Grove, T. L. (1990). Cooling histories of lavas from Serocki volcano. *Proceedings of the Ocean Drilling Program, Scientific Results* **106/109**, 3–8.
- Grove, T. L. & Beatty, D. W. (1980). Classification, experimental petrology and possible volcanic histories of the Apollo 11 high-K basalts. *Proceedings of the Eleventh Lunar and Planetary Science Conference*, 149–177.
- Grove, T. L. & Bryan, W. B. (1983). Fractionation of pyroxene-phyric MORB at low pressure: An experimental study. *Contributions to Mineralogy and Petrology* **84**, 293–309.
- Grove, T. L., Elkins-Tanton, L. T., Parman, S. W., Chatterjee, N., Müntener, O. & Gaetani, G. A. (2003). Fractional crystallization and mantle-melting controls on calc-alkaline differentiation trends. *Contributions to Mineralogy and Petrology* **145**, 515–533.
- Grove, T. L., Gerlach, D. C. & Sando, T. W. (1982). Origin of calc-alkaline series lavas at Medicine Lake Volcano by fractionation, assimilation and mixing. *Contributions to Mineralogy and Petrology* **80**, 160–182.
- Grove, T. L. & Juster, T. C. (1989). Experimental investigations of low-Ca pyroxene stability and olivine-pyroxene-liquid equilibria at 1-atm in natural basaltic and andesitic liquids. *Contributions to Mineralogy and Petrology* **103**, 287–305.
- Grove, T. L. & Vaniman, D. T. (1978). Experimental petrology of very low Ti (VLT) basalts. *Mare Crisium; The View from Luna 24*, 445–471.
- Hanson, B. & Jones, J. H. (1998). The systematics of Cr<sup>+3</sup> and Cr<sup>+2</sup> partitioning between olivine and liquid in the presence of spinel. *American Mineralogist* **83**, 669–684.
- Herd, C. D. K., Schwandt, C. S., Jones, J. H. & Papike, J. J. (2002). An experimental and petrographic investigation of Elephant Moraine 79001 lithology A: Implications for its petrogenesis and the partitioning of chromium and vanadium in a martian basalt. *Meteoritics & Planetary Science* **37**, 987–1000.

- Huebner, J. S., Lipin, B. R. & Wiggins, L. B. (1976). Partitioning of chromium between silicate crystals and melts. *Proceedings of the Seventh Lunar Science Conference*, 1195–1220.
- Irving, A. J., Merrill, R. B. & Singleton, D. E. (1978). Experimental partitioning of rare earth elements and scandium among armalcolite, ilmenite, olivine and mare basalt liquid. *Proceedings of the Ninth Lunar and Planetary Science Conference*, 601–612.
- Johnston, A. D. & Draper, D. S. (1992). Near-liquidus phase relations of an anhydrous high-magnesia basalt from the Aleutian Islands: Implications for arc magma genesis and ascent. *Journal of Volcanology and Geothermal Research* **52**, 27–41.
- Jurewicz, A. J. G., Mittlefehldt, D. W. & Jones, J. H. (1993). Experimental partial melting of the Allende (CV) and Murchison (CM) chondrites and the origin of asteroidal basalts. *Geochimica et Cosmochimica Acta* **57**, 2123–2139.
- Jurewicz, A. J. G., Mittlefehldt, D. W. & Jones, J. H. (1995). Experimental partial melting of the St Severin (LL) and Lost City (H) chondrites. *Geochimica et Cosmochimica Acta* **59**, 391–408.
- Jurewicz, A. J. G. & Watson, E. B. (1988). Cations in olivine, Part 1: Calcium partitioning and calcium-magnesium distribution between olivines and coexisting melts, with petrologic applications. *Contributions to Mineralogy and Petrology* **99**, 176–185.
- Juster, T. C., Grove, T. L. & Perfit, M. R. (1989). Experimental constraints on the generation of FeTi basalts, andesites, and rhyodacites at the Galapagos Spreading Center, 85°W and 95°W. *Journal of Geophysical Research* **94**, 9251–9274.
- Kadik, A. A., Biggar, G. M., Lukanin, O. A. & Dmitriev, L. V. (1982). An experimental study of the crystallization of Atlantic tholeiites at a given oxygen fugacity. *Geochemistry International* **19**, 104–127.
- Kennedy, A. K., Grove, T. L. & Johnson, R. W. (1990). Experimental and major element constraints on the evolution of lavas from Lihir Island, Papua New Guinea. *Contributions to Mineralogy and Petrology* **104**, 722–734.

- Kilinc, A., Carmichael, I. S. E., Rivers, M. L. & Sack, R. O. (1983). The ferric-ferrous ratio of natural silicate liquids equilibrated in air. *Contributions to Mineralogy and Petrology* **83**, 136–140.
- Kinzler, R. J. & Grove, T. L. (1985). Crystallization and differentiation of Archaean komatiite lavas from northeast Ontario: phase equilibrium and kinetic studies. *American Mineralogist* **70**, 40–51.
- Kinzler, R. J., Grove, T. L. & Recca, S. I. (1990). An experimental study on the effect of temperature and melt composition on the partitioning of nickel between olivine and silicate melt. *Geochimica et Cosmochimica Acta* **54**, 1255–1265.
- Kohut, E. J. & Nielsen, R. L. (2003). Low-pressure phase equilibria of anhydrous anorthite-bearing mafic magmas. *Geochemistry, Geophysics, Geosystems* **4**, 1057, doi:10.1029/2002GC000451.
- Longhi, J. & Pan, V. (1988). A reconnaissance study of phase boundaries in low-alkali basaltic liquids. *Journal of Petrology* **29**, 115–147.
- Longhi, J. & Pan, V. (1989). The parent magmas of the SNC meteorites. *Proceedings of the Nineteenth Lunar and Planetary Science Conference*, 451–464.
- McKay, G. A. & Weill, D. F. (1977). KREEP petrogenesis revisited. *Proceedings of the Eighth Lunar Science Conference*, 2339–2355.
- Merrill, R. B. & Williams, R. J. (1975). The system anorthite-forsterite-fayalite-silica to 2 kbar with lunar petrologic applications. *Proceedings of the Sixth Lunar Science Conference*, 959–971.
- Murck, B. W. & Campbell, I. H. (1986). The effects of temperature, oxygen fugacity and melt composition on the behaviour of chromium in basic and ultrabasic melts. *Geochimica et Cosmochimica Acta* **50**, 1871–1887.
- Nielsen, R. L., Davidson, P. M. & Grove, T. L. (1988). Pyroxene-melt equilibria: an updated model. *Contributions to Mineralogy and Petrology* **100**, 361–373.
- Parman, S. W., Dann, J. C., Grove, T. L. & deWit, M. J. (1997). Emplacement conditions of komatiite magmas from the 3.49 Ga Komati Formation, Barberton Greenstone Belt, South Africa. *Earth and Planetary Science Letters* **150**, 303–323.

- Rhodes, J. M., Lofgren, G. E. & Smith, D. P. (1979). One atmosphere melting experiments on ilmenite basalt 12008. *Proceedings of the Tenth Lunar and Planetary Science Conference*, 1025–1027.
- Sack, R. O. & Carmichael, I. S. F. (1984).  $\text{Fe}^{2+} \leftrightarrow \text{Mg}^{2+}$  and  $\text{TiAl}_2 \leftrightarrow \text{MgSi}_2$  exchange reactions between clinopyroxenes and silicate melts. *Contributions to Mineralogy and Petrology* **85**, 103–115.
- Sack, R. O., Walker, D. & Carmichael, I. S. E. (1987). Experimental petrology of alkalic lavas: constraints on cotectics of multiple saturation in natural basic liquids. *Contributions to Mineralogy and Petrology* **96**, 1–23.
- Sato, H. (1989). Mg-Fe partitioning between plagioclase and liquid in basalts of Hole 504B, ODP Leg 111; a study of melting at 1 atm. *Proceedings of the Ocean Drilling Program, Scientific Results* **111**, 17–26.
- Shi, P. (1993). Low-pressure phase relationships in the system  $\text{Na}_2\text{O}-\text{CaO}-\text{FeO}-\text{MgO}-\text{Al}_2\text{O}_3-\text{SiO}_2$  at 1100°C, with implications for the differentiation of basaltic magmas. *Journal of Petrology* **34**, 743–762.
- Singletary, S. J. & Grove, T. L. (2003). Early petrologic processes on the ureilite parent body. *Meteoritics and Planetary Science* **38**, 95–108.
- Singletary, S. J. & Grove, T. L. (2006). Experimental constraints on ureilite petrogenesis. *Geochimica et Cosmochimica Acta* **70**, 1291–1308.
- Snyder, D., Carmichael, I. S. E. & Wiebe, R. A. (1993). Experimental study of liquid evolution in an Fe-rich, layered mafic intrusion: constraints of Fe-Ti oxide precipitation on the T- $f\text{O}_2$  and T- $\square\square$  paths of tholeiitic magmas. *Contributions to Mineralogy and Petrology* **113**, 73–86.
- Snyder, D. A. & Carmichael, I. S. E. (1992). Olivine-liquid equilibria and the chemical activities of FeO, NiO,  $\text{Fe}_2\text{O}_3$ , and MgO in natural basic melts. *Geochimica et Cosmochimica Acta* **56**, 303–318.
- Stolper, E. (1977). Experimental petrology of eucritic meteorites. *Geochimica et Cosmochimica Acta* **41**, 587–611.
- Thy, P. (1991). High and low-pressure phase equilibria of a mildly alkalic lava from the 1965 Surtsey eruption: Experimental results. *Lithos* **26**, 223–243.

- Thy, P. (1992). Low-pressure melting relations of a basalt from Hole 797C in the Yamato Basin of the Japan Sea. *Proceedings of the Ocean Drilling Program, Scientific Results* **127–128, Part 2**, 861–868.
- Thy, P. (1995a). Experimental constraints on the evolution of transitional and mildly alkalic basalts: crystallization of spinel. *Lithos* **36**, 103–114.
- Thy, P. (1995b). Low-pressure experimental constraints on the evolution of komatiites. *Journal of Petrology* **36**, 1529–1548.
- Thy, P., Leshner, C. E. & Fram, M. S. (1998). Low pressure experimental constraints on the evolution of basaltic lavas from site 917, southeast Greenland continental margin. *Proceedings of the Ocean Drilling Program, Scientific Results* **152**, 359–372.
- Thy, P., Leshner, C. E., Nielsen, T. F. D. & Brooks, C. K. (2006). Experimental constraints on the Skaergaard liquid line of descent. *Lithos* **92**, 154–180.
- Thy, P., Lofgren, G. E. & Imsland, P. (1991). Melting relations and the evolution of the Jan Mayen magma system. *Journal of Petrology* **32**, 303–332.
- Toplis, M. J. & Carroll, M. R. (1995). An experimental study of the influence of oxygen fugacity on Fe-Ti oxide stability, phase relations, and mineral-melt equilibria in ferro-basaltic systems. *Journal of Petrology* **36**, 1137–1170.
- Toplis, M. J., Libourel, G. & Carroll, M. R. (1994). The role of phosphorus in crystallization processes of basalt: An experimental study. *Geochimica et Cosmochimica Acta* **58**, 797–810.
- Tormey, D. R., Grove, T. L. & Bryan, W. B. (1987). Experimental petrology of normal MORB near the Kane Fracture Zone: 22°N–25°N, mid-Atlantic ridge. *Contributions to Mineralogy and Petrology* **96**, 121–139.
- Walker, D. & Grove, T. (1993). Ureilite smelting. *Meteoritics* **28**, 629–636.
- Walker, D., Kirkpatrick, R. J., Longhi, J. & Hays, J. F. (1976). Crystallization history of lunar picritic basalt sample 12002: Phase-equilibria and cooling-rate studies. *Geological Society of America Bulletin* **87**, 646–656.
- Walker, D., Longhi, J., Stolper, E. M., Grove, T. L. & Hays, J. F. (1977). Slowly cooled microgabbros 15065 and 15555. *Proceedings of the Eighth Lunar Science Conference*, 964–966.

- Walker, D., Shibata, T. & DeLong, S. E. (1979). Abyssal tholeiites from the Oceanographer Fracture Zone. *Contributions to Mineralogy and Petrology* **70**, 111–125.
- Wang, Z. & Gaetani, G. A. (2008). Partitioning of Ni between olivine and siliceous eclogite partial melt: experimental constraints on the mantle source of Hawaiian basalts. *Contributions to Mineralogy and Petrology* **156**, 661–678.
- Yang, H.-J., Kinzler, R. J. & Grove, T. L. (1996). Experiments and models of anhydrous, basaltic olivine-plagioclase-augite saturated melts from 0.001 to 10 kbar. *Contributions to Mineralogy and Petrology* **124**, 1–18.

## Supplementary Material Tables

Table A1. Results of the mass balance calculations using the experimental data of Roeder and Emslie (1970)

| Run #           | liq   | ol    | sp           | plag  | liq FeO | liq Fe <sub>2</sub> O <sub>3</sub> | $\chi^2$ | SSR  | bulk $\Delta$ FeO* | K <sub>D</sub> <sup>all</sup> | K <sub>D</sub> <sup>mg</sup> | $\Delta$ QFM |
|-----------------|-------|-------|--------------|-------|---------|------------------------------------|----------|------|--------------------|-------------------------------|------------------------------|--------------|
| 7-1-654         | 0.882 | 0.110 | <b>0.008</b> |       | 5.979   | 5.878                              | 1.12     | 0.62 | 8.85               | 0.330(28)                     | 0.362(31)                    | 2.06         |
| 7-2-654         | 0.904 | 0.091 | 0.005        |       | 7.903   | 3.464                              | 2.71     | 0.10 | 2.73               | 0.293(25)                     | 0.298(25)                    | 1.75         |
| 7-3-654         | 0.931 | 0.065 | 0.004        |       | 8.146   | 3.515                              | 0.50     | 0.17 | 2.03               | 0.302(26)                     | 0.312(26)                    | 1.46         |
| 7-5-654         | 0.895 | 0.083 | <b>0.022</b> |       | 7.406   | 3.611                              | 1.43     | 0.94 | 7.40               | 0.287(24)                     | 0.330(28)                    | 1.92         |
| 7-6-654         | 0.966 | 0.032 | 0.003        |       | 8.295   | 3.042                              | 1.18     | 0.33 | -4.70              | 0.290(25)                     | 0.281(24)                    | 1.17         |
| 7-9-654         | 0.940 | 0.057 | 0.003        |       | 8.268   | 3.148                              | 1.73     | 0.09 | -0.50              | 0.302(26)                     | 0.294(25)                    | 1.30         |
| 7-10-654        | 0.976 | 0.022 | 0.002        |       | 8.262   | 2.894                              | 0.17     | 0.02 | -5.02              | 0.311(26)                     | 0.314(27)                    | 1.03         |
| 7-11-654        | 0.984 | 0.014 | 0.002        |       | 8.351   | 3.084                              | 0.46     | 0.10 | -3.74              | 0.321(27)                     | 0.311(26)                    | 0.89         |
| 6-1-654         | 0.952 | 0.043 | <b>0.005</b> |       | 4.945   | 6.695                              | 0.19     | 0.07 | -1.12              | 0.329(28)                     | 0.348(30)                    | 2.45         |
| 6-2-654         | 0.974 | 0.020 | 0.006        |       | 6.804   | 4.678                              | 0.82     | 0.20 | -3.01              | 0.300(26)                     | 0.289(25)                    | 2.18         |
| 6-3-654         | 0.967 | 0.026 | 0.007        |       | 6.942   | 4.619                              | 1.69     | 0.29 | -1.16              | 0.308(26)                     | 0.293(25)                    | 2.34         |
| 8-1-654         | 0.815 | 0.122 | 0.004        | 0.058 | 8.456   | 2.927                              | 2.09     | 1.12 | -1.38              | 0.321(27)                     | 0.302(26)                    | 0.96         |
| 8-2-654         | 0.912 | 0.085 | 0.003        |       | 9.115   | 2.320                              | 0.36     | 0.30 | 1.42               | 0.315(27)                     | 0.310(26)                    | 0.68         |
| 8-3-654         | 0.942 | 0.056 | 0.002        |       | 9.027   | 1.888                              | 3.76     | 0.86 | -6.72              | 0.320(27)                     | 0.292(25)                    | 0.39         |
| <b>8-4-654</b>  | 0.934 | 0.063 | 0.003        |       | 8.817   | 2.507                              | 0.86     | 0.22 | 2.20               | 0.311(26)                     | 0.327(28)                    | 0.07         |
| 9-1-654         | 0.841 | 0.143 |              | 0.015 | 8.695   | 1.896                              | 3.62     | 1.10 | 0.89               | 0.295(25)                     | 0.309(26)                    | -0.01        |
| <b>10-3-654</b> | 0.951 | 0.049 |              |       | 9.562   | 1.096                              | 1.65     | 1.25 | -1.10              | 0.328(28)                     | 0.344(29)                    | -1.94        |
| <b>10-4-654</b> | 0.921 | 0.079 |              |       | 9.270   | 1.423                              | 3.28     | 1.88 | 1.31               | 0.319(27)                     | 0.344(29)                    | -1.64        |
| <b>10-5-654</b> | 0.892 | 0.106 | 0.002        |       | 9.334   | 1.166                              | 0.44     | 0.47 | 0.21               | 0.325(28)                     | 0.328(28)                    | -1.35        |
| <b>11-2-654</b> | 0.911 | 0.089 |              |       | 9.789   | 0.819                              | 3.03     | 1.86 | 1.87               | 0.322(27)                     | 0.340(29)                    | -2.65        |
| 7-1-C71         | 0.918 | 0.079 | 0.003        |       | 8.970   | 2.903                              | 1.35     | 0.62 | 4.01               | 0.271(23)                     | 0.273(23)                    | 1.30         |
| 7-2-C71         | 0.941 | 0.056 | 0.003        |       | 8.189   | 2.546                              | 8.36     | 2.70 | -3.68              | 0.301(26)                     | 0.343(29)                    | 1.03         |
| 7-4-C71         | 0.962 | 0.036 | 0.002        |       | 8.745   | 1.983                              | 0.99     | 1.26 | -8.51              | 0.277(24)                     | 0.279(24)                    | 0.69         |
| 7-1-C218        | 0.955 | 0.040 | <b>0.005</b> | 0.000 | 8.474   | 3.811                              | 0.74     | 0.92 | 6.73               | 0.253(21)                     | 0.260(22)                    | 1.75         |

Notes: Bold and italicized run numbers indicate experiments conducted in alumina crucibles; all other experiments were conducted in Ag-Pd alloy capsules. Phase abbreviations: liq = liquid, ol = olivine, sp = Cr-spinel or magnetite, plag = plagioclase; values under these heading are phase proportions in weight fractions; values in bold and italics under the sp-heading indicate magnetite. In run 7-1-C218, the mass balance calculation returned a plagioclase mode of zero; the qualitative plagioclase mode in Roeder and Emslie's unpublished data table (REUPDT) is "trace". Liquid FeO and liquid Fe<sub>2</sub>O<sub>3</sub> are the wt % concentrations of these oxides in the liquid calculated by mass balance. SSR = sum of squared residuals from the mass balance. BulkΔFeO\* is the difference (in %) between the bulk FeO\* content determined by microprobe (probe) on each of the glassed starting materials and the wet chemistry (wc) bulk FeO and Fe<sub>2</sub>O<sub>3</sub> measurements on each of the experimental charges:  $100 \times [(FeO + 0.89981 \times Fe_2O_3)_{wc} - FeO^*_{probe}] / FeO^*_{probe}$ .  $K_D^{all}$  is the olivine-liquid exchange coefficient calculated using liquid FeO content based on a mass balance using all oxides and phases with the exception that clinopyroxene in runs 7-1-654 and 9-1-654 were assumed to be negligible;  $K_D^{mg}$  is the exchange coefficient with liquid FeO determined following the procedure of Roeder and Emslie (1970). Values in parentheses are 1s uncertainties calculated by propagating the 1s errors associated with FeO and MgO in liquid and olivine, respectively; uncertainties on the phase compositions are described below. ΔQFM is the  $\log fO_2$  of the experiment relative to the QFM buffer (O'Neill, 1987). Bulk compositions for the three starting materials are from Table 1 of Roeder and Emslie (1970) with the exception that the bulk FeO\* value in each mass balance calculation was replaced by the wet chemical measurements of bulk FeO and Fe<sub>2</sub>O<sub>3</sub> for each experiment; wet chemical data are taken from REUPDT. Cr contents for the three bulk compositions (not reported in Table 1 of Roeder and Emslie, 1970) were estimated using Cr and MgO contents for lavas from Kilauea (1084 points) and Hualalai (77 points) from the GeoRoc database (<http://georoc.mpch-mainz.gwdg.de/georoc/>). The equation: Cr (ppm) = a + b × log(MgO, wt%), yielded fits with correlation coefficients (R) of 0.95 (Kilauea) and 0.90 (Hualalai), respectively and Cr<sub>2</sub>O<sub>3</sub> contents in wt % of 0.0879 (Kilauea, 654), 0.0604 (Hualalai, C218), and 0.1009 (Hualalai, C71) for the MgO contents of the three bulk compositions; a and b values for the two sets of data are: -1375.17, 1959.79 (Kilauea) and -1705.77, 2318.70 (Hualalai). Olivine compositions are based on reported forsterite and fayalite values (REUPDT) and were converted into oxide wt % of SiO<sub>2</sub>, FeO, and MgO. The sum of the three oxides was fixed to that of the reported wt % sum of Fo and Fa, i.e., if Fo + Fa in a given experiment summed to 98 wt %, then the sum of SiO<sub>2</sub>, FeO, and MgO for olivine from that experiment was also fixed at 98 wt %. Spinels

compositions were estimated using the algorithm of Poustovetov and Roeder (2001). When Cr-spinel was included in the mass balance, the Cr content of the melt was set to zero. The model of Poustovetov and Roeder (2001) does not require a liquid  $\text{Cr}_2\text{O}_3$  value and including  $\text{Cr}_2\text{O}_3$  as an unknown in the melt leads to the Cr mass balance equation being under-constrained. The model does require FeO and  $\text{Fe}_2\text{O}_3$  liquid values and thus Cr-spinel compositions were calculated simultaneously during the mass balance minimization. We also tested the liquid-magnetite model of Ariskin and Barmina (1999) for the more oxidized experiments, i.e.,  $\geq\text{QFM}+1.75$  (the model of Poustovetov and Roeder is not well calibrated under these more oxidizing conditions). When magnetite was used in the mass balance, liquid and bulk  $\text{Cr}_2\text{O}_3$  contents were set to zero. For the six spinel-bearing experiments run at  $\geq\text{QFM}+1.75$ , the choice of which mass balance model to accept (Cr-spinel or magnetite) depended on which gave the lowest  $\chi^2$  value and a non-zero spinel mode. With two exceptions, the choice of Cr-spinel or magnetite had little effect on the calculated ol-liq  $K_D$ ; in runs 7-1-654 and 6-1-654, ol-liq  $K_D$  decreased from 0.394 to 0.330 and 0.362 to 0.329, respectively when magnetite was used in place of Cr-spinel. For the four experiments that contained plagioclase, we used the model of Putirka (2005) to calculate a coexisting plagioclase composition. FeO and  $\text{Fe}_2\text{O}_3$  contents in the liquid were calculated based on the following constraints: (1)  $\text{FeO}^{\text{liq}} + 0.89981 \times \text{Fe}_2\text{O}_3^{\text{liq}} = \text{FeO}^{*\text{liq}}$  (as measured by microprobe); (2)  $a_1 \times \text{FeO}^{\text{liq}} + a_2 \times \text{FeO}^{\text{ol}} + a_3 \times \text{FeO}^{\text{sp}} = \text{FeO}^{\text{bulk}}$ ; and (3)  $a_1 \times \text{Fe}_2\text{O}_3^{\text{liq}} + a_3 \times \text{Fe}_2\text{O}_3^{\text{sp}} = \text{Fe}_2\text{O}_3^{\text{bulk}}$ ; where the  $a_1$ ,  $a_2$ , and  $a_3$  are the calculated mass fractions of the phases. Since sodium is known to be volatile in 1-atm experiments (e.g., Tsuchiyama et al., 1981), we allowed bulk  $\text{Na}_2\text{O}$  to vary in order to minimize  $\chi^2$ ; the closure constraint was applied to the bulk composition in that if bulk  $\text{Na}_2\text{O}$  decreased, the remaining oxides in the bulk increased by a proportional amount. Bulk  $\Delta\text{Na}_2\text{O}$  values (the difference in percent between the bulk  $\text{Na}_2\text{O}$  content required to minimize  $\chi^2$  and the bulk  $\text{Na}_2\text{O}$  as measured by microprobe on the glassed starting material) for 22 of the mass balance calculations are less than the uncertainty on the sodium microprobe measurement ( $\pm 9\%$ ); for runs 10-4-654 and 7-2-C71,  $\Delta\text{Na}_2\text{O}$  is 10.2% and 9.3%, respectively. It is clear from the liquid compositions that those experiments run in  $\text{Al}_2\text{O}_3$  crucibles gained alumina. For these five experiments, we allowed the bulk  $\text{Al}_2\text{O}_3$  to vary along with  $\text{Na}_2\text{O}$  and again the remaining oxide concentrations in the bulk increased or decreased depending on the relative changes in  $\text{Al}_2\text{O}_3 + \text{Na}_2\text{O}$ . For these five experiments, bulk  $\Delta\text{Al}_2\text{O}_3$  values range from  $\sim 5$  to 31% and show a broad positive correlation with run temperature and run time. Uncertainties on the bulk, liquid, and solid phase compositions are based on the relative errors reported in Roeder and Emslie (1970). Specifically, fractional errors for  $\text{SiO}_2$ ,  $\text{TiO}_2$ ,  $\text{Al}_2\text{O}_3$ ,  $\text{FeO}^*$ ,  $\text{MgO}$ ,  $\text{CaO}$ ,  $\text{Na}_2\text{O}$  and  $\text{K}_2\text{O}$  are 0.04, 0.04, 0.04, 0.04, 0.06, 0.05, 0.09, and 0.08, respectively (for olivine we lowered the

uncertainty for MgO to 0.04 on the assumption that the high concentration of MgO in olivine would allow for more precise analyses). For Cr<sub>2</sub>O<sub>3</sub> in Cr-spinel and the bulk composition we arbitrarily used a fractional error of 0.04. For the wet chemical FeO and Fe<sub>2</sub>O<sub>3</sub> contents in the bulk composition, we used the FeO and Fe<sub>2</sub>O<sub>3</sub> measurements and their reported uncertainties from Hill and Roeder (1974) to calculate fractional errors and plot them as a function of FeO and Fe<sub>2</sub>O<sub>3</sub> concentrations—the data sets are well fit by the following equations: FeO fract. error = 0.050691/(FeO, wt %); R = 0.98 and Fe<sub>2</sub>O<sub>3</sub> fract. error = 0.167676/(Fe<sub>2</sub>O<sub>3</sub>, wt %); R = 0.95. For the calculated Fe<sub>2</sub>O<sub>3</sub> liquid contents, we used the expression above for the 1s uncertainties since the uncertainties are rather large (for the range of bulk Fe<sub>2</sub>O<sub>3</sub> measurements, fractional errors vary from 0.419 to 0.025). For the measured range of bulk FeO contents (5.3 to 10.8 wt %), fractional errors are substantial smaller than the FeO\* microprobe uncertainty (0.01–0.005 vs. 0.04) and for this reason we added a constant term of 0.014 to the FeO fractional error equation when we applied it to the calculated FeO liquid contents. This brought the calculated errors on the liquid FeO concentrations more in line with the microprobe uncertainties but nevertheless allowed us to retain the concentration dependence.

Table A2. Compositions (in wt %) used for olivine-addition calculations

|                         | SiO <sub>2</sub> | TiO <sub>2</sub> | Al <sub>2</sub> O <sub>3</sub> | Cr <sub>2</sub> O <sub>3</sub> | FeO*  | MnO   | MgO  | CaO   | Na <sub>2</sub> O | K <sub>2</sub> O | P <sub>2</sub> O <sub>5</sub> |
|-------------------------|------------------|------------------|--------------------------------|--------------------------------|-------|-------|------|-------|-------------------|------------------|-------------------------------|
| MK low-Si <sup>a</sup>  | 48.75            | 2.63             | 13.89                          | 0.044                          | 11.57 | 0.169 | 7.89 | 11.30 | 2.42              | 0.393            | 0.215                         |
| MK high-Si <sup>a</sup> | 51.40            | 2.44             | 13.46                          | 0.045                          | 10.43 | 0.166 | 7.39 | 11.24 | 2.22              | 0.383            | 0.202                         |
| ML <sup>b</sup>         | 51.90            | 2.04             | 13.84                          | 0.051                          | 10.41 | 0.166 | 7.62 | 10.70 | 2.22              | 0.339            | 0.206                         |
| Kil <sup>c</sup>        | 50.65            | 2.42             | 13.20                          | 0.070                          | 11.06 | 0.168 | 7.96 | 10.83 | 2.25              | 0.426            | 0.233                         |

<sup>a</sup> Mauna Kea low-SiO<sub>2</sub> and high-SiO<sub>2</sub> compositions based on glass compositions with  $\geq 7$  wt % MgO reported in Stolper *et al.* (2004); Cr<sub>2</sub>O<sub>3</sub> contents based on whole rock Cr vs. MgO regressions (Cr calculated at MgO values of 7.89 and 7.39 wt %, respectively); whole rock data from Rhodes and Vollinger (2004). Definition of glass and whole rock low-SiO<sub>2</sub> and high-SiO<sub>2</sub> compositions from Stolper *et al.* (2004).

<sup>b</sup> Mauna Loa composition represents the average of glass compositions with  $\geq 7$  wt % MgO from the GeoRock database (<http://georoc.mpch-mainz.gwdg.de/georoc/>). Cr content calculated from Mauna Loa bulk rock data (Rhodes, 1996) as described in the note for the Mauna Kea low-Si composition.

<sup>c</sup> Kilauea composition is the average of glass compositions from the GeoRock database with  $\geq 7$  wt % MgO.

Table A3. Compositions of calculated parental Hawaiian magmas (in wt %)

|     | $K_D$ | $Mg^{\#ol}$ | $\Delta QFM$ | SiO <sub>2</sub> | TiO <sub>2</sub> | Al <sub>2</sub> O <sub>3</sub> | FeO*  | MnO  | MgO   | CaO  | Na <sub>2</sub> O | K <sub>2</sub> O | P <sub>2</sub> O <sub>5</sub> |
|-----|-------|-------------|--------------|------------------|------------------|--------------------------------|-------|------|-------|------|-------------------|------------------|-------------------------------|
| MK1 | 0.30  | 0.90        | -0.5         | 47.09            | 2.11             | 11.18                          | 11.73 | 0.17 | 15.52 | 9.15 | 1.94              | 0.32             | 0.17                          |
| MK1 | 0.30  | 0.90        | -2.0         | 46.81            | 2.03             | 10.74                          | 11.83 | 0.17 | 16.71 | 8.80 | 1.87              | 0.30             | 0.17                          |
| MK1 | 0.30  | 0.91        | -0.5         | 46.77            | 2.00             | 10.60                          | 11.60 | 0.17 | 17.30 | 8.68 | 1.84              | 0.30             | 0.16                          |
| MK1 | 0.30  | 0.91        | -2.0         | 46.48            | 1.92             | 10.13                          | 11.68 | 0.16 | 18.57 | 8.31 | 1.76              | 0.29             | 0.16                          |
| MK1 | 0.34  | 0.90        | -0.5         | 46.53            | 1.94             | 10.29                          | 11.92 | 0.16 | 17.93 | 8.44 | 1.79              | 0.29             | 0.16                          |
| MK1 | 0.34  | 0.90        | -2.0         | 46.19            | 1.85             | 9.77                           | 12.05 | 0.16 | 19.33 | 8.02 | 1.70              | 0.28             | 0.15                          |
| MK1 | 0.34  | 0.91        | -0.5         | 46.17            | 1.82             | 9.65                           | 11.75 | 0.16 | 19.92 | 7.92 | 1.68              | 0.27             | 0.15                          |
| MK1 | 0.34  | 0.91        | -2.0         | 45.83            | 1.72             | 9.10                           | 11.86 | 0.16 | 21.40 | 7.48 | 1.58              | 0.26             | 0.14                          |
| MK1 | 0.34  | 0.91        | -1.0         | 46.04            | 1.78             | 9.43                           | 11.79 | 0.16 | 20.50 | 7.75 | 1.64              | 0.27             | 0.15                          |
| MK2 | 0.34  | 0.91        | -1.0         | 48.18            | 1.73             | 9.55                           | 10.92 | 0.16 | 18.98 | 8.04 | 1.57              | 0.27             | 0.14                          |
| ML  | 0.34  | 0.917       | -1.8         | 48.01            | 1.35             | 9.15                           | 10.81 | 0.16 | 21.22 | 7.14 | 1.46              | 0.22             | 0.14                          |
| Kil | 0.34  | 0.908       | -0.7         | 47.74            | 1.74             | 9.49                           | 11.37 | 0.16 | 19.02 | 7.84 | 1.61              | 0.31             | 0.17                          |
| Kil | 0.34  | 0.908       | -1.4         | 47.54            | 1.69             | 9.24                           | 11.43 | 0.16 | 19.73 | 7.64 | 1.57              | 0.30             | 0.16                          |

MK1 = Mauna Kea low-SiO<sub>2</sub> composition; MK2 = Mauna Loa high-SiO<sub>2</sub> composition; ML = Mauna Loa composition; Kil = Kilauea composition (all from Table A2).  $K_D$  is the constant value Fe<sup>+2</sup>-Mg exchange coefficient between olivine and liquid used for each calculation;  $Mg^{\#ol}$  is the Mg/(Mg+Fe), atomic, of the target olivine;  $\Delta QFM$  is the  $fO_2$  relative to QFM (O'Neill, 1987) used for each calculation. Starting with each average glass composition in Table A2, 0.0001 weight fraction of equilibrium olivine was repeatedly added to each composition until the evolving composition was in equilibrium with the target olivine; at each step Fe<sup>+3</sup>/Fe<sup>+2</sup> in the liquid was calculated using eqn. 12 of Jayasuriya *et al.* (2004), the specified  $fO_2$ , and the temperature calculated using the expression of Beattie (1993); olivine MnO and CaO contents calculated using the expression of Beattie *et al.* (1991) for MnO and a cation-based

version of the algorithm of Libourel (1999) for CaO; cation-based Al and Cr partition coefficients between olivine and liquid were 0.005 and 0.6, respectively (Bédard, 1994). Parental Cr<sub>2</sub>O<sub>3</sub> contents not listed. See the main text for a discussion of the target olivine compositions and  $f_{O_2}$ s of Hawaiian lavas.

### Supplementary Material Figure Captions

**Fig. A1.** Molar FeO/MgO in olivine (ol) vs. molar FeO/MgO in the coexisting liquid (liq) from the 27 experiments used by Roeder and Emslie (1970) to determine the value of the olivine-liquid Fe<sup>+2</sup>-Mg exchange coefficient ( $K_D$ ). Liquid FeO was determined by mass balance following the procedure described by Roeder and Emslie (1970): phases other than olivine and glass (spinel, clinopyroxene, and plagioclase) were ignored; the proportions of glass and olivine in each experiment were calculated using MgO contents of the glass, olivine, and bulk composition, respectively; FeO in the glass was calculated using the proportions of liquid and olivine and the measured FeO contents of the olivine and the bulk charge. The unweighted least-squares line is forced through the origin and yields a  $K_D$  of  $0.305 \pm 0.005$ . The relative positions of the points are extremely similar to those seen in Fig. 4 of Roeder and Emslie (1970).

**Fig. A2.** (a) Histogram of individual ol-liq  $K_{D,Fe^{+2}-Mg}$  values from the 27 experiments of Roeder and Emslie (1970); liquid FeO for each experiment calculated as described by Roeder and Emslie and in the caption to Fig. A1. The three different bulk compositions are denoted by dark (olivine basalt: 654), stippled (ankaramite: C71), and no shading (alkali olivine basalt: C218), respectively. The overall spread in  $K_D$  values is from 0.260 to 0.362. Although there is a tendency for experiments on the bulk compositions with lower silica contents (C71 and C218) to plot to the left of the diagram (to low  $K_D$ s), one experiment on C71 produced a  $K_D$  of 0.343. (b) Histogram of individual ol-liq  $K_{D,Fe^{+2}-Mg}$  values

distinguished by capsule material: red = either Ag<sub>55</sub>Pd<sub>45</sub> or Ag<sub>60</sub>Pd<sub>40</sub> alloy capsules; black = Al<sub>2</sub>O<sub>3</sub> crucibles. Note that the Al<sub>2</sub>O<sub>3</sub> crucible experiments yield tightly clustered  $K_D$  values (0.344–0.327), while those from the Ag-Pd alloy runs range from 0.260–0.362.

**Fig. A3.** SiO<sub>2</sub> vs. MgO (both in wt %) in the experimental glasses from the Kilauea olivine basalt (bulk composition 654) experiments showing the anomalous silica value in run 7-8-654 relative to the other glasses. Note that the SiO<sub>2</sub> content of the glass in 7-5-654 is also somewhat high relative to that seen in the remaining experiments.

**Fig. A4.** CaO vs. MgO (both in wt %) in the experimental glasses from the olivine basalt (bulk composition 654) experiments showing that the two clinopyroxene (cpx)-bearing experiments (open circles) are consistent with the CaO-MgO trend defined by the clinopyroxene-free experiments (filled circles). The solid black line is an unweighted least-squares fit to the clinopyroxene-free glasses.

**Fig. A5.** Calculated olivine modes (a) and spinel modes (b) as a function of run temperature (°C). Only the 7-X-654 series of experiments are plotted (where X denotes the run number). Modes calculated using all oxides and all phases except clinopyroxene (this study). The filled circles define tight linear arrays that are negatively correlated with temperature, whereas run 7-5-654 plots substantially off the olivine and spinel trends. The

calculated spinel mode for 7-5-654 is insensitive to the whether Cr-spinel or magnetite is used in the mass balance calculation.

**Fig. A6.** (a) Olivine-liquid (ol-liq)  $K_{D,Fe^{+2}-Mg}$  (R&E; MgO) where liquid FeO is calculated using the approach of Roeder and Emslie (1970) vs. ol-liq  $K_{D,Fe^{+2}-Mg}$  (all oxides) where liquid FeO is calculated using all oxides, a weighted mass balance approach, and with the compositions of all coexisting phases, except for clinopyroxene (this study). Symbol color denotes the experimental container material: either an Ag-Pd alloy or alumina. Error bars ( $1\sigma$ ) for both sets of  $K_D$  values are calculated by propagating FeO and MgO uncertainties associated with liquid and olivine compositions (uncertainties in FeO liquid for the Roeder and Emslie  $K_{DS}$  were assumed to be the same as those for FeO liquid in the complete mass balance calculation, see notes to Table A1 for more discussion). Unweighted mean and  $1\sigma$  values for both sets of  $K_{D,Fe^{+2}-Mg}$  s are given in the lower right corner of the figure. Note that both mean values are based on 24 experiments (i.e., the three rejected experiments, 8-2-C218, 7-5-654 and 7-8-654 were not included in the  $K_{D,Fe^{+2}-Mg}$  averages. (b) Ratio of  $K_{DS}$  ( $K_{D,R\&E\ using\ MgO}/K_{D,\ using\ all\ oxides}$ ) vs.  $\Delta FeO^*$  liquid defined as the percentage difference between the calculated  $FeO + 0.89981 \times Fe_2O_3$  value from the mass balance (mb) and the microprobe (probe) glass  $FeO^*$  value for each experiment:  $100 \times [(FeO + 0.89981 \times Fe_2O_3)_{mb} - FeO^*_{probe}] / FeO^*_{probe}$ . Symbol color denotes the experimental container material (see legend).

**Fig. A7.** Ol-liq  $K_{D,Fe^{+2}-Mg}$  (liquid FeO for each experiment calculated using a weighted mass balance approach, all oxides, and all coexisting phases except clinopyroxene) vs. bulk  $\Delta FeO^*$  in percent. Bulk  $\Delta FeO^*$  is defined as the percent difference between the wet chemistry (wc) measurements on each experimental charge ( $FeO + 0.89981 \times Fe_2O_3$ ) and  $FeO^*$  measured by electron microprobe (probe) on each of the glassed starting materials:  $100 \times [(FeO + 0.89981 \times Fe_2O_3)_{wc} - FeO^*_{probe}] / FeO^*_{probe}$ . Symbol color denotes the run container: red for an Ag-Pd alloy or black for alumina. Error bars on  $K_{D,Fe^{+2}-Mg}$  are  $1\sigma$  and are based on FeO and MgO uncertainties in olivine and glass, respectively.

**Fig. A8.** (a)  $\ln(Fe^{+3}/Fe^{+2})$  molar vs.  $\ln fO_2$  for the  $\sim 1200^\circ C$  superliquidus or near-liquidus experiments on bulk composition RHB (Hill and Roeder, 1974). FeO and  $Fe_2O_3$  determined by wet chemistry (see Hill and Roeder, 1974 for a discussion of analytical methods). Temperature range for the eight experiments is  $1195\text{--}1202^\circ C$ ; only the Pt capsule air experiment is below the liquidus. Error bars associated with  $\ln(Fe^{+3}/Fe^{+2})$  are one sigma and are based on the FeO and  $Fe_2O_3$  uncertainties reported in Hill and Roeder (1974); for all but the two most reducing experiments, one sigma errors are smaller than the size of the symbols. (b) Histogram of  $\ln(fO_2)$  coefficients (the slope of the line in panel a) at constant temperature and liquid composition for a wide range of non-magmatic systems (e.g., iron oxide slags), magmatic liquids (e.g., natural silicate liquids), and model expressions designed for magmatic liquids (e.g., equations for estimating  $Fe^{+3}/Fe^{+2}$  as a function of temperature,  $fO_2$ , and liquid composition; the 654 bulk composition of Roeder and Emslie (1970) was used for calculating temperature dependences shown in the figure).

Experimental data references: Larson and Chipman, 1953; Fudali, 1965; Shibata, 1967; Timucin and Morris, 1970; Hill and Roeder, 1974; O'Horo and Levy, 1978; Schreiber *et al.*, 1980; Bowker *et al.*, 1981; Mysen and Virgo, 1983; Virgo *et al.*, 1983; Mysen *et al.*, 1984; Schreiber *et al.*, 1986; Dingwell and Virgo, 1987; Kress and Carmichael, 1988, 1989; Iwase *et al.*, 1998; references for  $\text{Fe}^{3+}/\text{Fe}^{2+}$  models: Sack *et al.*, 1980; Kilinc *et al.*, 1983; Kress and Carmichael, 1988; Kress and Carmichael, 1991; Nikolaev *et al.*, 1996; Jayasuriya *et al.*, 2004.

**Fig. A9.** Calculated  $\ln(\text{Fe}^{+3}/\text{Fe}^{+2})$  in glass vs.  $\ln(f\text{O}_2)$  for the experiments of Roeder and Emslie (1970) on the 654 bulk composition; liquid  $\text{Fe}_2\text{O}_3$  and FeO from mass balance calculations using all oxides and phases (except clinopyroxene). Experiments from 1152–1153°C are plotted in (a), from 1175–1180°C in (b), from 1195–1212°C in (c), and from 1214–1228°C in (d). Regression lines and accompanying slopes are unweighted fits to the data: red solid lines are fits to the Ag-Pd capsule experiments plotted in each panel; solid black lines are fits to the  $\text{Al}_2\text{O}_3$  crucible experiments; and black dashed lines are fits to all the points in a given panel. Error bars (often smaller than the size of the symbols) are one sigma and are based on estimates of the uncertainties associated with the calculated FeO and  $\text{Fe}_2\text{O}_3$  in the glass (see text for further discussion).

**Fig. A10.**  $\ln(\text{Fe}^{+3}/\text{Fe}^{+2})$  vs.  $\ln(f\text{O}_2)$  for the ~1200°C alumina crucible experiments on bulk composition 654 (Roeder and Emslie, 1970) and RHB (Hill and Roeder, 1974). Slope is

from an unweighted fit to the data; error bars are one sigma and are calculated as described in the caption to Fig. A9.

**Fig. A11.** Histogram of temperature coefficients ( $10^4/T$ , K) for  $\ln(\text{Fe}^{+3}/\text{Fe}^{+2})$  in non-magmatic and magmatic liquids and from model expressions (e.g., equations for estimating  $\text{Fe}^{+3}/\text{Fe}^{+2}$  as a function of temperature,  $f\text{O}_2$ , and liquid composition). Data sources: Kennedy (1948), Johnston (1964), Sack *et al.* (1980), Kilinc *et al.* (1983), Mysen and Virgo (1983), Mysen *et al.* (1985ab), Kress and Carmichael (1988, 1991), Borisov and Shapkin (1989), Ghiorso and Kress (2004), Lange and Carmichael (1989), Ohashi *et al.* (2000), and Jayasuriya *et al.* (2004).

**Fig. A12.**  $\ln(\text{Fe}^{+3}/\text{Fe}^{+2})$  corrected to a reference temperature of 1155°C vs.  $\ln(f\text{O}_2)$  for the five alumina and 12 Ag-Pd experiments that have provisionally passed all of the previously described tests that are described in the text. The solid line is a weighted fit to the data and the dashed curves represent the 95% confidence interval for the regression. Error bars associated with each point are  $2\sigma$  and are calculated as described in the caption to Fig. A9.

**Fig. A13.**  $K_{\text{D,Fe}^{+2}\text{-MgS}}$  (liquid FeO for each experiment calculated using a weighted mass balance approach, all oxides, and all coexisting phases except clinopyroxene) vs. bulk  $\Delta\text{FeO}^*$  in percent (defined in the caption to Fig. A7). Error bars are  $1\sigma$  and are calculated as described in the caption to Fig. A6. Only the experiments plotted in Fig. A12 are shown here. Compare to Fig. A7.

**Fig. A14.** The sensitivity of  $K_{D,Fe^{+2}-Mg}$  to changes in bulk FeO, liquid MgO, and Fo and Fa contents of the equilibrium olivine. The filled black circle is the result of the mass balance calculation for run 7-3-654 (Table A1). The green curve denotes the effect on  $K_{D,Fe^{+2}-Mg}$  and liquid FeO of increasing or decreasing the bulk FeO by the specified amount and rerunning the mass balance. Changing the olivine composition from Fo<sub>79</sub>Fa<sub>20</sub> to either Fo<sub>78</sub>Fa<sub>21</sub> or Fo<sub>80</sub>Fa<sub>19</sub> (weight units) and rerunning the mass balance results in the open blue circles. The effect of changing the liquid MgO content by  $\pm 2\sigma$  is denoted by the open orange circles (uncertainties for bulk FeO and liquid MgO are listed in the notes to Table A1).

**Fig. A15.** (a)  $S/(C + M + A + S)$  vs. ol-liq  $K_{D,Fe^{+2}-Mg}$  for the 1-atm QFM $\pm 0.25$  experiments compiled from the literature as part of this study. Small open black circles are data from the literature;  $S/(C + M + A + S)$  calculated as described in the Supplement;  $K_{D,Fe^{+2}-Mg}$  calculated using FeO in each of the glass compositions as predicted by Jayasuriya *et al.*, 2004 at the temperature and  $fO_2$  of that experiment. The curved black line is an unweighted least-squares fit to this data using the expression:  $K_{D,Fe^{+2}-Mg} = a + b \times \exp(c \times "S")$  where "S" is equal to  $S/(C + M + A + S)$ , the values of the coefficients a, b, and c are given in the Supplement. The two larger open black circles are representative points that illustrate the effect of being moved parallel to the black line (path denoted by the two red lines with arrows) to an "S" value of 0.5; their projected positions are given by

the two open blue circles. The smaller filled blue circles represent the projected positions of all the other open black circles. (b) “S” projected ol-liq  $K_{D,Fe^{+2}-Mg}$  ( $[K_{D,Fe^{+2}-Mg}]_{0.5}$ ) vs. coexisting olivine  $Mg/(Mg+Fe)$ , atomic, values. The filled and open blue circles are the same as those in Fig. A15a. The black line is an unweighted least-squares fit using the equation:  $[K_{D,Fe^{+2}-Mg}]_{0.5} = d + e \times [Mg/(Mg+Fe)]^{ol}$  (values of the coefficients are given in the Supplemental text). Red lines show the movement of two representative points (the same two points as in panel a) parallel to the black line to an olivine composition of  $Fo_{88}$ . This represents the second projection. The filled gray circles define the now twice-projected ol-liq  $K_D$  values. It is these twice-projected values that are plotted in histogram form in Fig. 4 in the main article.

**Fig. A16.** A comparison of unprojected ol-liq  $K_{D,Fe^{+2}-Mg}$  (a) and “S” and olivine  $Mg\#$  projected values (b); both sets of  $K_{D,Fe^{+2}-Mg}$  calculated using experiments from the literature at  $QFM \pm 0.25$  and eqn 12 of Jayasuriya *et al.* (2004) to estimate the FeO content of the experimental glasses. The mean and standard deviation (stdev) for each set of  $K_{D,Fe^{+2}-Mg}$  is listed in each panel.

**Fig. A17.** Ol-liq  $K_{D,Fe^{+2}-Mg}$  as a function of temperature comparing  $K_{D,Fe^{+2}-Mg}$  calculated using olivine and liquid compositions from the experiments from this study to those calculated using the parameterizations of Ford *et al.* (1983) and Toplis (2005). Filled black circles are calculated using liquid FeO contents as estimated by eqn 12 of Jayasuriya *et al.*

(2004), liquid MgO contents, and olivine compositions; open circle indicates the  $K_{D,Fe^{+2}-Mg}$  calculated using the wet chemistry FeO liquid determination. Blue and red circles are  $K_{D,Fe^{+2}-Mg}$ s calculated using the temperatures,  $fO_2$ s, and liquid compositions of the experiments and the parameterizations of Ford *et al.* (1983) and Toplis (2005), respectively.

**Fig. A18.**  $(Fe^{+3}/Fe^{+2})_{Jay12}/(Fe^{+3}/Fe^{+2})_{Sack}$  (molar) vs. temperature ( $^{\circ}C$ ) of the experimental glasses from the 1-atm QFM $\pm$ 0.25 data set compiled as part of this study. “Jay12” and “Sack” in the y-axis label refer to Jayasuriya *et al.* (2004) eqn 12 and Sack *et al.* (1980), respectively.

**Fig. A19.** Distribution of run temperatures from 1-atm experiments (a) and high-pressure experiments (b) included in the calibration data set of the Toplis (2005) olivine-liquid  $Fe^{+2}$ -Mg exchange model. Literature references are from the captions to Fig. 1, 8, 9, and 10 of Toplis, and we assumed that all olivine-liquid-bearing experiments from these sources were used. The pressure range in panel (b) is from 5 to 144 kbar and pressure and temperature show a strong positive correlation.

## Supplementary Material Figures

Fig. A1.

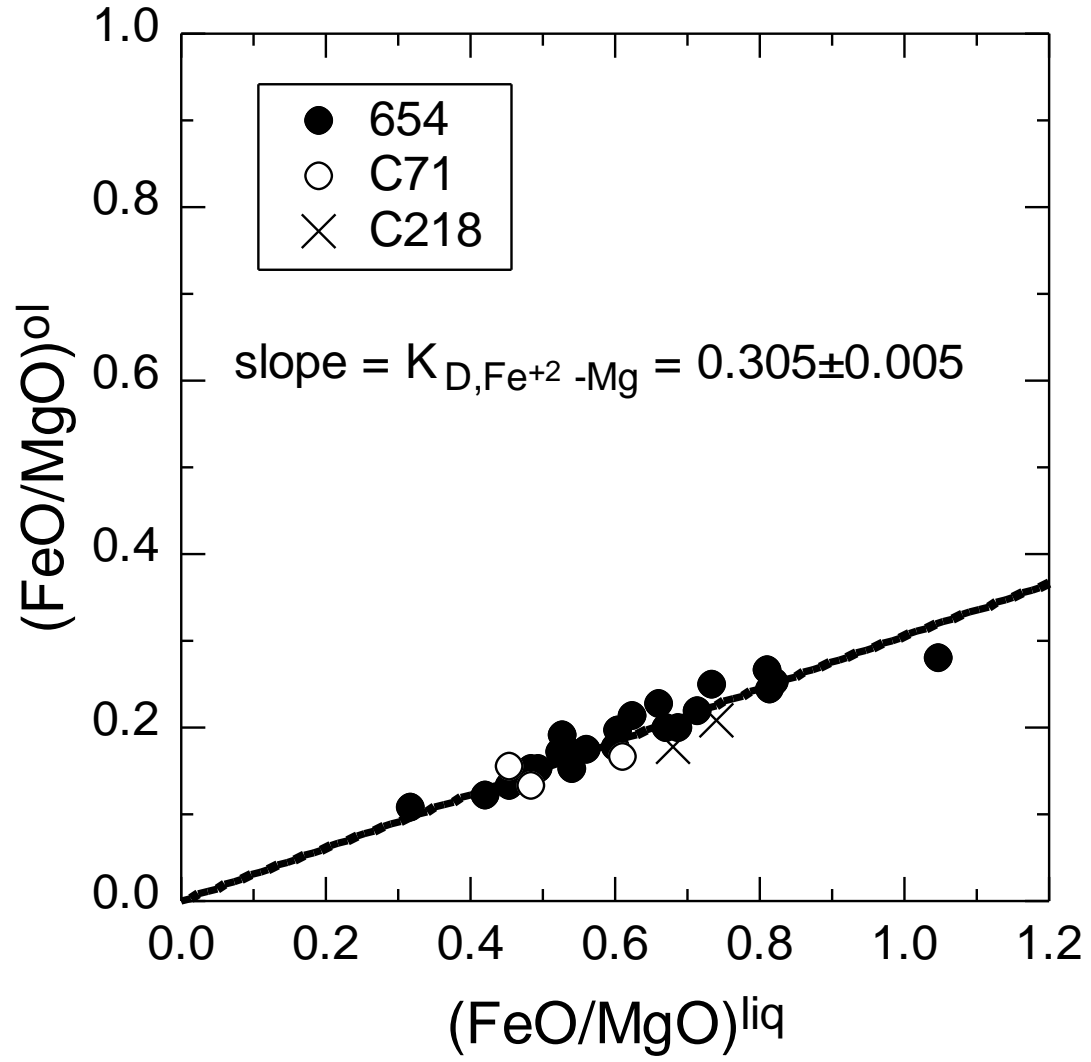


Fig. A2.

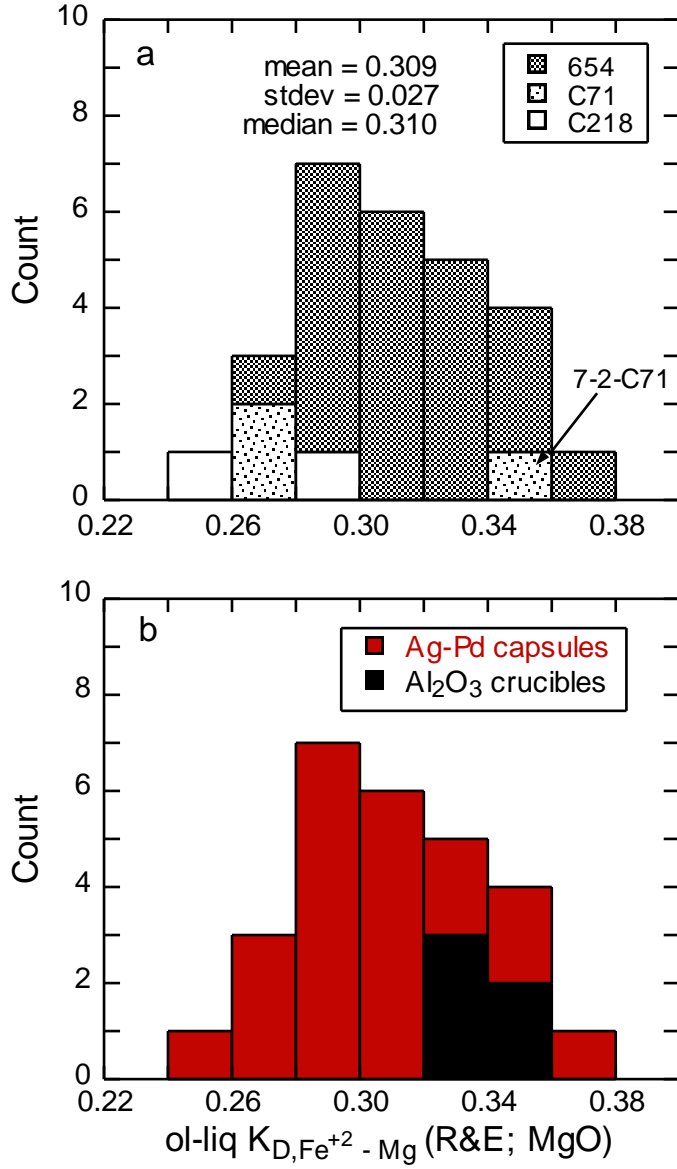


Fig. A3

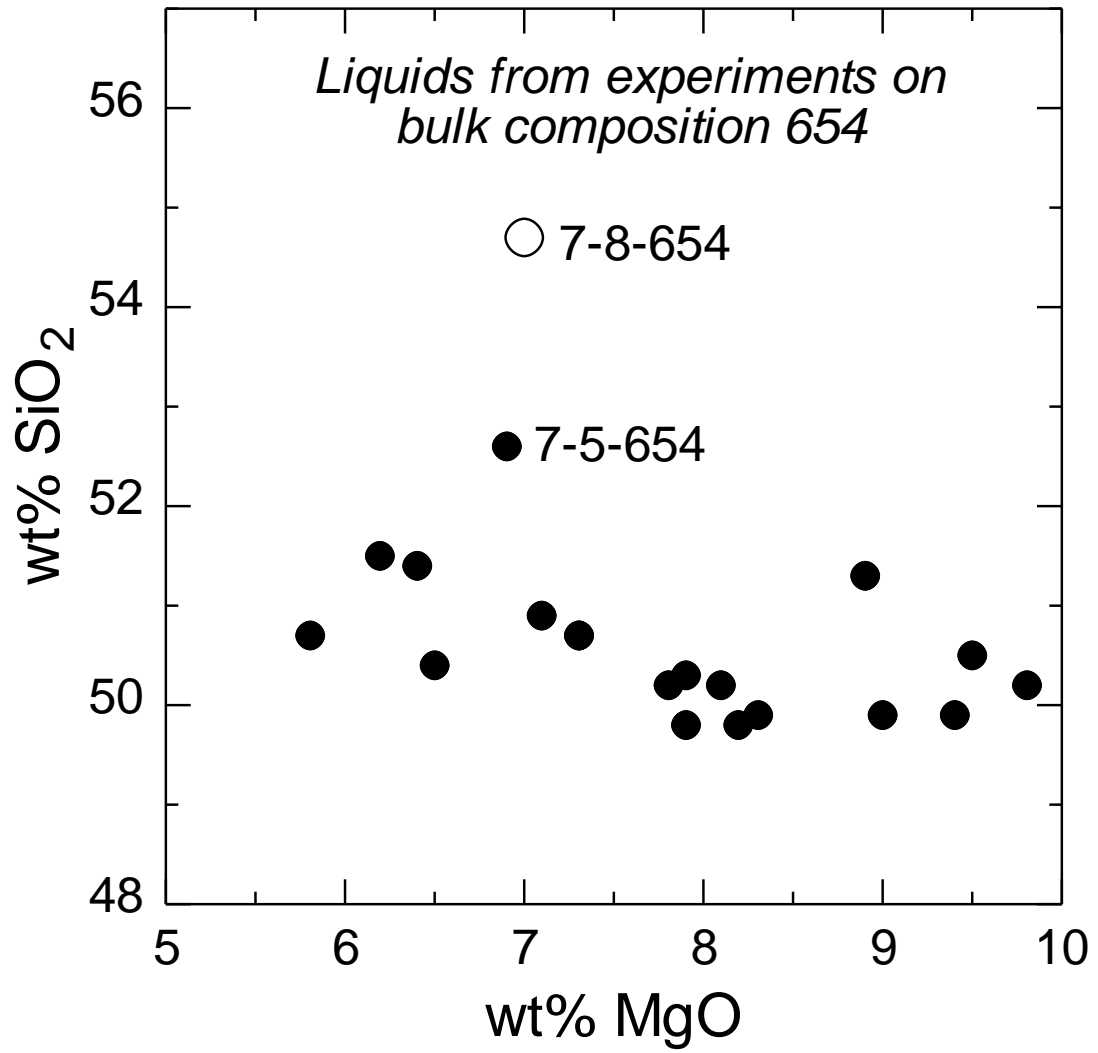


Fig. A4.

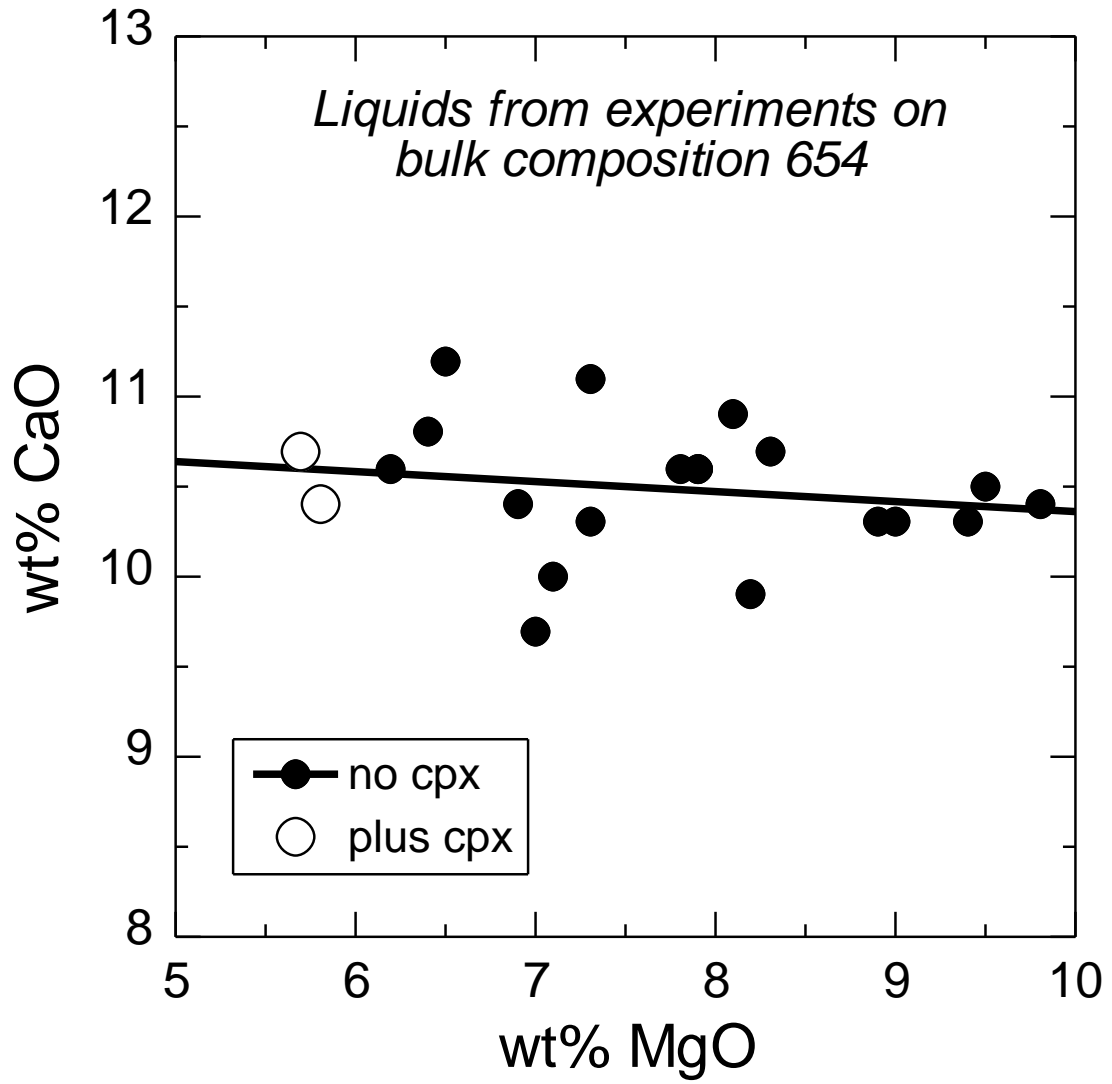


Fig. A5.

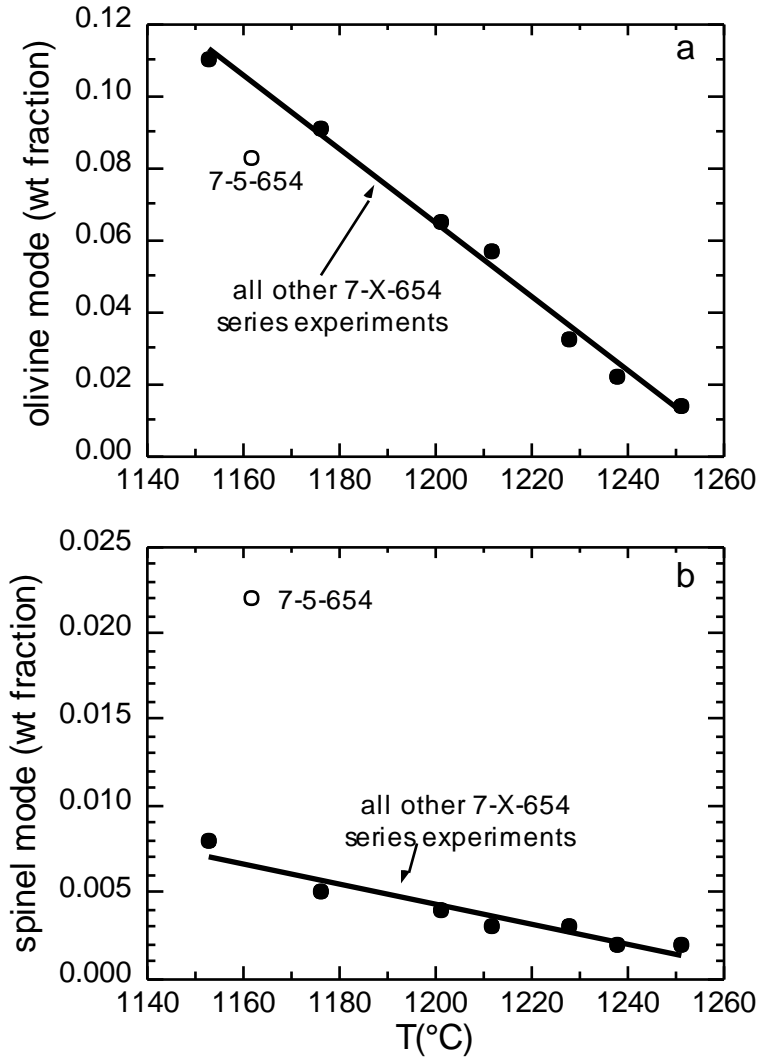
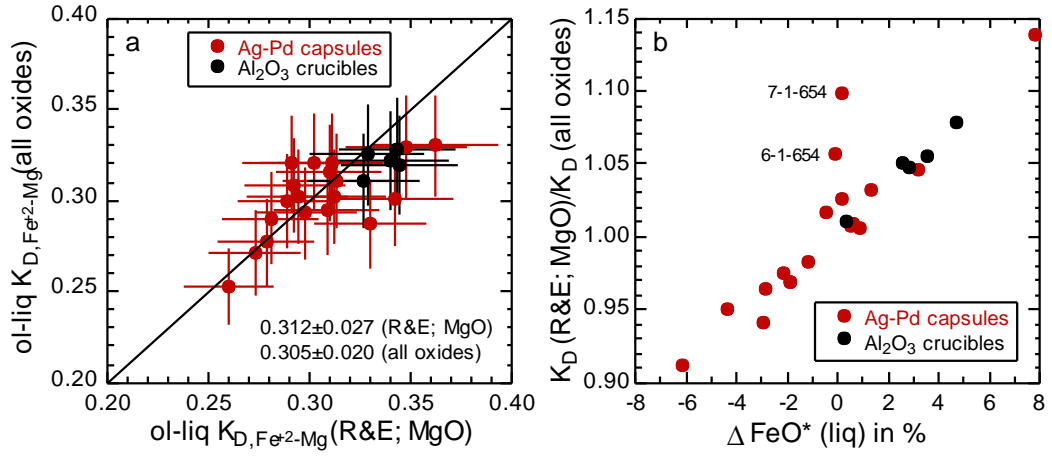


Fig. A6.



|

Fig. A7.

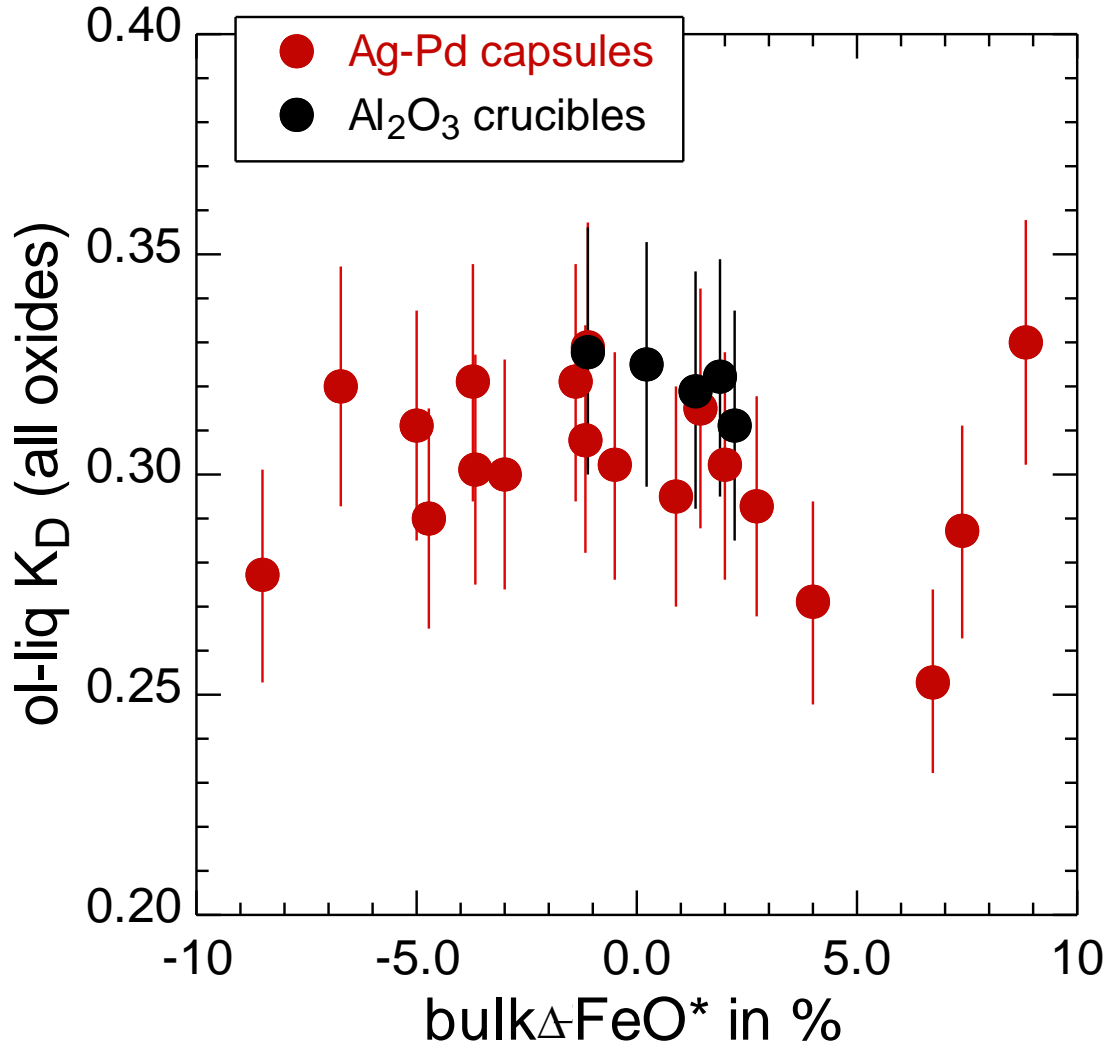


Fig. A8.

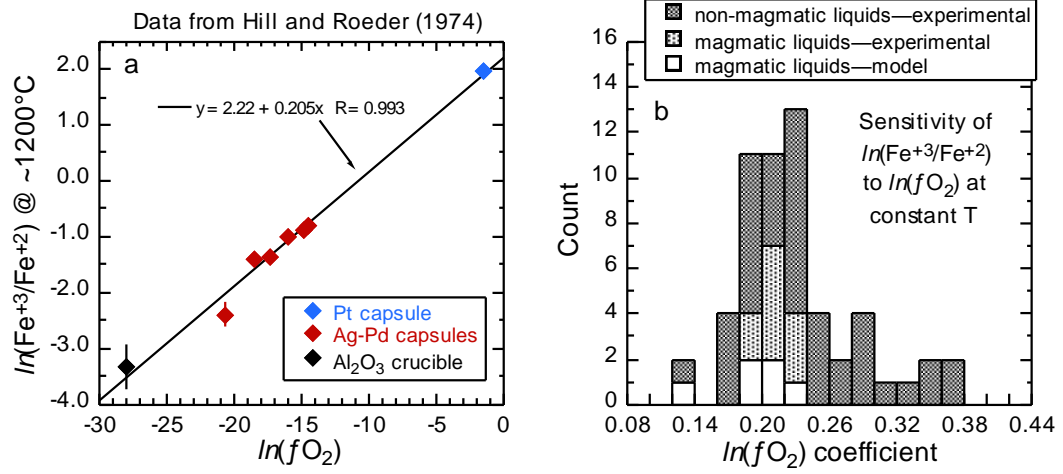


Fig. A9.

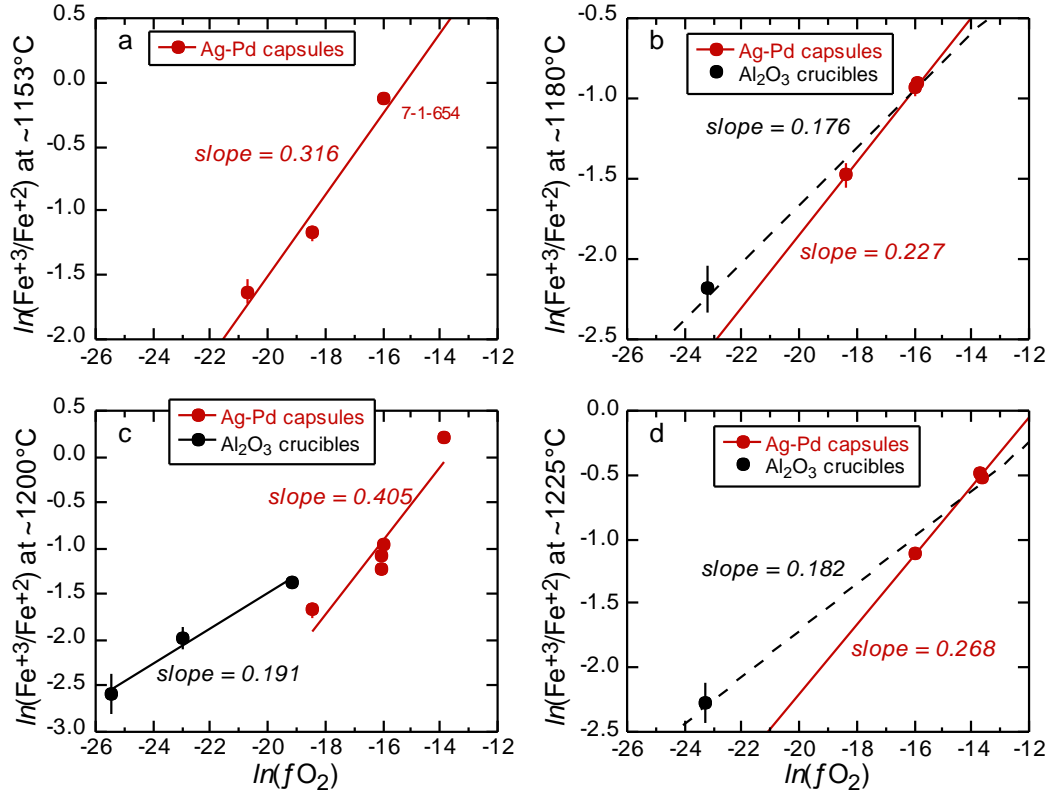


Fig. A10.

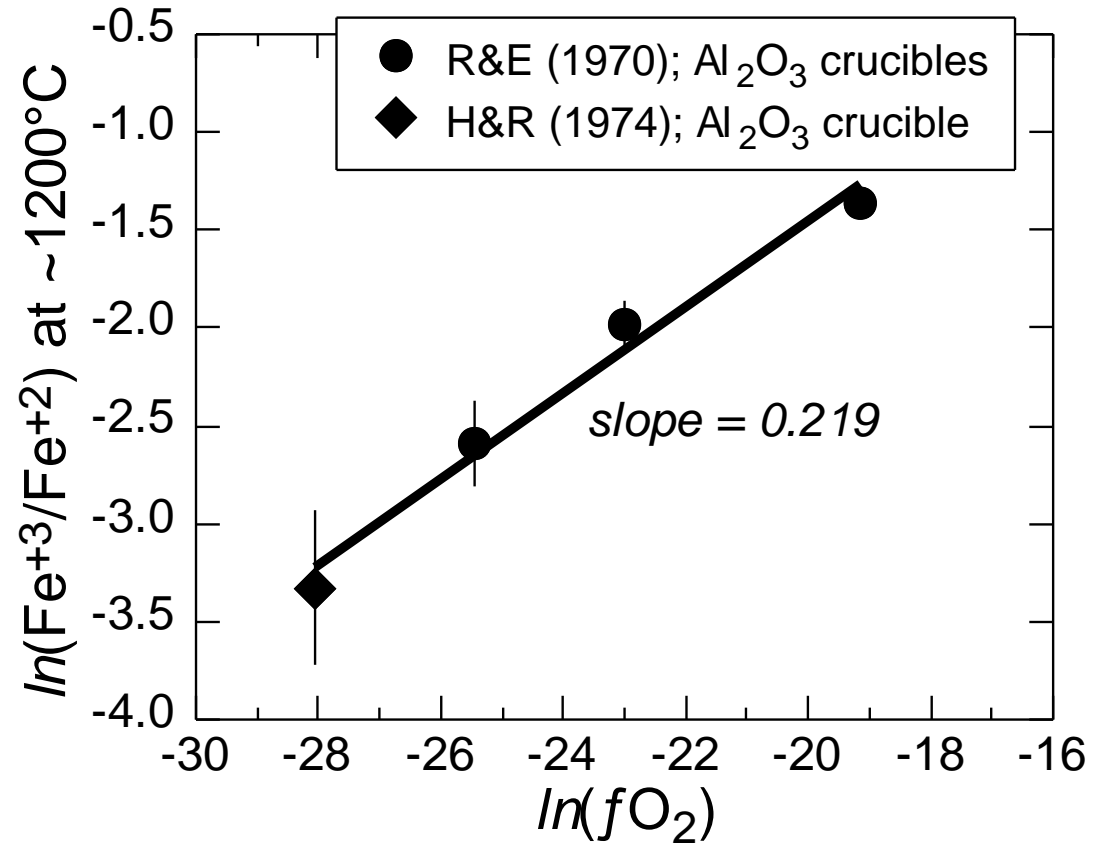


Fig. A11.

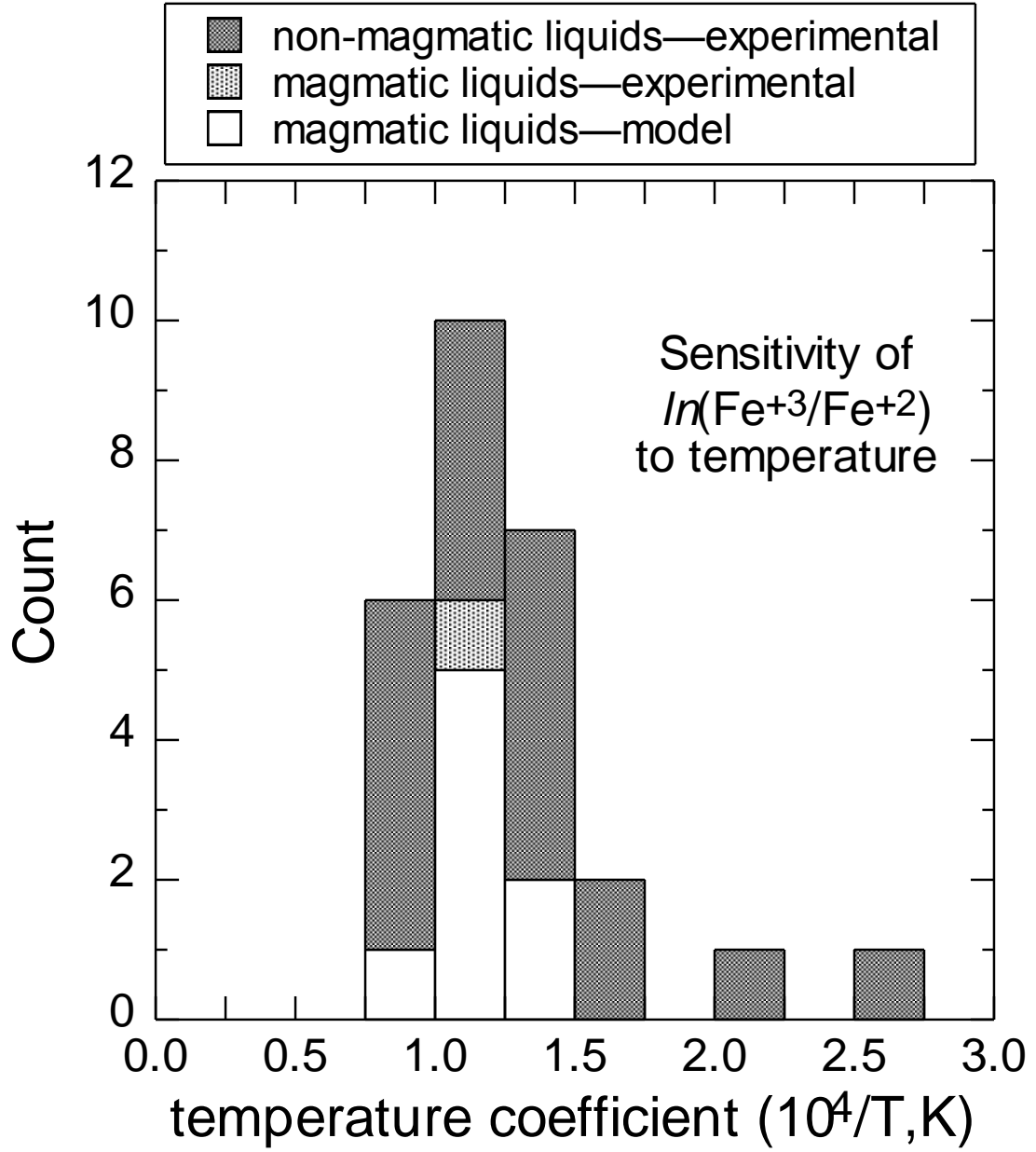


Fig. A12.

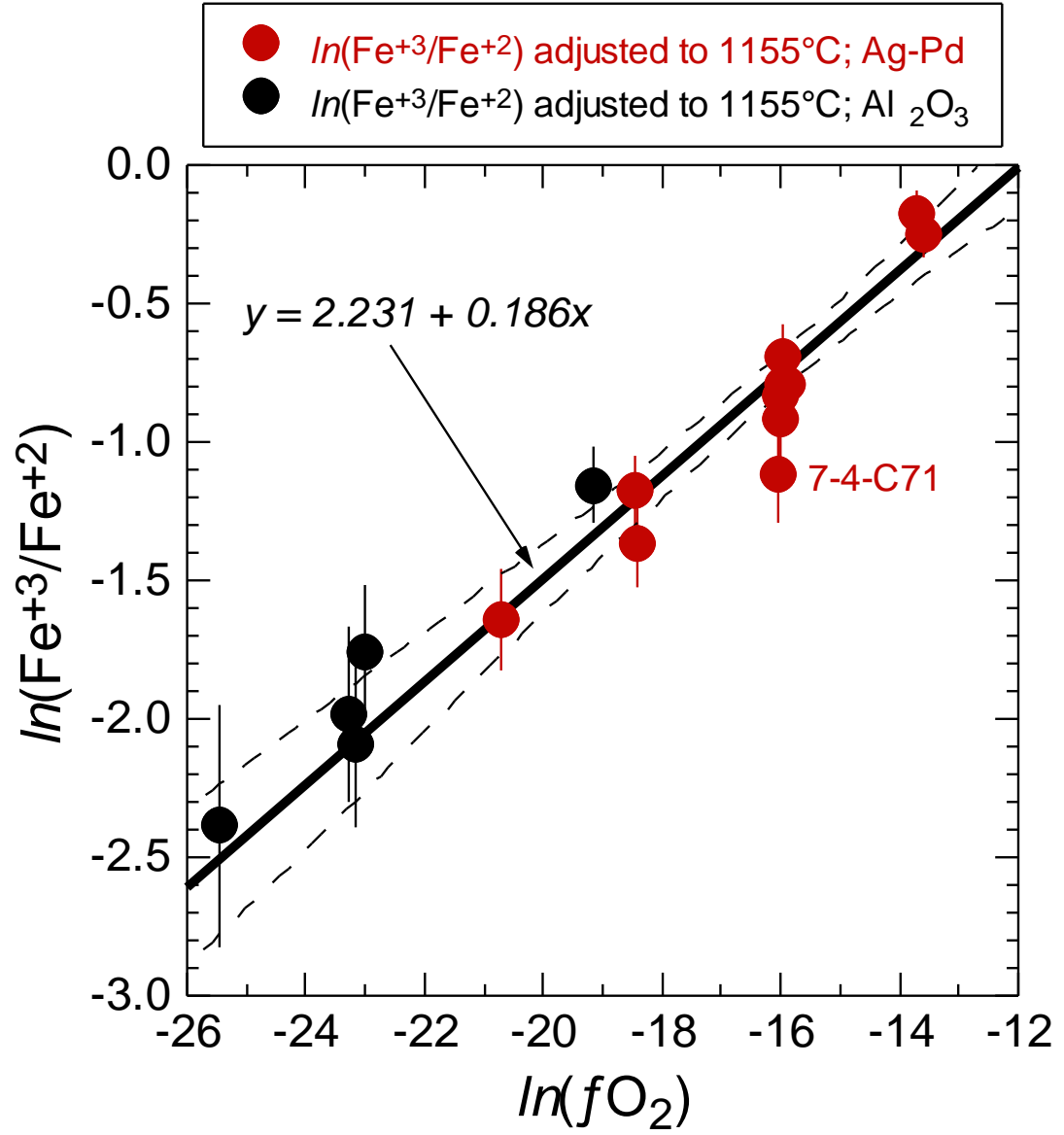


Fig. A13.

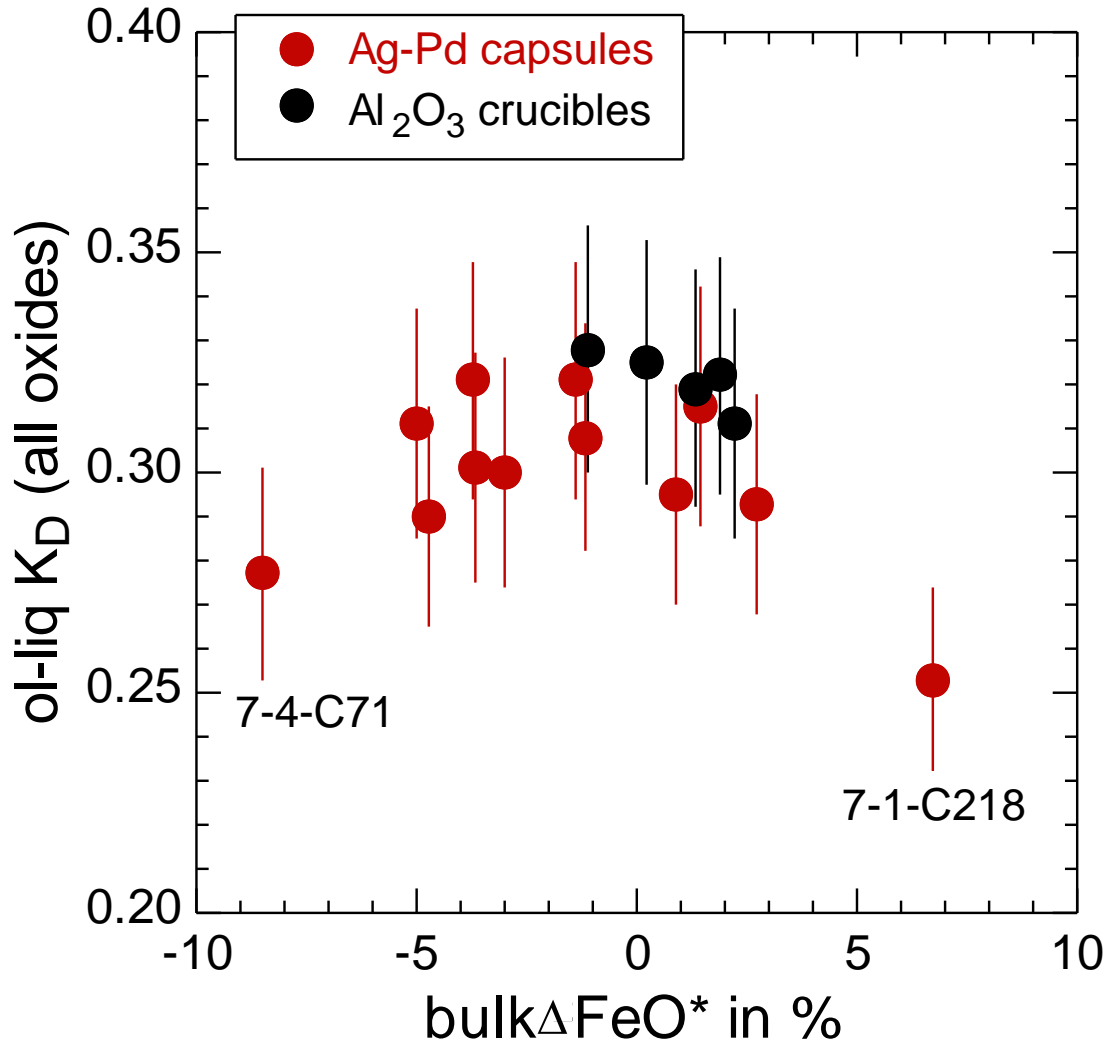


Fig. A14.

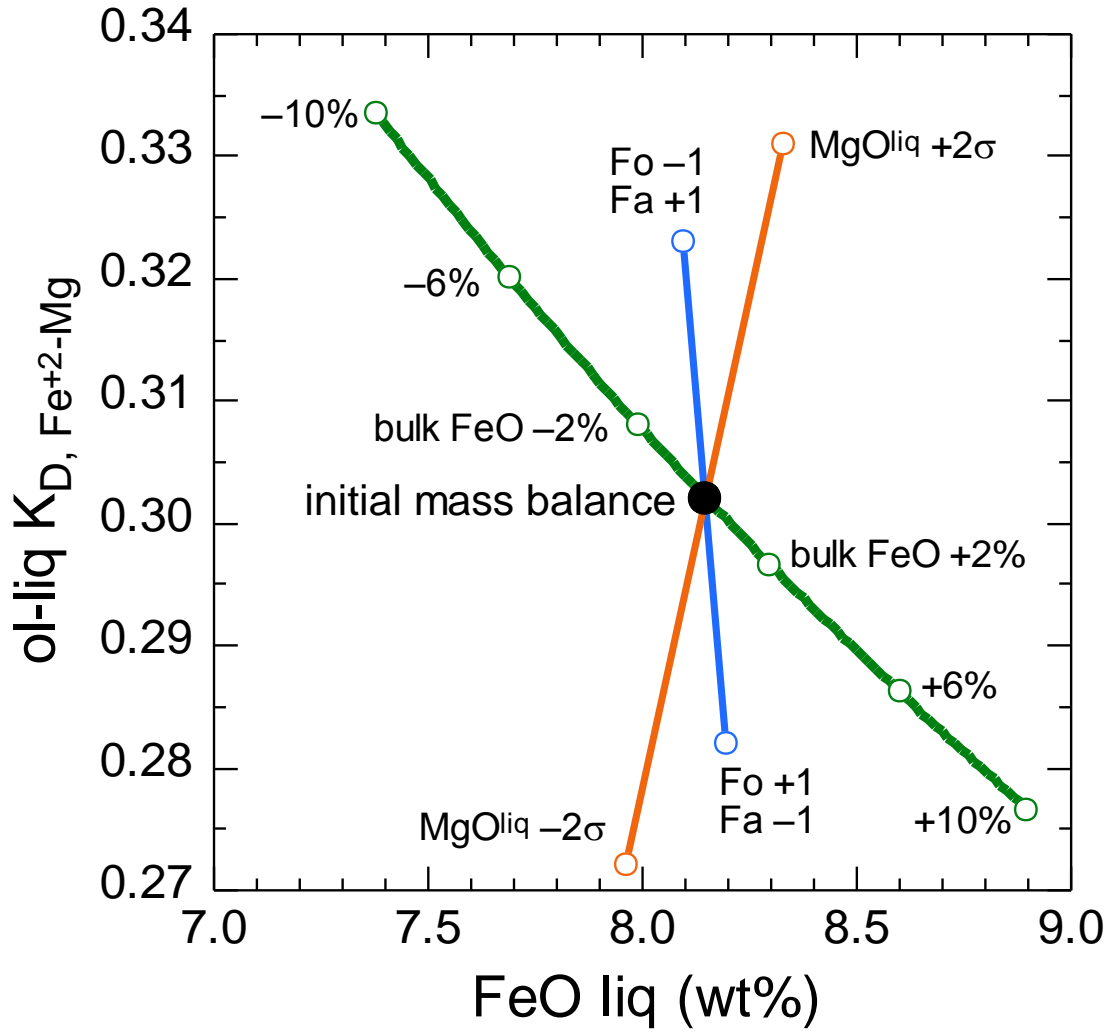


Fig. A15.

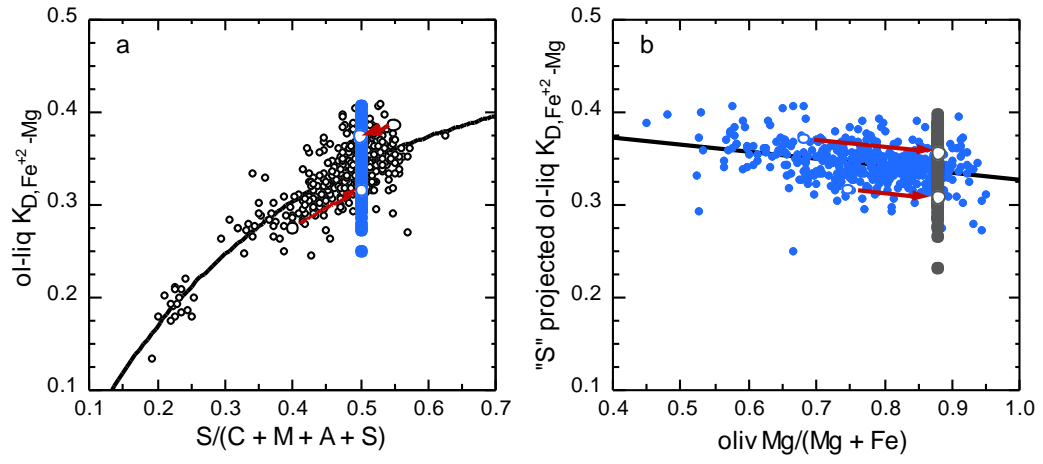


Fig. A16.

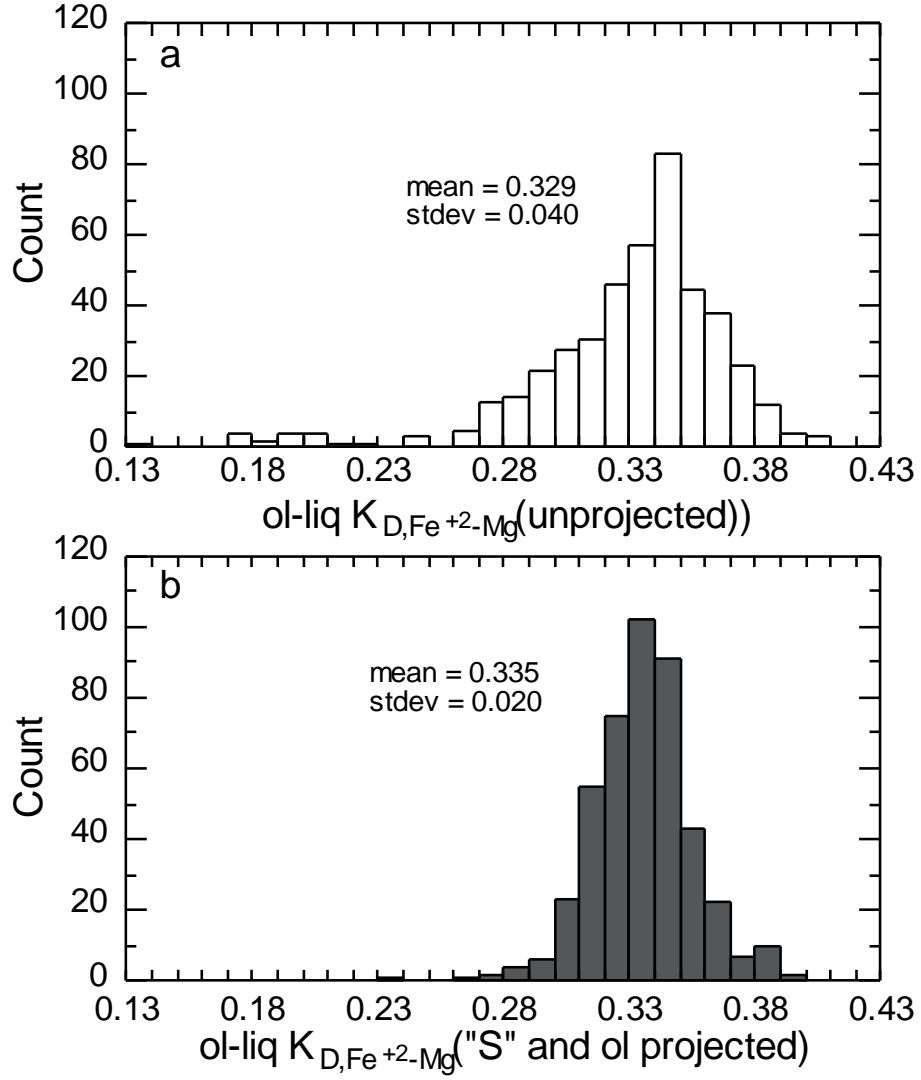


Fig. A17.

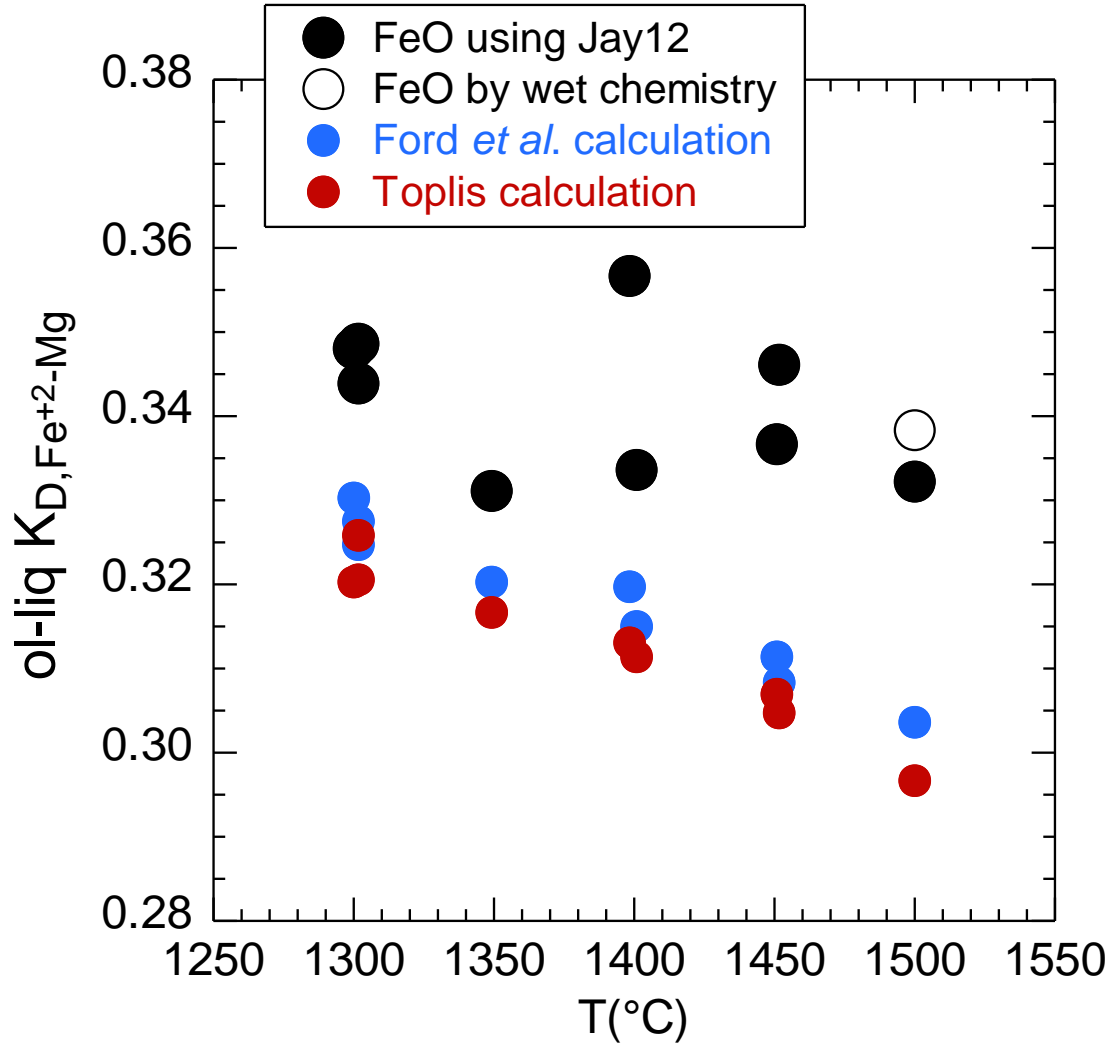


Fig. A18.

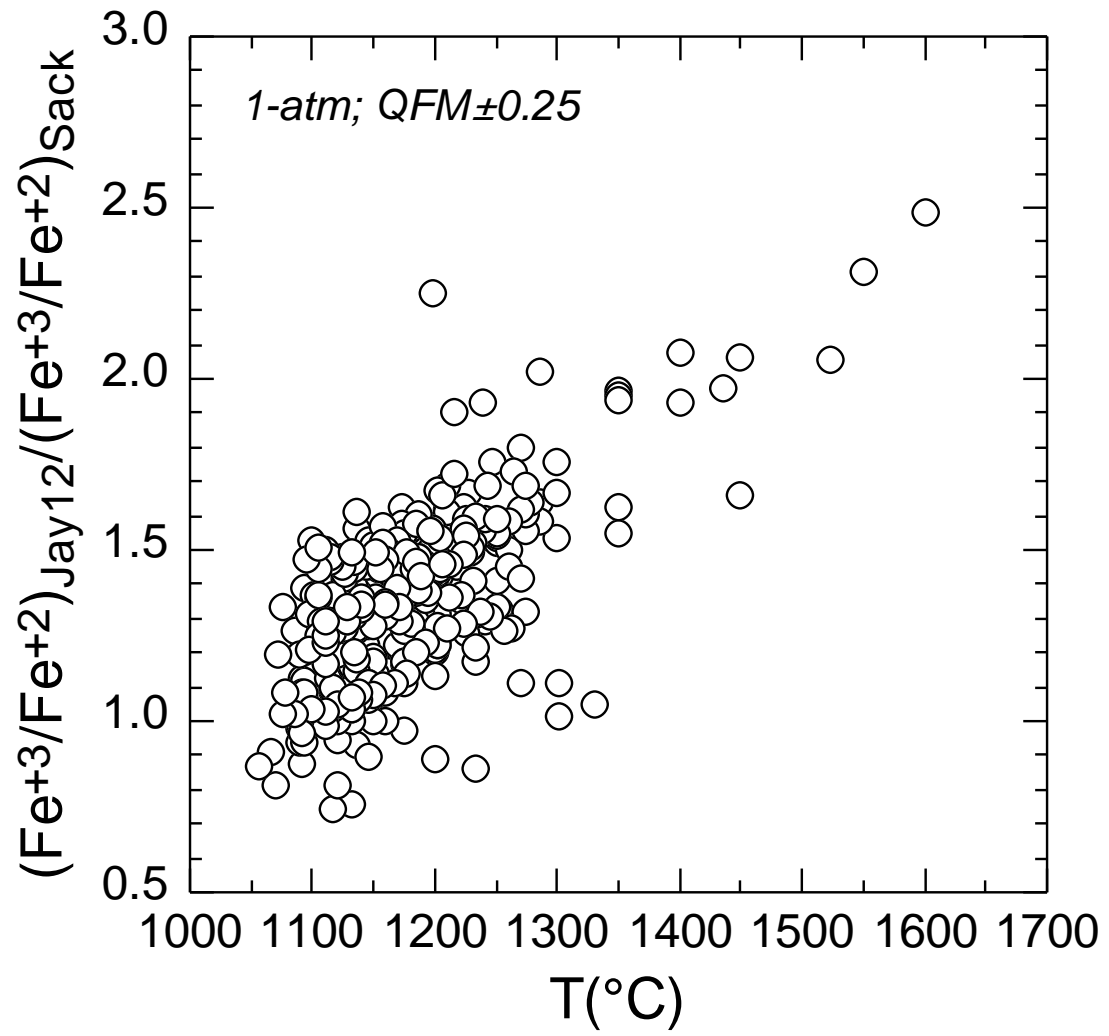
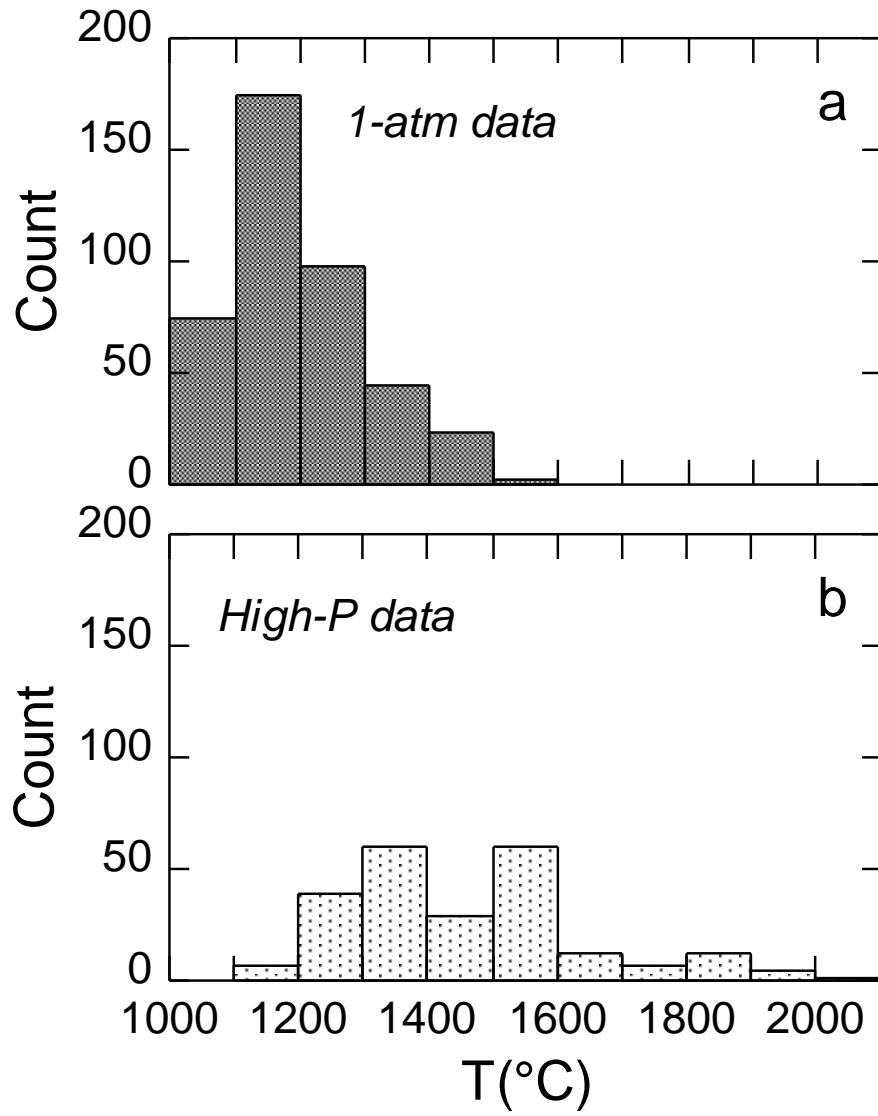


Fig. A19.



III-1

*Chapter 3*

Fe-Mg PARTITIONING BETWEEN OLIVINE AND BASALTIC MARTIAN MELTS

Andrew K. Matzen

John R. Beckett

Michael B. Baker

Edward M. Stolper

For submission to

*Meteoritics and Planetary Science*

January 5, 2012

**ABSTRACT**

We reviewed published experiments on model Martian compositions to determine the appropriate value(s) for the olivine (ol)-liquid (liq) exchange coefficient,  $K_{D, \text{Fe}^{+2}\text{-Mg}} = (\text{FeO/MgO})^{\text{ol}}/(\text{FeO/MgO})^{\text{liq}}$  (by weight). The median of 17 published one-atmosphere experiments yields  $K_{D, \text{Fe}^{+2}\text{-Mg}} = 0.354 \pm 0.008$  (error is one mean absolute deviation, MAD). In higher-pressure experiments on model Martian compositions the  $f\text{O}_2$ s and temperatures are less well constrained; however, correcting for the presence of ferric iron and considering only those experiments run above 1150°C leads to a median  $K_{D, \text{Fe}^{+2}\text{-Mg}}$  of  $0.365 \pm 0.024$  (MAD). The median  $K_{D, \text{Fe}^{+2}\text{-Mg}}$ s for the high-pressure and one-atm experiments overlap at one MAD, and both are notably higher than the canonical value of 0.30.

We then use this value to test whether any of the ol-phyric shergottites represent liquids. For each meteorite, we assume a liquid composition equal to that of the bulk (when available we also use estimates of the oxygen fugacity and temperature) and compare that liquid to the most Mg-rich olivine found. Using  $K_{D, \text{Fe}^{+2}\text{-Mg}} = 0.30$  leads to the conclusion that none of the olivine cores in olivine-phyric shergottites are in equilibrium with liquids equivalent to their bulk. However, using our  $K_{D, \text{Fe}^{+2}\text{-Mg}}$ , leads to the possibility that Yamato 980459, Northwest Africa 5789, 2990, and Elephant Moraine A79001 are liquid compositions (others are not), similar to the recent results of Filiberto and Dasgupta (2011). Accounting for  $\text{Fe}^{3+}$  in the liquid also allows us to constrain plausible  $f\text{O}_2$ s during cooling when independent measures are unavailable or not yet determined; e.g., if the olivines in Northwest Africa 2990 are in equilibrium with a liquid whose composition is that of the bulk meteorite, crystallization must have occurred under reducing conditions, approximately half of a log unit above the iron-wüstite buffer at one atm.

## INTRODUCTION

The partitioning of elements between solid and liquid phases is a useful tool for understanding and modeling igneous processes. Olivine is of particular interest due to its presence in a broad range of mafic and ultramafic lavas throughout the solar system (BVSP, 1981). In a landmark study, Roeder and Emslie (1970) showed that the olivine (ol)-liquid (liq) exchange coefficient,  $K_{D, Fe^{+2}-Mg} = (FeO/MgO)^{ol}/(FeO/MgO)^{liq}$  (by weight), is  $0.30 \pm 0.03$  and is independent of temperature and liquid composition. While later work (e.g., Sack et al., 1987) has shown that liquid composition does, in fact, play a significant role, the canonical value of 0.30 is still widely used in both terrestrial and Martian (e.g., Falloon et al., 2007; Peslier et al., 2010, respectively) applications. Despite the widespread use of the canonical value of 0.30, experimental work on both meteorite (Stolper, 1977) and low-Ti lunar model compositions (Longhi et al., 1978) indicate that a higher  $K_{D, Fe^{+2}-Mg}$  (0.33 or greater) may be more appropriate for extraterrestrial applications. It is important to note that a higher  $K_{D, Fe^{+2}-Mg}$  is not an esoteric consideration: Fe-Mg equilibrium is often used as a criteria for an experiment reaching equilibrium (e.g., Filiberto et al., 2010b), and differences of this magnitude in the exchange coefficient can lead to large differences in calculated parental magma compositions (e.g., Matzen et al., 2011) which, in turn, has petrogenetic significance, such as the temperature at which magmas are formed (e.g., Falloon et al., 2007; Putirka et al., 2007). In this work, we review a large database of experiments in order to determine the appropriate  $K_{D, Fe^{+2}-Mg}(s)$  for Martian bulk compositions and under what, if any, conditions  $K_{D, Fe^{+2}-Mg}$  can safely be approximated as a constant.

## EXPERIMENTS ON MARTIAN COMPOSITIONS

### *One-Atmosphere Martian Experiments.*

Calculating or measuring the ferric and ferrous iron present in experimental run products is crucial to computing an accurate  $K_{D, Fe^{+2}-Mg}$ . The most rigorous way to compute a  $K_{D, Fe^{+2}-Mg}$  is by directly measuring the  $Fe^{+3}/Fe^{+2}$  in the glass, in addition to measuring the compositions of coexisting glass and olivine. Although we are unaware of any experiments on Martian bulk compositions with coexisting olivine where  $Fe^{+3}/Fe^{+2}$  in the liquid is known by direct measurement, when the oxygen fugacity is measured independently (via a solid-state oxygen detector or by gas volumes)  $Fe^{+3}/Fe^{+2}$  can be calculated using a formulation for that express purpose (e.g., Sack et al., 1980). Given the experimental conditions and glass composition, there are many formulations available to calculate  $Fe^{+3}/Fe^{+2}$  of the glass. In this study, we use the expression of O'Neill et al. (2006) because it incorporates a pressure term that, although irrelevant for one-atm experiments, will become important in the following section where we consider high-pressure experiments. The median  $K_{D, Fe^{+2}-Mg}$  of 17 one-atm experiments on Martian bulk compositions whose analytical totals (post  $Fe^{+3}/Fe^{+2}$  correction for glasses) are between 98 and 102 wt. % (Filiberto et al., 2008; Herd et al., 2009) is  $0.354 \pm 0.008$  (error is one mean absolute deviation, MAD), significantly higher than the canonical value of 0.30, and in good agreement with the results of Filiberto and Dasgupta (2011) who argued that a  $K_{D, Fe^{+2}-Mg}$  of  $0.35 \pm 0.01$  is more appropriate for Martian bulk compositions. Fig. 1 shows the tight distribution of the  $K_{D, Fe^{+2}-Mg}$ s from these 17 experiments.

Matzen et al. (2011) illustrated the effect that  $Fe^{+3}/Fe^{+2}$  expressions can have on the resulting  $K_{D, Fe^{+2}-Mg}$ s, using primarily a large database of previously published one-atm experiments. Matzen et al. (2011) choose eq. 12 from Jayasuriya et al. (2004) because for comparable liquid compositions it predicted a similar  $K_{D, Fe^{+2}-Mg}$  in both highly reducing

experiments where the ferric iron is negligible, and in more oxidizing experiments where the correction for ferric iron is significant. We feel that it is important to note that though we chose the  $\text{Fe}^{+3}/\text{Fe}^{+2}$  expression of O'Neill et al. (2006) over that of Jayasuriya et al. (2004) for the reasons stated above, using eq. 12 of Jayasuriya et al. (2004) results in calculated  $K_{D, \text{Fe}^{+2}\text{-Mg}}$ s that, on average, differ by only 0.001. Thus, the result that the  $K_{D, \text{Fe}^{+2}\text{-Mg}}$  for Martian compositions is higher than the canonical value of Roeder and Emslie (1970) is not simply an artifact of choosing the  $\text{Fe}^{+3}/\text{Fe}^{+2}$  expression of O'Neill et al. (2006).

Most Martian basalts have higher FeO and lower  $\text{Al}_2\text{O}_3$  contents than the terrestrially-relevant liquids that were used to parameterize the  $\text{Fe}^{+3}/\text{Fe}^{+2}$  expression of O'Neill et al. (2006) and other previous expressions (e.g., Kilinc et al., 1983; Sack et al., 1980). Caution should be used when applying these (largely empirical) functions to Martian liquids because all calculations will involve an extrapolation in composition space. Righter et al. (2010) acknowledged this fact and reported a possible discrepancy between their XANES measurements and the  $\text{Fe}^{+3}/\text{Fe}^{+2}$  prediction of Kress and Carmichael (1991) for a model shergottite composition. We acknowledge this possible discrepancy, and eagerly await a complete description of both the experiments and the resulting data described briefly by Righter et al. (2010).

#### *High-Pressure Martian Experiments.*

In an attempt to expand the compositional range and the number of experiments under consideration, it is necessary to include higher pressure experiments; many experiments on Martian bulk compositions were conducted at high pressures in an attempt to mimic the conditions under which Martian basalts are thought to form. As stated earlier, knowledge of the  $\text{Fe}^{+3}/\text{Fe}^{+2}$  contents of experimentally produced glasses is paramount in calculating an accurate  $K_{D, \text{Fe}^{+2}\text{-Mg}}$ .

Unfortunately, like the one-atm experiments, we are unaware of any high-pressure experiments with coexisting glass and olivine where the  $\text{Fe}^{+3}/\text{Fe}^{+2}$  contents of the glass have been measured. Unlike one-atm experiments where there is good control over the temperature and oxygen fugacity, high-pressure experiments have (relatively) poor control over the temperature and the oxygen fugacity is often not buffered (i.e., with Ni-NiO or Fe-FeO), nor is the oxygen fugacity measured independently. Even though they are un-buffered, given consistent preparation of the starting materials, the oxygen fugacity of experiments run in graphite capsules in the piston-cylinder apparatus can be approximated at 0.8 log units below the graphite-carbon monoxide (CCO) buffer (Medard et al., 2008). However, it is important to realize that the increased uncertainty in both the temperature and oxygen fugacity, when compared to one-atm experiments, lead to larger uncertainties on the calculated  $\text{Fe}^{+3}/\text{Fe}^{+2}$  ratio (again, assuming we can successfully apply our  $\text{Fe}^{+3}/\text{Fe}^{+2}$  expression calibrated with terrestrially-relevant liquids to Martian liquids), and the resulting  $K_{D, \text{Fe}^{+2}\text{-Mg}}$ . Although this estimated oxygen fugacity (CCO-0.8) is reducing, it is not so reducing that the presence of ferric iron is negligible; for example, correcting for the presence of ferric iron in experiment H-12 (11.7 kbar and 1365°C) of Filiberto et al. (2008) increases the  $K_{D, \text{Fe}^{+2}\text{-Mg}}$  from 0.366 (assuming all Fe is FeO) to 0.380 (using the expression of O'Neill et al., 2006), a difference of 0.014. The median increase in  $K_{D, \text{Fe}^{+2}\text{-Mg}}$  for all high-pressure experiments with acceptable analytical totals is 0.013, and although the increase is not huge (it would be greater if we used a  $\text{Fe}^{+3}/\text{Fe}^{+2}$  expression without a pressure term) a difference of 0.013 can have significant petrogenetic consequences (e.g. Matzen et al. 2011). The median  $K_{D, \text{Fe}^{+2}\text{-Mg}}$  for all 77 high-pressure experiments (see caption to Fig. 2 for references) with acceptable analytical totals is  $0.369 \pm 0.024$  (MAD), a value that overlaps with the median of the one-atm experiments discussed in the previous section, albeit with more scatter. For the high-pressure experiments, the  $\text{Fe}^{+3}/\text{Fe}^{+2}$

ratio was calculated on an anhydrous basis following Moore et al. (1995) who observed no change in oxidation state with the addition of water. This observation was challenged by both Baker and Rutherford (1996), and Gaillard et al. (2003) who suggested that under reducing condition the addition of water results in an increase of the  $\text{Fe}^{+3}/\text{Fe}^{+2}$  ratio; see Botcharnikov (2005) for a discussion.

In the high-pressure experiments, there appears to be an increase in  $K_{D, \text{Fe}^{+2}\text{-Mg}}$  with decreasing temperature below  $\sim 1150^\circ\text{C}$ . The studies of Nekvasil et al. (2009), McCubbin et al. (2008), and Filiberto (2008) all suggest that the  $K_{D, \text{Fe}^{+2}\text{-Mg}}$  increases from approximately 0.35 to 0.40 as the temperature decreases from  $\sim 1150$  to  $1000^\circ\text{C}$ ; the increase in  $K_{D, \text{Fe}^{+2}\text{-Mg}}$  is surprising given the numerous studies that have shown that  $K_{D, \text{Fe}^{+2}\text{-Mg}}$  is insensitive to changes in temperatures (e.g., Roeder et al., 1970). It is important to note that these experiments are inherently difficult due to the low temperature and the presence of multiple ( $\geq 4$ ) phases both of which make the attainment of equilibrium challenging. Further experiments are needed to assess whether the apparent increase in  $K_{D, \text{Fe}^{+2}\text{-Mg}}$  at these low temperatures is a property inherent to these highly fractionated liquids, a consequence of the low temperature, or simply an experimental artifact. In the following sections we will only consider the results of experiments run at or above  $1150^\circ\text{C}$ , being careful not to use the results of these experiments in any calculations below  $1150^\circ\text{C}$ . If we consider only the high-pressure experiments run at temperatures at or above  $1150^\circ\text{C}$  that have analytical totals from 98-102 wt. %, the resulting median  $K_{D, \text{Fe}^{+2}\text{-Mg}}$  decreases to  $0.365 \pm 0.016$  (MAD). Fig. 2 shows that the high-pressure experiments have slightly more scatter, however their  $K_{D, \text{Fe}^{+2}\text{-Mg}}$  overlaps with the one-atm Martian dataset and is, again, significantly higher than the canonical value of  $0.30 \pm 0.03$ .

*Compositional Dependence of  $K_{D,Fe^{2+}-Mg}$ .*

The landmark work of Roeder and Emslie (1970) showed that the  $K_{D, Fe^{2+}-Mg}$  was independent of temperature and composition. While later work has shown that the  $K_{D, Fe^{2+}-Mg}$  is, indeed, a function of composition (e.g., Gee et al., 1988; Sack et al., 1987), over limited ranges in composition space  $K_{D, Fe^{2+}-Mg}$  can still be safely approximated as a constant (Matzen et al., 2011). Do the experiments presented in the previous section span a small enough range in composition space to allow  $K_{D, Fe^{2+}-Mg}$  to be approximated as a constant? To answer this question we used Spearman's rank correlation coefficient (implemented in MATLAB) to show that there are no statistically significant correlations between the computed  $K_{D, Fe^{2+}-Mg}$ s and the composition of the coexisting glass and olivine (where the compositions are in oxide wt. %). The independence of the  $K_{D, Fe^{2+}-Mg}$  for both the high-pressure and one-atm experiments with respect to composition is illustrated in Fig. 3 that shows the  $K_{D, Fe^{2+}-Mg}$  vs. the MgO and Na<sub>2</sub>O content of liquids.

It is convenient that, for the experiments introduced above,  $K_{D, Fe^{2+}-Mg}$  does not show a compositional dependence, i.e., calculations utilizing  $K_{D, Fe^{2+}-Mg}$  need only one number instead of a functional form. However, this constant  $K_{D, Fe^{2+}-Mg}$  is limiting because it can only be applied to compositions within the range of experiments used to calibrate our model. Therefore, an important step before using  $K_{D, Fe^{2+}-Mg} = 0.36$ , as argued in the previous section, is to show that the compositions of both the solid and liquid fall within the experimental range used to construct this value. Later, we will use our calculated  $K_{D, Fe^{2+}-Mg}$  to test if the bulk of any olivine-phyric shergottites represent liquids. The upper panels in Fig. 3 show that the experiments discussed previously nearly encompass the bulk shergottite compositions used in the following sections, giving us confidence that a constant  $K_{D, Fe^{2+}-Mg}$  is well suited to our application.

## COMPARISON WITH OTHER ONE-ATM EXPERIMENTS

Up to this point our discussion has been limited to experiments on model Martian bulk compositions. As we have shown, the resulting  $K_{D, \text{Fe}^{+2}\text{-Mg}}$  from these experiments is higher than the canonical value of 0.30. It is well known that shergottite bulk compositions are Fe-rich and Al-poor relative to most terrestrial magmas. We can compare the experiments on model Martian compositions to the terrestrially-relevant database assembled by Matzen et al. (2011) to see if there is a systematic difference between model Martian and terrestrially-relevant experiments. To compare these two datasets we use a compositional distance parameter defined, for each experiment, as the square root of the sum of the squared differences between the median of the model Martian experimental liquids and the liquid composition of experiment  $i$  on an oxide basis:

$$dist_i = \sqrt{\sum (x_{med}^j - x_i^j)^2}$$

where  $x_i^j$  is the wt. % of oxide  $j$  in experiment  $i$ , and  $x_{med}^j$  is the median (in wt. %) of oxide  $j$  in the model Martian experiments, discussed above. The terrestrially-relevant database was filtered to remove those experiments with (1) unacceptable analytical totals (outside 98-102 wt. %), (2) more than 6 wt. %  $\text{TiO}_2$  in the glass, and (3) more than 6 wt. % NiO or CoO in the olivine (Matzen et al., 2011); only those experiments that pass the filter are considered further. Fig. 4 shows that the terrestrially-relevant experiments whose compositions are closest to that of the model Martian experiments have equivalent

$K_{D, \text{Fe}^{+2}\text{-Mg}}$  s. With increasing compositional distance there is a decrease in the average  $K_{D, \text{Fe}^{+2}\text{-Mg}}$ ; however, due to the scatter in the data, it is unclear whether the  $K_{D, \text{Fe}^{+2}\text{-Mg}}$  actually decreases or the range of permissible  $K_{D, \text{Fe}^{+2}\text{-Mg}}$ s increases. In either case, the terrestrially-relevant database is in clear agreement with the experiments on model Martian bulk compositions. One additional note regarding Fig. 4: a large majority of experiments (both terrestrial and Martian) have  $K_{D, \text{Fe}^{+2}\text{-Mg}}$ s above the canonical value of 0.30.

### OLIVINE-PHYRIC SHERGOTTITES

As shown in Fig. 3 and discussed above, for the compositional range encompassed by the experiments on model Martian compositions,  $K_{D, Fe^{+2}-Mg}$  is not a strong function of composition, and, although not shown,  $K_{D, Fe^{+2}-Mg}$  is not correlated with temperature. Thus, a constant  $K_{D, Fe^{+2}-Mg}$  is well suited to test if bulk olivine-phyric shergottites represent liquids. In Fig. 5, we compare Mg#s (where  $Mg\# = Mg/[Fe^{+2}+Mg]$ , atomic) of bulk meteorites to that of the most Mg-rich olivine phenocryst. To calculate the Mg# of the bulk, when available, we used estimates of oxygen fugacity and the maximum temperature (Gross et al., 2011; Herd, 2003; McCanta et al., 2009; Peslier et al., 2010; Shearer et al., 2006) along with the  $Fe^{+3}/Fe^{+2}$  model of O'Neill et al. (2006). When temperature and redox estimates are unavailable, we assumed that all Fe in the bulk was as FeO, recognizing that this is a lower limit for the Mg# of the bulk. If the core of the most Mg-rich phenocryst is in equilibrium with the Mg# of the bulk, the meteorite represents a possible liquid. Using a  $K_{D, Fe^{+2}-Mg}$  of 0.30 leads to the conclusion that none of the olivine cores in olivine-phyric shergottites are in equilibrium with liquids equivalent to their bulk compositions. However, applying a  $K_{D, Fe^{+2}-Mg}$  value of 0.36 leads to the possibility that bulk compositions of Yamato 980459, Northwest Africa 5789, 2990, and Elephant Moraine A79001 represent liquid compositions, similar to the results of Filiberto and Dasgupta (2011).

An implicit assumption of the above treatment is that we have accurate measurements of both the bulk and the most Mg-rich olivine phenocryst. It is possible that the heterogeneous distribution of phenocrysts between splits can lead to erroneous measures of a bulk composition; however, the magnitude of these errors can be minimized by comparing analyzed bulks to those calculated from modal analysis on other sections. An interesting feature of Fig. 5 is that all of the

meteorites that are not possible liquids lie above and to the left of the equilibrium  $K_{D, \text{Fe}^{+2}\text{-Mg}} = 0.36$  line. There are a few possible explanations for this phenomenon: (1) the bulk may have accumulated olivine or other Mg-rich phases (e.g., Filiberto et al., 2011), (2) the cores of olivine phenocrysts may have diffusively re-equilibrated with their more Fe-rich rims, (3) we have, simply, not found the most Mg-rich phenocryst, or (4) any combination thereof. We believe that finding the most-Mg rich olivine phenocryst may be problematic due to the fact that olivine phenocrysts are often zoned (e.g., Peslier et al., 2010) raising the possibility that more Mg-rich regions lie either above or below the plane that constitutes the thin (or thick) section. If all olivines are of equal size, and spherically zoned in the same way (i.e., the compositions of every olivine from core to rim are the same) then a plane through a random selection of olivines should intersect very close to the center of many olivine grains (Cashman et al., 1988) and, therefore, recover the maximum Mg# (if this is true, the area and Mg# of all measured olivines should correlate). The preceding argument should hold true when there are large numbers of olivines in each section, however the details of what might happen when a thin section has a paucity of olivines is less clear. We believe that a rigorous determination of the likelihood of finding an olivine phenocryst of arbitrarily-high Mg content would be a very useful undertaking, considering how often these values are used in both terrestrial and planetary studies (e.g., Filiberto et al., 2011; Matzen et al., 2011), and the corresponding implications that may be able to be drawn regarding the mantle sources of these Mg-rich phenocrysts.

### **USING $K_{D, \text{Fe}^{+2}\text{-Mg}}$ TO ESTIMATE OXYGEN FUGACITY**

Perhaps the primary advantage of explicitly correcting for the presence of  $\text{Fe}^{3+}$  in the calibration of our constant  $K_{D, \text{Fe}^{+2}\text{-Mg}}$  model is that our result can now be applied across a range of oxygen

fugacities. This allows us, for example, to constrain plausible oxygen fugacities during cooling where independent measures are unavailable or not yet determined. More specifically, we are unaware of any measurements constraining the oxygen fugacity of NWA 2990; however, we can examine under what condition the most Mg-rich olivine is in equilibrium with the Mg # of bulk. In our calculation, we take the bulk composition of NWA 2990 as a liquid and then vary the oxygen fugacity and pressure (the temperature is calculated using the expression of Beattie, 1993). At each pressure- $f_{O_2}$  point we compute the  $Fe^{+3}/Fe^{+2}$  of the liquid according to O'Neill et al (2006). Given this, we can then calculate the Mg# of the bulk, and a  $K_{D, Fe^{+2}-Mg}$ . Fig. 5 can be used to provide a more visual guide to this process: at constant pressure, as we increase the oxygen fugacity, ferrous iron in the liquid is converted into ferric iron, which increases the Mg# of the bulk; the Mg# of the bulk, combined with that of the most Mg-rich olivine, allows us to compute a  $K_{D, Fe^{+2}-Mg}$ . The results of our calculation are shown in Fig. 6 which shows contours of  $K_{D, Fe^{+2}-Mg}$  as a function of pressure and oxygen fugacity. If the olivines in NWA 2990 are in equilibrium with a liquid whose composition is equal to that of the bulk meteorite, crystallization must have occurred under reducing conditions where the  $Fe^{3+}/\sum Fe$  is small, approximately half of a log unit above the iron-wüstite (IW) buffer at one atm or  $\sim IW+1$  at 1 GPa.

## CONCLUSIONS

We reviewed previously-published experiments on model Martian compositions to determine the appropriate  $K_{D, Fe^{+2}-Mg}$  when modeling olivine-liquid equilibria of Martian basalts. Due to a lack of direct measurements, we used the expression of O'Neill et al. (2006) to calculate the  $Fe^{+3}/Fe^{+2}$  of liquid coexisting with olivine. One-atm experiments have much tighter control over temperature and oxygen fugacity compared to the high-pressure experiments run in graphite capsules, which

leads to smaller uncertainties in the calculated  $K_{D, \text{Fe}^{+2}\text{-Mg}}$ . The median  $K_{D, \text{Fe}^{+2}\text{-Mg}}$  of 17 one-atm experiments is  $0.354 \pm 0.008$  (error is one MAD), and 77 higher-pressure experiments run above  $1150^\circ\text{C}$  have a median  $K_{D, \text{Fe}^{+2}\text{-Mg}}$  of  $0.365 \pm 0.024$  (MAD), both significantly higher than the canonical value of 0.30. Excluding those high-pressure experiments run below  $1150^\circ\text{C}$ , we observe no significant correlation between  $K_{D, \text{Fe}^{+2}\text{-Mg}}$  and the composition of the liquid, olivine, or temperature. Using a  $K_{D, \text{Fe}^{+2}\text{-Mg}}$  of  $0.36 \pm 0.02$ , we conclude that Y 980459, NWA 5789, 2990, and EETA 79001 are possible liquid compositions. Calculating the amount of ferric iron present in a liquid also allows us to comment on plausible oxygen fugacities when independent measurements are not available: if we assume a liquid composition equal to that of the bulk of NWA 2990 we conclude that the most Mg-rich phenocrysts were in equilibrium with that liquid under only relatively reducing conditions,  $\sim\text{IW}+0.5$  at 1 atm. The accuracy of these conclusions would be improved by either a direct measurement of the  $\text{Fe}^{+3}/\text{Fe}^{+2}$  ratio of a glass coexisting with olivine, or a systematic study of how the  $\text{Fe}^{+3}/\text{Fe}^{+2}$  ratio of a Martian basalt changes as a function of temperature and composition.

**REFERENCES**

- Agee C. B. and Draper D. S. 2004. Experimental constraints on the origin of Martian meteorites and the composition of the Martian mantle. *Earth and Planetary Science Letters* 224:415-429.
- Anand M., James S., Greenwood R. C., Johnson D., Franchi I. A., and Grady M. M. 2008. Mineralogy and geochemistry of shergottite RBT 04262 (abstract # 2173). 39<sup>th</sup> Lunar and Planetary Science Conference.
- Baker L. L. and Rutherford M. J. 1996. The effect of dissolved water on the oxidation state of silicic melts. *Geochimica et Cosmochimica Acta* 60(12):2179-2187.
- Barrat J. A., Jambon A., Bohn M., Gillet P., Sautter V., Gopel C., Lesourd M., and Keller F. 2002. Petrology and chemistry of the picritic shergottite North West Africa 1068 (NWA 1068). *Geochimica et Cosmochimica Acta* 66(19):3505-3518.
- Beattie P. 1993. Olivine-melt and ortho-pyroxene-melt equilibria. *Contributions to Mineralogy and Petrology* 115(1):103-111.
- Bertka C. M. and Holloway J. R. 1994a. Anhydrous partial melting of an iron-rich mantle I: subsolidus phase assemblages and partial melting relations at 10 to 30 kbar. *Contributions to Mineralogy and Petrology* 115:313-322.
- Bertka C. M. and Holloway J. R. 1994b. Anhydrous partial melting of an iron-rich mantle II: primary melt compositions at 15 kbar. *Contributions to Mineralogy and Petrology* 115:323-338.
- Blinova A. and Herd C. D. K. 2009. Experimental study of polybaric REE partitioning between olivine, pyroxene and melt of the Yamato 980459 composition: Insights into the

- petrogenesis of depleted shergottites. *Geochimica et Cosmochimica Acta* 73(11):3471-3492.
- Botcharnikov R., Freise M., Holtz F., and Behrens H. 2005. Solubility of C-O-H mixtures in natural melts: new experimental data and application range of recent models. *Annals of Geophysics* 48:633-646.
- Bunch T. E., Irving A. J., Wittke J. H., Rumble D., III, Korotev R. L., Gellissen M., and Palme H. 2009. Petrology and composition of Northwest Africa 2990; a new type of fine-grained, enriched, olivine-phyric shergottite (abstract # 2274). 40<sup>th</sup> Lunar and Planetary Science Conference.
- Burghel A., Dreibus G., Palme H., Rammensee W., Spettel B., Weckwerth G., and Waenke H. 1983. Chemistry of shergottites and the shergotty parent body (SPB); further evidence for the two component model of planet formation. *Abstracts of papers presented at the fourteenth Lunar and Planetary Science Conference*:80-81.
- BVSP 1981. *Basaltic Volcanism on the Terrestrial Planets* New York: Pergamon Press. 1286 p.
- Cashman K. V. and Marsh B. D. 1988. Crystal size distribution (CSD) in rocks and the kinetics and dynamics of crystallization II: Makaopuhi lava lake. *Contributions to Mineralogy and Petrology* 99:292-305.
- Dann J. C., Holzheid A. H., Grove T. L., and McSween Jr. H. Y. 2001. Phase equilibria of the Shergotty meteorite: Constraints on pre-eruptive water contents of martian magmas and fractional crystallization under hydrous conditions. *Meteoritics & Planetary Science* 36:793-806.

- Dreibus G., Spettel B., Haubold R., Jochum K. P., Palme H., Wolf D., and Zipfel J. 2000. Chemistry of a new shergottite; Sayh al Uhaymir 005. *Meteoritics & Planetary Science* 35(5, Suppl.):49.
- Falloon T. J., Danyushevsky L. V., Ariskin A., Green D. H., and Ford C. E. 2007. The application of olivine geothermometry to infer crystallization temperatures of parental liquids: Implications for the temperature of MORB magmas. *Chemical Geology* 241(3-4):207-233.
- Filiberto J. 2008. Experimental constraints on the parental liquid of the Chassigny meteorite: A possible link between the Chassigny meteorite and a Martian Gusev basalt. *Geochimica et Cosmochimica Acta* 72(2):690-701.
- Filiberto J. and Dasgupta R. 2011. Fe<sup>2+</sup>-Mg partitioning between olivine and basaltic melts: Applications to genesis of olivine-phyric shergottites and conditions of melting in the Martian interior. *Earth and Planetary Science Letters* 304(3-4):527-537.
- Filiberto J., Dasgupta R., Kiefer W. S., and Treiman A. H. 2010a. High pressure, near-liquidus phase equilibria of the Home Plate basalt Fastball and melting in the Martian mantle. *Geophysical Research Letters* 37.
- Filiberto J., Jackson C., Le L., and Treiman A. H. 2009. Partitioning of Ni between olivine and an iron-rich basalt: Experiments, partition models, and planetary implications. *American Mineralogist* 94(2-3):256-261.
- Filiberto J., Musselwhite D. S., Gross J., Burgess L. L. E., and Treiman A. H. 2010b. Experimental petrology, crystallization history, and parental magma characteristics of olivine-phyric shergottite NWA 1068: Implications for the petrogenesis of “enriched” olivine-phyric shergottites. *Meteoritics & Planetary Science* 45:1258-1270.

- Filiberto J., Treiman A. H., and Le L. 2008. Crystallization experiments on a Gusev Adirondack basalt composition. *Meteoritics & Planetary Science* 43(7):1137-1146.
- Gaillard F., Pichavant M., and Scaillet B. 2003. Experimental determination of activities of FeO and Fe<sub>2</sub>O<sub>3</sub> components in hydrous silicic melts under oxidizing conditions. *Geochimica et Cosmochimica Acta* 67(22):4389-4409.
- Gee L. L. and Sack R. O. 1988. Experimental petrology of melilite nephelinites. *Journal of Petrology* 29(6):1233-1255.
- Goodrich C. A. (2002) Petrogenesis of olivine-phyric shergottites Sayh al Uhaymir 005 and Elephant Moraine A79001 lithology A. In *Unmixing the SNCs; chemical, isotopic, and petrologic components of Martian meteorites* (eds. J. Jones and D. W. Mittlehehldt), pp. 17-18.
- Goodrich C. A. and Zipfel J. 2001. Magmatic inclusions in olivine and chromite in basaltic shergottite Sayh al Uhaymir 005; implications for petrogenesis and relationship to lherzolitic shergottites (abstract # 1174). 32<sup>nd</sup> Lunar and Planetary Science Conference.
- Gross J., Treiman A. H., Filiberto J., and Herd C. D. K. 2011. Primitive olivine-phyric shergottite NWA 5789: Petrography, mineral chemistry, and cooling history imply a magma similar to Yamato-980459. *Meteoritics & Planetary Science* 46(1):116-133.
- Herd C. D. K. 2003. The oxygen fugacity of olivine-phyric martian basalts and the components within the mantle and crust of Mars. *Meteoritics & Planetary Science* 38(12):1793-1805.
- Herd C. D. K., Dwarzski R. E., and Shearer C. K. 2009. The behavior of Co and Ni in olivine in planetary basalts: An experimental investigation. *American Mineralogist* 94(2-3):244-255.
- Irving A. J., Kuehner S. M., Herd C. D. K., Gellissen M., Korotev R. L., Puchtel I., Walker R. J., Lapen T. J., and Rumble D., III 2010. Petrologic, elemental and multi-isotopic

- characterization of permafic olivine-phyric shergottite Northwest Africa 5789: A primitive magma derived from depleted Martian mantle (abstract # 1547). 41<sup>st</sup> Lunar and Planetary Science Conference.
- Irving A. J., Kuehner S. M., Korotev R. L., and Hupe G. M. 2007. Petrology and bulk composition of primitive enriched olivine basaltic shergottite Northwest Africa 4468 (abstract # 1526). 38<sup>th</sup> Lunar and Planetary Science Conference.
- Jayasuriya K. D., O'Neill H. S., Berry A. J., and Campbell S. J. 2004. A Mossbauer study of the oxidation state of Fe in silicate melts. *American Mineralogist* 89(11-12):1597-1609.
- Kilinc A., Carmichael I. S. E., Rivers M. L., and Sack R. O. 1983. The ferric-ferrous ratio of natural silicate liquids equilibrated in air. *Contributions to Mineralogy and Petrology* 83(1-2):136-140.
- Kress V. C. and Carmichael I. S. E. 1991. The compressibility of silicate liquids containing Fe<sub>2</sub>O<sub>3</sub> and the effect of composition, temperature, oxygen fugacity and pressure on their redox states. *Contributions to Mineralogy and Petrology* 108(1-2):82-92.
- Kuehner S. M., Irving A. J., Herd C. D. K., Gellissen M., Lapen T. J., and Rumble D., III 2011. Pristine olivine-phyric shergottite Northwest Africa 6162; a primitive magma with accumulated crystals derived from depleted Martian mantle (abstract # 1610). 42<sup>nd</sup> Lunar and Planetary Science Conference.
- Longhi J., Walker D., and Hays J. F. 1978. The distribution of Fe and Mg between olivine and lunar basaltic liquids. *Geochimica et Cosmochimica Acta* 42:1545-1558.
- Matzen A. K., Baker M. B., Beckett J. R., and Stolper E. M. 2011. Fe–Mg Partitioning between Olivine and High-magnesian Melts and the Nature of Hawaiian Parental Liquids. *Journal of Petrology* 52(7-8):1243-1263.

- McCanta M. C., Elkins-Tanton L., and Rutherford M. J. 2009. Expanding the application of the Eu-oxybarometer to the Iherzolitic shergottites and nakhlites: Implications for the oxidation state heterogeneity of the Martian interior. *Meteoritics & Planetary Science* 44(5):725-745.
- McCubbin F. M., Nekvasil H., Harrington A. D., Elardo S. M., and Lindsley D. H. 2008. Compositional diversity and stratification of the Martian crust: Inferences from crystallization experiments on the microbasalt Humphrey from Gusev Crater, Mars. *Journal of Geophysical Research-Planets* 113:E11013.
- Medard E., McCammon C. A., Barr J. A., and Grove T. L. 2008. Oxygen fugacity, temperature reproducibility, and H<sub>2</sub>O contents of nominally anhydrous piston-cylinder experiments using graphite capsules. *American Mineralogist* 93(11-12):1838-1844.
- Mellin M. J., Liu Y., Schnare D. W., and Taylor L. A. 2008. Revised compositional estimate of EETA79001 lithology A groundmass (abstract # 2150). 39<sup>th</sup> Lunar and Planetary Science Conference.
- Mikouchi T., Kurihara T., and Miyamoto M. 2008. Petrology and mineralogy of RBT 04262; implications for stratigraphy of the Iherzolitic shergottite igneous block (abstract # 2403). 39<sup>th</sup> Lunar and Planetary Science Conference.
- Mikouchi T., Miyamoto M., and McKay G. A. 2001. Mineralogy and petrology of the Dar al Gani 476 martian meteorite: Implications for its cooling history and relationship to other shergottites. *Meteoritics & Planetary Science* 36(4):531-548.
- Monders A. G., Médard E., and Grove T. L. 2007. Phase equilibrium investigations of the Adirondack class basalts from the Gusev plains, Gusev crater, Mars. *Meteoritics and Planetary Science* 42:131-148.

- Moore G., Righter K., and Carmichael I. S. E. 1995. The effect of dissolved water on the oxidation state of iron in natural silicate liquids. *Contributions to Mineralogy and Petrology* 120:170-179.
- Musselwhite D. S., Dalton H. A., Kiefer W. S., and Treiman A. H. 2006. Experimental petrology of the basaltic shergottite Yamato-980459: Implications for the thermal structure of the Martian mantle. *Meteoritics & Planetary Science* 41(9):1271-1290.
- Nekvasil H., McCubbin F. M., Harrington A., Elardo S., and Lindsley D. H. 2009. Linking the Chassigny meteorite and the Martian surface rock Backstay: Insights into igneous crustal differentiation processes on Mars. *Meteoritics & Planetary Science* 44(6):853-869.
- O'Neill H. S. C., Berry A. J., McCammon C., Jayasuriya K. D., Campbell S. J., and Foran G. J. 2006. An experimental determination of the effect of pressure on the  $\text{Fe}^{+3}/\Sigma\text{Fe}$  ratio of anhydrous silicate melt to 3.0 GPa. *American Mineralogist* 91:404-412.
- Papike J. J., Karner J. M., Shearer C. K., and Burger P. V. 2009. Silicate mineralogy of martian meteorites. *Geochimica et Cosmochimica Acta* 73(24):7443-7485.
- Peslier A. H., Hnatyshin D., Herd C. D. K., Walton E. L., Brandon A. D., Lapen T. J., and Shafer J. T. 2010. Crystallization, melt inclusion, and redox history of a Martian meteorite: Olivine-phyric shergottite Larkman Nunatak 06319. *Geochimica et Cosmochimica Acta* 74(15):4543-4576.
- Putirka K. D., Perfit M., Ryerson F. J., and Jackson M. G. 2007. Ambient and excess mantle temperatures, olivine thermometry, and active vs. passive upwelling. *Chemical Geology* 241(3-4):177-206.

- Righter K., Danielson L. R., Martin A. M., Sutton S., Newville M., and Choi Y. 2010. Iron Redox Systematics of Shergottites and Martian Magmas (abstract # 5339). 73<sup>rd</sup> Annual Meteoritical Society Meeting.
- Roeder P. L. and Emslie R. F. 1970. Olivine-liquid equilibrium. *Contributions to Mineralogy and Petrology* 29(4):275-289.
- Sack R. O., Carmichael I. S. E., Rivers M., and Ghiorso M. S. 1980. Ferric-ferrous equilibria in natural silicate liquids at 1bar. *Contributions to Mineralogy and Petrology* 75(4):369-376.
- Sack R. O., Walker D., and Carmichael I. S. E. 1987. Experimental petrology of alkalic lavas: constraints on cotectics of multiple saturation in natural basic liquids. *Contributions to Mineralogy and Petrology* 96:1-23.
- Sarbadhikari A. B., Day J. M. D., Liu Y., Rumble D., and Taylor L. A. 2009. Petrogenesis of olivine-phyric shergottite Larkman Nunatak 06319: Implications for enriched components in martian basalts. *Geochimica et Cosmochimica Acta* 73(7):2190-2214.
- Shearer C. K., McKay G., Papike J. J., and Karner J. M. 2006. Valence state partitioning between olivine-melt: Estimates of the oxygen fugacity of Y980459 and application to other olivine-phyric martian basalts. *American Mineralogist* 91:1657-1663.
- Shirai N. and Ebihara M. 2004. Chemical characteristics of a Martian meteorite, Yamato 980459. *Antarctic Meteorite Research* 17:55-67.
- Shirai N., Humayun M., and Irving A. J. 2009. The bulk composition of coarse-grained meteorites from laser ablation analysis of their fusion crusts (abstract # 2170). 40<sup>th</sup> Lunar and Planetary Science Conference.

- Steele I. M. and Smith J. V. 1982. Mineralogy of Elephant Moraine EETA 79001 Two-Component Achondrite with Resemblances to Shergotty. *Abstracts of papers presented at the thirteenth Lunar and Planetary Science Conference*:764-765.
- Stolper E. 1977. Experimental petrology of eucritic meteorites. *Geochimica et Cosmochimica Acta* 41:587-611.
- Taylor L. A., Nazarov M. A., Shearer C. K., McSween H. Y., Cahill J., Neal C. R., Ivanova M. A., Barsukova L. D., Lentz R. C., Clayton R. N., and Mayeda T. K. 2002. Martian meteorite Dhofar 019: A new shergottite. *Meteoritics & Planetary Science* 37(8):1107-1128.
- Usui T., McSween H. Y., and Floss C. 2008. Petrogenesis of olivine-phyric shergottite Yamato 980459, revisited. *Geochimica et Cosmochimica Acta* 72(6):1711-1730.
- Yukio I. 1994. Petrography and petrology of the ALHA77005 shergottite. *Proceedings of the Seventh NIPR Symposium on Antarctic Meteorites*.
- Zipfel J., Scherer P., Spettel B., Dreibus G., and Schultz L. 2000. Petrology and chemistry of the new shergottite Dar al Gani 476. *Meteoritics & Planetary Science* 35(1):95-106.

## FIGURE CAPTIONS

**Fig. 1**  $D_{\text{Fe}^{+2}} = \text{FeO}^{\text{ol}} / \text{FeO}^{\text{liq}}$  and  $D_{\text{Mg}} = \text{MgO}^{\text{ol}} / \text{MgO}^{\text{liq}}$  (both by wt.) along with lines of constant  $K_{\text{D, Fe}^{+2}\text{-Mg}}$ . 17 one-atm experiments on Martian bulk compositions (Filiberto et al., 2008; Herd et al., 2009) have a nearly uniform  $K_{\text{D, Fe}^{+2}\text{-Mg}}$  of  $\sim 0.35$ , significantly higher than the canonical value of 0.30

**Fig. 2**  $D_{\text{Fe}^{+2}}$  vs.  $D_{\text{Mg}}$  (as defined in Fig. 1) for both one-atm (red squares) and high-pressure (blue circles) along with lines of constant  $K_{\text{D, Fe}^{+2}\text{-Mg}}$ . Both high-pressure and one-atm experiments have  $K_{\text{D, Fe}^{+2}\text{-Mg}} \sim 0.36 \pm 0.2$  after accounting for the presence of ferric iron in the melt. High-pressure experiments were taken from the following sources: Agee et al. (2004), Bertka et al. (1994a, b), Blinova et al. (2009), Dann et al. (2001), Filiberto (2008), Filiberto et al. (2010a), Filiberto et al. (2009), Filiberto et al. (2010b), Filiberto et al. (2008), McCubbin et al. (2008); Monders et al. (2007), Musselwhite et al. (2006), Nekvasil et al. (2009)

**Fig. 3** Lower panels:  $K_{\text{D, Fe}^{+2}\text{-Mg}}$  as a function of concentrations of oxides (wt. %) in experimental glasses; symbols for high-pressure and one-atm experiments as in Fig. 2. Upper panels: concentrations of oxides in the bulk (wt. %) for all olivine-phyric shergottites shown on Fig. 5. Compositions of bulk shergottites from: Anand et al. (2008), Barrat et al. (2002), Bunch et al. (2009), Burghele et al. (1983), Dreibus et al. (2000), Irving et al. (2010), Kuehner et al. (2011), Mellin et al. (2008), Sarbadhikari et al. (2009), Shirai et al. (2004); Shirai et al. (2009), Taylor et al. (2002), Zipfel et al. (2000)

**Fig. 4**  $K_{D, Fe+2-Mg}$  as a function of compositional distance (as defined in text). Symbols on model Martian bulk compositions as in previous figures; filtered, one-atm, terrestrially-relevant database assembled by Matzen et al. (2011) shown as small black points

**Fig. 5** Mg# of a liquid equal in composition to that of the bulk of the meteorite as a function of the Mg# of the most Mg-rich olivine found. Constant  $K_{D, Fe+2-Mg}$  contours of 0.30 and  $0.36 \pm 0.02$  are shown for reference. Olivine compositions from Peslier et al. (2010), Usui et al. (2008), Gross et al. (2011), Bunch et al. (2009), Mikouchi et al. (2001), Taylor et al. (2002), Papike et al. (2009), Mikouchi et al. (2008), Goodrich et al. (2001), Kuehner et al. (2011), Irving et al. (2007), Goodrich (2002), Yukio (1994), Steele et al. (1982). For each meteorite we calculate the Mg# of the bulk assuming all Fe as FeO, and, where available, we also use the maximum temperature and  $fO_2$  estimate (Gross et al., 2011; Herd, 2003; McCanta et al., 2009; Peslier et al., 2010; Shearer et al., 2006) to calculate the FeO content of the bulk (using the expression of O'Neill et al. (2006)). Our results suggest that, NWA 5789, 2990, EETA79001, and Y980459 represent possible liquid compositions; Northwest Africa 1068, 6126, 4468, Elephant Moraine A79001, Allan Hills A77005, Dar al Gani 476, Roberts Massif 04262, Dhofar 019, Sayh al Uhaymir 005, and Larkman Nunatak 06319 do not.

**Fig. 6**  $K_{D, Fe+2-Mg}$  as a function of pressure and  $fO_2$  (in log units relative to the Iron-Wüstite, IW, buffer) for NWA 2990. Temperature is estimated using the thermometer of Beattie (1993), and at each pressure- $fO_2$  point the  $Fe^{+3}/Fe^{+2}$  in the bulk is calculated using the expression of O'Neill et al.

(2006), resulting in a calculated  $K_{D, \text{Fe}+2\text{-Mg}}$ . The calculated  $K_{D, \text{Fe}+2\text{-Mg}}$ s are then contoured; for clarity, the +1 and +2 MAD contours are labeled (0.38 and 0.40).

Fig. 1.

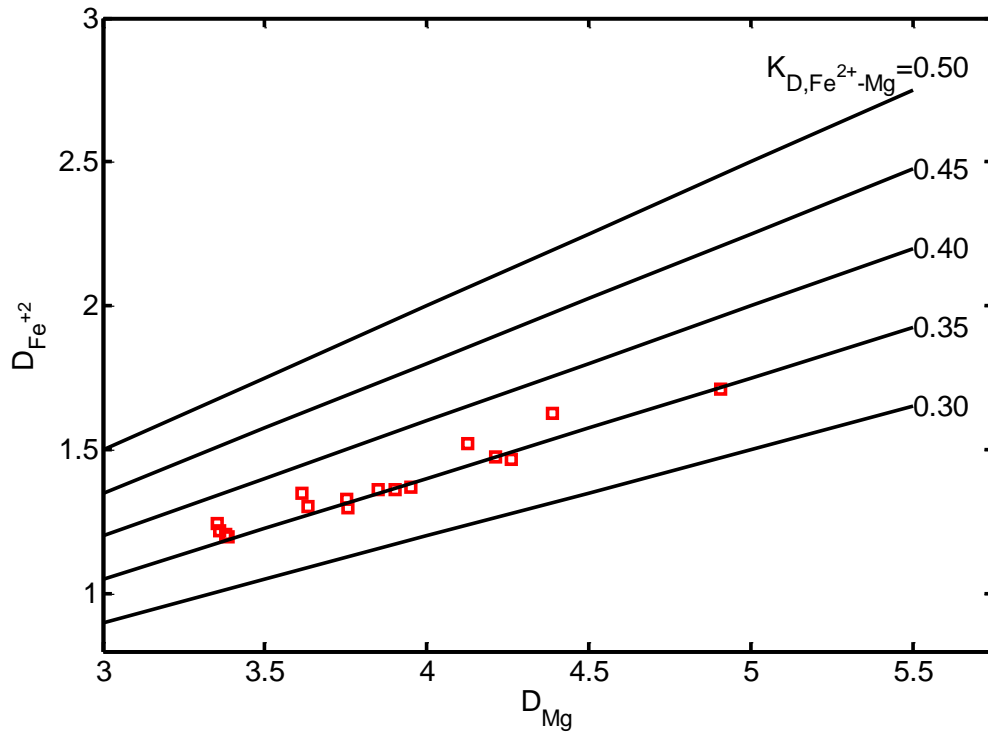


Fig. 2

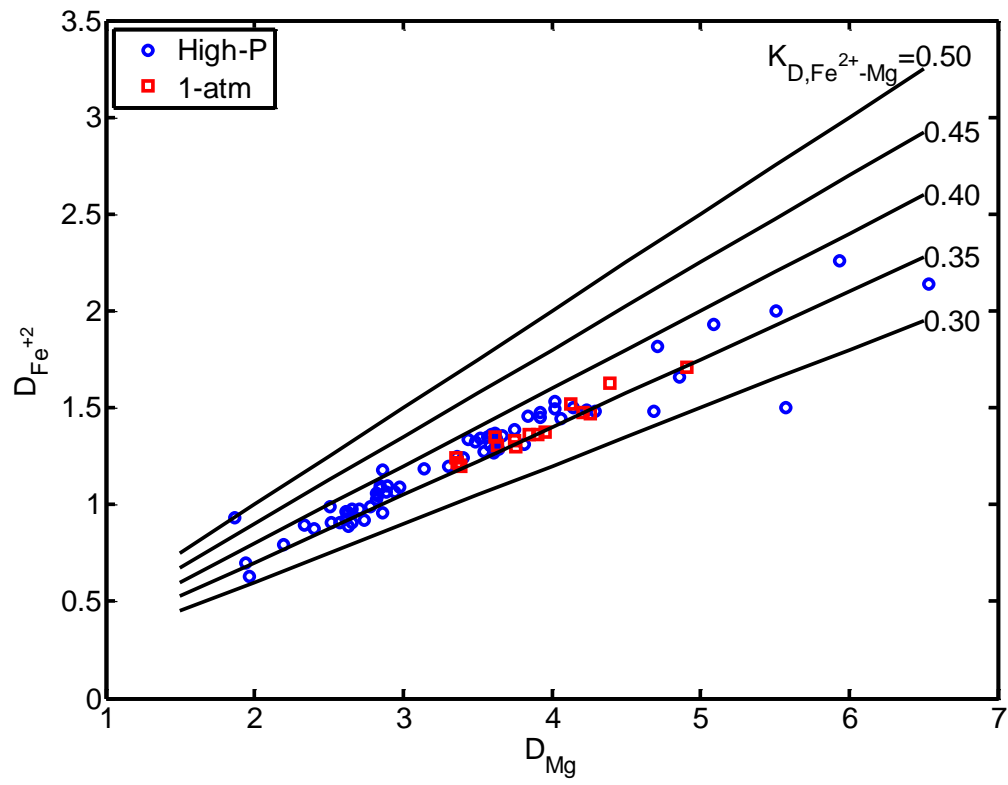


Fig. 3

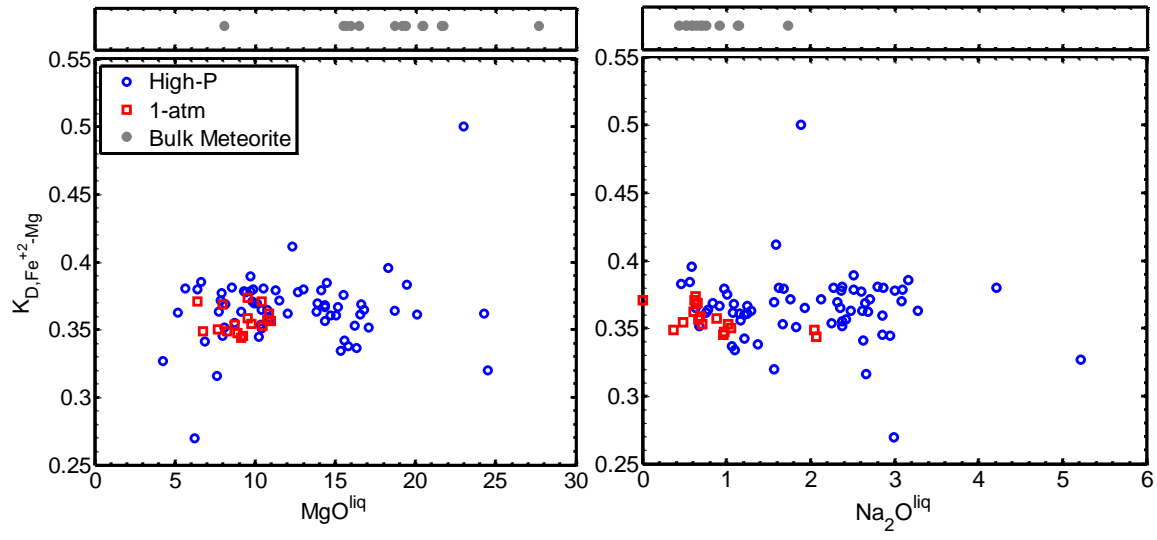


Fig. 4

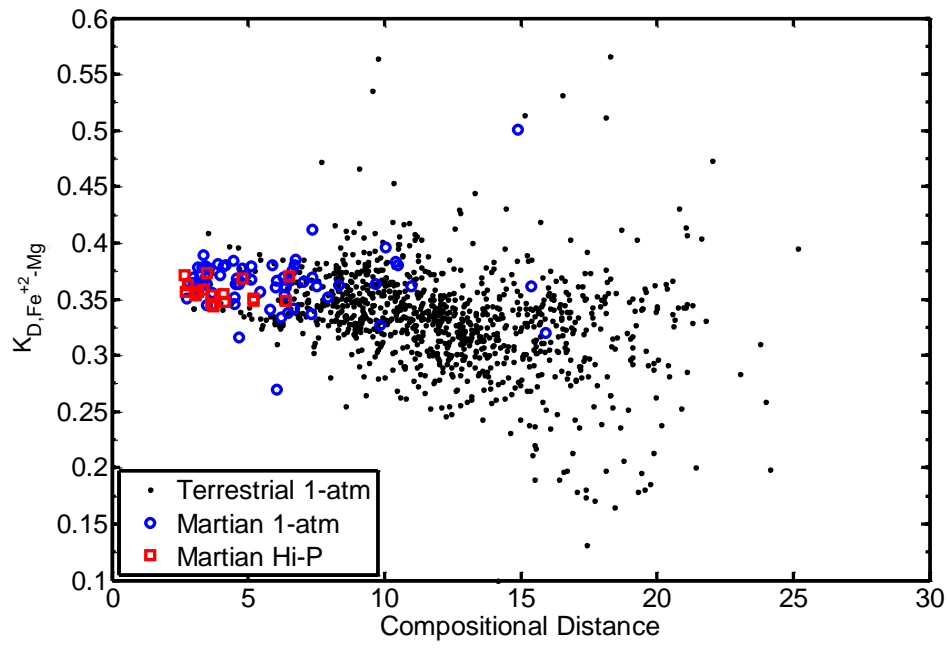


Fig. 5

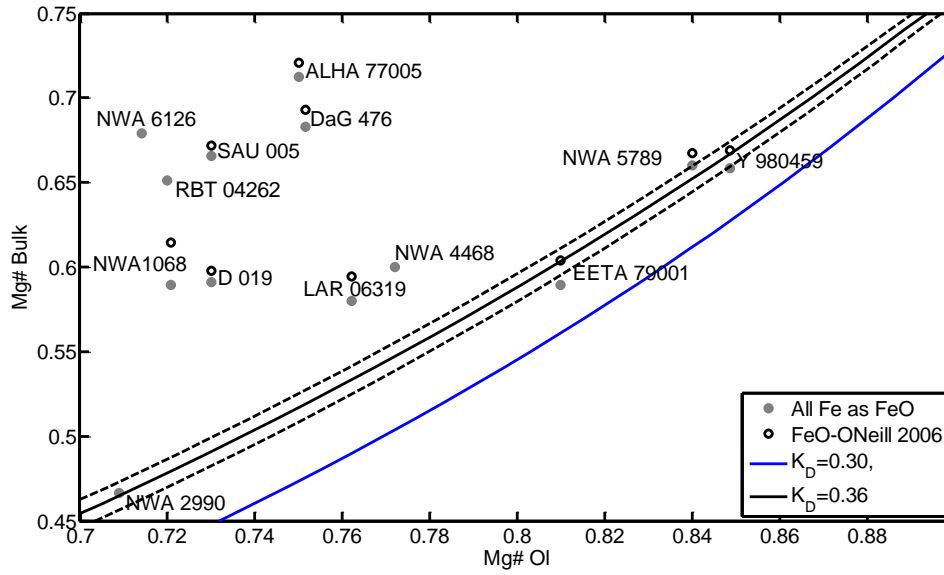
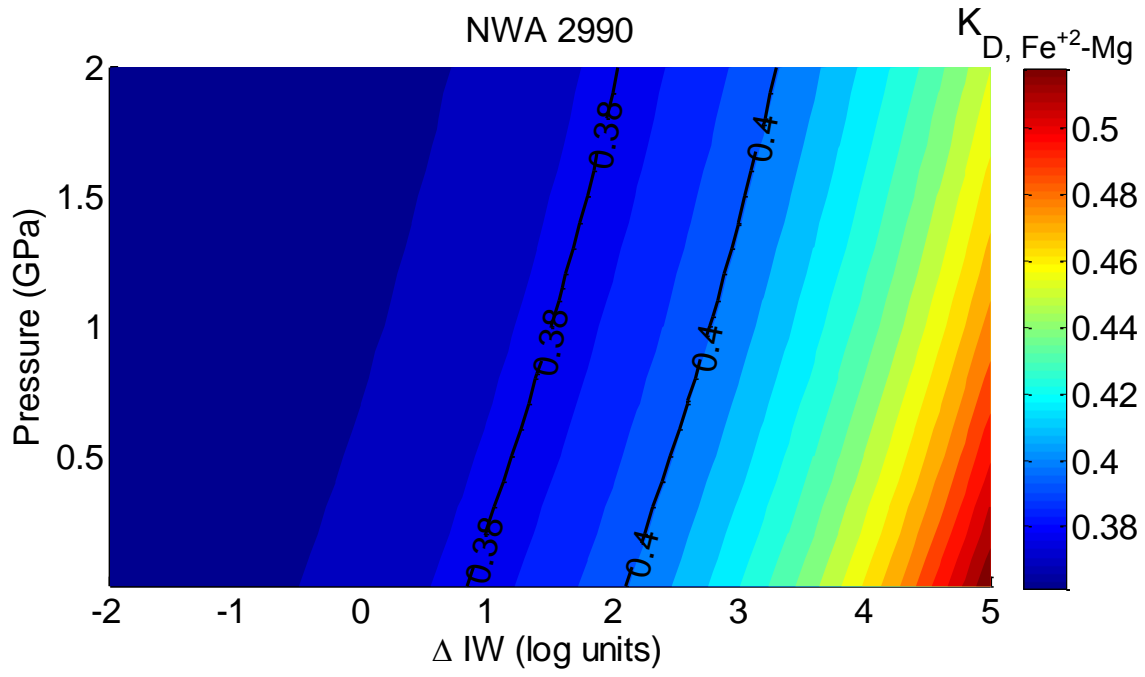


Fig. 6



IV-1

*Chapter 4*

**THE TEMPERATURE AND PRESSURE DEPENDENCE OF NICKEL  
PARTITIONING BETWEEN OLIVINE AND SILICATE MELT**

Andrew K. Matzen

Michael B. Baker

John R. Beckett

Edward M. Stolper

For submission to

*Contributions to Mineralogy and Petrology*

January 5, 2012

**ABSTRACT**

We measured Ni partitioning in experiments on mid-ocean ridge basalt (MORB) embedded in powdered olivine at pressures from 1-atm to 3.0 GPa and temperatures from 1400-1550°C. We present a reversed series of experiments where the pressure and temperature were changed in concert to obtain liquids with approximately the same composition (~18 wt. % MgO<sup>liq</sup>). This approach allowed us to separate the effects of composition from those of temperature and pressure. Our experiments show that the partition coefficient for Ni between olivine and liquid,  $D_{Ni}^{ol/liq}$ , decreases from 5.0 to 3.8 as the temperature increases from 1400 to 1550°C. We fit thermodynamic expressions that describe  $D_{Ni}^{ol/liq}$  as a function of both temperature and liquid composition using the results of our experiments and data from the literature. We then combine these expressions with the results of partial melting experiments to show that when a deep (3.0 GPa) partial melt is brought to lower pressure (0.1 GPa) and allowed to crystallize, the low-pressure olivines have significantly higher NiO contents (~0.43 wt. %) than the 0.36 wt. % NiO in olivine in the mantle peridotites from which the melt was extracted.. This effect may contribute to the high-NiO contents observed in magnesian olivine phenocrysts from Hawaii and other ocean-island basalts.

**INTRODUCTION**

The abundance and distribution of Ni within the Earth is a recurring theme in petrology and geochemistry because it can provide constraints on core formation, accretionary processes, and partial melting and crystallization processes (e.g., Gaetani and Grove 1997; Häkli and Wright 1967; Li and Ripley 2010; Minarik et al. 1996; Ringwood 1956; Vogt 1923). It is the compatibility of Ni in olivine relative to silicate melt, which contrasts with the behavior of most

other minor and trace elements, that makes it so useful in constraining igneous petrogenesis: For example, Hart and Davis (1978) showed that Ni contents of melts are sensitive to the fractionation of olivine and that high-MgO basalts from Baffin Island and Kilauea volcano are unlikely to be primary olivine-rich liquids, but rather to result from olivine accumulation.

One consequence of the compatibility of Ni in olivine relative to other phases in peridotites (e.g., Mysen 1978) is that the Ni contents of residual olivine and bulk peridotites are relatively unaffected by the extraction of low degrees of partial melt. By the same reasoning, the first olivine to crystallize from a partial melt of an olivine-bearing mantle source is expected to closely approach the composition of residual olivine in the source. For MORBs this appears to be generally true: most MORB olivine phenocrysts have NiO contents between 0.19 and 0.36 wt. % (median is 0.28, with a maximum of 0.45; Sobolev et al. 2007), whereas olivines in spinel peridotites generally have 0.31-0.43 wt. % NiO with a median of 0.37 wt. % (Korenaga and Kelemen 2000). Olivines from some ocean islands (e.g., the Hawaiian Islands), however, often have NiO contents exceeding 0.5 wt. % (e.g., Clague et al. 1991; Korenaga and Kelemen 1998; Sobolev et al. 2007; Sobolev et al. 2005)—significantly higher than the olivines from spinel peridotites.

Given the difficulty of generating high-Ni olivines by partially melting normal peridotitic mantle, alternatives have been proposed to explain olivine phenocrysts with elevated Ni contents. For example, Ryabchikov (2003) suggested that the Ni content of the Hawaiian plume was elevated due to interaction with the Earth's core, and Humayan and coworkers (Humayun et al. 2004; Qin and Humayun 2008) supported the idea of a significant contribution of the core to the sources of Hawaiian magmas based on an analysis of Fe/Mn ratios. Alternatively, Sobolev et al. (e.g., 2007; 2005) expanded on a model of Kelemen et al. (1998), proposing that silica-rich partial

melts of eclogite react with peridotite to form olivine-free pyroxenites; in the absence of olivine, the bulk solid-liquid Ni partition coefficient for the pyroxenite is low, and consequently, high-Ni melts can be produced during subsequent partial melting of the metasomatic pyroxenite. If such a high-Ni partial melt is then mixed with enough “normal” partial melt obtained directly from peridotite, to bring olivine back onto the liquidus, then high-Ni olivines can crystallize from such melts. Another possibility, proposed by Wang and Gaetani (2008), is that when partial melt of an eclogite in equilibrium with olivine mixes with a tholeiitic liquid, high-Ni olivines can crystallize from a melt with only moderate Ni concentrations due to the control the liquid composition exerts on the olivine-liquid Ni partition coefficient (defined here as  $D_{Ni}^{ol/liq} = NiO^{ol}/NiO^{liq}$ , by wt.). Finally, if  $D_{Ni}^{ol/liq}$  is a function of temperature and pressure (e.g., Duke 1976; Mysen and Kushiro 1979) high-Ni olivines may crystallize following the ascent and cooling of partial melts of “normal” mantle peridotite (e.g., Li and Ripley 2010; Matzen et al. 2009; Putirka et al. 2011).

Each of the possibilities described above depends on the nature of Ni partitioning between olivine and melt; thus, our ability to quantitatively test these models requires a characterization of  $D_{Ni}^{ol/liq}$  that includes the effects of variables that (1) substantially affect  $D_{Ni}^{ol/liq}$  and that (2) change during generation, transportation, and crystallization of magmas (e.g., pressure, temperature, melt composition,  $fO_2$ ). Although many experimental studies have measured olivine-liquid partitioning of Ni, most of them were conducted under 1 atmosphere of pressure. At constant pressure, for a given bulk composition, temperature and the compositions of coexisting olivine and melt are correlated (e.g., Herd et al. 2009; Wang and Gaetani 2008), and as a result, it has proven difficult to deconvolve the effects of temperature and melt composition on  $D_{Ni}^{ol/liq}$  (e.g., Arndt 1977; Hart and Davis 1978; Takahashi 1978). In the face of this difficulty, most authors have used either temperature (e.g., Arndt 1977; Hart and Davis 1978; Kelemen et al. 1998) *or* some aspect of the

melt composition (commonly MgO, but sometimes SiO<sub>2</sub>; e.g., Hart and Davis 1978; Kinzler et al. 1990) as the single independent variable to model variations in  $D_{Ni}^{ol/liq}$ . The use of  $D_{Mg}^{ol/liq}$  as the independent variable (e.g., Beattie 1993a; Beattie et al. 1991; Jones 1984) is essentially equivalent because  $D_{Mg}^{ol/liq}$  is strongly correlated with both temperature and melt composition. Models that parameterize  $D_{Ni}^{ol/liq}$  using liquid composition as the only independent variable (e.g., Hart and Davis 1978; Kinzler et al. 1990; Wang and Gaetani 2008), are widely used due to their ease of use and because the liquid composition during magmatic processes is generally more readily constrained than the temperature (e.g., Falloon et al. 2007; Putirka et al. 2007).

Although models that describe  $D_{Ni}^{ol/liq}$  in terms of a single independent variable (e.g., temperature or aspects of phase composition) are generally successful at describing experimental data, it is likely that  $D_{Ni}^{ol/liq}$  depends on multiple variables independently—temperature, pressure, and melt and mineral compositions (e.g., Hirschmann and Ghiorso 1994; Kinzler et al. 1990)—even if available experiments have not been optimized for deconvolving them. In nature, however, temperature and phase compositions may not co-vary in the same way as in currently available experiments. The objective of our study is to explicitly constrain the temperature dependence of  $D_{Ni}^{ol/liq}$  by conducting a series of experiments in which temperature and pressure are selected so that liquid and olivine compositions remain nearly constant, so that differences in  $D_{Ni}^{ol/liq}$  reflect mostly differences in temperature and pressure, not variations in phase chemistry. Preliminary reports on the work presented here are given in (Matzen et al. 2009, 2010).

## EXPERIMENTAL METHODS

A basic design constraint for our experiments was the need to reliably measure equilibrium partitioning between basaltic liquids and olivine as a function of pressure and temperature at a constant melt composition. In principle, this should be a simple matter: for a given melt composition, one need only determine the composition of the liquidus olivine as a function of pressure; since the liquid composition is constant in such experiments (provided one could determine the olivine composition sufficiently close to the liquidus temperature), variations of  $D_{Ni}^{ol/liq}$  would reflect only the effects of temperature and pressure. In practice, such experiments are not straightforward for high-pressure experiments using the standard Pt-graphite, double-capsule technique because Ni from the sample passes through the graphite to the enclosing Pt capsule, (e.g., J. Longhi, 2006, personal communication; unpublished data from our lab). Graphite-only capsules also fail to retain Ni (e.g., Filiberto et al. 2009). To minimize such Ni losses, we surrounded a small chip of homogenized Juan de Fuca MORB glass (6.6 wt. % MgO and NiO < 0.03 wt. %; see Table 1 for full analysis of all starting materials) with powdered Kilbourne Hole olivine (48.8 wt. % MgO and 0.36 wt. % NiO) in a Pt-graphite capsule; the mass of the glass chip is small compared to that of the olivine, accounting for, on average, only 4% of the weight of all starting materials. Once in the piston cylinder, the capsule was sintered  $\sim 15^\circ\text{C}$  below the solidus of the basalt for  $\sim 6$  hrs (see Table 2 for run conditions) and slightly below the final run pressure (i.e., most experiments were hot-piston-in, see Table 2), effectively transforming the powdered olivine into an inner container. After sintering, the temperature was then increased, above the solidus of the basalt, to the final run temperature, followed by a pressure increase to the final run pressure. Now the melt in the middle of the capsule is surrounded by (essentially) an olivine crucible. This inner olivine crucible is the important feature in our experiments because Ni

diffuses much more slowly in olivine than liquid, allowing the olivines and liquid in the center of the charge to exchange until reaching equilibrium. Analysis of our run products show that this strategy was successful in minimizing Ni loss: only a  $\sim 100$   $\mu\text{m}$  rind of sintered olivine immediately adjacent to the C capsule showed evidence of Ni loss, while the melt was typically at least 200  $\mu\text{m}$  from the edge of the inner C capsule. More importantly, mass balance calculations (discussed below) show that NiO was conserved in the interior portions of the sample.

We selected a specific set of pressures and temperatures so that the resulting liquid would have  $\sim 18$  wt. % MgO (17.1-18.9 wt%, excepting one experiment with 16.3 wt. % MgO). Another way to describe the overall experimental approach is that at each pressure, the temperature was chosen such that the MORB glass dissolved approximately the same amount of Kilbourne Hole olivine, resulting in a liquid composition that was similar in all experiments. All of the high-pressure experiments were run in a Rockland Research piston cylinder using a  $\text{CaF}_2$  assembly, graphite heaters, crushable MgO spacers, and W-3Re/W-25Re thermocouples housed in mullite at pressures at and below 2.5 GPa, and in 2-bore alumina at 3.0 GPa. To approach anhydrous conditions, the capsule was dried for approximately 3 hours at  $400^\circ\text{C}$  after loading and before being welded shut; crushable MgO was dried for about 18 hours at  $1000^\circ\text{C}$ . In addition to the Pt-graphite double capsule experiments described above, we also ran one experiment in a Re-foil capsule; this experiment had no C inner capsule, just powdered Kilbourne Hole olivine encased in Re foil surrounding a MORB chip. For all experiments, at pressures at and below 2.5 GPa turning off the power was sufficient to glass the high-temperature melt. Liquid from Run 30 (3.0 GPa) formed a quench mat upon cooling (analyzable glass pools were created in subsequent 3.0 GPa experiments using the pressure-drop quench technique of Putirka et al. (1996)).

Experiments were also done at 1 atm in a Del-Tech VT-31 gas mixing furnace using methods similar to Wang and Gaetani (2008): crucibles of single-crystal San Carlos olivine (49.0 wt. % MgO and 0.28 wt. % NiO) were drilled to form a 2.5 mm diameter, ~2.5 mm deep cavity, which was filled with a mixture of MORB and powdered Kilbourne Hole olivine and suspended by Pt wires. Oxygen fugacity was controlled using flowing H<sub>2</sub> and CO<sub>2</sub>; low flow rates (~4.8 cm/min) were used to minimize alkali loss (Tormey et al. 1987). The  $fO_2$  was ~1.7 log units below the quartz-fayalite-magnetite (QFM) buffer, a value similar to that of estimates for the  $fO_2$  of high-pressure experiments (QFM-2.2, Medard et al. 2008). For both the 1-atm and high-pressure experiments, reversals were conducted by doping the starting MORB glass with approximately 1 wt. % NiO (see Table 1).

Phase compositions measured on Caltech's JEOL JXA-8200 electron microprobe, processed using a modified ZAF procedure (CITZAF, Armstrong 1988) are reported in Table 1. Glasses were initially analyzed at 15 keV using a 10 nA beam and a 10  $\mu$ m spot (a 20- $\mu$ m-diameter spot was used to analyze the quench mat produced by Run 30); on-peak counting times ranged between 30-60 s and half of that on each of the high and low backgrounds. Secondary glass standards (BHVO-2g, BIR-1g, and BCR-2g) were all analyzed during each microprobe session; the mean BHVO-2g composition from each session coupled with the accepted composition of BHVO-2 ([http://minerals.cr.usgs.gov/geo\\_chem\\_stand/](http://minerals.cr.usgs.gov/geo_chem_stand/)) was used to reprocess the k-ratios for all glass analyses from a session. In subsequent instrumental sessions, Ni, Mn, and Cr were re-analyzed with a 200 nA beam, a 20  $\mu$ m spot, and longer counting times (~90 s on peak). This new data was then processed using the major and minor element concentrations from the low-beam current analyses. This dual-pass technique provides a dataset that contains both analyses of beam-

sensitive elements (e.g., Na<sub>2</sub>O, K<sub>2</sub>O, P<sub>2</sub>O<sub>5</sub>) and high-precision analyses of NiO; percent errors on the NiO content of the liquid average ~ 4% (where percent error = 100\*[standard deviation/mean]).

Olivine and pyroxene compositions were measured using a 1- $\mu$ m spot and a beam current of 100 nA; all analyses used an accelerating voltage of 15 keV. On-peak counting times for olivines ranged from 20 to 140 s (Ti and Al, respectively); Ni was counted for 90 s (extremely long counting times, e.g., 140 s for Al, are a result of only one element being analyzed on a given spectrometer). Olivine secondary standards (San Carlos and Guadeloupe) were repeatedly analyzed in each analytical session to monitor drift but no additional corrections were applied. Transects across near-melt olivine crystals (olivines typically range from ~20-100  $\mu$ m) from forward experiments revealed uniform NiO concentrations, but most analyses were collected within ~10  $\mu$ m from the edge of the olivine-glass interface. Near-melt olivines in reversal experiments are, however, zoned in Ni with NiO decreasing from the center to the edge of each crystal. In an effort to capture the equilibrium  $D_{Ni}^{ol/liq}$ , we performed a series of analyses with small step sizes (~2-4  $\mu$ m) approaching the ol-liq interface; we report (Table 3) the NiO contents of the analytical point closest to the interface that did not show contamination from the glass phase (e.g., an olivine from Run 17R was measured to have ~0.070 $\pm$ 0.003 wt. % Al<sub>2</sub>O<sub>3</sub>; either endpoint of the transect across the grain had ~0.36 wt. % Al<sub>2</sub>O<sub>3</sub>, which we interpret to be contamination from the glass phase that has 11 wt. % Al<sub>2</sub>O<sub>3</sub>). The uncertainty reported for the olivine compositions on the reversal experiments is the standard deviation of all analyses for each experiment taken ~10  $\mu$ m from the edge of the olivine-glass interface. These analytical procedures lead to errors of ~ 3% for the NiO contents in the olivines. Using the standard deviations reported in Table 3, the resulting uncertainty on the measured  $D_{Ni}^{ol/liq}$  is ~5%.

## EXPERIMENTAL RESULTS

### *Phase Compositions*

Glass: Ideally, the composition of the melt in each of our experiments represents that of the initial MORB glass, perturbed by the dissolution of surrounding Kilbourne Hole olivine, where the amount of dissolution at any pressure is dictated by the temperature. Since our objective was to evaluate  $D_{Ni}^{ol/liq}$  at a constant liquid composition, we explicitly chose a run temperature for each pressure (Table 2) that would lead to dissolution of approximately the same amount of olivine (based on MELTS predictions), thereby yielding a target melt with ~18 wt.% MgO. Glass compositions (Table 3) were all in the range of 16-19 wt. % MgO (11 of 13 were in the narrower 17.1-18.5 wt. % range). As expected, glass compositions generally reflect dissolution and precipitation of olivine, but as described below, about half of the experiments also experienced minor crystallization of pyroxene.

Although no phases other than olivine and glass are present in the run products from the 1.0 GPa experiments, some of the glasses are elevated in SiO<sub>2</sub> and lower in CaO relative to experiments at both higher and lower pressure with similar MgO contents. This reflects different degrees of permeation into the sintered olivine by the melt and thus different ratios of MORB to the amount of olivine that it interacted with from experiment to experiment. The CaO content of the melt decreases on interaction with larger amounts of olivine because the as-loaded Kilbourne Hole olivine has much lower CaO (~0.08 wt. %) than olivine in equilibrium with the melt (~0.24 wt. %). Calculations using MELTS (Ghiorso and Sack 1995) also predict that increasing the mass of olivine that the melt interacts with will result in an increase in the SiO<sub>2</sub> content of the liquid. These effects were smaller at pressures above 1.0 GPa because the hot-pressing process was more effective (thereby allowing less permeation into the olivine aggregate by the MORB melt) and

absent in the 1-atm experiments (which used a single crystal of olivine as the capsule). We confirmed this interpretation by sintering an assembly at 1.5 GPa before running at high temperature at 1.0 GPa (rather than the normal procedure of sintering at ~1.0 GPa); the glass in this experiment had SiO<sub>2</sub> contents lower than the other 1.0 GPa experiments (48.9 and an average of 49.8 wt. % SiO<sub>2</sub>, respectively) and was comparable to the one-atm experiments.

Incompatible minor elements, specifically TiO<sub>2</sub>, K<sub>2</sub>O and P<sub>2</sub>O<sub>5</sub>, show slight, albeit scattered, increases with increasing temperature and pressure, while SiO<sub>2</sub> decreases. It is well known that a basaltic melt with olivine on its low-pressure liquidus will achieve pyroxene saturation with increasing pressure. Thus, the experiments at 2.0, 2.5, and 3.0 GPa contained minor amounts of pyroxene in addition to olivine and melt (most were low-Ca, however Run 33 at 3.0 GPa contained both higher and low-Ca pyroxenes; both are described below). Based on mass balance calculations, the amounts of pyroxene in the capsules is < 0.5 wt. % at and below 2.5 GPa, increasing to as high as ~18 wt. % for one of the 3.0 GPa experiments. The crystallization of pyroxene in the highest pressure experiments resulted in decreases in the SiO<sub>2</sub> contents of the melts while simultaneously driving up the concentration of incompatible elements; thus, SiO<sub>2</sub> contents are as low as 45.40 and K<sub>2</sub>O is as high as 0.18 wt. % in the 3.0 GPa experiments. The decreases in SiO<sub>2</sub> and increases in K<sub>2</sub>O (and also TiO<sub>2</sub> and P<sub>2</sub>O<sub>5</sub>) in the higher-pressure experiments are quantitatively consistent with the results of our mass balance calculations described below. Consequently, we judge that despite these variations in melt composition, we achieved our objective of doing experiments at roughly constant melt composition over a significant range of pressure and temperature (i.e., these variations are small relative to the range from experiments in the literature. We will, however, include the effects of compositional variations in our

thermodynamic fits of the data, and are able to show that their expected effects on  $D_{Ni}^{ol/liq}$  are small compared to the systematic variation in  $D_{Ni}^{ol/liq}$  we have observed.

Olivine: Olivine compositions (see Table 3) show that olivine compositions are relatively constant for our experiments, as expected, based on the experimental design. Excluding Run 33R (Mg# = 88.1, Mg# = Mg/[Mg+Fe] atomic), which crystallized large amounts (18 wt. %) of pyroxene, the average Mg# of the near-melt olivines spans a narrow range, 89.6-90.3, encompassing the Mg# of the starting Kilbourne Hole olivine (90.1). In our high-pressure experiments, the CaO content of the olivines near the melt pool in the center of the experiment increases with pressure, from ~0.21 wt. % at 1.0 GPa to ~0.26 wt. % CaO at 3.0 GPa, qualitatively consistent with our inference that liquid interacts with a progressively smaller volumes of low-Ca olivine because sintering at higher pressure minimizes permeation of the olivine aggregate by the melt. Al<sub>2</sub>O<sub>3</sub> in olivines adjacent to melt increases from 0.04 wt. % at 1 atm to 0.15 wt. % Al<sub>2</sub>O<sub>3</sub> at 3.0 GPa. The Al<sub>2</sub>O<sub>3</sub> olivine-liquid partition coefficient increases with increasing pressure and temperature for our experiments with values that agree well with the model of Agee and Walker (1990).

Pyroxene: Low-Ca pyroxene (1.3-2.3 wt. % CaO) is touching the central melt pool in five of 13 experiments and a higher Ca-pyroxene (6.8 wt. % CaO) in one of these five (#33R); these occurrences are listed in Table 2 and pyroxene compositions are listed in Table 3. The SiO<sub>2</sub> contents of the low-Ca pyroxenes are higher than the glasses, spanning a narrow range from 54-56 wt. % (which is why the SiO<sub>2</sub> contents of glasses from the pyroxene-bearing experiments are lower than those in the pyroxene-absent experiments). The CaO concentration in the low-Ca pyroxenes increase with temperature (e.g., Davidson et al. 1982; Lindsley et al. 1981), going from ~1.3 wt. % at 1500°C to ~2.3 wt. % at 1550°C. The Na<sub>2</sub>O contents (of the low-Ca pyroxene) increase from 0.1 to 0.3 wt. % with temperature and pressure in our experiments. Overall, the compositions of

low-Ca pyroxene from our experiments are similar to those produced in the experiments of Hesse and Grove (2003) and Walter (1998). The higher Ca-pyroxene has a similar SiO<sub>2</sub> and a slightly lower MgO content than the low-Ca pyroxenes (53.7 and 30.0, respectively); overall its composition is very similar to the experimentally-produced pyroxenes of Yaxley (2000) and Salters et al. (2002).

### *Mass Balance*

As we have briefly highlighted above, high-pressure experiments run in graphite-only or Pt-C double capsules can lose substantial amounts of Ni on timescales that are short relative to typical experimental run-times. The loss of Ni is not limited to experiments with this particular configuration: Hart and Davis (1978) argued that loss of Ni from their samples to the supporting Pt loop could result in anomalously high  $D_{Ni}^{ol/liq}$ s: i.e., Ni is lost much faster from the liquid than the olivine because the diffusivity of Ni in silicate liquid is higher than that of olivine, and this can result in anomalously high  $D_{Ni}^{ol/liq}$ s relative to equilibrium values in what can appear to be fully equilibrated experiments. To overcome this issue Hart and Davis (1978) added additional Ni to their bulk starting material and showed that their experiments were run long enough for the olivine-liquid-loop system to reach equilibrium. Using this same approach (doping the bulk with significant amounts of Ni) in high-pressure experiments is problematic because (1) Pt-C double capsule experiments have a much higher Pt-to-sample ratio (i.e., extremely large quantities of Ni would need to be added to the starting material to saturate the Pt with Ni), and (2) the ultimate sink of Ni in the C-only capsule experiments is presently unknown. As mentioned above, our charges are experiencing time-dependent Ni loss while at high temperature, thus, we need to pay particular attention to the mass balance results of our experiments to gauge whether or not our experimental

setup was successful in limiting the Ni loss of the system to the olivine adjacent to the C capsule, thereby allowing the liquid and olivines in the center of the capsule to approach equilibrium.

The phase proportions in our experiments were determined using the non-linear approach of Albarède and Provost (1977), but the variable amount of interaction between melt and olivine from one experiment to the next requires an atypical approach to such mass balance calculations. We allowed the starting bulk composition to vary as a linear mixture of our starting materials, homogenized Juan de Fuca basalt glass and powdered Kilbourne Hole olivine. The NiO of the bulk for each experiment was allowed to vary (in addition to the Na<sub>2</sub>O of the bulk for one-atmosphere experiments; additional details are in the supplementary material). Results of the mass-balance calculation including phase proportions of glass, olivine, and pyroxene, percent Ni loss (and Na, when appropriate), and a goodness of fit value, Q, are given in Table 2. All experiments have mass balance solutions acceptable at the 95% confidence level (Press et al. 1992), suggesting that the variations in liquid composition, discussed above, is well explained by the simple presence of the phases listed in Table 3. Moreover, the overall results of these calculations are consistent with our observations of experimental run products: as pressure and temperature increase, compaction of the surrounding olivine powder becomes more complete and the liquid interacts with a smaller mass of olivine; in our photomicrographs this is evident by fewer and smaller melt pockets away from the center of the charge, and our mass-balance calculations output in a higher melt fraction.

The calculated change in the bulk NiO is listed for each experiment in Table 2; forward experiments were successful at conserving NiO—changes range from -16 to 2% relative (where a negative number indicates a decrease of NiO). This suggests that, although the outer ~100 μm rind of olivine that was closest to the graphite capsule in high pressure experiments lost Ni, our

experimental setup was largely successful in mitigating the loss of Ni from the central region of the capsule. Our mass-balance calculations also suggest that our high-pressure reversal experiments have gained 11-57% NiO. A possible reason for this apparent gain is that only compositions of near-liquid olivines, which gained significant NiO from the starting glass (the initial glass used in the reversal experiments has ~1 wt. % NiO), were entered into the calculation, giving our “system” an artificially high NiO content. In other words, the “system”, according to the mass balance calculation, likely involved olivine farther away from the central melt pool and this olivine did not experience the same level of Ni-enrichment as those close to the melt. Meanwhile, our calculation asks how much NiO it would take to enrich all of the olivines in the system to the NiO content measured for the near-melt olivine. This is an unrealistic demand, because we expect the NiO from the high-NiO glass to slowly diffuse away from the central melt pool. Improving the accuracy of the mass balance calculation for the reversal experiments would probably require mapping the olivine aggregate to obtain the true NiO contents and distribution of post-experiment “system” rather than simply measuring the near-liquid olivines.

#### *Attainment of Equilibrium*

To demonstrate that our experiments approached equilibrium  $D_{Ni}^{ol/liq}$  values, we conducted both time-series and reversal experiments. Time invariance is a necessary though insufficient condition for establishing equilibrium. We conducted a time series at 1.0 GPa and 1450°C, running experiments for 6, 12, and 18 hours. The partition coefficients from these experiments, shown in Fig. 1, range from 4.31 to 4.66 and overlap at  $1\sigma$ , suggesting that, for these run durations,  $D_{Ni}^{ol/liq}$  is not changing appreciably. As described above, we also performed reversal experiments. In a forward experiment (black symbols in Fig. 1), the starting glass chip had very low NiO (below

detection limit of 0.03 wt. %); i.e., at the start of the forward experiment the instantaneous  $D_{Ni}^{ol/liq}$  of the experiment was very high; over the course of the experiment, there was a net migration of Ni from the olivine into the liquid, so that the glass had 0.07-0.10 wt. % NiO at the end of an experiment. In the reversal experiments (red symbols on Fig. 1), the initial glass had ~1 wt. % NiO, making the initial  $D_{Ni}^{ol/liq}$  lower than the equilibrium value; NiO moves from the melt into the olivine during these experiments, and the recovered glass has 0.11-0.42 wt. % NiO. We conducted a total of five reversals at four different pressures (1-atm, and 1.0, 2.0 and 3.0 GPa); in all cases the reversed experiments have  $D_{Ni}^{ol/liq}$ s that overlap at  $1\sigma$  with all of the forward experiments run at the same conditions. The successful reversal of our experiments, along with our time series, strongly suggest that the  $D_{Ni}^{ol/liq}$  values reported here do, indeed, represent equilibrium values.

Additionally, the results from the Re-capsule experiment give a  $D_{Ni}^{ol/liq}$  that is indistinguishable from a Pt-C experiment conducted at the same pressure and temperature ( $D_{Ni}^{ol/liq}$  values are  $4.38 \pm 0.15$  and  $4.35 \pm 0.17$ , respectively; errors are  $1\sigma$ , propagated from reported values in Table 3), suggesting that our results are also independent of capsule material.

Figure 1a shows the  $D_{Ni}^{ol/liq}$  results of all of our experiments vs. temperature. Overall, Fig. 1a shows that the measured  $D_{Ni}^{ol/liq}$  decreases with increasing temperature and pressure for our experiments, decreasing from 5.0 at 1 atm (1400°C) to 3.7 at 3 GPa (1550°C). Correlation with either temperature or pressure is good, with  $R^2=0.72$ . Comparisons of our results with models from the literature for predicting  $D_{Ni}^{ol/liq}$  are described in more detail below, but Fig. 1b shows that none of the available models for predicting  $D_{Ni}^{ol/liq}$  accurately predict the results of our experiments: some predict smaller and some predict larger variations with temperature (and pressure) than our results (and some predict none at all). In the following sections, we explore the

relative contributions of temperature, pressure, and phase composition to the systematic variation of  $D_{Ni}^{ol/liq}$ .

## DISCUSSION

### *Possible Contributions of Melt Compositional Variations in our Experiments to the Observed Temperature and Pressure Dependence of $D_{Ni}^{ol/liq}$*

The salient feature of our experimental results is that for liquids of approximately constant composition (and especially MgO content), the partition coefficient decreases with increasing temperature and pressure, from 5.0 at 1 atm (1400°C) to 3.8 at 3 GPa (1550°C). The first issue we address is whether the small variations in melt composition in our experiments could contribute significantly to this decrease in  $D_{Ni}^{ol/liq}$ .

The stabilization of pyroxene at high pressures leads to a correlation between the observed partition coefficient and the SiO<sub>2</sub>, TiO<sub>2</sub>, K<sub>2</sub>O, and P<sub>2</sub>O<sub>5</sub> contents of the quenched liquid (i.e., as mentioned above, the stabilization of pyroxene simultaneously decreases the SiO<sub>2</sub> contents of the liquid while increasing the concentration of incompatible elements). Below we formulate expressions that describe the  $D_{Ni}^{ol/liq}$  as a function of the MgO and SiO<sub>2</sub> contents of the liquid; we then use these expressions to argue that the small variations of the MgO and SiO<sub>2</sub> contents of the liquid in our experiments have a much smaller effect on  $D_{Ni}^{ol/liq}$  than P and T. Before developing these models, however, there are a few observations we can make that also give us insight into the variables that control  $D_{Ni}^{ol/liq}$  in our experiments.

(1) Although there is a range in melt composition in our experiments, there is *not* a statistically significant correlation between  $D_{Ni}^{ol/liq}$  and the MgO content of the liquid, the variable

most widely used to describe variations of  $D_{Ni}^{ol/liq}$  (e.g., Hart and Davis 1978; Kinzler et al. 1990).

For example, glasses in Runs 25 (1-atm) and 30 (3.0 GPa) have essentially identical MgO contents (18.1 and 18.3 wt. %), yet the MgO-based models of Hart and Davis (1978) and Kinzler et al. (1990) predict a  $D_{Ni}^{ol/liq}$  that differs by only 0.1 for these two experiments, while the observed difference is 1.2.

(2) Glasses from the 1.0 GPa experiments showed a range in SiO<sub>2</sub> contents (48.9-50.2) over a narrow range of MgO contents (17.4-17.7) due to interaction with an increased volume of olivine (see above), yet they do not show a systematic variation in  $D_{Ni}^{ol/liq}$  with SiO<sub>2</sub> content.

(3) As mentioned above, pyroxene crystallization resulted in increases in the concentrations of incompatible elements in the highest-pressure experiments. However, the absolute increases for these incompatible elements is small (~0.6 wt. % for TiO<sub>2</sub> and ~0.07 wt. % for K<sub>2</sub>O and P<sub>2</sub>O<sub>5</sub>), making it unlikely that they are responsible for the large changes of  $D_{Ni}^{ol/liq}$  measured in our experiments.

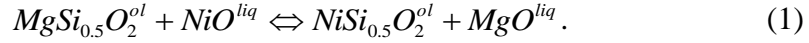
We conclude that although there are variations in melt composition in our experiments, these do not contribute significantly to the observed systematic decrease in  $D_{Ni}^{ol/liq}$  with increasing temperature and pressure. As mentioned above, we will demonstrate below the consistency of this conclusion with fits of our data and the data in the literature (which span a much larger range of melt composition) to thermodynamic functional forms that incorporate the effects of SiO<sub>2</sub> and MgO contents of liquids on  $D_{Ni}^{ol/liq}$ .

### *Fitting $D_{Ni}^{ol/liq}$ : Previous Partitioning Expressions*

As emphasized in the Introduction, knowing how temperature, pressure, and composition affect  $D_{Ni}^{ol/liq}$  is crucial for petrogenetic modeling; Fig. 1b compares our  $D_{Ni}^{ol/liq}$  measurements with various published models used for calculating  $D_{Ni}^{ol/liq}$ . Unsurprisingly, those models that attribute variations in  $D_{Ni}^{ol/liq}$  to olivine and liquid composition alone (Beattie et al. 1991; Hart and Davis 1978; Kinzler et al. 1990) predict essentially no change in  $D_{Ni}^{ol/liq}$  for our experiments (i.e., the melt and olivine compositions in our experiments are essentially constant) and therefore do a poor job explaining our data. On the other hand, models that attribute changes in  $D_{Ni}^{ol/liq}$  solely to temperature (Arndt 1977; Hart and Davis 1978; Kelemen et al. 1998) overpredict the temperature dependence (i.e., the predicted slope on  $D_{Ni}^{ol/liq}$  vs.  $T$  plot is more negative than in our data). As we show below, thermodynamic models suggest that both  $T$  and composition should affect  $D_{Ni}^{ol/liq}$ , thus it is not surprising that attributing changes to one or the other alone leads to models that over- or under-predict the actual variation in  $D_{Ni}^{ol/liq}$  under certain circumstances. The thermodynamically-inspired empirical fits of Li and Ripley (2010) and Putirka (2011) also overpredict the dependence of  $D_{Ni}^{ol/liq}$  vs.  $T$  for our experiments. The TEX model of Colson et al. (1988) and the MELTS thermodynamic model (Ghiorso and Sack 1995; Smith and Asimow 2005) are best at reproducing the temperature dependence of our data although the predicted  $D_{Ni}^{ol/liq}$  values are systematically high (by ~10% at 1400 and ~30% at 1550°C). In the following sections, we show that two relatively simple thermodynamic treatments can successfully describe both our data and those from the literature.

*Fitting  $D_{Ni}^{ol/liq}$  : Ideal Exchange Reaction*

We first fit our  $D_{Ni}^{ol/liq}$  data to an Ni-Mg exchange reaction (e.g., Hart and Davis 1978; Kinzler et al. 1990; Watson 1977):



Writing the equilibrium constant for reaction (1) yields

$$\Delta_{r(1)}G_{T,P}^{\circ} = -RT \ln \left( \frac{X_{NiSi_{0.5}O_2}^{ol} X_{MgO}^{liq}}{X_{MgSi_{0.5}O_2}^{ol} X_{NiO}^{liq}} \times \frac{\gamma_{NiSi_{0.5}O_2}^{ol} \gamma_{MgO}^{liq}}{\gamma_{MgSi_{0.5}O_2}^{ol} \gamma_{NiO}^{liq}} \right), \quad (2)$$

where  $\Delta_{r(1)}G_{T,P}^{\circ}$  is the standard-state Gibbs free energy change at the pressure and temperature of reaction 1, and  $X_i^{\phi}$  and  $\gamma_i^{\phi}$  are the mole fraction and activity coefficient of the  $i^{\text{th}}$  component in phase  $\phi$  (the selected molar components are defined in the notes to Table 3). We can write out the explicit dependence of  $\Delta_{r(1)}G_{T,P}^{\circ}$  on temperature and pressure:

$$\Delta_{r(1)}G_{T,P}^{\circ} = \Delta_{r(1)}H_{T_{ref},P_{ref}}^{\circ} + \int_{T_{ref}}^T \Delta_{r(1)}C_p^{\circ} dT - T \left( \int_{T_{ref}}^T \left( \frac{\Delta_{r(1)}C_p^{\circ}}{T} \right) dT + \Delta_{r(1)}S_{T_{ref},P_{ref}}^{\circ} \right) + \int_{P_{ref}}^P \Delta_{r(1)}V dP, \quad (3)$$

where  $\Delta_{r(1)}H_{T_{ref},P_{ref}}^{\circ}$  and  $\Delta_{r(1)}S_{T_{ref},P_{ref}}^{\circ}$  are the enthalpy and entropy changes of the reaction at the reference pressure,  $P_{ref}$ , and temperature,  $T_{ref}$ ,  $\Delta_{r(1)}C_p^{\circ}$  is the temperature-dependent, isobaric change in heat capacity of the reaction at  $P_{ref}$ , and  $\Delta_{r(1)}V$  is the temperature- and pressure-dependent volume change of the reaction at temperature and pressure, and the volume integral is taken along a constant temperature path at T. If we define the molar partition coefficient as

$$D_{Ni}^{molar} = X_{NiSi_{0.5}O_2}^{ol} / X_{NiO}^{liq} \text{ and combine Equations 2 and 3, we obtain}$$

$$\begin{aligned}
& -\frac{\Delta_{r(1)}H_{T_{ref},P_{ref}}^{\circ}}{RT} + \frac{\Delta_{r(1)}S_{T_{ref},P_{ref}}^{\circ}}{R} = \ln(D_{Ni}^{molar}) + \ln\left(\frac{X_{MgO}^{liq}}{X_{MgSi_0.5O_2}^{ol}}\right) + \ln\left(\frac{\gamma_{NiSi_0.5O_2}^{ol}\gamma_{MgO}^{liq}}{\gamma_{MgSi_0.5O_2}^{ol}\gamma_{NiO}^{liq}}\right) \\
& + \frac{\int_{T_{ref}}^T \Delta_{r(1)}C_p^{\circ} dT}{RT} - \frac{\int_{T_{ref}}^T \left(\Delta_{r(1)}C_p^{\circ}/T\right) dT}{R} + \frac{\int_{P_{ref}}^P \Delta_{r(1)}V dP}{RT}
\end{aligned} \quad (4)$$

Equation 4 is general, but it is usually simplified by various plausible and/or expedient assumptions. In particular, for exchange reactions such as reaction 1, it is usually assumed that  $\Delta_{r(1)}C_p^{\circ}$  and  $\Delta_{r(1)}V$  are small enough to be negligible. However, for the components in reaction 1, we have sufficient thermodynamic data to test this assumption. Specifically, the heat capacity of the olivines were taken from Berman (1988) and Hirschmann (1991), and constants were used for the heat capacity of the liquids (Chase 1998). To calculate the change in volume of reaction 1 we used expressions for the volume of forsterite from Berman and Aranovich (1996); following Hirschmann (1991), we fit the Ni-olivine data of Vokurka and Rieder (1987) to obtain the reference volume and thermal expansion coefficients, and took the compressibility from Bass et al. (1984). Liquids were modeled as stoichiometric olivine liquids (i.e.,  $NiSi_{0.5}O_2$ ) using a 3<sup>rd</sup>-order Birch-Murnaghan equation of state with a K' of five, assuming ideal volumes of mixing. For forsterite liquid, the reference volume and compressibility were taken from Ai and Lange (2008) and the thermal expansivity from Ghiorso (2004). Due to the absence of data on Ni-olivine liquid, we, like Hirschmann and Ghiorso (1994), used data for fayalite liquid; specifically, compressibility from Chen et al. (2002) and thermal expansivity from Ghiorso (2004). The reference volume for Ni-olivine liquid was set such that the volume change on melting (defined as  $\Delta_{me}V_t/V_{s,ol}$  at 1 bar), at the melting temperature, was 10%, similar to that of fayalite (9.9%) and forsterite (9.2%). For our experiments (choosing a reference temperature of 1662K),  $\Delta_{r(1)}C_p^{\circ}$  and  $\Delta_{r(1)}V$  are small

enough to be negligible: the sum of the final three terms (those involving  $\Delta_{r(1)}C_p^\circ$  and  $\Delta_{r(1)}V$ ) of Equation 4 ( $-1 \times 10^{-4}$  to  $5 \times 10^{-3}$ ) is an order of magnitude smaller than the errors on the sum of the

compositional terms  $\left[ \ln(D_{Ni}^{molar}) + \ln\left(\frac{X_{MgO}^{liq}}{X_{MgSi_2O_6}^{ol}}\right) \right]$  of the equation ( $3 \times 10^{-2}$  to  $9 \times 10^{-2}$ ). Thus for

reaction 1 we can safely approximate  $\Delta_{r(1)}C_p^\circ$  and  $\Delta_{r(1)}V$  as zero.

Additionally, a useful starting point for understanding compositional effects is to assume that the activity coefficients are all unity [or, equivalently in this case, that they are not unity but do cancel in Equation (4)]. Equation 4 then simplifies to

$$-\frac{\Delta_{r(1)}H_{T_{ref},P_{ref}}^\circ}{RT} + \frac{\Delta_{r(1)}S_{T_{ref},P_{ref}}^\circ}{R} = \ln(D_{Ni}^{molar}) + \ln\left(\frac{X_{MgO}^{liq}}{X_{MgSi_2O_6}^{ol}}\right). \quad (5)$$

Terms on the right hand side of Equation 5 can all be obtained from phase compositions in an experiment, so  $\Delta_{r(1)}H_{T_{ref},P_{ref}}^\circ$  and  $\Delta_{r(1)}S_{T_{ref},P_{ref}}^\circ$  are the only unknowns which, based on our stated assumptions, are independent of pressure and temperature. Equation 5 is a natural starting point for the fitting of experimentally determined Ni partitioning data (e.g., Hart and Davis 1978; Kinzler et al. 1990; Watson 1977) but even in this simplified version,  $D_{Ni}^{molar}$  depends on both temperature (provided  $\Delta_{r(1)}H_{T_{ref},P_{ref}}^\circ \neq 0$ ) and composition; for example,  $D_{Ni}^{molar}$  will decrease with increasing MgO content of the melt and increase with increasing forsterite content of the olivine (e.g., Hart and Davis 1978; Kinzler et al. 1990). Note that the form of Equation 5 is the same if the phases are Henrian but that the constant on the left hand side of the equation would then also include the activity coefficient terms. Below, the approximation of ideality will be relaxed by replacing mole fractions with more complex expressions for activities.

By design, phases from our experiments vary little in composition (particularly in the MgO content of the melt and the forsterite content of the coexisting olivine), and thus they provide direct constraints on  $\Delta_{r(1)}H_{T_{ref},P_{ref}}^{\circ}$  and  $\Delta_{r(1)}S_{T_{ref},P_{ref}}^{\circ}$ , assuming that the activity coefficients are not strong functions of temperature (e.g., Holzheid et al. 1997) or pressure, and that the resulting variations in the ratio of activity coefficients is small. We fit our data to Equation 5; the resulting values of

$$-\frac{\Delta_{r(1)}H_{T_{ref},P_{ref}}^{\circ}}{R} \text{ and } \frac{\Delta_{r(1)}S_{T_{ref},P_{ref}}^{\circ}}{R}$$

are 4380 K and -2.023, respectively (fits are shown graphically in Fig. 2 are listed in Table 4).

This fit does a good job describing our experiments: i.e., when the fit to the new data, presented here, is used to predict the  $D_{Ni}^{ol/liq}$  of each experiment, the average percent error is 4%, which is comparable to the analytical error of 5% from each experiment.

Our experiments were designed to isolate contributions of temperature and pressure to variations in  $D_{Ni}^{ol/liq}$  from those of phase compositions. Our experiments are, therefore, poorly posed to address the compositional dependences, and it is therefore necessary to utilize literature data to sort out the contribution of compositional variations to  $D_{Ni}^{ol/liq}$ . We constructed two datasets from the literature for the purpose of establishing the relationships between melt composition and  $D_{Ni}^{ol/liq}$ . In the first of these, we accepted our 13 experiments plus 312 experiments (from a literature database of 434 experiments; references for all experimental results in this database are listed in the supplemental information), whose glass and olivine analytical totals both fall in the range 98.5-101.5%. In our initial fits we noticed that some experiments from Leeman (1974) exhibited particularly large residuals, specifically those experiments with less than 0.05 wt. % NiO in the liquid; we excluded these experiments from all further consideration under the assumption that the low NiO content of the liquid and the analytical procedure combined to

produce a large uncertainty in the resulting  $D_{Ni}^{ol/liq}$ . We refer to this dataset, filtered primarily by analytical totals, as Filter-A. We also developed a more restrictive dataset, Filter-B, and the procedures for this are described in the following paragraph.

As we have emphasized above, experiments that experience a net loss of Ni may result in anomalously high  $D_{Ni}^{ol/liq}$  that appear to be in equilibrium (Hart and Davis 1978). In an attempt to filter out disequilibrium  $D_{Ni}^{ol/liq}$  due to such effects, we mass balanced all available olivine-liquid Ni partitioning experiments. Of the 312 experiments from the Filter-A dataset, 274 report enough information to be successfully mass balanced, and 197 of these experiments have mass balance solutions acceptable at the 95% confidence level. The details of the mass balance are given in the supplemental information; however, like the mass balance calculation for our experiments, the NiO content of the bulk was allowed to vary, giving us a quantitative measure of the amount of Ni lost (or gained) from the system; some of these successfully mass-balanced experiments have either gained or lost a large percentage (up to 91 and 96%, respectively) of their original NiO. However, an experiment losing a large percentage of its original NiO content does not mean it is necessarily a failed experiment; for example, Hart and Davis (1978) added extra NiO to their experiments (knowing that much of it would ultimately end up in the supporting Pt loop) and demonstrated that their run times were sufficient for Ni in the olivine, the Pt loop, and liquid to reach equilibrium (runs that gained significant NiO were typically either uncertain about the amount of NiO added to the bulk [e.g., “1-3 wt. %”; Takahashi (1978)] or run on Ni wire loops). Our Filter-B dataset includes those experiments that we are reasonably confident have reached equilibrium; namely those that have successfully mass balanced *and* show only moderate Ni-loss or gain (less than 65%, relative) *or* have explicitly experimentally demonstrated that  $D_{Ni}^{ol/liq}$  has reached equilibrium despite of large amounts of Ni loss (Arndt 1977; Campbell 1979; Drake and Holloway 1981; Hart

and Davis 1978; Kinzler et al. 1990; experiments from Leeman 1974 run above 1300°C and >144 hrs; Mysen 2007; Mysen 2006; Nabelek 1980; Seifert et al. 1988; Snyder and Carmichael 1992; experiments from Takahashi 1978 run above 1320°C and >15 hrs). See the supplemental information for details on construction of the Filter-B dataset. Of the 197 experiments from the literature with satisfactory mass balance solutions, 155 of them have lost or gained less than 65% of their initial NiO or demonstrated equilibrium in spite of large amounts of Ni loss and are included, along with the new work presented here, in the Filter-B dataset. The formulation of the Filter-B dataset began with only those experiments that passed the Filter-A dataset; therefore, by construction, all of the experiments in the Filter-B dataset are also in the Filter-A set. Although some olivines have high Ni-contents (the Filter-A database has olivines with up to 31.6 wt. % NiO), we ignored possible non-Henrian behavior (see Beattie 1993b for a discussion). The new work presented here also passes both the filters and is included in fits to the respective datasets.

The fits, using Equation 5, to the Filter-A and -B datasets are shown graphically in Fig. 2 and listed in Table 4; also listed in Table 4 are the average percent error between the predicted and measured  $D_{Ni}^{ol/liq}$ . Figure 2 shows that the fits for our experiments and both the Filter-A and -B datasets are very similar; the Fits to the Filter-A and -B datasets are essentially indistinguishable on

Fig. 2, and  $-\frac{\Delta_{r(1)}H_{T_{ref}, P_{ref}}^{\circ}}{R}$  and  $\frac{\Delta_{r(1)}S_{T_{ref}, P_{ref}}^{\circ}}{R}$  for all three fits overlap at one standard error. It is

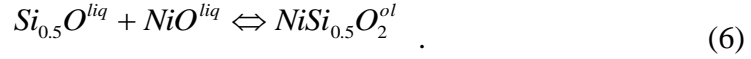
important to note that, although small, these datasets span an extremely wide range of composition: SiO<sub>2</sub> and MgO in the liquid range from 34-70 and 3-40 wt. % for the Filter-A dataset while the Filter-B dataset spans a similar range, 40-69 and 4-38 wt. % SiO<sub>2</sub> and MgO, respectively. The olivines from each dataset span an identical range, with Mg#s from 36 to 100. It should be noted that although not easily visible on Fig. 2, the Filter-A dataset has more scatter: the mean residual for the fit to the Filter-A dataset is ~2.5 times larger than the residuals of the fit to the Filter-B

dataset. A corollary of the increased scatter on Fig. 2 is that the mean percent error on  $D_{Ni}^{ol/liq}$  is larger for the Filter-A dataset (mean percent errors are 14 and 12% for the Filter-A and Filter-B datasets, respectively). Due to the similarity of the fit parameters, both datasets predict  $D_{Ni}^{ol/liq}$  from our experiments equally well: average error on  $D_{Ni}^{ol/liq}$  is 6.0%, only slightly larger than the fit to our data alone (3.9%).

Due to the similarity of the fits to data from the literature and the new work presented here, one might then ask whether our experiments that isolate the pressure-temperature effect cleanly from the compositional effect were even necessary; that is, simply taking the data from the literature and fitting them to the simple model described above results in a fit temperature dependence that is essentially identical to that derived from our experiments. However, the literature data it spans a very wide compositional range, and without the independent determination of the temperature dependence in the absence of such extreme compositional variation, it is unlikely that one could be confident in the reliability of the ideal corrections for composition and the inferred temperature dependence. Moreover, there is considerable scatter in the literature data, and although it would be difficult to avoid the conclusion that there is a non-negligible temperature dependence of the reaction, confidently constraining its value would be difficult. In other words, and as emphasized in the Introduction, without an independent constraint on the temperature dependence, errors in a compositional-dependence term can be readily offset by a compensating error in the temperature-dependence term, making it very difficult to isolate or quantify their effects. This is well illustrated in Fig. 1b, which demonstrates that previous efforts to quantify  $D_{Ni}^{ol/liq}$  in terms of temperature are inconsistent with our experiments. Our experiments allow confident resolution of this tradeoff and, as shown in Fig. 2, allow the full database currently available to be accounted for by what is, in effect, the simplest possible thermodynamic treatment.

*Fitting  $D_{Ni}^{ol/liq}$  : Ideal Formation Reaction*

In addition to working with the exchange reaction of Equation 1, we also fit our data together with those of the literature to an olivine-formation reaction



Writing an equilibrium constant expression for the reaction, defining the molar partition coefficient as above, and rearranging yields

$$\begin{aligned} -\frac{\Delta_{r(6)}H_{T_{ref},P_{ref}}^{\circ}}{RT} + \frac{\Delta_{r(6)}S_{T_{ref},P_{ref}}^{\circ}}{R} = \ln(D_{Ni}^{molar}) + \ln\left(\frac{1}{X_{Si_{0.5}O}^{liq}}\right) + \ln\left(\frac{\gamma_{NiSi_{0.5}O_2}^{ol}}{\gamma_{NiO}^{liq}\gamma_{Si_{0.5}O}^{liq}}\right) + \\ \frac{\int_{P_{ref}}^P \Delta_{r(6)}VdP}{RT} + \frac{\int_{T_{ref}}^T \Delta_{r(6)}C_p^{\circ}dT}{RT} - \frac{\int_{T_{ref}}^T \left(\frac{\Delta_{r(6)}C_p^{\circ}}{T}\right)dT}{R} \end{aligned} \quad (7)$$

Unlike the exchange reaction, for the Ni-olivine formation reaction  $\Delta_r C_p$  and  $\Delta_r V$  are not necessarily close to zero; the right-hand side of Equation 6 has only solid components, while the left-hand side has only liquid components. Choosing a relatively high reference temperature (1662K) reduces relative contributions from the heat capacity to differences in  $D_{Ni}^{ol/liq}$ ; however, the change in volume of this reaction is significant. For the experiments presented here, the

calculated  $\frac{\int_{P_{ref}}^P \Delta_{r(6)}VdP}{RT}$  ranges from zero (1-atm) to ~10% of  $\left[ \ln(D_{Ni}^{molar}) + \ln\left(\frac{1}{X_{Si_{0.5}O}^{liq}}\right) \right]$  (3.0 GPa).

Moreover, temperature and pressure are correlated for the larger experimental database; a failure to account for the change in volume of reaction 6 will lead to an incorrect value for  $\Delta_{r(6)}H_{T_{ref},P_{ref}}^{\circ}$ .

This is illustrated in Fig. 3 by the disagreement between our data and a fit to the Filter-A dataset (using Equation 7, assuming ideal behavior), that assumes  $\Delta_{r(6)}V$  of reaction 6 is zero. Calculating  $\Delta_{r(6)}V$  and re-fitting the data brings the larger experimental database and the new experiments presented here into agreement. Also shown on Fig. 3 are the predictions of equation 2b of Putirka et al. (2011) and equation 4 from Li and Ripley (2010), both of which use a similar functional form to our Equation 7. The disagreement between our data and their predictions may be due, in part, to the large standard state volume change of the formation reaction (Equation 6) which they did not attempt to correct for.

We fit both the Filter-A and Filter-B datasets using Equation 7, assuming ideal behavior. The fitted values for  $\Delta_{r(6)}H_{T_{ref}, P_{ref}}^{\circ}$  and  $\Delta_{r(6)}S_{T_{ref}, P_{ref}}^{\circ}$  as well as the average percent error of  $D_{Ni}^{o/liq}$  are listed in Table 4. Fits using the formation reaction (Equation 6) have larger average errors on  $D_{Ni}^{o/liq}$  than fits to the exchange reaction; this is true for the compilation of literature data (e.g., 17.5% vs. 13.9% avg. error on  $D_{Ni}^{o/liq}$  for the Filter-A dataset) as well as the new work presented here (8.2 and 6.0% avg. error on  $D_{Ni}^{o/liq}$  using the Filter-A fits to reproduce our experiments). As shown above, the formation reaction has non-zero  $\Delta_{r(6)}C_p^{\circ}$  and  $\Delta_{r(6)}V$ ; it is possible that the assumptions we made regarding the physical properties of the components of the reaction (specifically liquid NiO) are responsible for some of the misfit. However, the (relative) inability of the fits to the formation reaction to predict experimental results is likely due to the fact that the formation reaction is much more sensitive to changes in liquid chemistry. Previous work has demonstrated that the activity coefficients of liquid components are often correlated, effectively making ratios of activity coefficients approximately constant (e.g., O'Neill and Berry 2006). A formation reaction involves a product of activity coefficients of dissimilar components in the melt

(see Equation 7) whereas an exchange reaction involves a ratio of similar components (see Equation 4). Thus, it is not surprising that the fits to the exchange reaction are better than the fits to the formation reaction (assuming ideal behavior and the same number of fit parameters).

### *Fitting $D_{Ni}^{ol/liq}$ : Regular Solution Model*

The fits described in the previous section rely on the assumption of ideality. This is a sound first-order assumption for the olivines at high temperatures (e.g., Campbell and Roeder 1968; Nafziger and Muan 1967); for liquids, the assumption is much less likely to hold, particularly over the large compositional range represented by the database on Ni partitioning in olivine. In this section, we depart from a strict thermodynamic treatment of the data by adding simplified regular-solution-like terms to our model to explore the role of liquid composition in the observed variations in  $D_{Ni}^{ol/liq}$ ; the existing experimental database is not well posed for a full regular-solution treatment (e.g., Kinzler et al. 1990). While not thermodynamically rigorous, this approach nominally accounts simultaneously for the effects of MgO and SiO<sub>2</sub> in the melt, and it is important that we evaluate whether the small but non-negligible variations in MgO and SiO<sub>2</sub> contents of the melts in our experiments contribute to the observed variations in  $D_{Ni}^{ol/liq}$  in our experiments.

Using Equation 10 from Ghiorso et al. (1983) we can formulate expressions for the activity coefficients of liquid NiO, MgO, and Si<sub>0.5</sub>O in the Si<sub>0.5</sub>O-NiO-MgO ternary:

$$\begin{aligned}
 RT \ln \gamma_{MgO}^{liq} &= W_{Ni-Mg} X_{NiO}^{liq} (1 - X_{MgO}^{liq}) + W_{Mg-Si} X_{Si_{0.5}O}^{liq} (1 - X_{MgO}^{liq}) - W_{Ni-Si} X_{NiO}^{liq} X_{Si_{0.5}O}^{liq} \\
 RT \ln \gamma_{NiO}^{liq} &= W_{Ni-Mg} X_{MgO}^{liq} (1 - X_{NiO}^{liq}) + W_{Ni-Si} X_{Si_{0.5}O}^{liq} (1 - X_{NiO}^{liq}) - W_{Mg-Si} X_{MgO}^{liq} X_{Si_{0.5}O}^{liq} \\
 RT \ln \gamma_{Si_{0.5}O}^{liq} &= W_{Ni-Si} X_{NiO}^{liq} (1 - X_{Si_{0.5}O}^{liq}) + W_{Mg-Si} X_{MgO}^{liq} (1 - X_{Si_{0.5}O}^{liq}) - W_{Mg-Ni} X_{MgO}^{liq} X_{NiO}^{liq} . \quad (8)
 \end{aligned}$$

Although not thermodynamically rigorous, and without implying that these are the actual mixing species in the melt, we choose the  $\text{Si}_{0.5}\text{O}$ - $\text{NiO}$ - $\text{MgO}$  ternary because both Si (e.g., Li and Ripley 2010) and Mg (e.g., Hart and Davis 1978) are thought to influence Ni partitioning (also see the preceding discussion). Combining Equations 8 with both the exchange and formation reactions will make them both explicit functions of both the Mg and Si contents of the liquid. Substituting the expression for  $\gamma_{\text{NiO}}^{\text{liq}}$  and  $\gamma_{\text{MgO}}^{\text{liq}}$  into the exchange reaction (Equation 4) gives

$$\begin{aligned}
& -\frac{\Delta_{r(1)}H_{T_{\text{ref}},P_{\text{ref}}}^{\circ}}{RT} + \frac{\Delta_{r(1)}S_{T_{\text{ref}},P_{\text{ref}}}^{\circ}}{R} - \frac{W_{\text{Ni-Mg}}(X_{\text{NiO}}^{\text{liq}} - X_{\text{MgO}}^{\text{liq}})}{RT} - \frac{(W_{\text{Mg-Si}} - W_{\text{Si-Ni}})X_{\text{Si}_{0.5}\text{O}}^{\text{liq}}}{RT} = \ln(D_{\text{Ni}}^{\text{molar}}) \dots \\
& + \ln\left(\frac{X_{\text{MgO}}^{\text{liq}}}{X_{\text{MgSi}_{0.5}\text{O}_2}^{\text{ol}}}\right) + \frac{\int_{T_{\text{ref}}}^T \Delta_{r(1)}C_p^{\circ} dT}{RT} - \frac{\int_{T_{\text{ref}}}^T \left(\frac{\Delta_{r(1)}C_p^{\circ}}{T}\right) dT}{R} + \frac{\int_{P_{\text{ref}}}^P \Delta_{r(1)}V dP}{RT}
\end{aligned} \quad (9)$$

Similarly, substituting expressions for  $\gamma_{\text{NiO}}^{\text{liq}}$  and  $\gamma_{\text{Si}_{0.5}\text{O}}^{\text{liq}}$  into the formation reaction (Equation 7) gives

$$\begin{aligned}
& -\frac{\Delta_{r(6)}H_{T_{\text{ref}},P_{\text{ref}}}^{\circ}}{RT} + \frac{\Delta_{r(6)}S_{T_{\text{ref}},P_{\text{ref}}}^{\circ}}{R} = \ln(D_{\text{Ni}}^{\text{molar}}) + \ln\left(\frac{1}{X_{\text{Si}_{0.5}\text{O}}^{\text{liq}}}\right) + \frac{\int_{P_{\text{ref}}}^P \Delta_{r(6)}V dP}{RT} + \frac{\int_{T_{\text{ref}}}^T \Delta_{r(6)}C_p^{\circ} dT}{RT} \\
& - \frac{\int_{T_{\text{ref}}}^T \left(\frac{\Delta_{r(6)}C_p^{\circ}}{T}\right) dT}{R} + \frac{W_{\text{Ni-Mg}}X_{\text{MgO}}^{\text{liq}}(2X_{\text{NiO}}^{\text{liq}} - 1)}{RT} + \frac{W_{\text{Si-Mg}}X_{\text{MgO}}^{\text{liq}}(2X_{\text{Si}_{0.5}\text{O}}^{\text{liq}} - 1)}{RT} \\
& + \frac{W_{\text{Ni-Si}}(X_{\text{NiO}}^{\text{liq}}(2X_{\text{Si}_{0.5}\text{O}}^{\text{liq}} - 1) - X_{\text{Si}_{0.5}\text{O}}^{\text{liq}})}{RT}
\end{aligned} \quad (10)$$

In order to be self-consistent, we used a non-linear least-squares algorithm (Levenberg-Marquardt implemented in MATLAB) to simultaneously solve for the standard-state enthalpy and entropy of both the exchange (Equation 9) and formation reactions (Equation 10), along with the three common interaction parameters listed above. When Equations 9 and 10 were fit

simultaneously, we also ensured that the fitted standard-state parameters for both reactions were self-consistent e.g.,

$$\Delta_{r(6)} H_{T_{ref}, P_{ref}}^{\circ} = \Delta_{r(1)} H_{T_{ref}, P_{ref}}^{\circ} + H_{T_{ref}, P_{ref}}^{\circ} (X_{MgSi_0.5O_2}^{ol}) - H_{T_{ref}, P_{ref}}^{\circ} (X_{MgO}^{liq}) - H_{T_{ref}, P_{ref}}^{\circ} (X_{NiO}^{liq}) .$$

Fitted values for both the Filter-A and Filter-B datasets are listed in Table 4. For the exchange reaction and the Filter-B dataset, adding three new fit parameters does not appreciably change the quality of the fit (mean percent errors increase from 12.0 to 12.3%). The quality of the fit to the formation reaction, using the Filter-B dataset, improves markedly; mean percent errors on  $D_{Ni}^{ol/liq}$  decrease from 15.6 to 10.9%. The same general trend holds true for the larger Filter-A dataset: the quality of the fit for the exchange reaction shows marginal improvement when using the regular-solution model (13.9 to 12.9 mean percent error on  $D_{Ni}^{ol/liq}$ , respectively), whereas the formation reaction shows significant improvement (17.5 to 13.0 mean percent error on  $D_{Ni}^{ol/liq}$ , respectively). These results illustrate why working with an exchange reaction in complex systems is generally preferable to using a formation reaction approach if the objective is to limit the effect of melt composition on predictions of partitioning. Thus, it is not surprising that the fits to the formation reaction improve greatly when modeling of non-ideal behavior is included.

Although the quality of the fit improves by adding non-ideal terms, our model is too simplistic; the residuals of our non-ideal models are correlated with liquid components and higher-order combinations thereof. We do not pursue a more complicated model because even if one could evaluate the constants for all interaction parameters for a 7-12 component liquid, it is quite unlikely that a regular solution can be applied over the broad composition ranges accessed by available experiments. Properly resolving the compositional dependence of  $D_{Ni}^{ol/liq}$  would require considerably more experimentation. Our experiments provide a step in this direction by better

differentiating between contributions to variations in  $D_{Ni}^{ol/liq}$  from phase composition and temperature + pressure. Nevertheless, even our simplistic treatments via Equations 9 and 10 make the exchange reaction an explicit function of the Si content of the liquid and the formation reaction an explicit function of the Mg content of the liquid. This is important as it allows us to test whether or not our variations in liquid composition are the likely cause of the variation in  $D_{Ni}^{ol/liq}$  that we observe in our experiments or if it is an inherent pressure-temperature effect.

To perform this test we compare the measured  $D_{Ni}^{ol/liq}$  from our experiments to the predicted partition coefficient for an olivine-liquid pair of constant composition taken up pressure and temperature (from 1400°C and 1-atm to 1550°C and 3.0 GPa). Figure 4 shows the predicted partition coefficient using the fits to Equations 9 and 10 and the Filter-A and Filter-B databases, along with the measured  $D_{Ni}^{ol/liq}$  from each experiment. Our experiments, which do vary slightly in composition, are in good agreement with the prediction for a constant composition olivine-liquid pair, suggesting that the effect of temperature and pressure, rather than that of composition, is the dominant driver of the observed variation in  $D_{Ni}^{ol/liq}$ . Additionally, we can get a sense of the magnitude of the compositional effect by comparing the predicted partition coefficient for a constant-composition olivine-liquid pair to the prediction using the measured phase compositions listed in Table 3. For example, our high-pressure experiments crystallized pyroxene, decreasing the SiO<sub>2</sub> and increasing the incompatible element content of the glass (see preceding sections for further details). When we compare the predicted partition coefficient for the measured phase compositions of Run 33R (45.40 and 16.31 wt. % SiO<sub>2</sub> and MgO in the glass, respectively) one model (exchange reaction and our regular-solution model fit to the Filter-B dataset) predicts a  $D_{Ni}^{ol/liq}$  of 4.39. This predicted value is close to the prediction using the composition of Run 25

(48.26 and 17.17 wt. % SiO<sub>2</sub> and MgO in the glass, respectively) taken to 3.0 GPa and 1550°C, where the same model predicts a  $D_{Ni}^{ol/liq}$  of 4.17. This small (0.22) difference in  $D_{Ni}^{ol/liq}$  is well within our typical errors, and, as we stated earlier, these calculations suggest that the small changes in liquid composition observed in our experiments cannot account for the drop in  $D_{Ni}^{ol/liq}$  from ~5.0 at 1 atm to ~3.8 at 3.0 GPa and 1550°C.

Finally, since temperature and pressure co-vary in our experiments, we cannot, at this point, definitively separate the relative effects of these two variables. However, as we hope we have illustrated above, the reaction used to model partitioning can affect the apparent behavior of the partition coefficient. For example, by describing the experimental variations of  $D_{Ni}^{ol/liq}$  using a reaction that has a small  $\Delta_r V$ , we are left with an expression that is not a strong function of pressure. Alternatively if one chooses to describe the experimental variations of  $D_{Ni}^{ol/liq}$  using a reaction that has a large  $\Delta_r V$ , the resulting expression will be strongly pressure dependent. We also note that for some petrological applications, it may not be critical to separate pressure and temperature, as these two variables often co-vary in a predictable manner in natural systems. The exchange reaction has the added benefit that a regular-solution model does not greatly improve the quality of the fits; this, combined with the assumption that  $\Delta_{r(1)} C_p^\circ$  and  $\Delta_{r(1)} V$  can be safely approximated as zero, makes the partitioning expression using the exchange reaction relatively easy to compute. Below, we will use our preferred partitioning expression, Equation 5, to model the generation of high-NiO olivines from Hawaii and from komatiites.

### *Comparison of Ni with Other Divalent Cations*

Although an in-depth discussion of the partitioning behavior of other cations between olivine and liquid is beyond the scope of this work, it is nevertheless useful to compare Ni-Mg exchange with Co-Mg, Mn-Mg, and Fe-Mg exchange. In particular, it is well known that  $K_{D,Fe^{2+}-Mg}$  for olivine-melt equilibrium,  $K_{D,Fe^{2+}-Mg} = (FeO/MgO)^{ol}/(FeO/MgO)^{liq}$ , is essentially independent of

temperature (e.g., Roeder and Emslie 1970), yet the key message of our experiments and our analysis of the literature data for Ni-Mg exchange is that the equivalent parameter,

$(NiO/MgO)^{ol}/(NiO/MgO)^{liq}$  decreases significantly with increasing temperature (e.g., Figure 2).

That Ni-Mg exchange is indeed different from  $Fe^{2+}$ -Mg exchange, and indeed from Co-Mg and Mn-Mg exchange, is illustrated clearly by the experimental results of Takahashi (1978) shown in

Figure 5. Equation 5 can be rewritten with Mn, Co, and Fe in the place of Ni. Just as we did in Figure 2 for Ni, we have plotted in Fig. 5, using only the data from Takahashi (1978),  $\ln(K_D) =$

$$\ln(D_M^{mola}) + \ln\left(\frac{X_{MgO}^{liq}}{X_{MgO_2}^{ol}}\right) \text{ vs. } 1/T \text{ for where M is Ni, Mn, Co, or } Fe^{2+}.$$

It is clear from Fig. 5, especially the fits to the Takahashi (1978) data, that the temperature dependence of the Ni-Mg exchange differs from the other divalent cations shown. Moreover, fits to  $M^{2+}$ -Mg exchange for all the experiments in the Filter-A dataset are also shown on Fig. 5 and they agree well with the data of Takahashi (1978), demonstrating that this is a general result, not some artifact of the Takahashi dataset. Given this lack of temperature dependence for these exchange coefficients, especially that for  $Fe^{2+}$ -Mg exchange, it is not surprising that the conventional wisdom has been that Ni-Mg exchange would also not have a significant dependence on temperature (Hart and Davis 1978).

What is the origin of the anomalous behavior of Ni partitioning? A related question may be: Why is Ni so compatible in olivine in equilibrium with most naturally occurring silicate melts,

when it is actually incompatible in the  $\text{Ni}_2\text{SiO}_4\text{-Mg}_2\text{SiO}_4$  binary? Crystal-field stabilization energy (e.g., Burns and Fyfe 1966) and non-equivalent olivine sites (e.g., Wood 1974) are often-cited explanations for the unique behavior of Ni, however it is unclear to us how to prove that this is the case given that the structural environment of Ni in silicate melt is not well known, but is likely a function of temperature and composition (e.g., Galois and Calas 1993). Nevertheless, regardless of the ultimate explanation for the behavior of Ni, it is worth noting that it differs from that of other abundant cations in magmatic olivines. In the next section we show how the anomalous temperature-dependent behavior of Ni may lead to the generation of high-NiO olivine phenocrysts.

## **MODELING HIGH-NiO OLIVINES**

### *Ocean-Island magmas*

As described in the Introduction, given the compatibility of Ni in olivine, it was thought to be difficult to generate olivine phenocrysts with Ni concentrations higher than that of peridotite through low degrees of partial melting and crystallization alone. This led to several suggestions of how to explain olivine phenocrysts in primitive magmas, especially from Hawaii, that are significantly richer in Ni than most olivines in known mantle-derived peridotites (e.g., Ryabchikov 2003; Sobolev et al. 2007). However, given the temperature dependence of Ni partitioning between olivine and silicate melt, the presumption that olivine phenocrysts that crystallize near the earth's surface will reproduce the composition of the olivines of their mantle sources is not valid. In this section, we perform an illustrative calculation, using the temperature- and composition-dependent partitioning expressions developed above, to show how partial melting and crystallization at various temperatures and pressures has the potential to contribute to the crystallization of olivine phenocrysts with elevated Ni contents without appealing to core-mantle

interactions or mesomatic production of pyroxenites in the upper mantle (e.g., Rybchikov, 2003; Sobolev et al. 2007).

To illustrate the effects a temperature-dependent Ni partition coefficient can have on phenocryst compositions, we applied our preferred Ni partitioning expression (Equation 5) to the major element compositions of the 3.0 GPa experiments of Kushiro (1996). These four experiments, performed on a garnet-lherzolite bulk composition, represent some of the only low- to intermediate-degree (2.9-18.1 %), high-pressure (up to 3.0 GPa) melting experiments of a fertile upper mantle peridotite. We apply the same calculations to the liquid composition from all four experiments as a proxy for the effect of varying degrees of partial melting. Melting under Hawaii is thought to begin at great depths (e.g., Putirka 1999), but 3.0 GPa corresponds, roughly, to the thickness of the lithosphere under Hawaii (Priestley and Tilmann 1999) and is a conservative estimate for the depth of melt separation from the residual mantle. Kushiro's (1996) melts have 12-17 wt. % MgO and 45-47 wt. % SiO<sub>2</sub>, similar to some estimates of primary melt compositions (e.g., Green et al. 2001; Herzberg 2006), although they are less magnesian than the estimate of Matzen et al. (2011) for the Mauna Kea low-SiO<sub>2</sub> glasses (21.4 wt % MgO and 45.8 wt. % SiO<sub>2</sub>).

We first took each of the four 3 GPa melt compositions from Kushiro (1996) and computed the NiO concentration in the melt equilibrated with olivine containing 0.36 wt. % NiO at the measured temperature of each experiment (1460-1500°C) using  $D_{Ni}^{ol/liq}$  from Equation 5 with fit parameters for the Filter-B dataset (Table 4) [0.36 wt. % NiO in the olivine is based on sub-solidus partitioning of the DMM composition (Workman and Hart 2005) using the model of Baker et al. (2008) at 3.6 GPa, which agrees well with the olivines in spinel peridotites which have a median of 0.37 wt. % NiO (Korenaga and Kelemen 2000)]. We then used MELTS (Ghiorso and Sack 1995; Smith and Asimow 2005), assuming an oxygen fugacity two log units below the QFM buffer, to

calculate the temperature at 0.1 GPa (~3 km depth) at which 1 wt. % olivine crystallizes (1377-1402°C); this is not an arbitrary choice as erupted Hawaiian magmas are able to travel to the surface maintaining their individual chemical fingerprints (e.g., Stolper et al. 2004), and olivine phenocrysts are thought to crystallize in shallow level (0.2 GPa, ~6 km) magma chambers (Kauahikaua et al. 2000; Roedder 1983). The  $D_{Ni}^{ol/liq}$  expressions from this work give 0.1 GPa partition coefficients that are significantly higher than those at 3.0 GPa because the temperature is lower and, thus, these low-pressure olivines will have higher NiO contents than the source olivines, 0.41-0.43 wt. %. These calculations compare favorably with the Mauna Kea HSDP 2 olivines measured by Sobolev et al. (2007), falling roughly in the middle of the measured olivines with Mg#s that range from 88-90 (Fig. 6a). In this narrow Mg# range there are olivines with both higher (up to ~0.55 wt. % NiO) and lower (down to ~0.27 wt. % NiO) Ni contents. One way to generate olivines with higher NiO contents is to separate the melt from the residuum at higher pressure and temperature; when these melts are brought to the surface, the pressure and temperature drop between melting and crystallization will be greater than we assumed above, resulting in shallow crystallizing olivines with even higher NiO contents. Bear in mind that for our model calculation we made the conservative assumption that the melts separated from the residue at the base of the lithosphere. Thus, our calculations suggest that high NiO contents in early crystallizing olivine from Hawaii can be significantly influenced by the temperature difference between melt separation from the mantle and olivine crystallization at shallow depths. This effect is likely superimposed on variations in the NiO content of the source olivines. For example, Korneaga and Kelemen (2000) reported olivine NiO of  $0.37 \pm 0.03$  (1 MAD) for spinel lherzolite xenoliths. We use this distribution of NiO contents to create “error bars” on the calculated points in Fig. 6 by varying the source olivine composition over the range  $0.36 \pm 0.03$ . Note that, if a Ni

partitioning model with no temperature dependence were to be used, an increase in NiO for olivine phenocrysts crystallized at low pressure would be completely unexpected; for example, Kinzler et al.'s (1990) expression for  $D_{Ni}^{ol/liq}$  would yield, after 1% shallow crystallization, an olivine with ~0.37 wt. % NiO, essentially the same concentration as the source mantle olivine (0.36 wt. %).

Overall, our calculations demonstrate the potential for temperature differences between the mantle sources of basaltic magmas and the conditions of crystallization to affect the Ni contents of olivine phenocrysts. In particular, partial melting of olivine-bearing sources at elevated pressures and temperatures in the mantle, followed by melt segregation and transport toward the Earth's surface and crystallization of olivine at lower temperature will generate phenocrysts with variable (depending on the depths of segregation and crystallization), but inevitably higher, NiO contents than those of largely invariant olivines in the mantle source of the magmas. In Fig. 6b, we present the results of our calculations (Equation 5, Filter-B dataset 0.36 wt. % NiO in source olivine at 3.0 GPa) superimposed on the high-precision Hawaiian olivine dataset of Sobolev et al. (2007). Results of our relatively conservative calculations lie in the middle of the Hawaiian field.

Implicit in this discussion is that melts can be transported without significant crystallization or interaction with mantle olivines from their sources to near-surface environments in which they begin to crystallize; were the melt to equilibrate with mantle olivine as it ascended from its source, it would change in composition continuously, always saturated with olivines with ~0.36% NiO. In contrast, phenocrysts in basalts erupted on thick lithosphere tend to have elevated NiO (Sobolev et al. 2007), consistent with their having segregated from mantle sources below the base of the lithosphere and thus having experienced a temperature drop before the onset of olivine phenocryst formation. Although there are few constraints on the depths of crystallization of olivine phenocrysts, the presence of low-pressure fluid inclusions is often cited as evidence of shallow

formation (Roedder 1983); this, when coupled with the frequent occurrence of phenocrysts with  $Mg\#s \sim 90$  (i.e., suggesting that little prior crystallization from primary magmas occurred) is consistent with the idea that melts from mantle sources experience little crystallization of olivine between their mantle sources and near-surface environments.

### *Komatiites*

Komatiites are also thought to represent partial melts of the mantle, however the Ni contents of olivines from komatiites are not always as high as those from Hawaii (e.g., see Fig. 5b and Sobolev et al. 2005). The olivine phenocrysts in komatiites from the dataset of Sobolev et al. (2007) have maximum NiO contents of  $\sim 0.47$  wt. %; other authors have measured komatiitic olivines with slightly higher NiO contents ( $\sim 0.50$  wt. % NiO, Arndt et al. 2008, and references therein), however all are below the observed maximum of  $\sim 0.60$  wt. % NiO from Hawaii (e.g., Sobolev et al. 2005). Given the high temperatures associated with the eruption of komatiites ( $\sim 1600^\circ\text{C}$ ; Arndt et al. 2008; Herzberg et al. 2007; Nisbet et al. 1993), the temperature dependence of Ni partitioning between olivine and melt would be expected to have effects on the Ni contents of komatiitic olivines. However, as described in the previous section, the compositions of Ni in olivine phenocrysts is a consequence of both the absolute temperature and the *difference* in temperature between the depth at which the komatiitic magmas segregated from the mantle and that at which the phenocrysts crystallized, and thus it is not inevitable that the cores of komatiitic olivines would have anomalously high Ni contents. In this section, we use a calculation with a similar theoretical approach; again we must assume that komatiitic magmas do not crystallize olivine or interact with the mantle as they ascend from depth (either effect would lead to a decrease in the Ni content of the cores of olivine phenocrysts). However, komatiites are thought to erupt rapidly (e.g., Peslier et

al. 2008), which may promote disequilibrium transport and suppress crystallization. Additional potential complexities for komatiites are, (1) the rapid crystal growth rates that create spinifex olivines, characteristic of komatiites, may result in disequilibrium Ni contents such that our thermodynamic descriptions of equilibrium between olivine and melt are no longer applicable, (2) there is some uncertainty about the temperatures of formation and eruption of komatiitic magmas and eruption (e.g., Arndt et al. 2008; Grove and Parman 2004), (3) our previous assumptions about the volumes and compressibility of olivine and silicate liquid may be invalid at the high temperatures and pressures at which komatiites form, leading to a pressure effect that is distinct from that measured in our experiments, and (4) the NiO contents of olivines in equilibrium with a komatiitic melt at high pressure are poorly constrained (i.e., the solid-solid and solid-liquid Ni partition coefficients at ~5 GPa and 1700°C are not well known).

Uncertainties aside, based on the ideal treatment of the exchange reaction (Equation 5), the ratio of the partition coefficients of olivine between a melt of constant composition at two temperatures is a function of the difference in inverse temperature

$$\frac{D_{Ni}^{molar}(T_1)}{D_{Ni}^{molar}(T_2)} = \exp\left(\frac{\Delta_{r(1)}H_{T_{ref},P_{ref}}^\circ}{RT_2} - \frac{\Delta_{r(1)}H_{T_{ref},P_{ref}}^\circ}{RT_1}\right). \quad (11)$$

An important point is that komatiites are generally thought to have been much hotter than basalts when extruded (~1600°C, Arndt et al. 2008; Herzberg et al. 2007; Nisbet et al. 1993) vs. ~1400°C for primitive Hawaiian magmas (previous section, and Matzen et al. 2011).

Consequently, for a given temperature difference (i.e.,  $T_1 - T_2$  is constant), the difference in inverse temperature ( $1/T_1 - 1/T_2$ ) will be smaller for komatiites than for normal basaltic magma; thus Equation 11 implies that the ratio of  $D_{Ni}^{molar}$  at the near-surface sites of komatiitic phenocryst

formation to that in the source will be lower than that for basaltic melts, leading to a smaller amount of Ni enrichment in komatiitic phenocrysts than in Hawaiian phenocrysts.

To illustrate this quantitatively, we consider the Barberton komatiite K4-1BA, reported by Parman et al. (2004) and interpreted to be a liquid by Arndt et al. (2008), which has 46.8 wt. % SiO<sub>2</sub> and 30.3 wt. % MgO. We assume this liquid equilibrated with an olivine at 5.1 GPa and 1740°C, the estimated conditions at which the liquid separated from its source (Arndt et al. 2008). The residual olivine was assumed to have 0.36 wt. % NiO; FeO and MgO of the olivine was calculated assuming a  $K_{D, Fe^{+2}-Mg}$  of 0.34 (Matzen et al. 2011) and all Fe as FeO. This yields a composition similar to that of the most Mg-rich olivine observed; Mg#s of 93 and 94, respectively. As in the previous example, we then bring this liquid to low pressure (in this instance 1-atm rather than the 0.1 GPa used previously) and compute the  $D_{Ni}^{ol/liq}$  using the estimated eruptive temperature of 1600°C (Arndt et al. 2008). Using Equation 5 fit to the Filter-B dataset predicts an olivine with 0.42 wt. % NiO in the olivine. Fig. 6b shows that this prediction agrees well with the komatiites in the Sobolev et al. (2007) dataset which has a maximum NiO content of ~0.47 wt. %. The calculated NiO contents of olivine phenocrysts for the Barberton komatiite are similar to the results of the calculation presented above for a representative Hawaiian composition. The similarity of these results shows that both the temperature change (temperature between the separation of the melt from residuum at depth and near-surface crystallization) and absolute temperature are important in determining the enrichment of Ni in olivine phenocrysts; for komatiites the temperature drop is significantly larger (140°C) than that assumed for Hawaii (86°C, on average), however, the higher eruption temperature of the komatiite (1600°C, and an avg. of 1392°C for Hawaii) leads to approximately equivalent levels of NiO enrichment. Thus, a possible explanation for the moderate enrichment in Ni contents observed in some komatiitic olivines is the simple fact

that high absolute temperatures are needed to produce MgO-rich melts which then lead to a smaller difference in  $D_{Ni}^{ol/liq}$  between equilibration with the mantle olivines and the crystallization of olivine at or near the surface for the same  $\Delta T$ . It is interesting to note that although our model predicts that the Ni contents of the olivine phenocrysts will be moderate (when compared to Hawaii), it also predicts that the bulk-rock Ni content of a komatiite should be higher due to the lower  $D_{Ni}^{ol/liq}$  during partial melting.

## CONCLUSIONS

In olivine-saturated one-atmosphere experiments, temperature and liquid composition are correlated, making it difficult to determine their relative contributions to variations in  $D_{Ni}^{ol/liq}$ . We conducted olivine-liquid partitioning experiments on roughly constant liquid compositions but over a range of pressures and temperatures. Models that ascribe variations in  $D_{Ni}^{ol/liq}$  solely to differences in liquid composition or solely to temperature are inconsistent with the results of our experiments. Our work, which held the liquid composition approximately constant, has shown that temperature and pressure can drive significant changes in the observed partition coefficient. Using a Ni exchange reaction between olivine and liquid yields a functional form that does not include a pressure term. However, using formation reactions to describe the partitioning requires the incorporation of a pressure term if applications to high pressure are desired.

Using a simple model in which partial melting and crystallization takes place at two different pressures and temperatures, we have shown that the changing  $D_{Ni}^{ol/liq}$  can lead to the crystallization of high-NiO olivines from a melt that was in equilibrium with mantle with normal NiO concentrations. Furthermore, this conceptual model explains the observation that most high-NiO olivines come from places with thick lithosphere.

## ACKNOWLEDGMENTS

We thank Glenn Gaetani and Russ Colson for insights into their work, Ma Chi for guidance on the electron microprobe, Paul Asimow and Paula Antoshechkin for help with the MELTS calculations, and Jun Korenaga for supplying data. Funding was provided by National Science Foundation and National Aeronautics and Space Administration grant NNG04GG14G.

## REFERENCES

- Agee CB, Walker D (1990) Aluminum partitioning between olivine and ultrabasic silicate liquid to 6 GPa. *Contributions to Mineralogy and Petrology* 105:243-254
- Ai YH, Lange RA (2008) New acoustic velocity measurements on CaO-MgO-Al<sub>2</sub>O<sub>3</sub>-SiO<sub>2</sub> liquids: Reevaluation of the volume and compressibility of CaMgSi<sub>2</sub>O<sub>6</sub>-CaAl<sub>2</sub>Si<sub>2</sub>O<sub>8</sub> liquids to 25 GPa. *Journal of Geophysical Research-Solid Earth* 113 (B4).
- Albarède F, Provost A (1977) Petrological and geochemical mass-balance equations: an algorithm for least-square fitting and general error analysis. *Computers and Geosciences* 3:309-326
- Armstrong JT (1988) Quantitative analysis of silicate and oxide minerals: comparison of Monte Carlo, ZAF and  $\phi(\rho z)$  procedures. In: Newbury DE (ed) *Microbeam Analysis—1988*. San Francisco Press, pp 239–246
- Arndt N, Lesher CM, Barnes SJ (2008) *Komatiite*. Cambridge University Press, New York, NY
- Arndt NT (1977) Partitioning of nickel between olivine and ultrabasic and basic komatiite liquids. *Year Book - Carnegie Institution of Washington* (76):553-557
- Baker MB, Lesher CE, Stolper EM (2008) Predicting solidus temperatures and modes of mantle peridotites. *Geochimica et Cosmochimica Acta* 72 (12):A45-A45

- Bass JD, Weidner DJ, Hamaya N, Ozima M, Akimoto S (1984) Elasticity of the olivine and spinel polymorphs of  $\text{Ni}_2\text{SiO}_4$ . *Physics and Chemistry of Minerals* 10 (6):261-272
- Beattie P (1993a) Olivine-melt and ortho-pyroxene-melt equilibria. *Contributions to Mineralogy and Petrology* 115 (1):103-111
- Beattie P (1993b) On the occurrence of apparent non-Henry's Law behaviour in experimental partitioning studies. *Geochimica et Cosmochimica Acta* 57 (1):47-55
- Beattie P, Ford C, Russell D (1991) Partition coefficients for olivine-melt and orthopyroxene-melt systems. *Contributions to Mineralogy and Petrology* 109:212-224
- Berman RG (1988) Internally-consistent thermodynamic data for minerals in the system  $\text{Na}_2\text{O}-\text{K}_2\text{O}-\text{CaO}-\text{MgO}-\text{FeO}-\text{Fe}_2\text{O}_3-\text{Al}_2\text{O}_3-\text{SiO}_2-\text{TiO}_2-\text{H}_2\text{O}-\text{CO}_2$ . *Journal of Petrology* 29 (2):445-522
- Berman RG, Aranovich LY (1996) Optimized standard state and solution properties of minerals .1. Model calibration for olivine, orthopyroxene, cordierite, garnet, ilmenite in the system  $\text{FeO}-\text{MgO}-\text{CaO}-\text{Al}_2\text{O}_3-\text{TiO}_2-\text{SiO}_2$ . *Contributions to Mineralogy and Petrology* 126 (1-2):1-24
- Burns RG, Fyfe WS (1966) Behaviour of Nickel during Magmatic Crystallization. *Nature* 210:1147-1148
- Campbell FE, Roeder P (1968) The stability of olivine and pyroxene in the Ni-Mg-Si-O system. *American Mineralogist* 53 (1-2):257-268
- Campbell IH (1979) The influence of temperature and composition on nickel activity in silicate liquids. *Eos* 60 (18):402-403
- Chase MW (ed) (1998) NIST-JANAF Thermochemical Tables, 4th Edition. American Institute of Physics, Woodbury, New York

- Chen GQ, Ahrens TJ, Stolper EM (2002) Shock-wave equation of state of molten and solid fayalite. *Physics of the Earth and Planetary Interiors* 134 (1-2):35-52
- Clague DA, Weber WS, Dixon JE (1991) Picritic Glasses from Hawaii. *Nature* 353 (6344):553-556
- Colson RO, McKay GA, Taylor LA (1988) Temperature and compositional dependencies of trace element partitioning: Olivine/melt and low-Ca pyroxene/melt. *Geochimica et Cosmochimica Acta* 52:539-553
- Davidson PM, Grover J, Lindsley DH (1982)  $(\text{Ca,Mg})_2\text{Si}_2\text{O}_6$  Clinopyroxenes: A solution model based on nonconvergent site-disorder. *Contributions to Mineralogy and Petrology* 80 (1):88-102
- Drake MJ, Holloway JR (1981) Partitioning of Ni between olivine and silicate melt: the 'Henry's Law problem' reexamined. *Geochimica et Cosmochimica Acta* 45:431-437
- Duke JM (1976) Distribution of the period four transition elements among olivine, calcic clinopyroxene and mafic silicate liquid: experimental results. *Journal of Petrology* 17:499-521
- Falloon TJ, Danyushevsky LV, Ariskin A, Green DH, Ford CE (2007) The application of olivine geothermometry to infer crystallization temperatures of parental liquids: Implications for the temperature of MORB magmas. *Chemical Geology* 241 (3-4):207-233
- Filiberto J, Jackson C, Le L, Treiman AH (2009) Partitioning of Ni between olivine and an iron-rich basalt: Experiments, partition models, and planetary implications. *American Mineralogist* 94 (2-3):256-261

- Gaetani GA, Grove TL (1997) Partitioning of moderately siderophile elements among olivine, silicate melt, and sulfide melt: Constraints on core formation in the Earth and Mars. *Geochimica et Cosmochimica Acta* 61:1829-1846
- Galoisy L, Calas G (1993) Structural environment of nickel in silicate glass/melt systems: Part 1. Spectroscopic determination of coordination states. *Geochimica et Cosmochimica Acta* 57 (15):3613-3626
- Ghiorso MS (2004) An equation of state for silicate melts. III. Analysis of stoichiometric liquids at elevated pressure: Shock compression data, molecular dynamics simulations and mineral fusion curves. *American Journal of Science* 304 (8-9):752-810
- Ghiorso MS, Carmichael ISE, Rivers ML, Sack RO (1983) The Gibbs free-energy of mixing of natural silicate liquids- an expanded regular solution approximation for the calculation of magmatic intensive variables. *Contributions to Mineralogy and Petrology* 84 (2-3):107-145
- Ghiorso MS, Sack RO (1995) Chemical Mass-Transfer in Magmatic Processes .4. a Revised and Internally Consistent Thermodynamic Model for the Interpolation and Extrapolation of Liquid-Solid Equilibria in Magmatic Systems at Elevated-Temperatures and Pressures. *Contributions to Mineralogy and Petrology* 119 (2-3):197-212
- Green DH, Falloon TJ, Eggins SM, Yaxley GM (2001) Primary magmas and mantle temperatures. *European Journal of Mineralogy* 13 (3):437-452
- Grove TL, Parman SW (2004) Thermal evolution of the Earth as recorded by komatiites. *Earth and Planetary Science Letters* 219:173-187
- Häkli TA, Wright TL (1967) Fractionation of nickel between olivine and augite as a geothermometer. *Geochimica et Cosmochimica Acta* 31 (5):877-884

- Hart SR, Davis KE (1978) Nickel Partitioning between Olivine and Silicate Melt. *Earth and Planetary Science Letters* 40 (2):203-219
- Herd CDK, Dwarzski RE, Shearer CK (2009) The behavior of Co and Ni in olivine in planetary basalts: An experimental investigation. *American Mineralogist* 94 (2-3):244-255
- Herzberg C (2006) Petrology and thermal structure of the Hawaiian plume from Mauna Kea volcano. *Nature* 444:605-609
- Herzberg C, Asimow PD, Arndt N, Niu YL, Leshner CM, Fitton JG, Cheadle MJ, Saunders AD (2007) Temperatures in ambient mantle and plumes: Constraints from basalts, picrites, and komatiites. *Geochemistry Geophysics Geosystems* 8
- Hesse M, Grove TL (2003) Absarokites from the western Mexican Volcanic Belt: constraints on mantle wedge conditions. *Contributions to Mineralogy and Petrology* 146:10-27
- Hirschmann M (1991) Thermodynamics of multicomponent olivines and the solution properties of  $(\text{Ni,Mg,Fe})_2\text{SiO}_4$  and  $(\text{Ca,Mg,Fe})_2\text{SiO}_4$  olivines. *American Mineralogist* 76 (7-8):1232-1248
- Hirschmann MM, Ghiorso MS (1994) Activities of nickel, cobalt, and manganese silicates in magmatic liquids and applications to olivine/liquid and to silicate metal partitioning. *Geochimica et Cosmochimica Acta* 58:4109-4126
- Holzheid A, Palme H, Chakraborty S (1997) The activities of NiO, CoO and FeO in silicate melts. *Chemical Geology* 139:21-38
- Humayun M, Qin L, Norman MD (2004) Geochemical evidence for excess iron in the mantle beneath Hawaii. *Science* 306:91-94
- Jones JH (1984) Temperature-independent and pressure-independent correlations of olivine liquid partition-coefficients and their application to trace-element

- partitioning. *Contributions to Mineralogy and Petrology* 88 (1-2):126-132
- Kauahikaua J, Hildenbrand T, Webring M (2000) Deep magmatic structures of Hawaiian volcanoes, imaged by three-dimensional gravity models. *Geology* 28 (10):883-886
- Kelemen PB, Hart SR, Bernstein S (1998) Silica enrichment in the continental upper mantle via melt/rock reaction. *Earth and Planetary Science Letters* 164:387-406
- Kinzler RJ, Grove TL, Recca SI (1990) An experimental study on the effect of temperature and melt composition on the partitioning of nickel between olivine and silicate melt. *Geochimica et Cosmochimica Acta* 54 (5):1255-1265
- Korenaga J, Kelemen PB (1998) Melt migration through the oceanic lower crust: a constraint from melt percolation modeling with finite solid diffusion. *Earth and Planetary Science Letters* 156:1-11
- Korenaga J, Kelemen PB (2000) Major element heterogeneity in the mantle source of the North Atlantic igneous province. *Earth and Planetary Science Letters* 184:251-268
- Kushiro I (1996) Partial melting of a fertile mantle peridotite at high pressures: An experimental study using aggregates of diamonds. In: Basu A, Hart S (eds) *Earth Processes: Reading the Isotopic Code*, vol 95. *Geophysical Monograph Series*. American Geophysical Union, Washington, DC, pp 109–122
- Leeman WP (1974) Part I, Petrology of basaltic lavas from the Snake River Plain, Idaho; and Part II, Experimental determination of partitioning of divalent cations between olivine and basaltic liquid. Doctoral, University of Oregon, Eugene
- Li CS, Ripley EM (2010) The relative effects of composition and temperature on olivine-liquid Ni partitioning: Statistical deconvolution and implications for petrologic modeling. *Chemical Geology* 275 (1-2):99-104

- Lindsley DH, Grover JE, Davidson PM (1981) The thermodynamics of the  $\text{Mg}_2\text{Si}_2\text{O}_6$ - $\text{CaMgSi}_2\text{O}_6$  join: A review and an improved model. In: Newton RC, Navrotsky A, Wood BJ (eds) Advances in physical geochemistry vol Thermodynamics of minerals and melts. Springer-Verlag, New York, NY, pp 149-175
- Matzen AK, Baker MB, Beckett JR, Stolper EM (2009) The temperature and pressure dependence of Ni partitioning between olivine and MgO-rich silicate melt. *Geochimica et Cosmochimica Acta* 73 (13):A851-A851
- Matzen AK, Baker MB, Beckett JR, Stolper EM (2010) The temperature and pressure dependence of nickel partitioning between olivine and high-MgO silicate melt. Abstract #V13F-03, presented at 2010 Fall Meeting, AGU, San Francisco, Calif, 13-17 Dec
- Matzen AK, Baker MB, Beckett JR, Stolper EM (2011) Fe–Mg Partitioning between Olivine and High-magnesian Melts and the Nature of Hawaiian Parental Liquids. *Journal of Petrology* 52 (7-8):1243-1263
- Medard E, McCammon CA, Barr JA, Grove TL (2008) Oxygen fugacity, temperature reproducibility, and H<sub>2</sub>O contents of nominally anhydrous piston-cylinder experiments using graphite capsules. *American Mineralogist* 93 (11-12):1838-1844
- Minarik WG, Ryerson FJ, Watson EB (1996) Textural entrapment of core-forming melts. *Science* 272 (5261):530-533
- Mysen B (2007) Partitioning of calcium, magnesium, and transition metals between olivine and melt governed by the structure of the silicate melt at ambient pressure. *American Mineralogist* 92:844-862
- Mysen BO (1978) Experimental determination of nickel partition coefficients between liquid, pargasite, and garnet peridotite minerals and concentration limits of behavior according to

- Henry's law at high pressure and temperature. *American Journal of Science* 278 (2):217-243
- Mysen BO (2006) Redox equilibria of iron and silicate melt structure: Implications for olivine/melt element partitioning. *Geochimica et Cosmochimica Acta* 70 (12):3121-3138
- Mysen BO, Kushiro I (1979) Pressure-Dependence of Nickel Partitioning between Forsterite and Aluminous Silicate Melts. *Earth and Planetary Science Letters* 42 (3):383-388
- Nabelek PI (1980) Nickel Partitioning between Olivine and Liquid in Natural Basalts - Henrys Law Behavior. *Earth and Planetary Science Letters* 48 (2):293-302
- Nafziger RH, Muan A (1967) Equilibrium phase compositions and thermodynamic properties of olivines and pyroxenes in system MgO-"FeO"-SiO<sub>2</sub>. *American Mineralogist* 52 (9-10):1364-1385
- Nisbet EG, Cheadle MJ, Arndt NT, Bickle MJ (1993) Constraining the potential temperature of the Archaean mantle: A review of the evidence from komatiites. *Lithos* 30 (3-4):291-307
- O'Neill HSC, Berry AJ (2006) Activity coefficients at low dilution of CrO, NiO and CoO in melts in the system CaO-MgO-Al<sub>2</sub>O<sub>3</sub>-SiO<sub>2</sub> at 1400°C: Using the thermodynamic behaviour of transition metal oxides in silicate melts to probe their structure. *Chemical Geology* 231 (1-2):77-89
- Parman SW, Grove TL, Dann JC, de Wit MJ (2004) A subduction origin for komatiites and cratonic lithospheric mantle. *South African Journal of Geology* 107:107-118
- Peslier AH, Woodland AB, Wolff JA (2008) Fast kimberlite ascent rates estimated from hydrogen diffusion profiles in xenolithic mantle olivines from southern Africa. *Geochimica et Cosmochimica Acta* 72 (11):2711-2722

- Press WH, Teukolsky SA, Vetterling WT, Flannery BP (1992) Numerical Recipes. 2nd. edn.  
Cambridge University Press, Cambridge
- Priestley K, Tilmann F (1999) Shear-wave structure of the lithosphere above the Hawaiian Hot Spot from two-station Rayleigh wave phase velocity measurements. *Geophysical Research Letters* 26 (10):1493-1496
- Putirka K (1999) Melting depth and mantle heterogeneity beneath Hawaii and the East Pacific Rise: Constraints from Na/Ti and rare earth element ratios. *Journal of Geophysical Research* 104:2817-2829
- Putirka K, Johnson M, Kinzler R, Longhi J, Walker D (1996) Thermobarometry of mafic igneous rocks based on clinopyroxene-liquid equilibria, 0-30 kbar. *Contributions to Mineralogy and Petrology* 123:92-108
- Putirka K, Ryerson FJ, Perfit M, Ridley WI (2011) Mineralogy and Composition of the Oceanic Mantle. *Journal of Petrology* 52 (2):279-313
- Putirka KD, Perfit M, Ryerson FJ, Jackson MG (2007) Ambient and excess mantle temperatures, olivine thermometry, and active vs. passive upwelling. *Chemical Geology* 241 (3-4):177-206
- Qin L, Humayun M (2008) The Fe/Mn ratio in MORB and OIB determined by ICP-MS. *Geochimica et Cosmochimica Acta* 72:1660-1677
- Ringwood AE (1956) Melting relationships of Ni-Mg olivines and some geochemical implications. *Geochimica et Cosmochimica Acta* 10 (5-6):297-303
- Roedder E (1983) Geobarometry of ultramafic xenoliths from Loihi Seamount, Hawaii, on the basis of CO<sub>2</sub> inclusions in olivine. *Earth and Planetary Science Letters* 66 (1-3):369-379

- Roeder PL, Emslie RF (1970) Olivine-liquid equilibrium. *Contributions to Mineralogy and Petrology* 29 (4):275-289
- Ryabchikov ID (2003) High NiO content in mantle-derived magmas as evidence for material transfer from the Earth's core. *Doklady Earth Sciences* 389A:437-439
- Salters VJM, Longhi JE, Bizimis M (2002) Near mantle solidus trace element partitioning at pressures up to 3.4 GPa. *Geochemistry, Geophysics, Geosystems* 3:doi:10.1029/2001GC000148
- Seifert S, O'Neill HSC, Brey G (1988) The partitioning of Fe, Ni and Co between olivine, metal, and basaltic liquid: An experimental and thermodynamic investigation, with application to the composition of the lunar core. *Geochimica et Cosmochimica Acta* 52 (3):603-616
- Smith PM, Asimow PD (2005) *Adiabat\_1ph*: A new public front-end to the MELTS, pMELTS, and pHMELTS models. *Geochemistry, Geophysics, Geosystems* 6:Q02004, doi:02010.01029/02004GC000816.
- Snyder DA, Carmichael ISE (1992) Olivine-liquid equilibria and the chemical activities of FeO, NiO, Fe<sub>2</sub>O<sub>3</sub>, and MgO in natural basic melts. *Geochimica et Cosmochimica Acta* 56 (1):303-318
- Sobolev AV, Hofmann AW, Kuzmin DV, Yaxley GM, Arndt NT, Chung S-L, Danyushevsky LV, Elliott T, Frey FA, Garcia MO, Gurenko AA, Kamenetsky VS, Kerr AC, Krivolutsкая NA, Matvienkov VV, Nikogosian IK, Rocholl A, Sigurdsson IA, Sushchevskaya NM, Teklay M (2007) The amount of recycled crust in sources of mantle-derived melts. *Science* 316:412-417
- Sobolev AV, Hofmann AW, Sobolev SV, Nikogosian IK (2005) An olivine-free mantle source of Hawaiian shield basalts. *Nature* 434:590-597

- Stolper E, Sherman S, Garcia M, Baker M, Seaman C (2004) Glass in the submarine section of the HSDP2 drill core, Hilo, Hawaii. *Geochemistry, Geophysics, Geosystems* 5:doi:10.1029/2003GC000553
- Takahashi E (1978) Partitioning of  $\text{Ni}^{2+}$ ,  $\text{Co}^{2+}$ ,  $\text{Fe}^{2+}$ ,  $\text{Mn}^{2+}$  and  $\text{Mg}^{2+}$  between Olivine and Silicate Melts - Compositional Dependence of Partition-Coefficient. *Geochimica Et Cosmochimica Acta* 42 (12):1829-1844
- Tormey DR, Grove TL, Bryan WB (1987) Experimental petrology of normal MORB near the Kane Fracture Zone: 22°N-25°N, mid-Atlantic ridge. *Contributions to Mineralogy and Petrology* 96:121-139
- Vogt JHL (1923) Nickel in igneous rocks. *Economic Geology* 18 (4):307-352
- Vokurka K, Rieder M (1987) Thermal expansion and excess volumes of synthetic olivines on the  $\text{Mg}_2\text{SiO}_4$ - $\text{Ni}_2\text{SiO}_4$  join. *Neues Jahrb Mineral-Monhefte (H3)*:97-106
- Walter MJ (1998) Melting of garnet peridotite and the origin of komatiite and depleted lithosphere. *Journal of Petrology* 39:29-60
- Wang Z, Gaetani GA (2008) Partitioning of Ni between olivine and siliceous eclogite partial melt: experimental constraints on the mantle source of Hawaiian basalts. *Contributions to Mineralogy and Petrology* 156 (5):661-678
- Watson EB (1977) Partitioning of manganese between forsterite and silicate liquid. *Geochimica et Cosmochimica Acta* 41 (9):1363-1374
- Wood BJ (1974) Crystal Field Spectrum of  $\text{Ni}^{2+}$  in Olivine. *American Mineralogist* 59 (3-4):244-248
- Workman RK, Hart SR (2005) Major and trace element composition of the depleted MORB mantle (DMM). *Earth and Planetary Science Letters* 231:53-72

Yaxley GM (2000) Experimental study of the phase and melting relations of homogeneous basalt plus peridotite mixtures and implications for the petrogenesis of flood basalts.

Contributions to Mineralogy and Petrology 139 (3):326-338

## TABLES

Table 1. Starting Compositions

| Sample                              | n  | SiO <sub>2</sub> | TiO <sub>2</sub> | Al <sub>2</sub> O <sub>3</sub> | Cr <sub>2</sub> O <sub>3</sub> | FeO*      | MnO     | MgO       | CaO      | Na <sub>2</sub> O | K <sub>2</sub> O | P <sub>2</sub> O <sub>5</sub> | NiO     | Sum    |
|-------------------------------------|----|------------------|------------------|--------------------------------|--------------------------------|-----------|---------|-----------|----------|-------------------|------------------|-------------------------------|---------|--------|
| TT152-21-35 <sup>a</sup>            | -  | 50.80            | 1.84             | 13.70                          | -                              | 12.40     | 0.22    | 6.67      | 11.50    | 2.68              | 0.15             | 0.19                          | -       | 100.15 |
| TT152-21-35 <sup>b</sup>            | -  | 50.92            | 2.02             | 13.70                          | -                              | 12.56     | 0.19    | 7.11      | 10.88    | 2.63              | 0.16             | -                             | -       | 100.17 |
| Fused TT152-21-35 <sup>c</sup>      | 3  | 50.45(7)         | 1.91(3)          | 14.04(9)                       | BDL                            | 12.06(10) | 0.21(2) | 6.97(2)   | 11.05(5) | 2.59(6)           | 0.16(1)          | 0.19(3)                       | BDL     | 99.63  |
| Fused TT152-21-35 +NiO <sup>d</sup> | 6  | 49.63(7)         | 1.92(3)          | 13.78(7)                       | BDL                            | 12.33(8)  | 0.22(1) | 6.98(5)   | 10.97(9) | 2.60(3)           | 0.16(1)          | 0.18(2)                       | 0.97(3) | 99.74  |
| Kilbourne Hole olivine <sup>e</sup> | 18 | 40.87(24)        | BDL              | 0.03(2)                        | 0.011(4)                       | 9.23(7)   | 0.13(1) | 48.80(28) | 0.088(5) | -                 | -                | -                             | 0.36(2) | 99.51  |
| San Carlos olivine <sup>f</sup>     | 4  | 40.47(6)         | BDL              | 0.02(2)                        | 0.021(5)                       | 9.17(29)  | 0.13(1) | 49.03(33) | 0.11(7)  | -                 | -                | -                             | 0.39(3) | 99.35  |

Note: All compositions in wt. %. Numbers in parenthesis are analytical uncertainties in terms of the least units cited, e.g., 50.46(2) corresponds to 50.46±0.02 where 0.02 is the standard deviation of n measurements. FeO\* = all Fe as FeO. A dash indicates that the element was not analyzed or reported. BDL = below detection limit

<sup>a</sup> Dixon et al. (1988)

<sup>b</sup> Fine and Stolper (1986)

<sup>c</sup> fused at 1 atm and 1240°C on a pre-doped Pt loop at QFM for 0.5 hr

<sup>d</sup> ~1 wt. % NiO was mixed with TT152-21-35 glass powder and then fused<sup>c</sup>.

<sup>e</sup> Composition of Kilbourne Hole olivine powder used in experiments.

<sup>f</sup> San Carlos olivine capsule used in experiment 25

Table 2. Run Conditions and Phase Information

| Run #                     | Final Run Conditions |                    |        | Hot Press Conditions |        |        | Capsule | Run Products <sup>a</sup><br>(wt. %) | Phase Proportions <sup>b</sup><br>(relative) | % NiO Change <sup>c</sup> | q-value |
|---------------------------|----------------------|--------------------|--------|----------------------|--------|--------|---------|--------------------------------------|--|---------------------------|---------|
|                           | T(°C)                | P(GPa)             | t(hrs) | T(°C)                | P(GPa) | t(hrs) |         |                                      |  |                           |         |
| kbh-ol-c-6                | 1450                 | 1.0                | 12.0   | 890                  | 0.88   | 6.0    | Pt-C    | gl, oliv                             | 7.2, 92.8                                    | -12.77                    | 0.85    |
| kbh-ol-c-7                | 1450                 | 1.0                | 18.0   | 890                  | 0.89   | 6.0    | Pt-C    | gl, oliv                             | 5.1, 94.9                                    | -11.63                    | 0.92    |
| kbh-ol-c-8                | 1450                 | 1.0                | 6.0    | 890                  | 0.89   | 6.0    | Pt-C    | gl, oliv                             | 9.2, 90.8                                    | -0.02                     | 0.25    |
| kbh-ol-nc-9 <sup>e</sup>  | 1500                 | 2.0                | 12.2   | 940                  | 1.89   | 6.3    | Re      | gl, oliv                             | 12.7, 87.3                                   | 1.82                      | 0.38    |
| kbh-ol-c-10               | 1500                 | 2.0                | 12.0   | 940                  | 1.75   | 6.0    | Pt-C    | gl, oliv, px                         | 8.1, 91.4, -                                 | 2.45                      | 0.96    |
| kbh-ol-c-13               | 1525                 | 2.5                | 12.0   | 965                  | 2.20   | 6.0    | Pt-C    | gl, oliv, px                         | 17.1, 82.6, 0.3                              | 1.15                      | 0.96    |
| kbh-ol-c-17R              | 1450                 | 1.0                | 12.0   | 890                  | 0.89   | 6.0    | Pt-C    | gl, oliv                             | 5.8, 94.2                                    | 17.19                     | 0.72    |
| kbh-ol-c-25               | 1399                 | 1x10 <sup>-4</sup> | 8.0    | -                    | -      | -      | SCOI    | gl, oliv                             | 99.96, 0.02                                  | -16.35                    | 0.81    |
| kbh-ol-c-28R <sup>e</sup> | 1500                 | 2.0                | 10.7   | 940                  | 1.81   | 6.0    | Pt-C    | gl, oliv, px                         | 13.6, 86.4, -                                | 57.36                     | 0.97    |
| kbh-ol-c-30               | 1550                 | 3.0                | 12.0   | 990                  | 2.65   | 6.0    | Pt-C    | gl, oliv, px                         | 48.6, 41.6, 9.8                              | 1.78                      | 0.88    |
| kbh-ol-32R <sup>f</sup>   | 1402                 | 1x10 <sup>-4</sup> | 8.0    | -                    | -      | -      | SCOI    | gl, oliv                             | 86.0, 14.0                                   | -16.38                    | 0.09    |
| kbh-ol-c-33R              | 1550                 | 3.0                | 12.0   | 990                  | 2.70   | 6.1    | Pt-C    | gl, oliv, px, px                     | 50.7, 31.0, 0.1, 18.2                        | 11.73                     | 0.97    |
| kbh-ol-c-45R              | 1450                 | 1.0                | 12.2   | 915                  | 1.50   | 16.4   | Pt-C    | gl, oliv                             | 5.2, 94.8                                    | 46.48                     | 0.90    |

Note: Sample names followed by the letter R denote a reversal experiment. One-atmosphere experiments, runs 25 and 32R, were conducted at  $fO_2$ s ~1.7 log units below the QFM buffer ( $\log_{10} fO_2 = -8.07$  and  $-8.09$ , respectively). Runs 25 and 32R lost and gained, respectively, 19.8 and 3.5% (relative) of the bulk Na<sub>2</sub>O over the course of the experiment. The glass composition from run 32R (listed in Table 3) was renormalized to 100% before being entered into the mass balance.

<sup>a</sup> Run products abbreviations: gl=glass (quenched liquid), oliv=olivine, px=pyroxene.

<sup>b</sup> Phase proportions, calculated by mass balance, are given in the same order as listed in the run products column. Calculated pyroxene proportions for experiment 33R correspond to the order in which they appear in Table 3.

<sup>c</sup> Relative change (in percent) of NiO from the bulk composition based on mass balance; negative sign denotes a decrease while a positive sign indicates an increase in the NiO content of the bulk.

<sup>d</sup> Goodness of fit measure; values above 0.05 indicate a high confidence in results of the mass balance.

<sup>e</sup> Upon heating to the final-run temperature pressure increased above the desired final-run pressure. Pressure was slowly bled off until final run-pressure was reached; colloquially, these experiments were hot-piston out.

<sup>f</sup> The glass composition used to mass balance run 32R was renormalized to 100.

Table 3. Phase Compositions

| Name         | phase | SiO <sub>2</sub> | TiO <sub>2</sub> | Al <sub>2</sub> O <sub>3</sub> | Cr <sub>2</sub> O <sub>3</sub> <sup>a</sup> | FeO*        | MnO      | MgO       | CaO      | Na <sub>2</sub> O | K <sub>2</sub> O | P <sub>2</sub> O <sub>5</sub> | NiO <sup>a</sup> | Sum   |
|--------------|-------|------------------|------------------|--------------------------------|---|-------------|----------|-----------|----------|-------------------|------------------|-------------------------------|------------------|-------|
| kbh-ol-c-6   | gl    | 49.91(15)        | 1.41(4)          | 11.10(10)                      | 0.015(1)                                    | 10.73(7)    | 0.20(2)  | 17.66(8)  | 7.41(4)  | 1.95(2)           | 0.12(1)          | 0.11(2)                       | 0.073(3)         | 100.7 |
|              | oliv  | 40.74(17)        | 0.022(4)         | 0.070(4)                       | 0.013(3)                                    | 9.94(4)     | 0.14(1)  | 48.56(19) | 0.21(1)  | --                | --               | --                            | 0.324(8)         | 100.0 |
| kbh-ol-c-7   | gl    | 50.18(7)         | 1.44(2)          | 11.29(7)                       | 0.014(2)                                    | 10.31(9)    | 0.19(2)  | 17.36(3)  | 7.18(3)  | 1.98(3)           | 0.13(1)          | 0.13(2)                       | 0.071(4)         | 100.3 |
|              | oliv  | 40.50(16)        | 0.02(1)          | 0.069(3)                       | 0.013(2)                                    | 9.86(4)     | 0.14(1)  | 48.50(11) | 0.20(1)  | --                | --               | --                            | 0.329(12)        | 99.6  |
| kbh-ol-c-8   | gl    | 49.57(15)        | 1.45(3)          | 11.20(8)                       | 0.016(1)                                    | 10.66(7)    | 0.21(2)  | 17.40(9)  | 7.56(4)  | 1.92(4)           | 0.12(1)          | 0.13(2)                       | 0.086(4)         | 100.3 |
|              | oliv  | 40.29(19)        | 0.018(3)         | 0.07(1)                        | 0.013(4)                                    | 9.99(3)     | 0.14(1)  | 48.11(15) | 0.22(1)  | --                | --               | --                            | 0.371(5)         | 99.2  |
| kbh-ol-nc-9  | gl    | 47.84(15)        | 1.34(4)          | 9.75(5)                        | 0.019(2)                                    | 11.45(5)    | 0.20(2)  | 18.87(7)  | 7.93(5)  | 1.67(3)           | 0.12(1)          | 0.13(1)                       | 0.087(3)         | 99.4  |
|              | oliv  | 40.88(20)        | 0.009(4)         | 0.09(2)                        | 0.011(2)                                    | 9.47(9)     | 0.13(1)  | 48.97(22) | 0.21(2)  | --                | --               | --                            | 0.381(5)         | 100.2 |
| kbh-ol-c-10  | gl    | 48.40(15)        | 1.47(3)          | 10.62(5)                       | 0.016(1)                                    | 10.77(10)   | 0.19(2)  | 18.37(6)  | 7.75(3)  | 1.84(3)           | 0.14(1)          | 0.13(2)                       | 0.088(3)         | 99.8  |
|              | oliv  | 41.02(24)        | 0.01(1)          | 0.08(1)                        | 0.010(3)                                    | 9.64(4)     | 0.136(4) | 48.73(31) | 0.204(4) | --                | --               | --                            | 0.381(6)         | 100.2 |
|              | px    | 56.17(33)        | 0.13(3)          | 2.59(13)                       | 0.05(1)                                     | 6.41(10)    | 0.13(1)  | 33.30(28) | 1.30(12) | 0.10(1)           | --               | --                            | 0.15(2)          | 100.3 |
| kbh-ol-c-13  | gl    | 47.19(13)        | 1.62(4)          | 11.32(6)                       | 0.018(2)                                    | 10.76(7)    | 0.20(2)  | 17.18(9)  | 8.75(5)  | 2.11(5)           | 0.15(1)          | 0.17(3)                       | 0.089(4)         | 99.6  |
|              | oliv  | 41.03(12)        | 0.02(1)          | 0.14(6)                        | 0.013(3)                                    | 9.83(4)     | 0.14(1)  | 47.92(24) | 0.27(1)  | --                | --               | --                            | 0.370(7)         | 99.7  |
|              | px    | 55.10(32)        | 0.16(3)          | 4.09(62)                       | 0.05(1)                                     | 6.63(30)    | 0.13(1)  | 31.75(52) | 1.77(46) | 0.19(3)           | --               | --                            | 0.13(1)          | 100.0 |
| kbh-ol-c-17R | gl    | 49.34(15)        | 1.45(4)          | 11.11(10)                      | 0.015(2)                                    | 10.61(6)    | 0.20(2)  | 17.77(8)  | 7.53(05) | 1.99(4)           | 0.12(1)          | 0.14(2)                       | 0.111(4)         | 100.4 |
|              | oliv  | 40.95(8)         | 0.029(4)         | 0.070(3)                       | 0.013(3)                                    | 9.55(2)     | 0.14(1)  | 48.51(13) | 0.22(1)  | --                | --               | --                            | 0.497(16)        | 100.0 |
| kbh-ol-c-25  | gl    | 48.26(17)        | 1.44(4)          | 10.51(6)                       | 0.018(1)                                    | 11.55(6)    | 0.20(3)  | 18.09(7)  | 8.32(6)  | 1.55(3)           | 0.10(1)          | 0.12(2)                       | 0.081(3)         | 100.2 |
|              | oliv  | 41.07(18)        | 0.02(1)          | 0.04(1)                        | 0.018(14)                                   | 9.38(4)     | 0.140(3) | 48.84(28) | 0.27(1)  | --                | --               | --                            | 0.408(10)        | 100.2 |
| kbh-ol-c-28R | gl    | 48.34(25)        | 1.57(3)          | 11.34(6)                       | 0.017(1)                                    | 10.76(6)    | 0.21(2)  | 17.17(7)  | 8.43(4)  | 2.05(3)           | 0.15(1)          | 0.14(3)                       | 0.170(4)         | 100.3 |
|              | oliv  | 41.03(40)        | 0.02(1)          | 0.10(2)                        | 0.011(2)                                    | 9.76(12)    | 0.143(4) | 48.15(14) | 0.25(1)  | --                | --               | --                            | 0.782(12)        | 100.2 |
|              | px    | 55.72(26)        | 0.16(2)          | 3.05(20)                       | 0.05(1)                                     | 6.57(15)    | 0.13(1)  | 32.30(21) | 1.59(5)  | 0.12(1)           | --               | --                            | 0.35(5)          | 100.0 |
| kbh-ol-c-30  | gl    | 46.38(91)        | 1.59(9)          | 10.92(18)                      | 0.015(2)                                    | 11.65(1.01) | 0.20(2)  | 18.28(80) | 8.99(18) | 1.62(38)          | 0.13(6)          | 0.17(4)                       | 0.102(8)         | 100.1 |
|              | oliv  | 41.14(5)         | 0.0016(2)        | 0.14(2)                        | 0.008(3)                                    | 9.91(21)    | 0.140(5) | 48.39(27) | 0.25(4)  | --                | --               | --                            | 0.390(9)         | 100.4 |
|              | px    | 55.27(11)        | 0.15(3)          | 4.11(11)                       | 0.04(1)                                     | 6.57(9)     | 0.13(1)  | 31.59(17) | 2.01(6)  | 0.23(1)           | --               | --                            | 0.13(1)          | 100.2 |
| kbh-ol-32R   | gl    | 48.82(24)        | 1.44(3)          | 10.69(7)                       | BDL   | 11.51(7)    | 0.20(2)  | 17.06(6)  | 8.46(5)  | 2.09(4)           | 0.11(1)          | 0.12(2)                       | 0.418(7)         | 100.9 |
|              | oliv  | 41.16(34)        | 0.022(5)         | 0.03(1)                        | 0.018(3)                                    | 9.68(4)     | 0.147(3) | 47.13(17) | 0.26(2)  | --                | --               | --                            | 2.063(38)        | 100.5 |
| kbh-ol-c-33R | gl    | 45.40(38)        | 1.90(3)          | 11.76(6)                       | BDL   | 12.40(7)    | 0.20(2)  | 16.31(8)  | 8.97(3)  | 2.31(4)           | 0.18(1)          | 0.18(1)                       | 0.396(4)         | 100.0 |
|              | oliv  | 41.00(5)         | 0.02(1)          | 0.15(3)                        | 0.011(4)                                    | 11.30(22)   | 0.147(5) | 46.71(32) | 0.29(2)  | --                | --               | --                            | 1.476(68)        | 101.1 |
|              | px    | 54.30(29)        | 0.17(2)          | 5.27(34)                       | 0.04(1)                                     | 7.10(6)     | 0.14(1)  | 29.99(25) | 2.32(11) | 0.31(2)           | --               | --                            | 0.58(2)          | 100.2 |
|              | px    | 53.69(25)        | 0.21(4)          | 5.87(30)                       | 0.05(1)                                     | 7.00(9)     | 0.17(1)  | 24.83(69) | 6.83(42) | 0.87(7)           | --               | --                            | 0.59(5)          | 100.1 |
| kbh-ol-c-45R | gl    | 48.87(10)        | 1.44(3)          | 11.10(7)                       | 0.023(1)                                    | 10.46(6)    | 0.20(2)  | 17.41(8)  | 7.19(4)  | 1.96(3)           | 0.13(1)          | 0.12(2)                       | 0.134(3)         | 99.0  |
|              | oliv  | 40.54(10)        | 0.019(5)         | 0.064(3)                       | 0.016(2)                                    | 9.86(5)     | 0.14(1)  | 48.28(19) | 0.20(1)  | --                | --               | --                            | 0.612(29)        | 99.7  |

Note: All compositions listed in wt. %. Abbreviations as in Table 2. Numbers in parenthesis are analytical uncertainties in terms of the least units cited, e.g., 49.91(15) corresponds to 49.91±0.15 where 0.15 is one standard sample deviation; when the error is ≥1.0, we include the decimal point. FeO\* = all Fe as FeO. Dashed line indicates that the element was not analyzed. BDL = below detection limit. For fitting purposes, the liquid and olivine compositions were transformed into mole fractions. For the liquids, components are as listed,

with the exception of  $\text{SiO}_2$  which was calculated as  $\text{Si}_{0.5}\text{O}$ . Olivine analyses were transformed into olivine components;  $\text{SiO}_2$ ,  $\text{FeSi}_{0.5}\text{O}_2$ ,  $\text{MgSi}_{0.5}\text{O}_2$ ,  $\text{MnSi}_{0.5}\text{O}_2$ ,  $\text{CaSi}_{0.5}\text{O}_2$ ,  $\text{NiSi}_{0.5}\text{O}_2$ , and  $\text{CoSi}_{0.5}\text{O}_2$ .

<sup>a</sup> Element analyzed with a 200 nA beam current, see text

Table 4. Fit Parameters

| Reaction Fit  | Dataset Used | $-\Delta_r H_{T_{ref}, P_{ref}}^\circ / R$<br>(K) <sup>a</sup> | $\Delta_r S_{T_{ref}, P_{ref}}^\circ / R$<br>(K) | $W_{Ni-Mg}/R$<br>(K) | $W_{Mg-Si}/R$<br>(K) | $W_{Si-Ni}/R$<br>(K) | Mean Percent Errors of Dataset <sup>b</sup> |          |           |
|---|--------------|--|--|----------------------|----------------------|----------------------|---|----------|-----------|
|   |              |  |  |                      |                      |                      | Fit   | Filter-B | This Work |
| Ex, Ideal <sup>c</sup>                                | This work    | 4,375(1,050)   | -2.023(602)                                      | -                    | -                    | -                    | 3.9   | 12.2     | 3.9       |
| Ex, Ideal   | Filter-A     | 4,362(156)   | -1.970(95)                                       | -                    | -                    | -                    | 13.9  | 12.0     | 6.0       |
| Ex, Ideal   | Filter-B     | 4,338(208)   | -1.956(126)                                      | -                    | -                    | -                    | 12.0  | 12.0     | 6.0       |
| Fm, Ideal <sup>d</sup>                                | Filter-A     | 9,931(232)   | -3.144(141)                                      | -                    | -                    | -                    | 18.4  | 17.6     | 8.6       |
| Fm, Ideal, $\Delta_r C_p$ , $\Delta_r V$ <sup>e</sup> | This work    | 8,795(798)   | -2.620(457)                                      | -                    | -                    | -                    | 3.1   | 17.5     | 3.1       |
| Fm, Ideal, $\Delta_r C_p$ , $\Delta_r V$              | Filter-A     | 10,749(215)  | -3.664(130)                                      | -                    | -                    | -                    | 17.5  | 16.0     | 8.2       |
| Fm, Ideal, $\Delta_r C_p$ , $\Delta_r V$              | Filter-B     | 11,239(255)  | -3.970(154)                                      | -                    | -                    | -                    | 15.6  | 15.6     | 6.2       |
| Ex, $W_{Ni-Mg-Si}$ <sup>f</sup>                       | Filter-A     | 2,942  | -2.006   | 581.1                | 3248                 | 5277                 | 12.9  | 12.1     | 4.0       |
| Ex, $W_{Ni-Mg-Si}$                                    | Filter-B     | 2,660  | -1.390   | -738.3               | 4906                 | 6156                 | 12.3  | 12.3     | 5.5       |
| Fm, $W_{Ni-Mg-Si}$                                    | Filter-A     | 5,498  | -2.582   | 581.1                | 3248                 | 5277                 | 13.0  | 11.5     | 6.1       |
| Fm, $W_{Ni-Mg-Si}$                                    | Filter-B     | 3,814  | -1.741   | -738.3               | 4906                 | 6156                 | 10.9  | 10.9     | 8.3       |

Note: For each fit we list the reaction, the dataset used, and the resulting fit parameters. We also report the mean percent errors between the predicted and measured  $D_{Ni}^{molar}$  for the dataset used in the fit, the Filter-B dataset, and this work.

<sup>a</sup> For all fit parameters units are listed in parenthesis in the column header, and are unit-less when not available. Number in parenthesis is the standard error of the fit parameter in terms of the last unit cited (e.g., -1.970(95) should be read as -1.970 with an estimated standard error of 0.095; standard errors are estimated using the robustfit function in MATLAB).

<sup>b</sup> Mean percent errors are defined as  $100 * [\text{predicted } D_{Ni}^{ol/liq} - \text{measured } D_{Ni}^{ol/liq}] / \text{measured } D_{Ni}^{ol/liq}$ .

<sup>c</sup> Equation 5

<sup>d</sup> Equation 7, assuming ideality and that  $\Delta_r C_p$  and  $\Delta_r V$  are both zero

<sup>e</sup> Equation 7, assuming ideality and calculating  $\Delta_r C_p$  and  $\Delta_r V$  as described in the text

<sup>f</sup> Simultaneous fit of Equations 9 and 10 as described in the text

## FIGURE CAPTIONS

**Fig. 1**  $D_{Ni}^{ol/liq}$  as a function of temperature. (a) Experiments from this study. Error bars are 1 standard deviation of the calculated partition coefficient based on the uncertainties in average NiO contents of the glass and olivine. For clarity, we offset points by as much as 10 degrees from the actual run temperature (e.g., all experiments plotting close to 1450°C were conducted at 1450°C). Black symbols indicate forward experiments and red the reversals. Circles represent Pt-graphite double capsule experiments while the square represents the Re-capsule experiment. (b) Predictions, based on literature models, for data from our experiments, which are also shown along with a linear least-squares regression assuming that  $D_{Ni}^{ol/liq}$  is a function only of temperature (red line). Symbols for our data are as in panel **a**. Each literature line was constructed by first calculating  $D_{Ni}^{ol/liq}$  for each experiment according to the authors' models using the compositions given in Table 3. The resulting set of points for each expression was then fit using an unweighted linear function of temperature. A77: Arndt (1977); AW90-TMg and AW90T-Si: expressions from Agee and Walker (1990) assuming that  $D_{Ni}^{ol/liq}$  depends on temperature and either  $MgO^{liq}$  (A&W90-TMg) or  $SiO_2^{liq}$  (A&W90T-Si), B91: Beattie et al. (1991); C88: Colson et al. (1988); HD-Mg and HD-T: Hart and Davis (1978) expressions assuming  $D_{Ni}^{ol/liq}$  to be functions of  $MgO^{liq}$  and T, respectively; Kel98: Kelemen et al. (1998); Kin90: Equation 4 from Kinzler et al. (1990); LR10: Li and Ripley (2010); MELTS: MELTS calculations (these were calculated by taking the run #25 (1-atm) glass composition and varying temperature at each pressure [1-atm to 3.0 GPa in 0.5 GPa increments] until a small amount of olivine crystallized); P11-2a, P11-2b, and P11-2c: Equations 2a, 2b, and 2c, respectively, from Putirka et al. (2011). Unlabeled line is a least-squares fit to the new experiments presented here.

**Fig. 2**  $\ln(D_{Ni}^{mol ar}) + \ln\left(\frac{X_{MgO}^{liq}}{X_{Fe}^{ol}}\right)$  as a function of  $1/T(K)$  (see Equation 5, where  $X_{Fo}^{ol} = X_{MgO}^{ol}$ ).

Each point represents the result for an individual experiment, and lines are robust fits to a given dataset. Experiments passing Filter-A only are shown as blue crosses (all points passing Filter B are also included in this dataset but are not plotted separately). The robust fit for Filter-A data is shown as a solid blue line. Data passing Filter-B are shown as brown circles, and the robust fit to these experiments as a dashed brown line (data from this study also pass Filter-B and are included in the fit but are plotted separately). Data from this work are plotted as closed red circles and the corresponding robust fit by a solid red line

**Fig. 3** Measured olivine-liquid Ni partition coefficients (by weight) from this work and Filter-A data as a function of temperature. Also shown are the predictive equations 2b of Putirka et al. (2011) and Equation 4 from Li and Ripley (2010). As in Fig. 2, lines are linear fits to predicted partition coefficients using phase compositions listed in Table 3. Fits to the formation reaction (Equation 9) for the Filter-A dataset are shown in gray, one fit assuming  $\Delta_r C_p$  and  $\Delta_r V$  is zero, and the second after calculating the  $\Delta_r C_p$  and  $\Delta_r V$  for each experiment. Calculating  $\Delta_r C_p$  and  $\Delta_r V$  leads to a much better fit to our experimental data, with mean % errors decreasing from 9% to 6%

**Fig. 4** Measured and predicted  $D_{Ni}^{ol/liq}$  (by wt.) vs. temperature. In both panels of the figure, measured  $D_{Ni}^{ol/liq}$ s from our experiments are shown as filled black circles with their corresponding error bars. In panel (a), all fits use Equation 9 (regular-solution exchange reaction). The lines correspond to the predicted partition coefficient for a liquid and olivine of constant composition

(run 25) being taken up pressure and temperature simultaneously; the prediction using the Filter-A dataset is a solid blue line, while the prediction of the fit to the Filter-B dataset is a brown dashed line. Panel (b) shows fits to Equation 10 (regular-solution formation reaction). Symbols in (b) are the same as panel (a) except that all predicted partition coefficients used regular-solution fits to the formation reaction

**Fig. 5**  $M^{2+}$ -Mg exchange showing the data from Takahashi (1978). Ni: black triangles; Co: blue triangles; Mn: green triangles;  $Fe^{2+}$ : pink squares. Robust least-squares fits to the Takahashi (1978) data are shown as solid lines with colors corresponding to the data as above. Dashed lines are robust least-squares fits to the Filter-A dataset (Filter A-data points not shown). Red circles are the new Ni-partitioning data presented in this work

**Fig. 6a** NiO vs. Mg# of olivines. Open red circles are from Mauna Kea, obtained by the Hawaiian Scientific Drilling Project and reported by Sobolev et al. (2007). Closed gray symbols refer to olivine compositions obtained using the calculation described in the text. Briefly, melts whose compositions are equal to the 3.0 GPa experiments of Kushiro (1996) are equilibrated with olivines that have 0.36 wt. % NiO at 3.0 GPa and the temperature of each experiment. These melts are then brought to low pressure (0.1 GPa) and allowed to cool until 1 wt. % olivine forms (temperature and olivine compositions from MELTS). This calculation is done independently for each of the four experimental liquids. The resulting low-pressure olivines for fits to the Filter-B dataset using Equation 5 are shown

**Fig. 6b** NiO vs. Mg# of olivine phenocrysts. Hawaii, MORB, Iceland, Other OIB, and Komatiites from Sobolev et al. (2007). Results of our schematic calculations for both Hawaii and a Barberton komatiite are shown in gray (Filter-B dataset fit to Equation 5 with a source region containing olivine with NiO = 0.36 wt. %). Note that (1) calculated NiO contents of phenocrysts crystallized at shallow depths are higher than those of olivines in the source and (2) the calculated olivine compositions closely resemble those observed from Hawaii and other komatiites

## FIGURES

Fig. 1

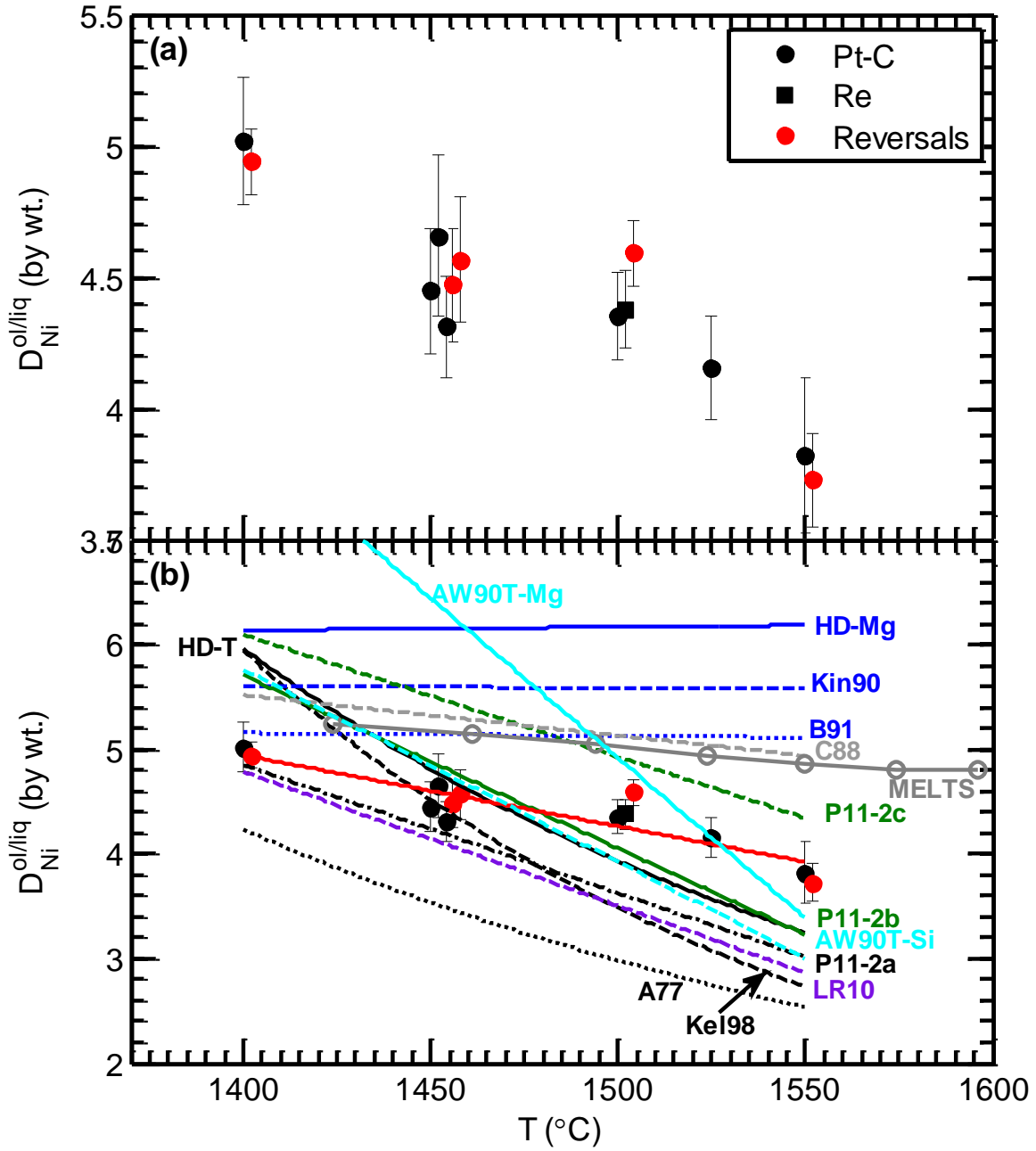


Fig 2

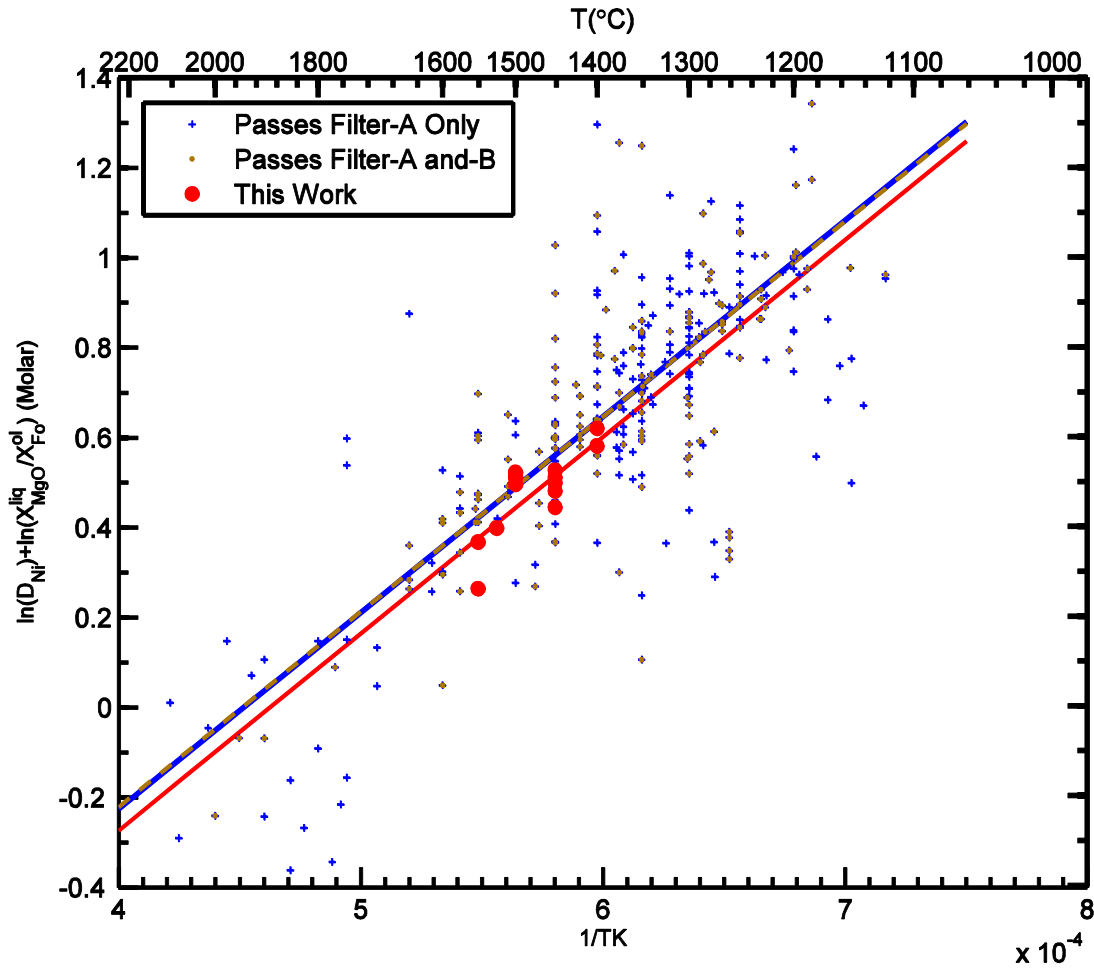


Fig. 3

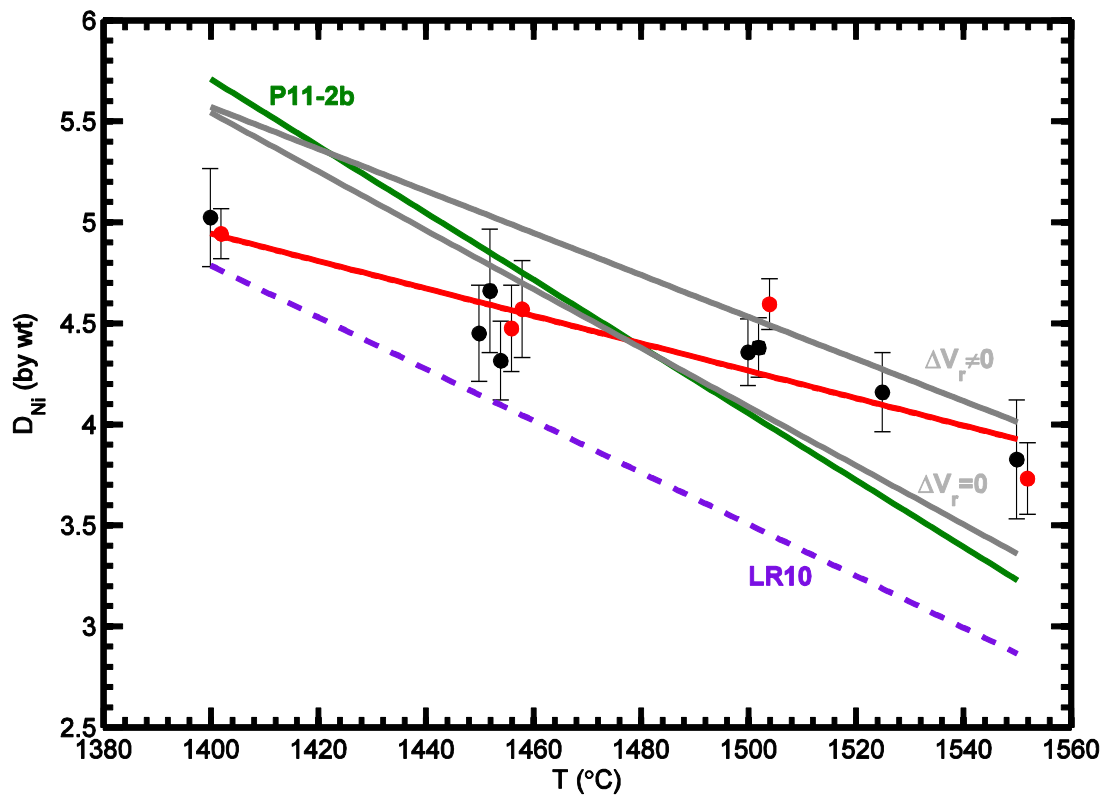


Fig. 4

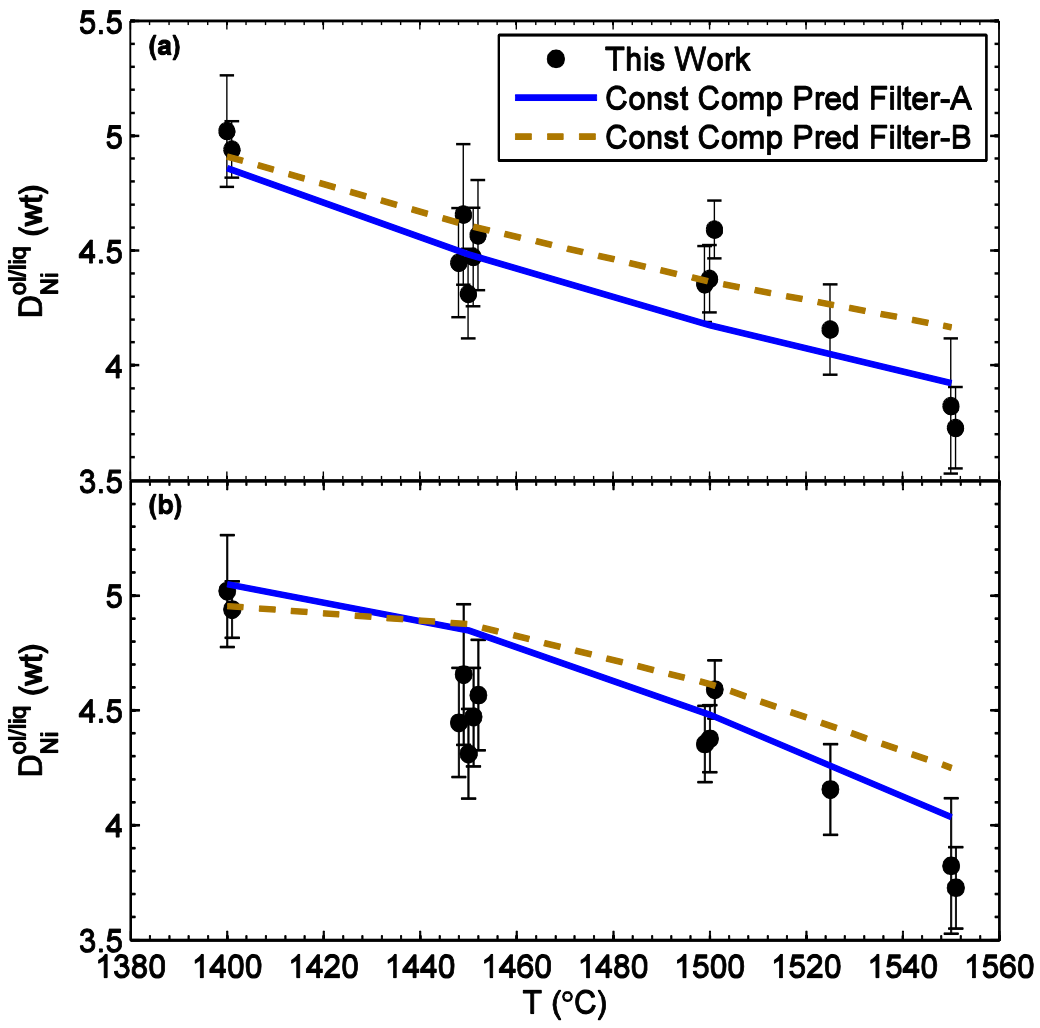


Fig. 5

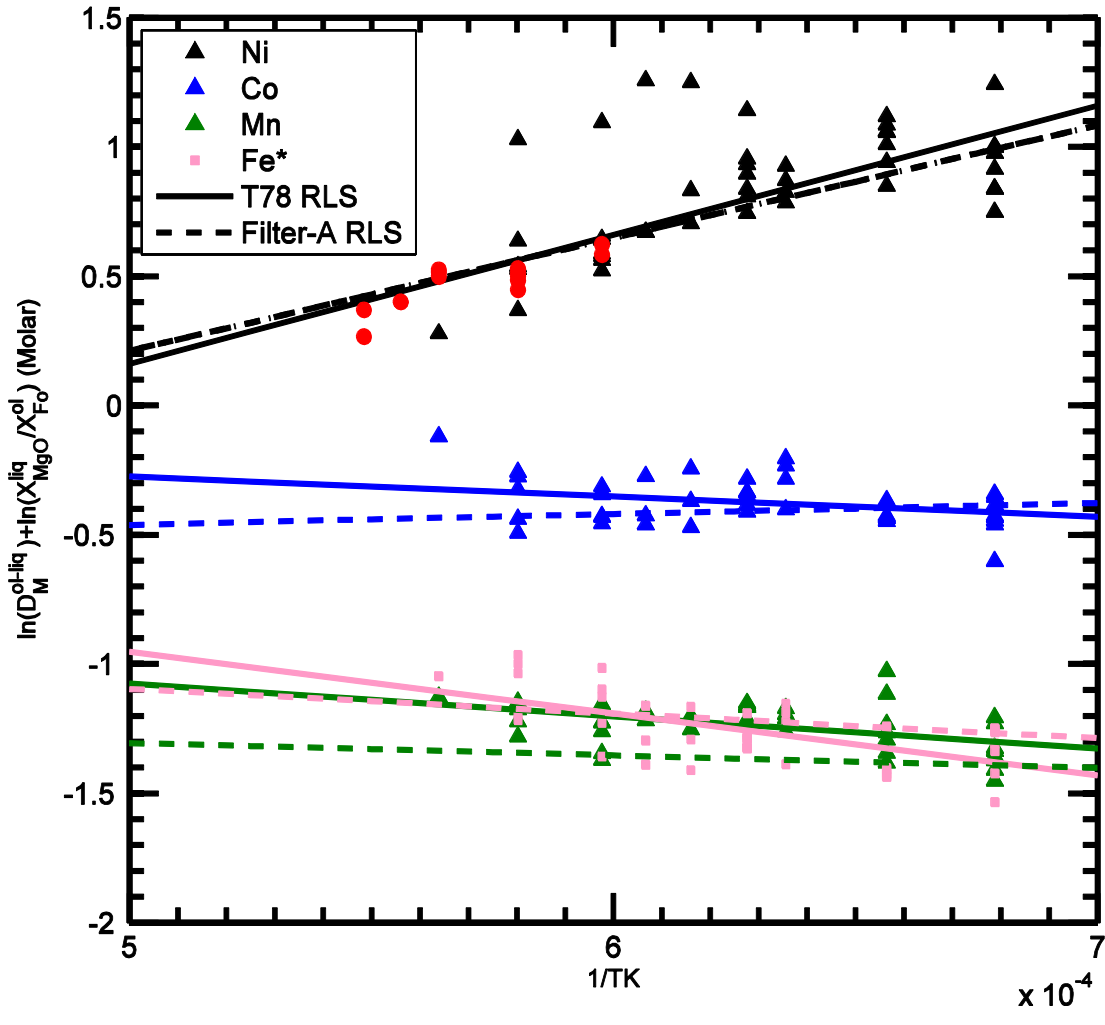


Fig. 6a

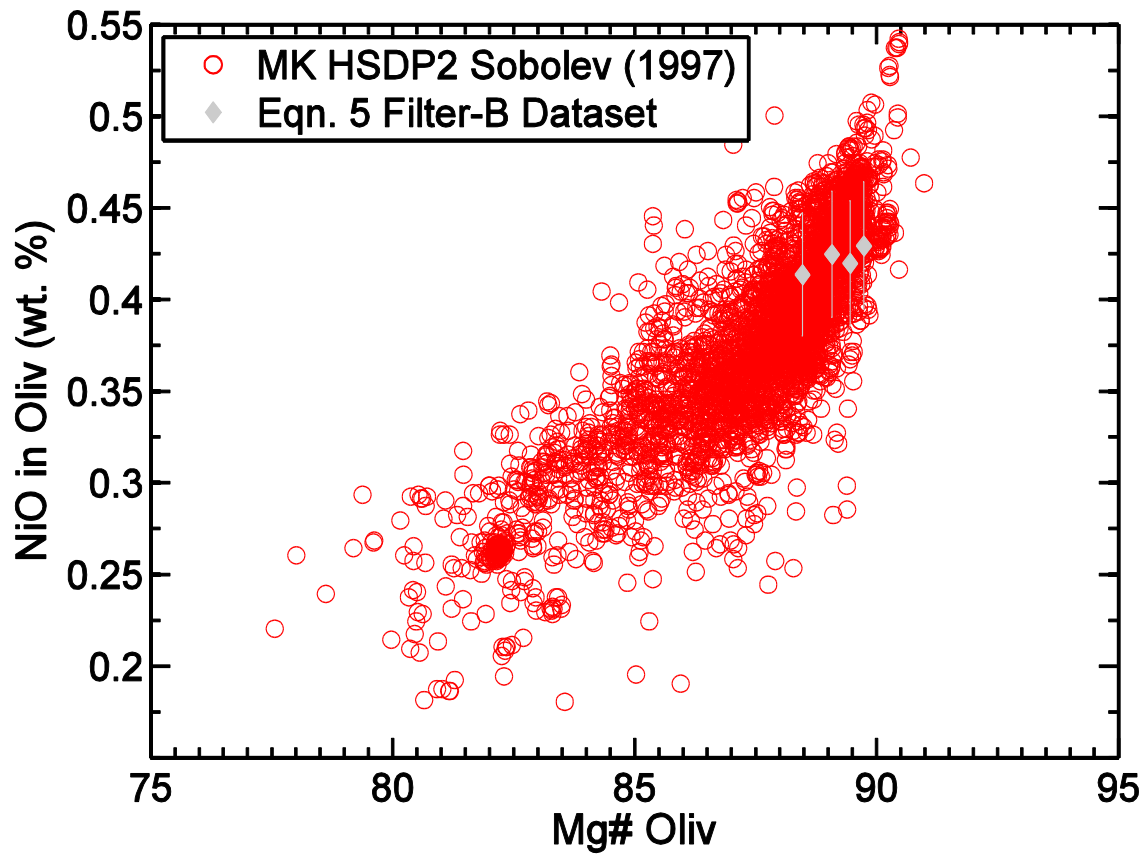
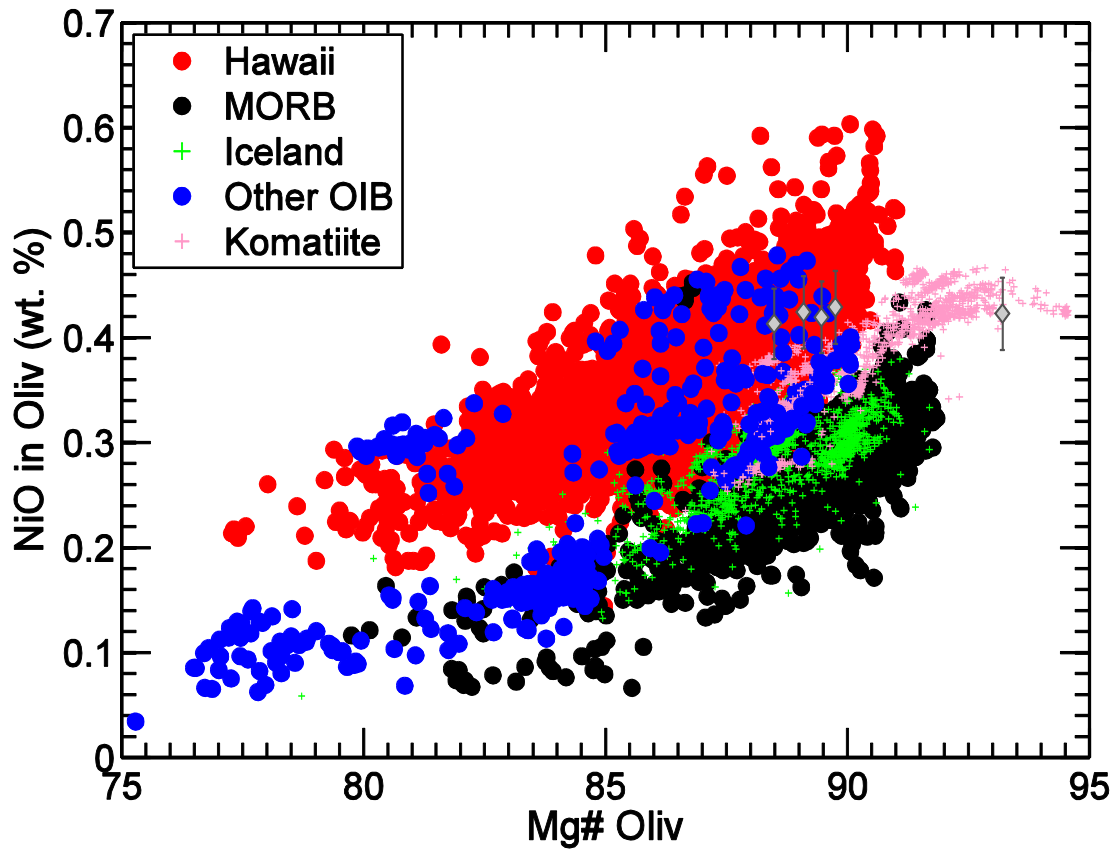


Fig. 6b



## SUPPLEMENTARY MATERIAL

In this Supplement we provide five sections that expand and/or illustrate specific topics presented in the main text. The first section is an example calculation using our preferred partitioning expression, Equation 5, from the main text. Section 2 compares our fitted values of  $-\frac{\Delta_r H_{T_{ref}, P_{ref}}^\circ}{R}$  and  $\frac{\Delta_r S_{T_{ref}, P_{ref}}^\circ}{R}$  for Equation 5 to those calculated using tabulated thermodynamic data. In Section 3 we present the details of the mass-balance calculations used to evaluate the experiments from both this work and the literature, and in Section 4 we describe in detail the construction of the Filter-B dataset. Finally, Section 5 lists all of the references incorporated into our database on olivine-liquid Ni partitioning.

### 1. Example Calculation Using Our Preferred Partitioning Expression (Equation 5) from the Main Text

Although one of the simplest equations listed in the text, we think it useful to present a detailed accounting of how to use Equation 5, along with the fitted parameters presented in Table 4, to predict  $D_{Ni}^{ol/liq}$  (where  $D_{Ni}^{ol/liq} = \text{NiO}^{ol}/\text{NiO}^{liq}$ , by wt.) given the temperature and compositions of the coexisting olivine and liquid. In our example calculation we predict the partition coefficient for one of our 1.0 GPa experiments, kbh-ol-c-6. Below, we will display initial values truncated to 2 or 4 decimal places. We then use the truncated values in the calculation, showing the calculated values to 4 decimal places; this in no way a reflection on the precision of the measurements or the resulting prediction, rather it is meant to aid in the reproduction of the calculation.

#### 1.1 Initial Information

Temperature (K) = 1723.15

Liquid composition (wt. %)

|                                |        |
|--------------------------------|--------|
| SiO <sub>2</sub>               | 49.91  |
| TiO <sub>2</sub>               | 1.41   |
| Al <sub>2</sub> O <sub>3</sub> | 11.10  |
| Cr <sub>2</sub> O <sub>3</sub> | 0.0121 |
| FeO*                           | 10.73  |
| MnO                            | 0.20   |
| MgO                            | 17.66  |
| CaO                            | 7.41   |
| Na <sub>2</sub> O              | 1.95   |
| K <sub>2</sub> O               | 0.1204 |
| P <sub>2</sub> O <sub>5</sub>  | 0.1120 |
| NiO                            | 0.0729 |

Olivine composition (wt. %)

|                                |        |
|--------------------------------|--------|
| SiO <sub>2</sub>               | 40.74  |
| TiO <sub>2</sub>               | 0.0223 |
| Al <sub>2</sub> O <sub>3</sub> | 0.0703 |
| Cr <sub>2</sub> O <sub>3</sub> | 0.0130 |
| FeO*                           | 9.94   |
| MnO                            | 0.1415 |
| MgO                            | 48.56  |
| CaO                            | 0.2128 |
| Na <sub>2</sub> O              | 0      |
| K <sub>2</sub> O               | 0      |
| P <sub>2</sub> O <sub>5</sub>  | 0      |
| NiO                            | 0.3243 |

For reference, the measured  $D_{Ni}^{ol/liq}$  (using the truncated data listed above) = 4.4486.

### ***1.2 Transforming to Molar Components***

Fits to the equations presented in the text are performed using mole fractions; therefore, to predict a partition coefficient it is necessary to transform a composition from weight percent into mole fractions. Transforming the liquid composition is relatively straightforward (dividing the wt. % values by the gram-formula weight). Note that we choose to use the liquid component Si<sub>0.5</sub>O, instead of the more common SiO<sub>2</sub>, to facilitate writing the formation reaction in the main text.

## Liquid composition (moles) and components

| Components                     | Moles  | Formula weights |
|--------------------------------|--------|-----------------|
| Si <sub>0.5</sub> O            | 1.6613 | 30.04215        |
| TiO <sub>2</sub>               | 0.0177 | 79.8658         |
| Al <sub>2</sub> O <sub>3</sub> | 0.1089 | 101.9613        |
| Cr <sub>2</sub> O <sub>3</sub> | 0.0001 | 151.9904        |
| FeO*                           | 0.1494 | 71.8444         |
| MnO                            | 0.0028 | 70.9374         |
| MgO                            | 0.4382 | 40.3044         |
| CaO                            | 0.1321 | 56.0774         |
| Na <sub>2</sub> O              | 0.0315 | 61.9789         |
| K <sub>2</sub> O               | 0.0013 | 94.196          |
| P <sub>2</sub> O <sub>5</sub>  | 0.0008 | 141.9445        |
| NiO                            | 0.0010 | 74.6928         |
| CoO                            | 0      | 74.9326         |

Renormalizing by the sum of the total number of moles in the liquid (2.5449) gives the liquid composition in mole fractions.

## Liquid composition (mole fractions) and components

| Components                     | Mole fract. |
|--------------------------------|-------------|
| Si <sub>0.5</sub> O            | 0.6528      |
| TiO <sub>2</sub>               | 0.0069      |
| Al <sub>2</sub> O <sub>3</sub> | 0.0428      |
| Cr <sub>2</sub> O <sub>3</sub> | 0.0000      |
| FeO*                           | 0.0587      |
| MnO                            | 0.0011      |
| MgO                            | 0.1722      |
| CaO                            | 0.0519      |
| Na <sub>2</sub> O              | 0.0124      |
| K <sub>2</sub> O               | 0.0005      |
| P <sub>2</sub> O <sub>5</sub>  | 0.0003      |
| NiO                            | 0.0004      |
| CoO                            | 0           |

Transforming the olivine composition into olivine components is only slightly more involved: First, the composition in wt. % is transformed into moles and mole fractions of the components listed in Table 3 (i.e., Si is as SiO<sub>2</sub>).

## Olivine composition (moles) and components

| Components                     | Moles  | Formula weights |
|--------------------------------|--------|-----------------|
| SiO <sub>2</sub>               | 0.6780 | 60.0843         |
| TiO <sub>2</sub>               | 0.0003 | 79.8658         |
| Al <sub>2</sub> O <sub>3</sub> | 0.0007 | 101.9613        |
| Cr <sub>2</sub> O <sub>3</sub> | 0.0001 | 151.9904        |
| FeO*                           | 0.1384 | 71.8444         |
| MnO                            | 0.0020 | 70.9374         |
| MgO                            | 1.2048 | 40.3044         |
| CaO                            | 0.0038 | 56.0774         |
| Na <sub>2</sub> O              | 0      | 61.9789         |
| K <sub>2</sub> O               | 0      | 94.196          |
| P <sub>2</sub> O <sub>5</sub>  | 0      | 141.9445        |
| NiO                            | 0.0043 | 74.6928         |
| CoO                            | 0      | 74.932          |

Renormalizing by the total number of the moles (2.0324) gives the olivine composition in mole fractions.

## Olivine composition (mole fractions) and components

|                                |        |
|--------------------------------|--------|
| SiO <sub>2</sub>               | 0.3336 |
| TiO <sub>2</sub>               | 0.0001 |
| Al <sub>2</sub> O <sub>3</sub> | 0.0003 |
| Cr <sub>2</sub> O <sub>3</sub> | 0.0000 |
| FeO*                           | 0.0681 |
| MnO                            | 0.0010 |
| MgO                            | 0.5928 |
| CaO                            | 0.0019 |
| Na <sub>2</sub> O              | 0      |
| K <sub>2</sub> O               | 0      |
| P <sub>2</sub> O <sub>5</sub>  | 0      |
| NiO                            | 0.0021 |
| CoO                            | 0      |

A transformation matrix,

|   |      |      |      |      |      |      |
|---|------|------|------|------|------|------|
| 1 | -0.5 | -0.5 | -0.5 | -0.5 | -0.5 | -0.5 |
| 0 | 1    | 0    | 0    | 0    | 0    | 0    |
| 0 | 0    | 1    | 0    | 0    | 0    | 0    |
| 0 | 0    | 0    | 1    | 0    | 0    | 0    |
| 0 | 0    | 0    | 0    | 1    | 0    | 0    |
| 0 | 0    | 0    | 0    | 0    | 1    | 0    |
| 0 | 0    | 0    | 0    | 0    | 0    | 1    |

is then multiplied by a vector containing the mole fractions of SiO<sub>2</sub>, FeO, MnO, MgO, CaO, NiO, and CoO, transforming the olivine composition into moles of end-member olivine components.

Olivine composition (moles) and components

|                                    |        |
|------------------------------------|--------|
| SiO <sub>2</sub>                   | 0.0007 |
| FeSi <sub>0.5</sub> O <sub>2</sub> | 0.0681 |
| MnSi <sub>0.5</sub> O <sub>2</sub> | 0.0010 |
| MgSi <sub>0.5</sub> O <sub>2</sub> | 0.5928 |
| CaSi <sub>0.5</sub> O <sub>2</sub> | 0.0019 |
| NiSi <sub>0.5</sub> O <sub>2</sub> | 0.0021 |
| CoSi <sub>0.5</sub> O <sub>2</sub> | 0      |

The resulting vector is then renormalized by its sum (0.6665), completing the transformation of an olivine analysis in wt. % to mole fractions of olivine components and SiO<sub>2</sub>.

Olivine composition (mole fraction) and components

|                                    |        |
|------------------------------------|--------|
| SiO <sub>2</sub>                   | 0.0010 |
| FeSi <sub>0.5</sub> O <sub>2</sub> | 0.1021 |
| MnSi <sub>0.5</sub> O <sub>2</sub> | 0.0015 |
| MgSi <sub>0.5</sub> O <sub>2</sub> | 0.8894 |
| CaSi <sub>0.5</sub> O <sub>2</sub> | 0.0028 |
| NiSi <sub>0.5</sub> O <sub>2</sub> | 0.0032 |
| CoSi <sub>0.5</sub> O <sub>2</sub> | 0      |

Again, for reference, the measured  $D_{Ni}^{molar}$  (as defined in the text, using the truncated data presented here) is 8.3569.

### ***1.3 Predicting a Partition Coefficient***

Now that we have transformed our analyses into the proper molar components we have the information we need to predict the partition coefficient. Equation 5 from the main text

$$-\frac{\Delta_r H_{T_{ref}, P_{ref}}^\circ}{RT} + \frac{\Delta_r S_{T_{ref}, P_{ref}}^\circ}{R} = \ln(D_{Ni}^{molar}) + \ln\left(\frac{X_{MgO}^{liq}}{X_{MgSi_{0.5}O_2}^{ol}}\right)$$

can be rearranged to

$$D_{Ni}^{molar} = \exp\left[-\frac{\Delta_r H_{T_{ref}, P_{ref}}^\circ}{RT} + \frac{\Delta_r S_{T_{ref}, P_{ref}}^\circ}{R} - \ln\left(\frac{X_{MgO}^{liq}}{X_{MgSi_{0.5}O_2}^{ol}}\right)\right].$$

Using the fits to the Filter-B dataset ( $-\frac{\Delta_r H_{T_{ref}, P_{ref}}^\circ}{R}$  and  $\frac{\Delta_r S_{T_{ref}, P_{ref}}^\circ}{R}$  are 4337.9665 and -1.9563, respectively) results in a predicted molar partition coefficient of 9.0537.

#### 1.4 Converting $D_{Ni}^{molar}$ to $D_{Ni}^{ol/liq}$

In this specific case a molar partition coefficient is useful in that we can compare it to the experimentally measured value (the prediction has an error of ~8%); however, in most applications it is preferable to work with the traditional weight-based  $D_{Ni}^{ol/liq}$ . To convert a molar partition coefficient into a weight-based partition coefficient we need to multiply  $D_{Ni}^{molar}$  by the ratio of the renormalizing constants used in the olivine transformation to the renormalizing constants used in the liquid transformation. In our example we renormalized our olivine composition twice (molar sums were 2.0324 and 0.6665) and we renormalized our liquid composition once (molar sum was 2.5449), therefore we need to multiply  $D_{Ni}^{molar}$  by 0.5323 [i.e., (2.0324 0.6665)/2.5449] to transform our molar partition coefficient to our more familiar, weight-based,  $D_{Ni}^{ol/liq}$ . The predicted  $X_{start}^{ol}$  for this experiment is 4.8195 (again, the error of the predicted value is ~8%).

## 2. Comparing Fitted and Tabulated Standard-State Enthalpies and Entropies

We can compare our fitted values of  $-\frac{\Delta_r H_{T_{ref}, P_{ref}}^\circ}{R}$  and  $\frac{\Delta_r S_{T_{ref}, P_{ref}}^\circ}{R}$  from Equation 5 to those calculated using tabulated thermodynamic data (e.g., Robie et al. 1978). More specifically, we used data from Robie et al. (1978) whenever possible, and Barin (1995) when the data was not available in Robie et al. (1978) [e.g., the enthalpy of melting of NiO]; along with the heat capacity expression of Hirschmann (1991) for Ni-olivine. Using this tabulated thermodynamic data leads to values of  $-\frac{\Delta_r H_{T_{ref}, P_{ref}}^\circ}{R}$  and  $\frac{\Delta_r S_{T_{ref}, P_{ref}}^\circ}{R}$  of  $-2171$  and  $-1.6$ , respectively. The result of this calculation predicts a slope of  $-\frac{\Delta_r H_{T_{ref}, P_{ref}}^\circ}{R}$  that is opposite in sign to that predicted using our experimental data and data from the literature, as discussed in the main text. Although seemingly at odds with the large body of experimental data, the slope calculated using the tabulated thermodynamic data ( $-2171$ ) is in rough agreement with the slope using the high-temperature portion ( $1767$  to  $1896^\circ\text{C}$ ) of the  $\text{Ni}_2\text{SiO}_4\text{-Mg}_2\text{SiO}_4$  phase diagram from Ringwood (1956) ( $-9483/\text{K}$ ); the compositions of coexisting solid and liquid as extracted from the phase diagram over this temperature interval were used to calculate partitioning coefficients, that were then treated in the same manner as our experimental data. One possible explanation for the difference in sign in the  $-\frac{\Delta_r H_{T_{ref}, P_{ref}}^\circ}{R}$  term would be the apparent discontinuity between the behavior of Ni in the  $\text{Ni}_2\text{SiO}_4\text{-Mg}_2\text{SiO}_4$  binary and in more complex silicate melts (e.g., Burns and Fyfe 1966). The poor agreement between the fit parameters based on the large body of experimental data and the expected values from thermodynamic tables and data from simple systems reminds us: (1) that our experiments likely carry some contribution from non-ideality, and (2) the danger of extrapolating

simple system results to more complex systems or vice versa where the differences in activity-composition relations may be great; thus, the substantial disagreement is not entirely surprising. Ultimately, the overall objective is to fit experimental data in reasonably complex systems with a thermodynamically- inspired functional form. Although our preferred fit does not reproduce the values calculated from thermodynamic tables, as discussed in the main text, it does quite a good job describing our experiments and those from the literature.

### 3. Mass-Balance Calculations

The mass-balance calculations for our experiments, and those from the literature, use the non-linear form of the  $\chi^2$  function that includes uncertainties on the oxide values of the bulk composition and each of the phases. Our experiments and the 1-atm olivine-crucible experiments of Ehlers et al. (1992) and Wang and Gaetani (2008) present a particular problem with respect to mass balance. The issue is that the bulk composition for a given experiment is not given by the compositions and mass fractions of the starting olivine and glass, since during the experiment the evolving liquid does not react with the entire mass of olivine in the charge. Thus, at the end of the experiment the bulk composition actually lies somewhere along the join defined by the starting olivine and glass compositions. Our approach for mass balancing the results of this sort of experimental design is to do a one-dimensional search along this join for the mass fraction of the starting olivine ( $X_{start}^{ol}$ ; the mass fraction of starting glass is:  $1 - X_{start}^{ol}$ ) that produces a bulk composition that in turn yields a minimum  $\chi^2$  value for the mass balance using the final glass and olivine compositions. It is important to note that the two minimizations are not done simultaneously—the existence of a single minimum along the join is tested by starting at  $X_{start}^{ol} = 0.99$  and calculating  $\chi^2$ , then decreasing  $X_{start}^{ol}$  by 0.025 and again calculating  $\chi^2$ , and continuing

this process till  $X_{start}^{ol} = 0.015$ . Once the minimum is bracketed (multiple minima were not encountered for any experiments), it is refined using inverse parabolic interpolation (e.g., Press et al. 1992).

Since the bulk composition varies as  $X_{start}^{ol}$  varies, this approach requires a flexible method for calculating one-sigma uncertainties on the bulk. We have calculated fractional errors ( $\sigma/\text{mean}$ ) for large numbers of analyses of different microprobe standards (both glasses and minerals) in the Caltech collection using the same set of analytical conditions that we used for determining the major-element chemistry of our experimental glasses. Standards were chosen so as to cover a broad range of concentrations for the following oxides: SiO<sub>2</sub>, TiO<sub>2</sub>, Al<sub>2</sub>O<sub>3</sub>, Cr<sub>2</sub>O<sub>3</sub>, FeO\* (all Fe as FeO), MnO, MgO, CaO, Na<sub>2</sub>O, K<sub>2</sub>O, and P<sub>2</sub>O<sub>5</sub>. For example, SiO<sub>2</sub>, FeO\*, and MgO concentrations ranged from ~41 to 66, ~6 to 16, and ~0.9 to 49 wt. %, respectively. Our expectation is that fractional errors for a given oxide should be approximately constant for concentrations above a certain value (generally in the range of 1 to 2 wt. %, although this will vary with the oxide). Below this concentration range fractional errors increase, rapidly eventually reaching and exceeding a value of one; a concentration that yields a fractional error of one is presumably close to the detection limit. For the ranges of silica and iron concentrations reported above, fractional errors were, not surprisingly, uncorrelated with concentration, and we calculated the following mean values: 0.003829 and 0.008303. Thus for a given bulk SiO<sub>2</sub> value, the corresponding standard deviation would be:  $[\text{SiO}_2] \cdot 0.003829$  (where the square brackets denote an oxide concentration in wt. %). For MgO, fractional errors are not constant over the concentration range of 0.9 to 49 wt. % and have been fit using the following power law expression:  $a + b [\text{MgO}]^c$ , (where  $a$ ,  $b$ , and  $c$  are the fit parameters). The remaining oxides also spanned a sufficient compositional range so as to have non-constant fractional errors which were fit using either:

$a$  (oxide concentration of  $i$ ) <sup>$b$</sup>  or  $a + b$  (oxide concentration of  $i$ ) <sup>$c$</sup> . Fig. S1 shows fits for MgO and K<sub>2</sub>O.

Note that NiO is not in the above list of oxides. This is because we treat bulk NiO as a free parameter in our mass balance calculations since it is the one element that can be most easily lost from our high-pressure experiments if melt comes in contact with the graphite inner capsule. To insure a good mass balance fit for Ni (and thus an accurate estimate of Ni loss or gain) we fix the fractional error for NiO in all phases and in the bulk at 0.001. The difference between NiO<sup>bulk</sup> required for mass balance and the NiO concentration calculated using the optimal value of  $X_{start}^{ol}$  and the NiO contents of the starting olivine and glass denotes the extent to which NiO has been conserved in a given experiment. In the 1-atm olivine-capsule experiments bulk Na<sub>2</sub>O and K<sub>2</sub>O are also allowed to vary, since the volatility of sodium, and to a lesser extent potassium, under such conditions is well known (e.g., Corrigan and Gibb 1979; Kilinc et al. 1983; Yamanaka et al. 1996). If the concentration of bulk NiO and/or Na<sub>2</sub>O and K<sub>2</sub>O (in 1-atm runs) changes, then the remaining oxide concentrations in the bulk change inversely by a proportional amount (i.e., the bulk oxide sum remains fixed at 100%). For each experiment, the minimum  $\chi^2$  value along with the number of degrees of freedom is used to calculate a  $Q$  value, a statistical measure of goodness-of-fit (the degrees of freedom are decreased by the number of oxides in the bulk that are allowed to vary).

Several further points concerning our mass balance approach for olivine-capsule experiments are worth discussing: the method is based on the assumption that dissolution/precipitation of olivine is the dominant process that causes the liquid to evolve in composition. If the liquid composition at the end of an experiment is largely controlled by differing rates of diffusion of components into and out of the olivine capsule, we would expect that this mass balance approach would not yield successful solutions. The fact that we do generate

successful solutions suggests that dissolution/reprecipitation is probably the dominant mechanism generating a change in liquid composition. Finally, our approach does fail if the final liquid and olivine compositions are too similar to those of the starting olivine and glass—i.e., little dissolution/reprecipitation has occurred during the experiment—since in this case the starting olivine and glass pair and the final olivine and glass pair are, within error, collinear.

For experiments from the literature run on wire loops or in precious metal capsules  $\pm$  graphite, the bulk composition is in principal fixed and the mass balance exercise is much more straight forward; although as stated above the inclusion of errors on the phase compositions makes the  $\chi^2$  equation non-linear. However, only a subset of studies in our database report analytical uncertainties on the average phase compositions, and very few studies provide estimates of the uncertainties on their bulk compositions. Thus a consistent approach is required for estimating these uncertainties. To take into consideration the fact that experimental olivine-liquid Ni partitioning studies in our database span a period of close to 40 years and much of the data was collected using earlier generations of microprobes, we have used the large body of average experimental glass compositions and uncertainties published by the MIT group (all collected on a JEOL 733 microprobe) to calculate fractional errors for the following oxides: SiO<sub>2</sub>, TiO<sub>2</sub>, Al<sub>2</sub>O<sub>3</sub>, Cr<sub>2</sub>O<sub>3</sub>, FeO\* (all Fe as FeO), MnO, MgO, CaO, Na<sub>2</sub>O, K<sub>2</sub>O, and P<sub>2</sub>O<sub>5</sub>. As was the case above, fractional errors for SiO<sub>2</sub> are independent of concentration in the range 35–71 wt. % and have a mean value of 0.006480. For the remaining oxides, power law fits adequately describe the variation of fractional error with concentration. Again, the fractional error for NiO in all phases and in the bulk was set to 0.001 and bulk NiO was a free parameter in the mass balance calculations. For the 1-atm wire loop and Mo crucible experiments, bulk FeO\*, Na<sub>2</sub>O, and K<sub>2</sub>O concentrations were also allowed to vary: the alkalis for reasons of volatility and FeO\* because

even with pre-saturation of the sample container the silicate charge can still gain or lose Fe. Further, in the experiments of Synder and Carmichael (1992) a subset of the runs were done on Fe-wire loops and the silicate charges gained substantial amounts of iron (note that this does not necessarily mean that these experiments have not closely approached equilibrium). For the high-pressure experiments in the database, only bulk Ni was allowed to vary. Finally, a goodness-of-fit parameter  $Q$  was calculated for each mass balance calculation using the  $\chi^2$  value and the number of degrees of freedom.

#### 4. Constructing the Filter-B Dataset

We constructed our Filter-A dataset based solely on having acceptable analytical totals (98.5-101.5). When we fit this loosely-filtered dataset the resulting residuals are fairly large (e.g., using Equation (5) the mean percent error on  $D_{Ni}^{ol/liq}$  is ~14%). As discussed in the main text, a flux of Ni out of the silicate portion of the charge and into the container or wire-loop can lead to anomalous  $D_{Ni}^{ol/liq}$  values. Thus, a fundamental question arises: Is the scatter in the fits to our models a result of the shortcomings of our models or the presence of experiments in our database that have not reached equilibrium, at least with respect to Ni partitioning? In an attempt to answer this inherently difficult question, we developed a more restrictive Filter-B dataset. Ideally this dataset would contain only well-analyzed, equilibrium experiments; operationally achieving that goal proves to be more difficult. To begin, in this dataset we only consider experiments with mass balance solutions acceptable at the 95% confidence level. This gives us confidence that, excluding Ni, the phases reported and the analyses thereof constitute an adequate description of the system. As discussed in the main text (and mentioned above), the flux of Ni out of an experiment can lead to anomalous  $D_{Ni}^{ol/liq}$  s. Thus, for the first step in constructing our Filter-B dataset we consider only

those experiments that have acceptable mass balance solutions **and** have either experienced only a small amount of Ni-loss or gain (less than 15%, relative), *or* have explicitly demonstrated experimentally (e.g., via time-series experiments) that  $D_{Ni}^{ol/liq}$  has reached equilibrium, despite large amounts of Ni loss (Arndt 1977; Campbell 1979; Drake and Holloway 1981; Hart and Davis 1978; Kinzler et al. 1990; experiments from Leeman 1974, run above 1300°C and >144 hrs; Mysen 2007; Mysen 2006; Nabelek 1980; Seifert et al. 1988; Snyder and Carmichael 1992; experiments from Takahashi 1978, run above 1320°C and >15 hrs). For example, Run 14 from Hart and Davis (1978) passes our mass balance test and our calculations suggest that it has lost 58% of the initial NiO in the bulk composition. Despite the large amount of Ni-loss Hart and Davis (1978) demonstrated that their run times were sufficient for Ni to equilibrate between the olivine, liquid, and Pt wire loop or Pt capsule, and thus Run 14 is included in the first step of the Filter-B dataset. Not all of the experiments in Hart and Davis (1978) are included in this initial set; Run 7 gained ~6% NiO, however the mass balance solution for the other elements is not satisfactory (at the 95% confidence level) and it is, therefore, not included. From this starting point we can examine how the fits change as we include experiments that while satisfying mass balance for oxides other than Ni, show increasing extents of Ni loss from the bulk. More specifically, as we add experiments that have gained or lost progressively more NiO and subsequently refit the dataset, the residual sum of squares begins to increase rapidly when we include those experiments that lost or gained upwards of ~70% of their initial NiO. We interpret this increase in the residual sum of squares as a possible indication that an increasing number of experiments that are not in equilibrium with respect to Ni are being included in the fit. Thus, the final Filter-B dataset includes only those experiments where the bulk Ni has changed by less than 65%, relative—and all other oxide satisfy mass balance. It is important to note that even if an experiment passes these well-defined criteria, it is not necessarily

an equilibrium experiment. For example, an extremely short duration experiment will (likely) lose little Ni and pass our mass-balance criteria, even though the phases have not had sufficient time to reach equilibrium. Thus, even though we have tried to capture only equilibrium experiments, it is possible that some of the experiments in our Filter-B dataset fall short of this goal.

#### **References for Sections 1-4**

- Arndt NT (1977) Partitioning of nickel between olivine and ultrabasic and basic komatiite liquids. Year Book - Carnegie Institution of Washington (76):553-557
- Barin I (1995) Thermochemical data of pure substances. VCH, New York
- Burns RG, Fyfe WS (1966) Behaviour of Nickel during Magmatic Crystallization. Nature 210:1147-1148. doi:10.1038/2101147a0
- Campbell IH (1979) The influence of temperature and composition on nickel activity in silicate liquids. Eos 60 (18):402-403
- Corrigan G, Gibb FGF (1979) Loss of Fe and Na from a Basaltic Melt During Experiments Using the Wire-Loop Method. Mineralogical Magazine 43 (325):121-126
- Drake MJ, Holloway JR (1981) Partitioning of Ni between olivine and silicate melt: the 'Henry's Law problem' reexamined. Geochimica et Cosmochimica Acta 45:431-437
- Ehlers K, Grove TL, Sisson TW, Recca SI, Zervas DA (1992) The effect of oxygen fugacity on the partitioning of nickel and cobalt between olivine, silicate melt, and metal. Geochimica et Cosmochimica Acta 56:3733-3743
- Hart SR, Davis KE (1978) Nickel Partitioning between Olivine and Silicate Melt. Earth and Planetary Science Letters 40 (2):203-219

- Hirschmann M (1991) Thermodynamics of multicomponent olivines and the solution properties of  $(\text{Ni,Mg,Fe})_2\text{SiO}_4$  and  $(\text{Ca,Mg,Fe})_2\text{SiO}_4$  olivines. *American Mineralogist* 76 (7-8):1232-1248
- Kilinc A, Carmichael ISE, Rivers ML, Sack RO (1983) The ferric-ferrous ratio of natural silicate liquids equilibrated in air. *Contributions to Mineralogy and Petrology* 83 (1-2):136-140
- Kinzler RJ, Grove TL, Recca SI (1990) An experimental study on the effect of temperature and melt composition on the partitioning of nickel between olivine and silicate melt. *Geochimica et Cosmochimica Acta* 54 (5):1255-1265
- Leeman WP (1974) Part I, Petrology of basaltic lavas from the Snake River Plain, Idaho; and Part II, Experimental determination of partitioning of divalent cations between olivine and basaltic liquid. Doctoral, University of Oregon, Eugene
- Mysen B (2007) Partitioning of calcium, magnesium, and transition metals between olivine and melt governed by the structure of the silicate melt at ambient pressure. *American Mineralogist* 92:844-862
- Mysen BO (2006) Redox equilibria of iron and silicate melt structure: Implications for olivine/melt element partitioning. *Geochimica et Cosmochimica Acta* 70 (12):3121-3138
- Nabelek PI (1980) Nickel Partitioning between Olivine and Liquid in Natural Basalts - Henrys Law Behavior. *Earth and Planetary Science Letters* 48 (2):293-302
- Press WH, Teukolsky SA, Vetterling WT, Flannery BP (1992) *Numerical Recipes*. 2nd. edn. Cambridge University Press, Cambridge
- Ringwood AE (1956) Melting relationships of Ni-Mg olivines and some geochemical implications. *Geochimica et Cosmochimica Acta* 10 (5-6):297-303

- Robie RA, Hemingway BS, Fisher JR (1978) Thermodynamic properties of minerals and related substances at 298.15 K and 1 bar ( $10^5$  Pascals) pressure and at higher temperatures. Geological Survey Bulletin 1452
- Seifert S, O'Neill HSC, Brey G (1988) The partitioning of Fe, Ni and Co between olivine, metal, and basaltic liquid: An experimental and thermodynamic investigation, with application to the composition of the lunar core. *Geochimica et Cosmochimica Acta* 52 (3):603-616. doi:10.1016/0016-7037(88)90322-5
- Snyder DA, Carmichael ISE (1992) Olivine-liquid equilibria and the chemical activities of FeO, NiO, Fe<sub>2</sub>O<sub>3</sub>, and MgO in natural basic melts. *Geochimica et Cosmochimica Acta* 56 (1):303-318
- Takahashi E (1978) Partitioning of Ni<sup>2+</sup>, Co<sup>2+</sup>, Fe<sup>2+</sup>, Mn<sup>2+</sup> and Mg<sup>2+</sup> between Olivine and Silicate Melts - Compositional Dependence of Partition-Coefficient. *Geochimica Et Cosmochimica Acta* 42 (12):1829-1844
- Wang Z, Gaetani GA (2008) Partitioning of Ni between olivine and siliceous eclogite partial melt: experimental constraints on the mantle source of Hawaiian basalts. *Contributions to Mineralogy and Petrology* 156 (5):661-678
- Yamanaka A, Tsuchiyama A, Tachibana S, Kawamura K (1996) Measurements of evaporation rates of sodium and potassium from silicate melts. Papers Presented to the Symposium on Antarctic Meteorites 21:210-212

## 5. Experimental Database References

In addition to the data from this work we considered experiments from the following sources. See the main text and Section 4 of this Supplement for the criterion by which subsets of this dataset were selected.

Agee CB, Walker D (1990) Aluminum partitioning between olivine and ultrabasic silicate liquid to 6 GPa. *Contributions to Mineralogy and Petrology* 105:243-254

Arndt NT (1977) Partitioning of nickel between olivine and ultrabasic and basic komatiite liquids. *Year Book - Carnegie Institution of Washington* (76):553-557

Bickle MJ, Ford CE, Nisbet EG (1977) Petrogenesis of Peridotitic Komatiites - Evidence from High-Pressure Melting Experiments. *Earth and Planetary Science Letters* 37 (1):97-106

Brenan JM, McDonough WF, Ash R (2005) An experimental study of the solubility and partitioning of iridium, osmium and gold between olivine and silicate melt. *Earth and Planetary Science Letters* 237 (3-4):855-872

Campbell IH, Naldrett AJ, Roeder PL (1979) Nickel activity in silicate liquids; some preliminary results. *Canadian Mineralogist* 17:495-505

Drake MJ, Holloway JR (1981) Partitioning of Ni between olivine and silicate melt: the 'Henry's Law problem' reexamined. *Geochimica et Cosmochimica Acta* 45:431-437

Ehlers K, Grove TL, Sisson TW, Recca SI, Zervas DA (1992) The effect of oxygen fugacity on the partitioning of nickel and cobalt between olivine, silicate melt, and metal. *Geochimica et Cosmochimica Acta* 56:3733-3743

- Filiberto J, Jackson C, Le L, Treiman AH (2009) Partitioning of Ni between olivine and an iron-rich basalt: Experiments, partition models, and planetary implications. *American Mineralogist* 94 (2-3):256-261
- Hart SR, Davis KE (1978) Nickel Partitioning between Olivine and Silicate Melt. *Earth and Planetary Science Letters* 40 (2):203-219
- Herd CDK, Dwarzski RE, Shearer CK (2009) The behavior of Co and Ni in olivine in planetary basalts: An experimental investigation. *American Mineralogist* 94 (2-3):244-255. doi:10.2138/am.2009.2768
- Herzberg C, Zhang J (1996) Melting experiments on anhydrous peridotite KLB-1: Compositions of magmas in the upper mantle and transition zone. *Journal of Geophysical Research* 101:8271-8295
- Jurewicz AJG, Mittlefehldt DW, Jones JH (1993) Experimental partial melting of the Allende (CV) and Murchison (CM) chondrites and the origin of asteroidal basalts. *Geochimica et Cosmochimica Acta* 57 (9):2123-2139
- Kinzler RJ, Grove TL, Recca SI (1990) An experimental study on the effect of temperature and melt composition on the partitioning of nickel between olivine and silicate melt. *Geochimica et Cosmochimica Acta* 54 (5):1255-1265
- Le Roux V, Dasgupta R, Lee CTA (2011) Mineralogical heterogeneities in the Earth's mantle: Constraints from Mn, Co, Ni and Zn partitioning during partial melting. *Earth and Planetary Science Letters* 307 (3-4):395-408. doi:10.1016/j.epsl.2011.05.014
- Leeman WP (1974) Part I, Petrology of basaltic lavas from the Snake River Plain, Idaho; and Part II, Experimental determination of partitioning of divalent cations between olivine and basaltic liquid. Doctoral, University of Oregon, Eugene

- Longhi J, Durand SR, Walker D (2010) The pattern of Ni and Co abundances in lunar olivines. *Geochimica et Cosmochimica Acta* 74 (2):784-798. doi:10.1016/j.gca.2009.10.001
- Matzen AK, Baker MB, Beckett JR, Stolper EM (2011) Fe–Mg Partitioning between Olivine and High-magnesian Melts and the Nature of Hawaiian Parental Liquids. *Journal of Petrology* 52 (7-8):1243-1263. doi:10.1093/petrology/egq089
- Mibe K, Fujii T, Yasuda A, Ono S (2006) Mg-Fe partitioning between olivine and ultramafic melts at high pressures. *Geochimica Et Cosmochimica Acta* 70 (3):757-766
- Mysen B (2007a) Partitioning of calcium, magnesium, and transition metals between olivine and melt governed by the structure of the silicate melt at ambient pressure. *American Mineralogist* 92:844-862
- Mysen BO (2006) Redox equilibria of iron and silicate melt structure: Implications for olivine/melt element partitioning. *Geochimica et Cosmochimica Acta* 70 (12):3121-3138
- Mysen BO (2007b) Olivine/melt transition metal partitioning, melt composition, and melt structure - Influence of Al<sup>3+</sup> for Si<sup>4+</sup> substitution in the tetrahedral network of silicate melts. *Geochimica Et Cosmochimica Acta* 71 (22):5500-5513
- Mysen BO (2008) Olivine/melt transition metal partitioning, melt composition, and melt structure - Melt polymerization and Q(n)-speciation in alkaline earth silicate systems. *Geochimica Et Cosmochimica Acta* 72 (19):4796-4812
- Nabelek PI (1980) Nickel Partitioning between Olivine and Liquid in Natural Basalts - Henrys Law Behavior. *Earth and Planetary Science Letters* 48 (2):293-302
- Seifert S, O'Neill HSC, Brey G (1988) The partitioning of Fe, Ni and Co between olivine, metal, and basaltic liquid: An experimental and thermodynamic investigation, with application to

- the composition of the lunar core. *Geochimica et Cosmochimica Acta* 52 (3):603-616.  
doi:10.1016/0016-7037(88)90322-5
- Snyder DA, Carmichael ISE (1992) Olivine-liquid equilibria and the chemical activities of FeO, NiO, Fe<sub>2</sub>O<sub>3</sub>, and MgO in natural basic melts. *Geochimica et Cosmochimica Acta* 56 (1):303-318
- Takahashi E (1978) Partitioning of Ni<sup>2+</sup>, Co<sup>2+</sup>, Fe<sup>2+</sup>, Mn<sup>2+</sup> and Mg<sup>2+</sup> between Olivine and Silicate Melts - Compositional Dependence of Partition-Coefficient. *Geochimica Et Cosmochimica Acta* 42 (12):1829-1844
- Taura H, Yurimoto H, Kurita K, Sueno S (1998) Pressure dependence on partition coefficients for trace elements between olivine and coexisting melts. *Physics and Chemistry of Minerals* 25:469-484
- Tuff J, O'Neill HSC (2010) The effect of sulfur on the partitioning of Ni and other first-row transition elements between olivine and silicate melt. *Geochimica et Cosmochimica Acta* 74 (21):6180-6205. doi:10.1016/j.gca.2010.08.014
- Wang Z, Gaetani GA (2008) Partitioning of Ni between olivine and siliceous eclogite partial melt: experimental constraints on the mantle source of Hawaiian basalts. *Contributions to Mineralogy and Petrology* 156 (5):661-678

**Supplementary Material Figure Captions**

**Fig. S1** MgO (A) and K<sub>2</sub>O (B) fractional errors ( $\sigma/\text{mean}$ ) as a function of oxide concentration. Open circles represent fractional errors as calculated for at least 20 analyses on glass and mineral standards in the Caltech microprobe lab; analytical conditions were the same as those used for determining the major-element compositions of the experimental glasses, and are described in the main text. In (A) the best-fit parameters are:  $a = 0.0038425$ ,  $b = 0.026598$ ,  $c = -1.05476$ ; in (B)  $a = 0.017511$ ,  $b = -0.67532$ ; correlation coefficients for both fits are  $> 0.97$ .

## Supplementary Material Figure

Fig. S1

